# Alkane Activation by First, Second, and Third Row Transition Metal Ions: Organometallic Chemistry in the Gas Phase

Thesis by

Jason Kendrick Perry

In Partial Fulfillment of the Requirements

for the Degree of

Doctor of Philosophy

California Institute of Technology

Pasadena, California

1994

(Submitted December 3, 1993)

For my mother,

and for my father and sister for standing by her.

## Acknowlegements

First of all my most sincere thanks must go to Bill Goddard. Bill taught me how to think about chemistry and I found it could be fun. Bill also put his trust in me and as a result I ended up trusting myself, too. I'm glad that I entered the Holy Temple of GVB.

I'd also like to thank Jack Beauchamp. Jack taught me that experimentalists are my friends and I must not fear them. These include Peter Armentrout and Petra van Koppen.

Much of this work was done in collaboration with Gilles Ohanessian. Gilles introduced me to the field of gas phase organometallic chemistry three years ago with this funny problem about inequivalent bonds. I'm eternally grateful. I hope we can continue to collaborate in the future. It's certainly been a productive partnership so far.

Many people have come into my life during these years at Caltech. Although this is just a list, every name here holds a special meaning to me. Graduate school can be a difficult thing and it's these people that have made it bearable: Erik and Laura Bierwagen, Charles Musgrave, Len and Shelley Mueller, Kevin and Lisa Plaxco, Alan Mathiowetz, Jamil Tahir-Kheli, Jean-Marc Langlois, Elaine Marzluff, Karl Irikura, Vinay Sathe, Gordon Oliver, Eddie Schwartz, and Greg Hennessey.

I'd like to pay a special thanks to Siddharth Dasgupta for giving me the final nudge I needed to reconsider staying in graduate school.

Finally, I'd like to thank BP America for a fellowship which made my life a little more comfortable over the past few years.

## Abstract

Reactions of the atomic transition metal cations, $Co^+$, $Rh^+$, and $Ir^+$, with $H_2$, $CH_4$, and $C_2H_6$ in the gas phase are considered using high level *ab initio* techniques. The nature of complexation and oxidative addition, in particular, are discussed. We find that the third row metal, $Ir^+$, is significantly more reactive toward these small molecules in comparison to the first and second row metals. $Ir^+$ is capable of inserting into the H−H bond and leads to the facile dehydrogenation of $CH_4$ to form $IrCH_2^+$. $Co^+$ and $Rh^+$ form only molecular complexes with these molecules. All three metals exothermically dehydrogenate ethane but $Co^+$ has a barrier which prevents the reaction from being observed at room temperature. The mechanisms for dehydrogenation are distinctly different for each metal. For $Co^+$, the initial C−H insertion to form $Co(H)(C_2H_5)^+$ is rate limiting. This is followed by a multi-center elimination of $H_2$. For $Rh^+$, the concerted insertion into two C−H bonds to form $Rh(H)_2(C_2H_4)^+$ is seen without the intermediacy of $Rh(H)(C_2H_5)^+$. Reductive elimination of $H_2$ follows. For $Ir^+$, a number of reaction pathways are viable with the most favorable being a stepwise oxidative addition/$\beta$-H shift mechanism. Much of the difference in the chemistry of these metals stems from two principal factors: the atomic state splittings and the orbital sizes. For $Co^+$ and $Ir^+$, both the $s^1d^7$ and $d^8$ valence electron configurations are accessible, providing the flexibility needed to adapt to the changing ligation of the reaction profile. For $Rh^+$, the $s^1d^7$ state is high in energy, limiting the efficiency of this metal in these reactions. In addition, the $s$ and $d$ orbitals have dramatically different sizes for $Co^+$, which diminishes the effectiveness of $sd$ hybridization and leads to weaker bonds, particularly in highly ligated complexes. The $s$ and $d$ orbitals of $Rh^+$ and $Ir^+$ are more similar in size, providing strong $sd$ hybrid bonds. These two factors compromise the reactivity of $Co^+$ and $Rh^+$, leaving only $Ir^+$ near the ideal.

# Table of Contents

Chapter I

# Introduction

# Chapter I

# Introduction

## 1.1 Chemistry in the gas phase

The reactions of bare transition metal ions with organic molecules in the gas phase offer a unique perspective on the chemistry of many important catalytic processes. Unencumbered by stabilizing ligands or surface support, the chemistry of these ions provides a glimpse into the intrinsic features of metal-ligand bonding and organometallic reaction mechanisms. As one might expect, these features vary significantly from metal to metal and it has been the aim of hundreds of experimental and theoretical papers in the last 15 years to characterize trends among the rows and columns of the transition series.[1,2] While perhaps somewhat esoteric, this field, as it continues to evolve, serves to remove much of the mystery surrounding the chemistry of transition metal containing systems. In effect, with respect to condensed phase organometallic catalysts, the study of the chemistry of atomic transition metal ions in the gas phase is like taking a look under the hood of a car to see how the engine runs.

Of particular concern has been the reactions of transition metal cations with small alkanes. Fueled by the petroleum industry, there is a pervasive interest among those working in the field of catalysis as a whole in the chemistry of alkane C–H and C–C bond activation.[3–5] Methane, for instance, is the most abundant natural gas and has the potential for solving the world's energy needs well into the next century, yet methane deposits go largely untapped because of the difficulties associated with transportation. The search for a catalyst capable of efficiently converting methane to the more portable methanol is of top priority

for many oil companies and, indeed, many nations. The activation of C−C bonds is also of interest to the petroleum industry since this opens up the possibility of skeletal rearrangements and the conversion of linear alkanes to more useful branched alkanes. While chemists have been getting closer to the development of efficient catalysts for reactions of this nature, the chemistry of alkane C−H and C−C bond activation remains quite a challenge.

Studies of the reactions of alkanes with bare transition metal ions in the gas phase have demonstrated a high level of activity for C−H and C−C bond cleavage processes. Dehydrogenation and demethanation of alkanes, reactions (1) and (2) for instance,

$$M^+ + C_3H_8 \longrightarrow M(C_3H_6)^+ + H_2 \qquad (1)$$

$$\longrightarrow M(C_2H_4)^+ + CH_4, \qquad (2)$$

are two of the most common exothermic processes which are observed. Much of this chemistry is covered in an excellent review by Eller and Schwartz[1] and it is clear from the body of work described therein that the chemistry of these interactions is quite diverse. There appears to be no shortage of problems to study. However, there are many limitations of experiment which preclude a thorough understanding of the nature of the chemistry. By and large, the nature of the products is explicity limited to a knowledge of the ion masses and the nature of the intermediates is only inferred through careful reasoning. For a number of systems of interest, it has reached the point where theory now offers more valuable information than experiment and advances in just the last decade have provided the tools to make such theoretical studies of these difficult problems quantitative yet tractable.

In this work, we have chosen to take a comparitive look at the chemistry

of a particular column in the periodic table using methods of *ab initio* quantum chemistry. We wish to define the chemistry of $Co^+$, $Rh^+$, and $Ir^+$ in their interactions with $H_2$, $CH_4$, and $C_2H_6$. While limited in scope, a number of general principles can be made which can easily be applied to a wide variety of transition metal-alkane reactions. By way of introduction, we outline here the experimental approaches to this chemistry and provide a flavor of the types of reactions which have been observed.

## 1.2 Experimental methods

Reactions in the gas phase between ions and neutrals can be carried out under a variety of conditions. At low pressures, single collision conditions exist, and with no third body to remove the excess energy, the ion and neutral adduct must dissociate to either the reactants ($M^+ + AB$) or ion and neutral products ($MA^+ + B$).

$$M^+ + AB \longleftrightarrow M(AB)^+ \longrightarrow MA^+ + B \tag{3}$$

The products can result from just a simple bond cleavage or from a more complicated reaction sequence, but only under multi-collision conditions can the adduct [$M(AB)^+$] be thermally stabilized and be observed as a product.

The two key methods used in studying ion-molecule reactions under single collision conditions are Fourier-Transform Ion Cyclotron Resonance (FTICR) spectrometry[6] and guided-ion beam techniques.[7] The basic chemistry which can be observed with these techniques is described here. Additional methods to study these reactions under high pressure conditions[8] or to measure product kinetic energy release distributions (KERD)[9] are described elsewhere.

### 1.2.1 Fourier-Transform Ion Cyclotron Resonance

The practical advantage in studying the chemistry of metal ions rather than metal neutrals is the availability of mass spectrometry as a means of characterizing the ionic species. An FTICR spectrometer,[6] in addition to being highly sensitive, has the advantage of being able to trap ions for an extended period of time. This allows one to study the evolution of a reaction over time, affording the accumulation of information on the kinetics.

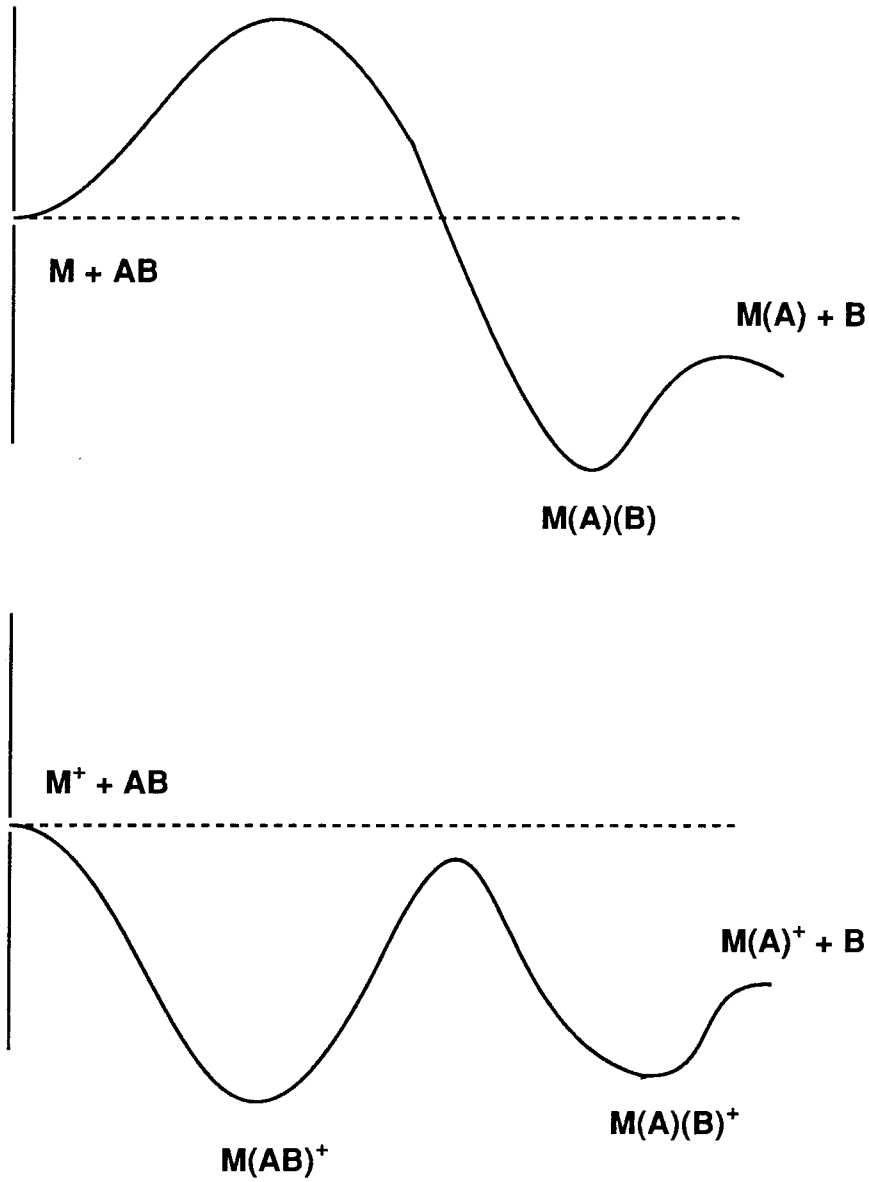


**Figure 1.** One difference in the reactivity of ionic metal atoms vs. neutral metal atoms is that the initial electrostatic attraction between the ionic metal ($M^+$) and the target molecule (AB) lowers the barrier to reaction with respect to the reactants. The neutral metal atoms (M) have no such attractive interaction.

FTICR is used to study *exothermic* reactions at room temperature. As a constraint, there must be no barriers along the potential energy surface in excess of the reactant energy in order for a reaction to occur. Efficiencies of these gas phase reactions, as measured against the Langevin-Gioumousis-Stevenson collision rate limit,[10] are then generally determined by how far *below* the reactant energy the rate limiting step lies. This point illustrates another advantage in studying the chemistry of ions over neutrals, as shown in Figure 1. Ions lead to an initial attractive electrostatic interaction with the target molecule which can be viewed as an energy source to drive the reaction. (The nature of such interactions will be described in detail in Chapters IV and V.) No such attraction exists for the neutrals and consequently barriers can be well above the limits of accessibility.

FTICR can also be used to provide some information on metal-ligand bond energies. For instance, the reaction,

$$Ir^+ + CH_4 \longrightarrow IrCH_2^+ + H_2, \tag{4}$$

has been observed to occur under ICR conditions.[11] Since the endothermicity of the reaction,

$$CH_4 \longrightarrow CH_2 + H_2 \tag{5}$$

is 111 kcal/mol,[12] the $Ir^+{=}CH_2$ bond strength must be $\geq$111 kcal/mol in order for the methane dehydrogenation reaction to be observed. In many cases, a clever comparison between various reactions can lead to lower and upper bounds on these metal-ligand bond strengths.

### 1.2.2 Guided-Ion Beams

With an ion beam apparatus,[7] it is possible to study both exothermic and endothermic reactions. By accelerating reactant ions to a well defined energy, upon collision with the neutral species, the extra translational energy is used to drive the reaction. As implemented by Armentrout,[13] the use of an octopole ion beam guide allows for the control of ion energy from as low as 0.1 eV to typically 10's of eVs. An ion beam guide also improves product collection such that quantitative results may be had. By modeling the threshold behavior for a given reaction to occur as a function of the ion kinetic energy, an accurate evaluation of the endothermicity or limiting barrier height can be made. For a reaction such as (6),

$$Fe^+ + H_2 \longrightarrow FeH^+ + H, \tag{6}$$

knowledge of the endothermicity allows for the determination of the $Fe^+-H$ bond energy, since the $H_2$ bond energy is known.[14] Such techniques have been used to obtain the $M^+-H$ and $M^+-CH_3$ bond energies for most of the first and second row transition metals.[15] The nature of these bonds will be discussed in Chapter III.

There are numerous variations to ion beam experiments. Most notably Collision Induced Dissociation (CID)[16] or Threshold Collisional Activation (TCA)[17] can lead to successive ligand binding energies or information on fragmentation processes. This is done by collision of a stabilized adduct ion or organometallic frament with an inert gas. Such techniques have been used to measure the successive $Fe(CH_4)_x^+$ bond energies,[18] for example (7),

$$Fe(CH_4)_2^+ \longrightarrow Fe(CH_4)^+ + CH_4. \tag{7}$$

These ion-alkane species will be described in Chapter V.

### 1.3 Basic reactions

The most common reactions which have been observed between transition metal ions and $H_2$, $CH_4$, and $C_2H_6$, include the following:

$$M^+ + H_2 \longrightarrow MH^+ + H \tag{8}$$

$$M^+ + CH_4 \longrightarrow MH^+ + CH_3 \tag{9}$$

$$\longrightarrow MCH_3^+ + H \tag{10}$$

$$\longrightarrow MCH_2^+ + H_2 \tag{11}$$

$$M^+ + C_2H_6 \longrightarrow MH^+ + C_2H_5 \tag{12}$$

$$\longrightarrow MCH_3^+ + CH_3 \tag{13}$$

$$\longrightarrow MCH_2^+ + CH_4 \tag{14}$$

$$\longrightarrow MC_2H_4^+ + H_2 \tag{15}$$

$$\longrightarrow MC_2H_2^+ + 2H_2 \tag{16}$$

$$\longrightarrow MH_2^+ + C_2H_4 \tag{17}$$

Of these reactions, only dehydrogenation (11, 15, and 16) has been observed to be exothermic for any metal.[1,2] The remaining reactions have all been endothermic for the metals studied and are not observed under ICR conditions.

Dehydrogenation of methane has only been observed to be exothermic for five metals of the third row ($Ta^+$, $W^+$, $Os^+$, $Ir^+$, and $Pt^+$).[11] (The second row metal, $Zr^+$, has also been observed to dehydrogenate methane, but due to the reported inefficiency of the reaction, 1%, it is suspected that an excited state of the metal was involved.)[19] First row metals (with the exception of $Mn^+$) have been observed to form stable adducts with methane under high pressure conditions.[8] Ion beam studies of the reactions of $Fe^+$ with methane indicate

the dominant pathways at higher energies are loss of hydrogen (9) and methyl radical (10) rather than loss of dihydrogen (11).[20]

The situation with ethane becomes a bit more interesting. Most of the second row metals[21] (and the first row metals, $Sc^+$ and $Ti^+$)[8,22] have been observed to exothermically dehydrogenate ethane (15). The third row metal, $Os^+$, has also been observed to doubly dehydrogenate ethane (16) to a large extent.[23] Still other metals, $Co^+$ and $Ni^+$, have been found *not* to react with ethane under ICR conditions, despite the fact that the dehydrogenation reaction is exothermic.[7,8,24] This indicates the presence of a barrier on the potential energy surface in excess of the reactant energy. The size of the barrier for $Co^+$ could not be determined quantitatively by ion beam studies due to competition from endothermic reactions, but the barrier is apparantly less than 1 eV. It should be noted that much of the third row metals have not yet been studied. Based on the observed chemistry with methane, most of these metals should also be reactive toward ethane.

As the alkanes become larger, more metals react with them, the reaction efficiencies increase, and more reaction channels are observed to be exothermic. Demethanation as well as dehydrogenation are observed in the reactions of $Fe^+$, $Co^+$, and $Ni^+$ with propane, for instance.[7,8,25] In contrast, for $Ru^+$, $Rh^+$, and $Pd^+$, only dehydrogenation is observed,[21] and $Os^+$ shows an unusual combined dehydrogenation and demethanation.[23]

The large differences in the chemistry of the transition metals are as yet not well understood.

## 1.4 Reaction mechamisms

With a few notable exceptions, the proposal of mechanisms operating in the dehydrogenation and dementhanation of alkanes has rested largely on isotopic labeling studies and the characterization of products. From this information it can be seen that the mechanisms operating in these reactions vary from metal to metal. For instance, dehydrogenation of *n*-butane occurs via a 1,3-mechanism for $Sc^+$,[26] a 1,4-mechanism for $Co^+$ and $Ni^+$,[25] and a 1,2-mechanism for $Ru^+$ and $Rh^+$.[21] The proposed reaction sequences for these processes and others generally involve C−H or C−C oxidative addition followed by a hydrogen or alkyl shift and reductive elimination of product. These mechanisms are outlined in Scheme 1. In most cases, there are a number of possible reaction pathways which can explain the observed products, but more detail on the nature of these potential energy surfaces has been difficult to come by.

The most insightful studies to date on the mechanisms operating in these gas phase reactions have been done for the dehydrogenation and demethanation of propane by $Co^+$ and more recently, $Fe^+$ and $Ni^+$.[27,28] Through a combination of isotopic labeling, threshold studies, kinetic energy release studies, and phase space modeling, van Koppen *et al.* have convincingly found the rate determining step for *both* the demethanation and dehydrogenation reaction pathways to be the initial C−H insertion step for all three of these metals. Thier suggested mechanisms for these processes are detailed in Scheme 2.

The basic mechanism involves an initial complexation to the propane followed by either primary or secondary C−H insertion. Insertion into the *secondary* C−H bond can lead only to $H_2$ loss, proposed to occur via a multi-center transition state. Insertion into the *primary* C−H bond can lead to either

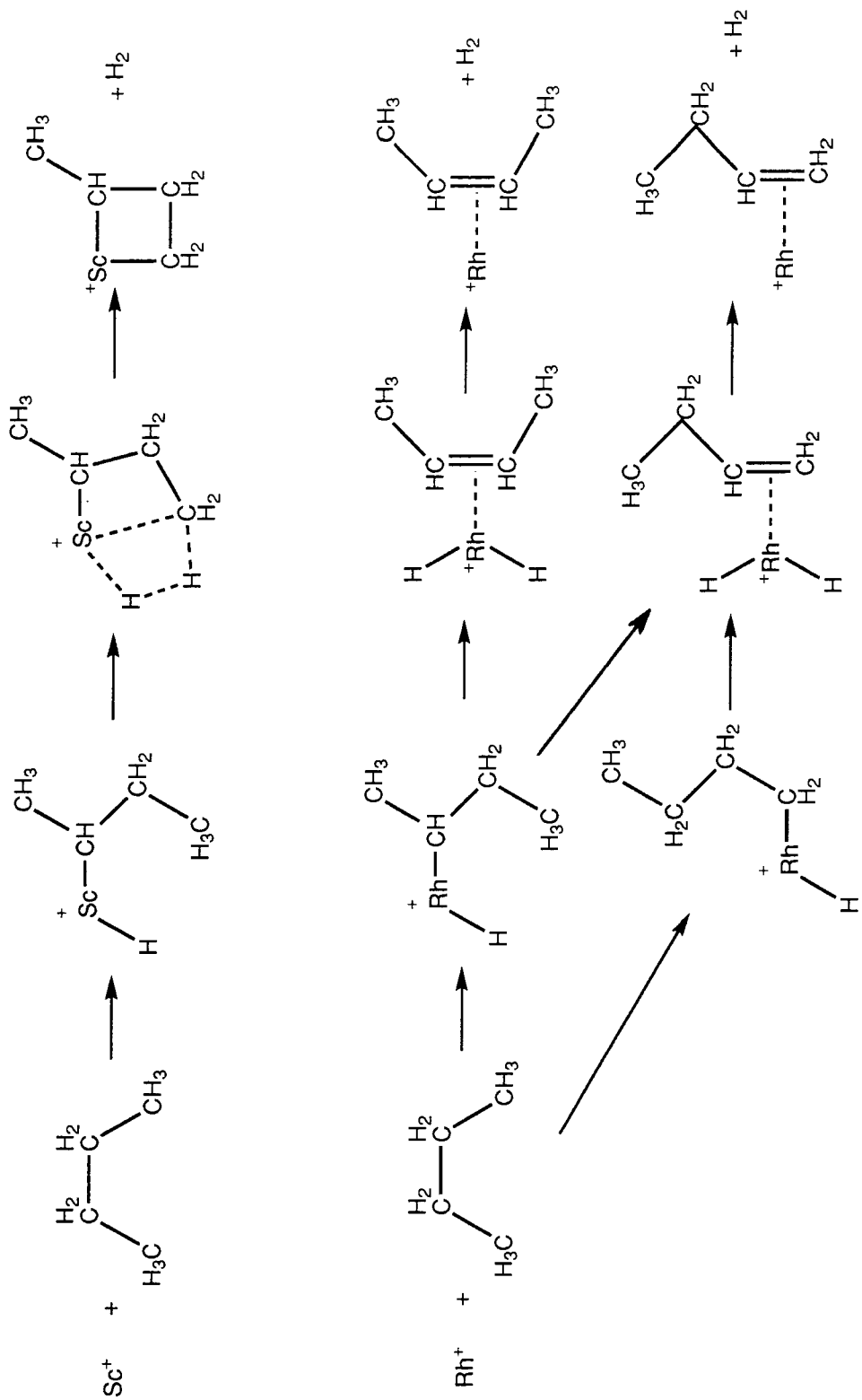
Sc+
Rh+
+ H2

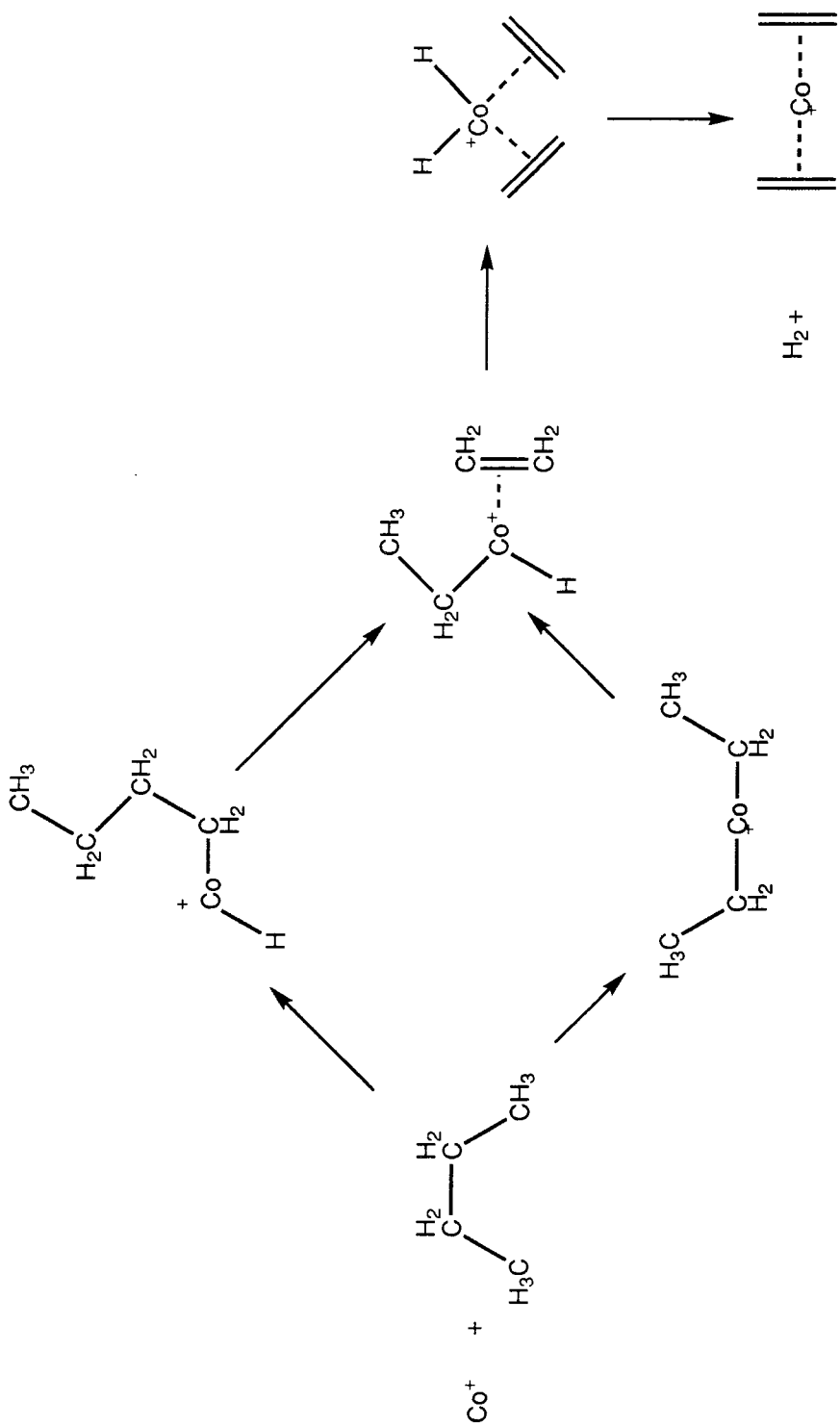

**Scheme 1**

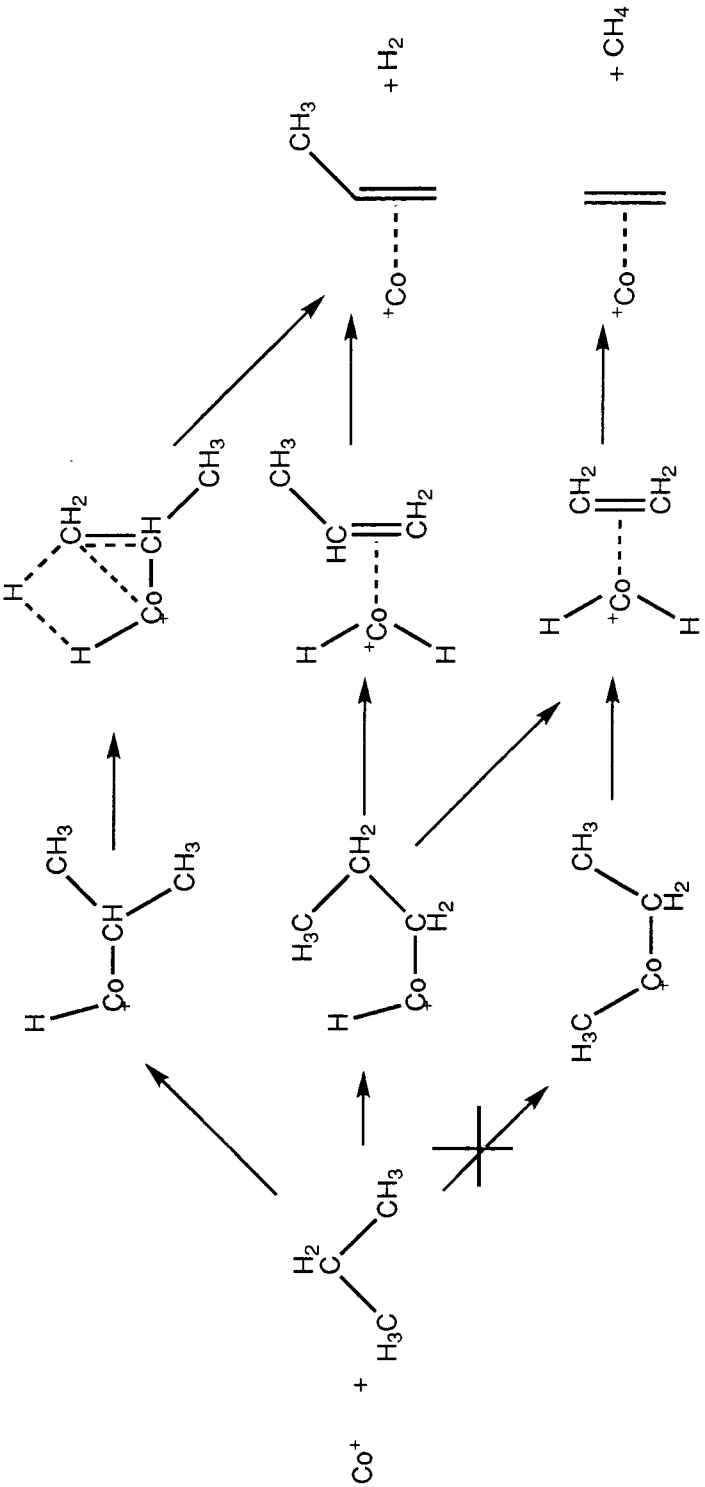

**Scheme 2**

$H_2$ loss, by $\beta$-H shift to form the $M(H)_2(C_3H_6)^+$ intermediate, or $CH_4$ loss, by $\beta$-$CH_3$ shift to form the $M(H)(CH_3)(C_2H_4)^+$ intermediate. (Note, the authors question the intermediacy of the hydrido methyl ethylene complex.) Moreover, at higher ion kinetic energies, increased demethanation is seen relative to dehydrogenation, suggesting a new reaction channel has become accessible. This probably corresponds to initial C−C insertion followed by $\beta$-H shift.

The barrier for initial primary C−H insertion was determined by phase space theory to lie only 2.5±0.7 kcal/mol below the threshold energy in the case of $Co^+$. This tight transition state is consistent with the low, 13%, reaction efficiency. In the reaction with ethane, the barrier is expected to be above the threshold energy, thus barring the exothermic dehydrogenation from occuring. We should also note that in a study by Schultz and Armentrout,[29] the barrier for initial C−C insertion was found to be 8 kcal/mol higher than the barrier for initial C−H insertion for $Fe^+$ reacting with propane.

In sum, there is a little information about many reactions and a lot of information about a few reactions. The broader question of what intrinsic differences between the metals lead to their varying reactivity remains unsettled.

## 1.5 Overview of research

In order to gain a better understanding of the nature of the processes just described, we have chosen to do a theoretical study of the chemistry of $Co^+$, $Rh^+$, and $Ir^+$ with $H_2$, $CH_4$, and $C_2H_6$. It is hoped that a number of general principles can be developed which will explain the differences in reactivity for these and other metals. It is also hoped that insight into the chemistry of larger alkanes might be had.

$Ir^+$ is far and away the most reactive metal toward $CH_4$.[11] It leads to dehydrogenation with an efficiency of 70%. The next best ion, $Pt^+$, has an efficiency of only 39%. Much of the aim of this work then is to understand what factors contribute to the high reactivity of $Ir^+$, by means of contrast to $Co^+$ and $Rh^+$. If these factors are correctly understood, it should be clear why additional metals are less reactive.

For $Co^+$ and $Rh^+$, the chemistry with ethane is perhaps more interesting. The fact that $Rh^+$ leads to dehydrogenation of ethane[21] while $Co^+$ does not[7,8] (despite the purported exothermicity of the reaction) may be the key to understanding much of the chemistry of these metals. For instance, if properly analyzed, it may be apparant why $Rh^+$ leads exclusively to 1,2-dehydrogenation of propane while $Co^+$ leads to both dehydrogenation and demethanation.

This work is presented in eight chapters. After a description of the methods used and other relevant computational details (Chapter II), the next four chapters will lay the foundation for understanding the chemistry of methane dehydrogenation and ethane dehdyrogenation detailed in Chapters VII and VIII.

This is of course a doctoral thesis and, as such, is very detailed. I hope that the broader issues aren't obscured by the minutiae, but it should be recognized

that this thesis has two purposes. The first is to answer the questions at hand and teach some chemistry. The second is to communicate how I think about chemistry. Due to the nature of the problem, this is really chemistry from the bottom up.

In particular, it is hoped that thinking about gas phase transition metal chemistry in the manner presented will be successfully applied to thinking about the chemistry of solution phase species. This is only touched upon here, but the future success of the field demands that such connections with the chemistry in the condensed phase be made.

## References


(1) Eller, K.; Schwartz, H. *Chem. Rev.* **1991**, *91*, 1121.

(2) Armentrout, P.B.; Beauchamp, J.L. *Acc. Chem. Res.* **1989**, *22*, 319.

(3) Satterfield, C.N. *Heterogeneous Catalysis in Industrial Practice, Ed. 2*; McGraw-Hill: New York, 1991.

(4) Shilov, A.E. *Activation of Saturated Hydrocarbons by Transition Metal Complexes*; Reidel: Dordrecht, 1984.

(5) Crabtree, R.H. *Chem. Rev.* **1985**, *85*, 245.

(6) (a) Beauchamp, J.L. *Ann. Rev. Phys. Chem.* **1971**, *22*, 527. (b) Gross, M.L.; Rempel, D.L. *Science* **1984**, *226*, 261. (c) Marshall, A.G. *Acc. Chem. Res.* **1985**, *18*, 316.

(7) Armentrout, P.B.; Beauchamp, J.L. *J. Chem. Phys.* **1981**, *74*, 2819.

(8) Tonkyn, R.; Ronan, M.; Weisshaar, J.C. *J. Phys. Chem.* **1988**, *92*, 92.

(9) Hanratty, M.A.; Beauchamp, J.L.; Illies, A.J.; van Koppen, P.; Bowers, M.T. *J. Am. Chem. Soc.* **1988**, *110*, 1.

(10) Gioumousis, G.; Stevenson, D.P. *J. Chem. Phys.* **1958**, *29*, 294.

(11) Irikura, K.K.; Beauchamp, J.L. *J. Phys. Chem.* **1991**, *95*, 8344.

(12) Bartmess, J.E.; Liebman, J.F.; Holmes, J.L.; Levin, R.D.; Mallard, W.G. *J. Phys. Chem. Ref. Data, Suppl.* **1988**, *17*, no.1.

(13) Ervin, K.M.; Armentrout, P.B. *J. Chem. Phys.* **1985**, *83*, 166.

(14) Elkind, J.L.; Armentrout, P.B. *J. Phys. Chem.* **1986**, *90*, 5736.

(15) Armentrout, P.B.; Georgiadis, R. *Polyhedron* **1988**, *7*, 1573.

(16) Schultz, R.H.; Crellin, K.C.; Armentrout, P.B. *J. Am. Chem. Soc.* **1991**, *113*, 8690.

(17) Schultz, R.H.; Armentrout, P.B. *J. Phys. Chem.* **1992**, *96*, 1662.

(18) Schultz, R.H.; Armentrout, P.B. *J. Phys. Chem.* **1993**, *97*, 596.

(19) Ranasinghe, Y.A.; MacMahon, T.J.; Freiser, B.S. *J. Phys. Chem.* **1991**, *95*, 7721.

(20) Schultz, R.H.; Elkind, J.L.; Armentrout, P.B. *J. Am. Chem. Soc.* **1988**, *110*, 411.

(21) Tolbert, M.A.; Mandich, M.L.; Halle, L.F.; Beauchamp, J.L. *J. Am. Chem. Soc.* **1986**, *108*, 5675.

(22) Sunderlin, L.S.; Armentrout, P.B. *Int. J. Mass Spectr.* **1989**, *94*, 149.

(23) Irikura, K.K.; Beauchamp, J.L. *J. Am. Chem. Soc.* **1989**, *111*, 75.

(24) Georgiadis, R.; Fisher, E.R.; Armentrout, P.B. *J. Am. Chem. Soc.* **1989**, *111*, 4251.

(25) Jacobson, D.B.; Freiser, B.S. *J. Am. Chem. Soc.* **1983**, *105*, 5197.

(26) Tolbert, M.A.; Beachamp, J.L. *J. Am. Chem. Soc.* **1984**, *106*, 8117.

(27) van Koppen, P.A.M.; Brodbelt-Lustig, J.; Bowers, M.T.; Dearden, D.V.; Beauchamp, J.L.; Fisher, E.R.; Armentrout, P.B. *J. Am. Chem. Soc.* **1991**, *113*, 2359.

(28) van Koppen, P.A.M.; Bowers, M.T.; Fisher, E.R.; Armentrout, P.B. *J. Am. Chem. Soc.*, submitted.

(29) Schultz, R.H.; Armentrout, P.B. *J. Am. Chem. Soc.* **1991**, *113*, 729.

# Chapter II

# Calculational Details

# Chapter II

## Calculational Details

### 2.1 Overview

We outline here the standard methods used in this work. Deviations from these methods or calculations of a highly specific nature will be detailed in the appendices to each chapter.

As in most of quantum chemistry, it is necessary to make approximations in order to handle a project of this scope. The trick then is to understand the nature of these approximations in order to obtain reliable results. To produce the large amount of data required for this study in a timetable acceptable to a graduate student (~3 years), the best approach is to find the cheapest method which gives consistently qualitatively correct results. By comparison to more accurate (*i.e.*, more expensive) methods for appropriate test cases, the shortcomings of the cheaper method may be easily quantified. For the most successful methods, these shortcomings will be systematic and appropriate corrections to the data will lead to the desired quantitative accuracy.

As a general rule, the procedures outlined here will underestimate the metal-ligand bond strength, some more so than others and some more systematically than others. This underestimation will vary depending on the nature of the bond. Contributions to this error come from the extent of electron correlation, the selection of the basis set, and the geometry optimization procedure. Details of these three aspects of the calculations follow.

## 2.2 Methods

As a general introduction to methods used by *ab initio* theorists, the book "Modern Quantum Chemistry: Introduction to Advanced Electronic Structure Theory" by Szabo and Ostlund[1] is recommended. We summarize here some of the features of the methods used in this work.

### 2.2.1 Hartree-Fock

The single determinant Hartree-Fock (HF) method is often the starting point for subsequent higher level calculations. It is based on simple Molecular Orbital (MO) theory. By itself, it can usually produce a qualitatively correct wavefunction (although not always), but it is significantly lacking in quantitative accuracy. This comes from the lack of static correlation and dynamic correlation. The absence of both of these works against the formation of bonds, and with transition metals in particular, bond energies can be underestimated by up to 80 kcal/mol in some cases.

All other methods presented here are designed to account for these deficiencies in the wavefunctions. GVB and CASSCF account for the static correlation–the basic correlation which takes care of near degeneracies and ensures a proper dissociation potential. The CI methods account for the dynamic correlation as well–the correlation which describes the instantaneous motions of electrons in response to other electrons.

### 2.2.2 Generalized Valence Bond and Complete Active Space Self-Consistent Field

The Generalized Valence Bond (GVB) method, and specifically the Perfect Pairing (GVB-PP) version of this method,[2] is the simplest way of accounting

for the deficiency in the static correlation of the HF wavefunction. In its most common use, molecular bonds are described by two configurations from the MO picture representing the occupation of the orthogonal bonding and antibonding orbitals as in (1)

$$\Psi_{GVB}(2/2) = (gg - \lambda uu)(\alpha\beta - \beta\alpha) \tag{1}$$

with the designation (2/2) meaning 2 electrons in 2 orbitals, $g$ and $u$ being the bonding and antibonding orbitals, and $\lambda$ being a variable coefficient. Effectively, the Valance Bond (VB) picture results from a transformation to nonorthogonal atomic orbitals as in (2)

$$\Psi_{GVB}(2/2) = (lr + rl)(\alpha\beta - \beta\alpha) \tag{2}$$

with $l$ being the bonding orbital on one fragment and $r$ being the bonding orbital on the other. It is computationally simpler to optimize the orthogonal orbitals rather than the nonorthogonal orbitals, but the result is the same either way.

The GVB wavefunction properly describes dissociation. Two fragments separated by a long distance can only be described by a wavefunction such as (2). Consequently, the GVB wavefunction is an improvement over the HF wavefunction, especially in the descriptions of bonds with small overlap between the atomic orbitals $r$ and $l$. Bond strengths for covalent transition metal bonds can typically be improved by 30 kcal/mol in using the GVB method instead of the HF method.

With GVB-PP, multiple bonds are described by restricting each correlated pair to the type of excitation in (1). Correlations between pairs are neglected. Thus, with two pairs, the wavefunction is as in (3)

$$\Psi_{GVB}(4/4) = (g_1g_1 - \lambda_1u_1u_1)(g_2g_2 - \lambda_2u_2u_2)(\alpha\beta - \beta\alpha)(\alpha\beta - \beta\alpha). \tag{3}$$

The Complete Active Space Self-Consistent Field (CASSCF) method[3] is similar to GVB (it is in fact also known as GVB-CI), but it removes all restrictions on the excitations between the electrons. That is, given a set of orbitals and a set of electrons, CASSCF will generate all possible configurations of those electrons within those orbitals. This more general method is useful for describing transition states where the bonding transforms from one GVB scheme to another.

### 2.2.3 Multi-Reference Configuration Interaction

The general term Multi-Reference Configuration Interaction (MRCI) refers to the multi-reference analogue of Hartree-Fock times Singles plus Doubles (HFSD). From a given set of reference configurations (perhaps the GVB or CASSCF wavefunctions), all single and double excitations of the valence electrons are made into all of the virtual orbitals. This expensive method introduces the dynamic correlation missing from the HF, GVB and CASSCF wavefunctions. This is absolutely critical in obtaining quantitative results, especially on transition metal systems.

The major shortcoming of this method, beyond its expense, is that it is not size consistent. While an improvement over the single-reference HFSD, it is the case that a single MRCI on fragments separated by a long distance is higher in energy than the sum of separate MRCI's on the individual fragments. This means that the quality of the wavefunction diminishes as the number of electrons being correlated increases. Thus a calculation on $CoCH_3^+$ would not be expected to be as accurate as a calculation on $CoH^+$ with this method.

The use of Davidson's correction[4] can remedy the problem to some extent by estimating the contribution from quadruple excitations. It has been our

experience that this MRCI+Q method is generally quantitative provided the reference space is adequate. We have used this method in our study of $M^+ + H_2$, M = Co, Rh, and Ir (Chapter IV).

### 2.2.4 Modified Coupled Pair Functional and Averaged Coupled Pair Functional

The Modified Coupled Pair Functional (MCPF)[5] and Averaged Coupled Pair Functional (ACPF)[6] methods represent size-consistent modifications of HFSD and MRCI, respectively. Size-consistency is achieved through partial normalization denominators in the energy functional. MCPF, in particular, leads to dramatically improved results over its HFSD counterpart at a comparable cost. The accuracy of this method is generally better than a typical MRCI and nearly as good as MRCI+Q. However, being a single-reference method, it is significantly cheaper than MRCI.

We find that the method does exceptionally well with electrostatic bonds, but in general, the strengths of covalent bonds will tend to be underestimated, particularly in the case of multiple covalent bonds. However, this underestimation appears to be by and large systematic. Because this method is cheap but acceptably accurate, and because the errors in the calculated energetics are systematic, we have opted to do the majority of calculations in this work with this method. When appropriate, an assessment is made as to the errors in the calculated energetics and our best estimates are reported.

The MCPF method is most reliable when the dominant configuration represents >90% of the wavefunction. This is true for most of the systems studied here. However, in cases of severe multi-configurational character, this single-reference based method is not sufficient. Altenatively, the multi-reference ACPF

method is one of the most accurate techniques available today. Unfortunately, it is just as expensive as MRCI, but often requires an expanded reference space. Too small a reference space can lead to instabilities in the wavefunction and unpredictable results. Because of its expense, we have used this method only for calculations on $MH^+$, M = Co, Rh, and Ir (Chapter III).

We should note that in all of the CI calcuations, only the valence electrons are correlated.

## 2.3 Basis sets and Effective Core Potentials

The choice of basis set can be just as important as the choice of correlation method. For the metals, the first consideration is the use of an Effective Core Potential (ECP). As the inner core electrons are relatively invariant to changes in the valence shell, including them in a potential can save considerable expense. Moreover, potentials are available which also include relativistic effects (RECP's). As the effects of relativity become particularly acute with the second and third row metals, this is an important consideration. Christiensen and Ermler and co-workers[7] have developed such RECP's for the entire transition series. They have published two sets, one which treats only the valence electrons explicitly and a second which treats both the valence and outer $s$ and $p$ core electrons explicitly. We have opted for the latter, as calculations with the potentials which do not treat the outer core electrons explicitly can often lead to poor results, particularly in correlated wavefunctions.

Valence triple-$\zeta$ basis sets have been optimized for these RECP's for the metals Co, Rh, and Ir by Ohanessian.[8] These basis sets were optimized in particular for the cations of the metals. We have also optimized two sets of 7 component $f$ functions for these metals. The first function was optimized at the HFSD level for the ground state of the cation. It is thus a correlation function. The second function is more diffuse and was optimized at the GVB level for the ground state of $MH^+$. It is thus a polarization function. These (4s4p3d2f) basis sets are given in Table I.

In Table II, we give calculated state splittings at the HF and MCPF levels for the $d^8$ $^3$F and $s^1d^7$ $^5$F states of $Co^+$, $Rh^+$, and $Ir^+$. The results at the MCPF level are in good agreement with experiment, reflecting both the quality

**Table I.** Basis sets for $Co^+$, $Rh^+$, and $Ir^+$ for use with the RECP's of reference 7.

| | $Co^+$ | | $Rh^+$ | | $Ir^+$ | |
|---|---|---|---|---|---|---|
| | Exponent | Coefficient | Exponent | Coefficient | Exponent | Coefficient |
| **S** | 56.12 | −0.013620 | 13.49 | −0.083935 | 12.140 | −0.181212 |
| | 18.92 | 0.064966 | 8.732 | 0.305789 | 9.5628 | 0.380150 |
| | 7.952 | −0.428446 | 4.410 | −0.819385 | 3.8891 | −0.973125 |
| | 2.198 | 0.666424 | 1.631 | 0.640072 | 1.6203 | 0.898216 |
| | 0.8467 | 1.000000 | 0.7330 | 1.000000 | 0.6827 | 1.000000 |
| | 0.1223 | 1.000000 | 0.1498 | 1.000000 | 0.1736 | 1.000000 |
| | 0.04417 | 1.000000 | 0.07413 | 1.000000 | 0.07754 | 1.000000 |
| **P** | 49.24 | −0.010215 | | | | |
| | 20.75 | −0.010807 | | | | |
| | 9.204 | −0.063664 | 31.14 | −0.004215 | 36.105 | −0.001966 |
| | 3.818 | 0.341285 | 4.788 | −0.147812 | 2.8117 | −1.582027 |
| | 1.588 | 0.559305 | 1.523 | 0.675414 | 2.4614 | 1.724003 |
| | 0.6247 | 1.000000 | 0.5796 | 1.000000 | 0.8901 | 1.000000 |
| | 0.2120 | 1.000000 | 0.2082 | 1.000000 | 0.3920 | 1.000000 |
| | 0.0651 | 1.000000 | 0.08190 | 1.000000 | 0.1447 | 1.000000 |
| **D** | 51.69 | 0.019049 | | | | |
| | 14.70 | 0.110260 | 18.92 | −0.009176 | 9.3910 | −0.012525 |
| | 4.851 | 0.317431 | 4.148 | 0.049155 | 1.3937 | 0.289711 |
| | 1.643 | 0.438641 | 1.610 | 0.398239 | 0.9188 | 0.204391 |
| | 0.5565 | 1.000000 | 0.6110 | 1.000000 | 0.4456 | 1.000000 |
| | 0.1881 | 1.000000 | 0.2124 | 1.000000 | 0.1649 | 1.000000 |
| **F** | 2.05 | 1.000000 | 1.05 | 1.000000 | 0.60 | 1.000000 |
| | 0.42 | 1.000000 | 0.30 | 1.000000 | 0.20 | 1.000000 |

**Table II.** Calculated splittings between the atomic $^3$F ($d^8$) and $^5$F ($s^1d^7$) states of $Co^+$, $Rh^+$, and $Ir^+$ at the HF and MCPF levels. Comparison is made to the experimental values[9] for $Co^+$ and $Rh^+$, averaging over $J$ levels. The $^3$F state is the ground state for $Co^+$ and $Rh^+$ and the $^5$F state is the ground State for $Ir^+$. Numbers in kcal/mol.

| | $Co^+$ | $Rh^+$ | $Ir^+$ |
|---|---|---|---|
| HF | −30.9 | +31.3 | −17.6 |
| MCPF | +4.0 | +45.2 | −6.6 |
| expt. | +9.9 | +49.1 | |

**Table III.** Comparison to experiment[10] of hydrocarbon thermochemistry calculated at the MCPF level.

| | $D_e$ | $D_0$ [a] | expt. | % error |
|---|---|---|---|---|
| $H_2 \rightarrow 2H$ | 107.2 | 100.9 | 104.4 | 3.2 |
| $CH_4 \rightarrow CH_3 + H$ | 108.6 | 99.0 | 104.7 | 5.4 |
| $CH_4 \rightarrow CH_2 + H_2$ | 113.8 | 102.7 | 111 | 7.5 |
| $C_2H_6 \rightarrow C_2H_5 + H$ | 105.3 | | 101.0[b] | |
| $C_2H_6 \rightarrow 2CH_3$ | 90.4 | 80.3 | 89.7 | 10.5 |
| $C_2H_6 \rightarrow C_2H_4 + H_2$ | 40.2 | 31.3 | 32.7 | 4.3 |
| $C_2H_6 \rightarrow CH_4 + CH_2$ | 94.0 | 85.7 | 96 | 10.7 |

[a] Zero-pont corrections were determined at the MP2 level.
[b] The stability of the $C_2H_5$ radical is taken from reference 11.

of the method and the basis set. It is generally the case, as indicated in the HF results, that calculations on transition metal state splittings favor the $s^1d^{n-1}$ states over the $d^n$ states. The tighter $d$ orbitals lead to more electron repulsion and thus having more electrons in this shell requires more correlation. Yet the error in the MCPF results is about 6 kcal/mol for $Co^+$ and 4 kcal/mol for $Rh^+$. The state splittings for $Ir^+$ have not been determined experimentally.[12]

For carbon and hydrogen, our standard basis set is of comparable triple-$\zeta$ plus double polarization quality. In all cases we use Huzinaga's $(11s7p/5s3p)$ basis set for carbon[13] and Dunning's $(6s/3s)$ basis set for hydrogen.[14] The two sets of $d$ polarization functions for carbon have exponents of $\alpha_d$=0.75 and $\alpha_d$=0.08. The more diffuse exponent was optimized for the polarizability of methane.[15] The polarization functions for hydrogen are from Dunning ($\alpha_p$=1.407 and $\alpha_p$=0.388).[16] In some cases, as noted, only one polarization function is used on the hydrogens ($\alpha_p$=1.00).

Using these TZ2P basis sets, comparison to experiment is made in Table III for MCPF determinations of the thermochemistry involved in the more pertinent reactions in this study. The comparison is reasonable, with bond energies generally being underestimated by 5−10%. Most of this error is from basis set incompleteness.

## 2.4 Geometry optimizations

Full geometry optimizations were generally performed at the HF level using analytic gradients. In some cases where the HF wavefunction leads to a poor description of the molecule, a geometry optimization was performed at the GVB level.

In most cases, these geometries are reasonably accurate, introducing errors of only a few kcals/mol (always underestimating well depths). Most of the error is in bond angles for covalently bonded ligands and bond lengths for electrostatically bonded ligands. In a number of cases where more accuracy is desired and easily obtained (Chapters IV and V, in particular), geometries were optimized in part at the CI level. This was done in a point by point manner by fitting a quadratic polynomial to three geometries near the minimum or by fitting a cubic polynomial to four geometries. For molecules with many degrees of freedom, such as the M(alkane)$^+$ complexes of Chapter V, this involved optimizing only the metal-ligand distance. Other coordinates were optimized subsequently at the HF level.

In some cases transition states are desired. We have found geometry optimizations at the lower levels of theory to be inadequate for this. While in absolute terms, the errors in these transition states may be comparable to the errors in the minima, there is a danger of underestimating the size of the barrier. This is appropriate if one is demonstrating that a barrier is prohibitively high for reaction to occur since the true barrier should be even higher, but in calculating barriers for viable pathways, we would rather err on the conservative side. In such cases, we have optimized a series of constrained geometries corresponding to the reaction pathway. Calculations at the higher level of theory using these

geometries then produce a barrier which should be an overestimate of the true barrier.

Calculations were performed using the following:

(1) GVB:[17] Used for HF, GVB and MCSCF wavefunctions and HF and GVB geometry optimizations.

(2) MOLECULE/SWEDEN:[18] Used for HF, CASSCF, MRCI, MCPF, and ACPF wavefunctions.

(3) Gaussian 92:[19] Used for HF wavefunctions and HF geometry optimizations.

Calculations were run on FPS 522, Alliant FX/80, HP 9000, and Cray Y-MP computers.

## 2.5 Error corrections

In a number of cases it is appropriate to epirically correct our calculated numbers to obtain the best approximation to the true numbers. This occurs in cases where the state splittings between the $s^1d^{n-1}$ and $d^n$ configurations are incorrect and there is substantial mixing of the two asymptotes in the wavefunction. To eliminate this error, an empirical correction can be made. This is done by first determining the extent of mixing between the two asymptotes. The most reliable guage of this is the $d$ shell populations. Generally these are intermediate to $n-1$ and $n$. The corrected energy of the complex should then be determined by a weighted average of the calculated energy with respect to the ground state of the ion and the calculated energy with respect to the excited state of the ion – the experimental promotion energy. This was done on most complexes of $Co^+$ and $Rh^+$ involving covalent bonds (Chapters III, VII, and VIII). This was also done for the molecular complexes of $Fe^+$ in Chapter V. Our corrected numbers are most consistent with experiment in the case of the $Fe^+$ complexes, supporting the legitimacy of the method.

More extensive corrections were made in Chapters VII and VIII in order to obtain our best estimate to these potential energy surfaces. While also reporting our calculated numbers (empirically corrected for the atomic state splittings as above), our estimated numbers include corrections for the error in the hydrocarbon energetics, the zero-point energy, and a general underestimation of the $M^+-R$ bond strengths. The following procedure was used:

(1) Calculate the energy of the complex, $D_e$, with respect to the metal + ligand fragments [*i.e.*, $Ir(H)_2(C_2H_4)^+$ with respect to $Ir^+ + 2H + C_2H_4$]. This leads to the total metal-ligand well depth.

(2) Estimate the zero-point correction for each metal-ligand bond from the $M^+-R$ stretching frequency scaled by 1.7 (empirically derived, this scale factor reasonably accounts for the contributions from the two additional modes per bond). This leads to the total metal-ligand bond energy, $D_0$.

(3) Scale the bond energy by 1.07. Since these bond energies are typically underestimated by 5–10%, a scale factor of 7% was deemed appropriate.

(4) If HF geometries are used, add 2 kcal/mol to the bond energy for each electrostatically bound ligand.

(5) Subtract the experimental $D_0$ for the appropriate hydrocarbon fragmentation reaction from the bond energy [*i.e.*, subtract $D_0$ for $C_2H_6 \rightarrow C_2H_4 + 2H$ from the bond energy of $Ir(H)_2(C_2H_4)^+$]. This leads to $D_0$ for the complex with respect to the metal ion + the free hydrocarbon.

While this process is involved, after a number of tries, we found this to be the most consistent means of correcting for the errors in the calculations.

## References


(1) Szabo, A.; Ostlund, N.S. *Modern Quantum Chemistry: Introduction to Advanced Electronic Structure Theory*; Macmillan: New York, 1989.

(2) Bobrowicz, F.W.; Goddard, W.A., III *Modern Theoretical Chemistry: Methods of Electronic Structure Theory*, Schaefer, H.F., III, Ed.; Plenum: New York, 1977.

(3) Siegbahn, P.E.M.; Almlöf, J.; Heiberg, A.; Roos, B. *J. Chem. Phys.* **1981**, *74*, 2384.

(4) Davidson, E.R. *The World of Quantum Chemistry*, Daudel, R.; Pullman, B., Eds.; Reidel: Dordrecht, 1974.

(5) (a) Chong, D.P.; Langhoff, S.R. *J. Chem. Phys.* **1986**, *84*, 5606. (b) See also Ahlrichs, R.; Scharf, P.; Ehrhardt, C. *J. Chem. Phys.* **1984**, *82*, 890.

(6) Gdanitz, R.J.; Ahlrichs, R. *Chem. Phys. Lett.* **1988**, *143*, 413.

(7) (a) Hurley, M.M.; Fenandez-Pacios, P.A.; Christiansen, P.A.; Ross, R.B.; Ermler, W.C. *J. Chem. Phys.* **1986**, *84*, 6840. (b) LaJohn, L.A.; Christiansen, P.A.; Ross, R.B.; Atashroo, T.; Ermler, W.C. *J. Chem. Phys.* **1987**, *87*, 2812. (c) Ross, R.B.; Powers, J.M.; Atashroo, T.; Ermler, W.C.; LaJohn, L.A.; Christiansen, P.A. *J. Chem. Phys.* **1990**, *93*, 6654.

(8) Perry, J.K.; Goddard, W.A., III; Ohanessian, G. *J. Chem. Phys.* **1992**, *97*, 7560.

(9) Moore, C.E. *Atomic Energy Levels*, NSRDS-NBS 35 (reprint of NBS circular 467); U.S. Government Printing Office: Washington, DC, 1971.

(10) Lias, S.G.; Barmess, J.E.; Liebman, J.F.; Holmes, J.L.; Levin, R.D.; Mallard, W.G. *J. Phys. Chem. Ref. Data, Suppl.* **1988**, *17*, no. 1.

(11) (a) Seakins, P.W.; Pilling, M.J.; Niiranen, J.T.; Gutman, D.; Krasnoperov, L.N. *J. Phys. Chem.* **1992**, *96*, 9847. (b) For a review see Berkowitz, J.; Ellison, G.B.; Gutman, D. *Ann. Rev. Phys. Chem.*, in press.

(12) (a) The splitting between the lowest $J$ levels of the two states is 6.5 kcal/mol, and can be found in van Kleef, T.A.M.; Metsch, B.C. *Physica* **1978**, *95C*, 251. (b) See also, Wyart, J.-F. *Opt. Pura Apl. (Spain)* **1977**, *10*, 177.

(13) Huzinaga, S.; Sakai, Y. *J. Chem. Phys.* **1969**, *50*, 1371.

(14) Dunning, T.H. *J. Chem. Phys.* **1971**, *55*, 716.

(15) Werner, H.J.; Meyer, W. *Mol. Phys.* **1976**, *31*, 855.

(16) Dunning, T.H. *J. Chem. Phys.* **1989**, *90*, 1007.

(17) GVB, a suite of electronic structure programs written at the California Institute of Technology under the supervision of Goddard, W.A., III.

(18) MOLECULE/SWEDEN, an electronic structure program system written by Almlöf, J.; Bauschlicher, C.W., Jr.; Blomberg, M.R.A.; Chong, C.P.; Heiberg, A.; Langhoff, S.R.; Malmqvist, P.-Å.; Rendell, A.P.; Roos, B.O.; Siegbahn, P.E.M.; Taylor, P.R.

(19) Gaussian 92, Revision A, Frisch, M.J.; Trucks, G.W.; Head-Gordon, M.; Gill, P.M.W.; Wong, M.W.; Foresman, J.B.; Johnson, B.G.; Schlegel, H.B.; Robb, M.A.; Replogle, E.S.; Gomperts, R.; Andres, J.L.; Raghavachari, K.; Binkley, J.S.; Gonzalez, C.; Martin, R.L.; Fox, D.J.; Defrees, D.J.; Baker, J.; Stewart, J.J.P.; Pople, J.A., Gaussian, Inc., Pittsburgh, PA, 1992.

Chapter III

# The Nature of the Metal-Alkyl and Metal-Hydride Bond

# Chapter III

## The Nature of the Metal-Alkyl and Metal-Hydride Bond

### 3.1 Introduction

In a thorough study of the mechanisms associated with alkane activation by transition metal ions, it is necessary to characterize a wide variety of metal-ligand bonds. These include metal-alkane, metal-hydride, metal-alkyl, metal-alkylidene, and metal-olefin bonds, and combinations thereof. We begin here with a study of the $M^+-H$, $M^+-CH_3$, and $M^+-C_2H_5$ bonds, for M = Co, Rh, and Ir. The strengths of these bonds and the nature of these bonds are directly relevant to the issue of C−H and C−C activation.

The largely covalent $M^+-H$ and $M^+-CH_3$ bonds have been well studied for the first and second row transition metals both theoretically[1−6] and experimentally,[7−10] and improvements in both *ab initio* and ion beam mass spectrometric techniques have led to a quantitative agreement between theory and experiment on the bond strengths associated with these species. The $M^+-C_2H_5$ bond has received only sporadic attention from experimentalists,[11] however, and the first comprehensive theoretical study of $M^+-CH_3$, $M^+-C_2H_5$, $M^+-C_3H_7$, and $M^+ - t\text{-}C_4H_9^+$ bond strengths was made by us only recently for M = Sc.[12] The chemistry of the third row metals has also received only scant attention from both theorists[1] and experimentalists,[13] yet the available data indicates that these metals (1) form stronger $M^+-H$ bonds and (2) are more chemically active in the gas phase.

Most of the concepts associated with the nature of the bonding in these $MR^+$ species have been well detailed in the literature. They will be reviewed

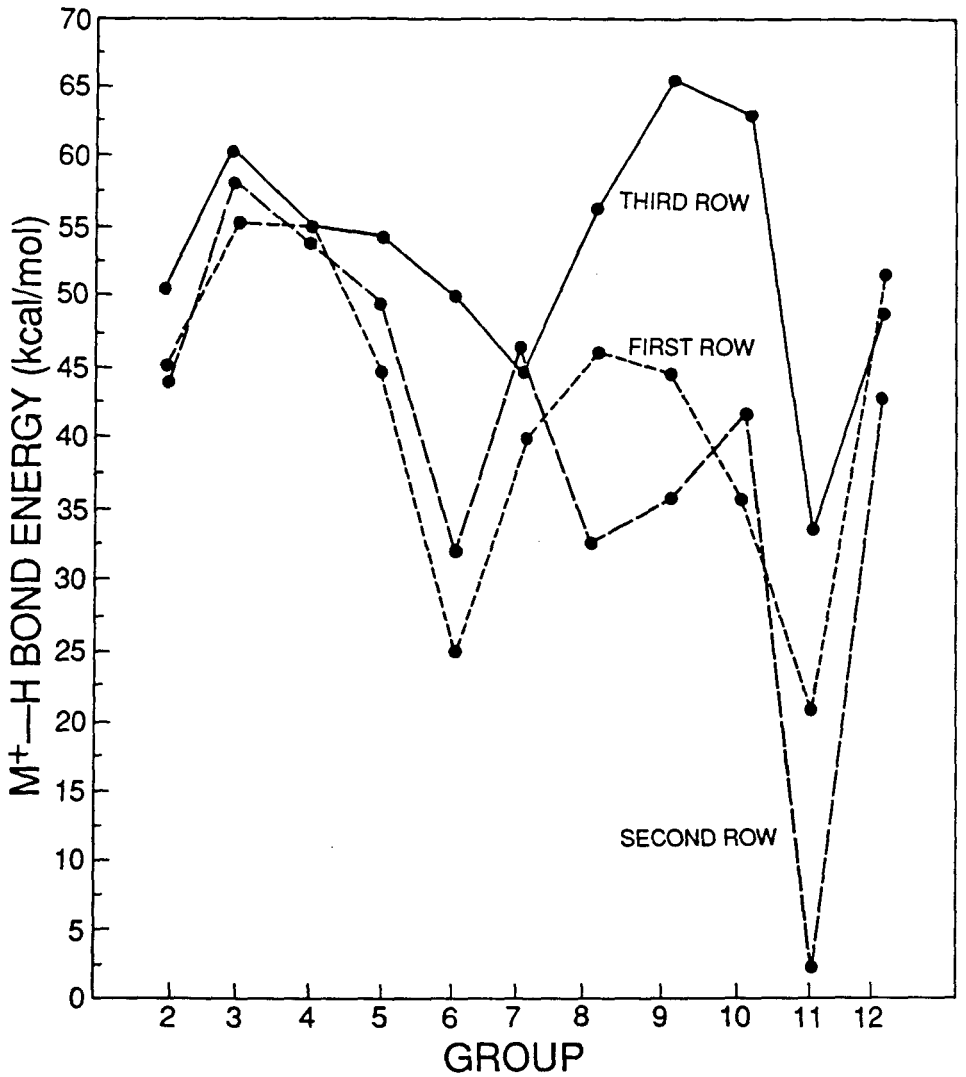


**Figure 1.** Trends in $M^+-H$ bond strengths for the entire transition metal series. From Ohanessian and Goddard.[1]

here breifly as they serve as a good introduction to the types of factors that should be considered in understanding the bonding of other ligands (alkanes, olefins, and alkylidenes) to transition metal ions. These concepts have already been quite successful in explaining the non-monotonic behavior of metal-ligand bond strengths across a given row of the transition series.[2] For instance, the trends in the $M^+-H$ bond energies are shown in Figure 1.[1] Consideration of exchange energy loss in particular explains why metals in the middle of each row generally have the weakest bonds. Further consideration of promotion energies and hybridization in the bonding orbitals leads to distinctions between each of the rows.

We interpret our results for $MH^+$, $MCH_3^+$, and $MC_2H_5^+$, M = Co, Rh, and Ir, in terms of these existing ideas. In a few instances, we point out a few subtleties in the bonding which haven't yet been addressed.

Importantly, we find that the most favorable situation is for the bonds to $Ir^+$ and this is clearly reflected in the thermochemistry. Early results on these energetics led Ohanessian and Goddard[14] to predict in advance of experiment a much higher level of alkane activation for the third row transition metals as compared to the first two rows. Irikura and Beauchamp[13] showed this to be the case with their study of methane dehydrogenation by third row transition metals.

### 3.2 Results

Using HF optimized geometries, we have performed ACPF calculations on the lowest lying doublet and quartet states of $MH^+$, M = Co, Rh, and Ir. We have also performed MCPF calculations on the ground states of $MCH_3^+$ and $MC_2H_5^+$, for M = Co, Rh, and Ir, as well as the excited states of these complexes for M = Co. Results are presented in Tables I and II and Figures 2–4. The ground states of all the $Co^+$ and $Ir^+$ complexes have quartet spin while the ground states of the $Rh^+$ complexes have doublet spin.

The use of the expensive ACPF method for the $MH^+$ species stems from the fact that the $^4\Phi$ and $^4\Sigma^-$ states of the $MH^+$ species exhibit significant multi-reference character. Use of the single-reference MCPF method for states such as these is risky. Pettersson *et al.*[3] used the MCPF method and a basis set comparable to, yet slightly larger than, ours in their study of the complete first and second row transition metal hydride positive ions. They obtained a binding energy for $CoH^+$ of $D_0$=42.5 kcal/mol which can be compared to our value of $D_0$=46.0 kcal/mol. The discrepancy in the numbers is perhaps small, but a more favorable comparison can be made between our value for the binding energy of $RhH^+$ ($D_0$=40.9 kcal/mol) and theirs ($D_0$=39.5 kcal/mol). The $^2\Delta$ ground state of $RhH^+$ is well described by a single configuration, as are the lowest lying states of the metal alkyls. This being the case, the more tractable MCPF method was used for the larger $MCH_3^+$ and $MC_2H_5^+$ calculations. In general, our results for the $MH^+$ and $MCH_3^+$ bond strengths compare well with previous theoretical results and with experiment (at least in the case of M = Co, see Table II). We expect the results for $MC_2H_5^+$ to have a comparable accuracy.

**Table I.** Calculated properties of $MH^+$, $MCH_3^+$ and $MC_2H_5^+$. The $d$ populations and charges on the metal are from a Mulliken population analysis.

| | $CoR^+$ | | | |
|---|---|---|---|---|
| | $CoH^+$ $^4\Phi$ | $CoH^+$ $^2\Delta$ | $CoCH_3^+$ $^4A_2$ | $CoCH_3^+$ $^2E$ |
| $D_e$ (kcal/mol)[a] | 48.7 | 29.8 | 47.5 | 21.3 |
| $r_e$ (Å) | 1.61 | 1.51 | 2.05 | 1.95 |
| $d_{pop}$ | 7.23 | 7.81 | 7.18 | 7.70 |
| $Q_{Co}$ | +0.92 | +0.85 | +0.66 | +0.71 |
| | | $CoC_2H_5^+$ $^4A''$ | $CoC_2H_5^+$ $^2A''$ | |
| $D_e$ (kcal/mol) | | 45.8 | 24.0 | |
| $r_e$ (Å) | | 2.09 | 1.96 | |
| $d_{pop}$ | | 7.17 | 7.72[b] | |
| $Q_{Co}$ | | +0.56 | +0.65[b] | |
| | $RhR^+$ | | | |
| | $RhH^+$ $^2\Delta$ | $RhH^+$ $^4\Phi$ | $RhCH_3^+$ $^2E$ | $RhC_2H_5^+$ $^2A''$ |
| $D_e$ (kcal/mol) | 43.9 | 29.7 | 38.9 | 46.2 |
| $r_e$ (Å) | 1.49 | 1.62 | 1.99 | 1.99 |
| $d_{pop}$ | 7.95 | 7.48 | 7.99 | 8.03 |
| $Q_{Rh}$ | +0.84 | +0.88 | +0.73 | +0.67 |
| | $IrR^+$ | | | |
| | $IrH^+$ $^4\Sigma^-$ | $IrH^+$ $^2\Delta$ | $IrCH_3^+$ $^4A_2$ | $IrC_2H_5^+$ $^4A''$ |
| $D_e$ (kcal/mol) | 74.9 | 59.6 | 70.3 | 70.2 |
| $r_e$ (Å) | 1.56 | 1.54 | 2.05 | 2.08 |
| $d_{pop}$ | 7.17 | 7.78 | 7.23 | 7.26 |
| $Q_{Ir}$ | +0.77 | +0.77 | +0.67 | +0.60 |

[a] In each case, the bond energies were adjusted to account for the error in the $^3F$-$^5F$ state splittings by using the $d$ populations as a guide to the extent of mixing of the $d^8$ and $s^1d^7$ configurations.

[b] We were unable to obtain the MCPF $d$ populations charges for this state so they were estimated based on the values for $^2E$ $CoCH_3^+$ and a comparison of the SCF properties for the two complexes.

**Table II.** Comparison of our calculated dissociation energies to previous theoretical results (Bauschlicher[2,6] and Ohanessian[1]) and to experiment (Armentrout[8]). All numbers are in kcal/mol and include the zero-point correction. The experimental numbers are adjusted to 0 K.

| | Present work[a] | Bauschlicher[b] | Ohanessian | Armentrout |
|---|---|---|---|---|
| $CoH^+$ | 46.4[a] | 42.5 (44.5) | 43.6 | 45.7±1.4 |
| $CoCH_3^+$ | 46.7 | 45.3 (48.3) | | 48±4 |
| $CoC_2H_5^+$ | 45.2 | | | |
| $RhH^+$ | 40.9 | 39.5 (41.5) | 34.8 | 35±3 (41±3)[c] |
| $RhCH_3^+$ | 38.1 | 34.1 (37.1) | | 46±5 |
| $RhC_2H_5^+$ | 45.6 | | | |
| $IrH^+$ | 71.5 | | 65.8 | |
| $IrCH_3^+$ | 69.4 | | | |
| $IrC_2H_5^+$ | 69.5 | | | |

[a] Zero-point corrections for $MH^+$ are taken from Ohanessian and Goddard.[1] Zero-point corrections for $CoCH_3^+$ and $RhCH_3^+$ are taken from Bauschlicher *et al.*[6] The zero-point correction was estimated for the remaining complexes based on these numbers.

[b] Number in parenthesis represents their "best estimate" to $D_0$.

[c] Number in parenthesis from Mandich, Halle, and Beauchamp.[10]

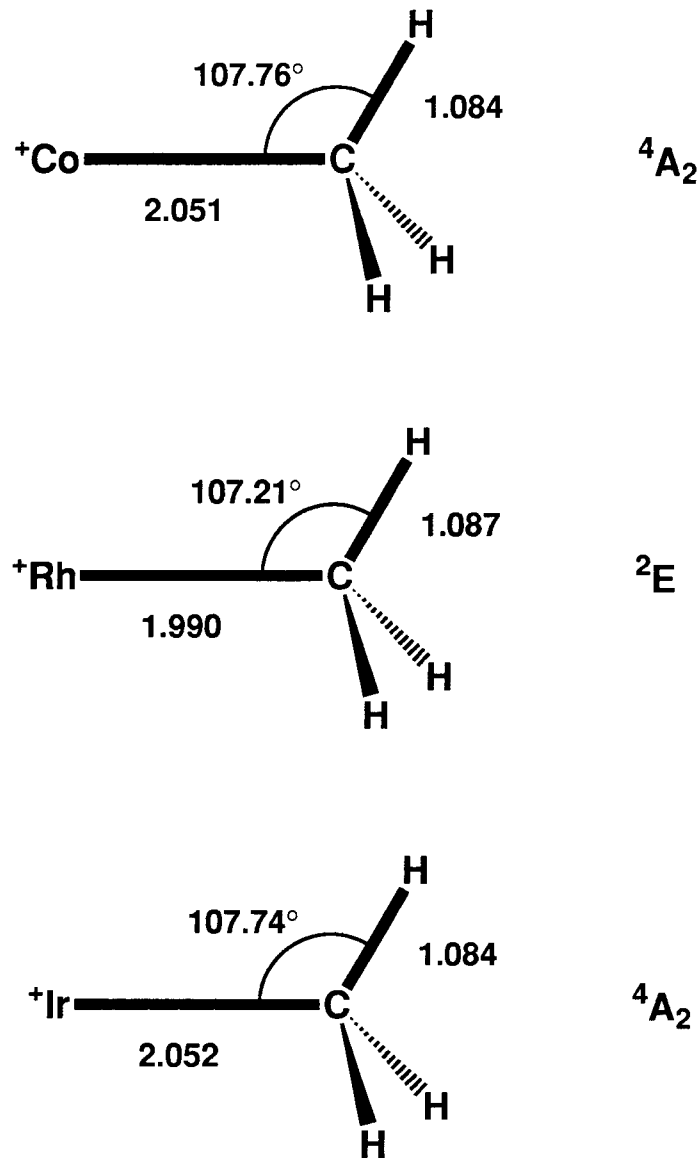


**Figure 2.** Geometries for the ground states of $MCH_3^+$, M = Co, Rh, and Ir.

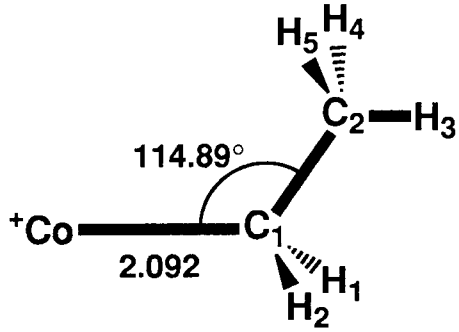


$C_s\ ^4A''\ CoC_2H_5^+$

| | | | |
|---|---|---|---|
| Co | 0.0000 | 0.0000 | 0.0000 |
| $C_1$ | 0.0000 | 0.0000 | 2.0919 |
| $C_2$ | 0.0000 | 1.3803 | 2.7324 |
| $H_1$ | 0.8831 | -0.5842 | 2.3303 |
| $H_2$ | -0.8831 | -0.5842 | 2.3303 |
| $H_3$ | 0.0000 | 1.2527 | 3.8131 |
| $H_4$ | 0.8813 | 1.9576 | 2.4751 |
| $H_5$ | -0.8813 | 1.9576 | 2.4751 |

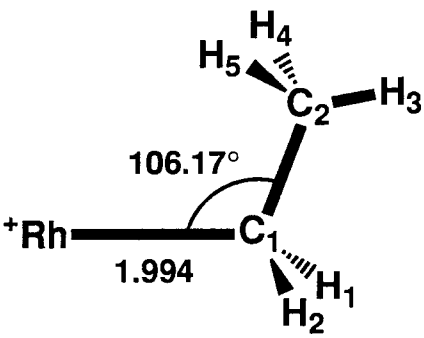


$C_s\ ^2A''\ RhC_2H_5^+$

| | | | |
|---|---|---|---|
| Rh | 0.0000 | 0.0000 | 0.0000 |
| $C_1$ | 0.0000 | 0.0000 | 1.9940 |
| $C_2$ | 0.0000 | 1.4456 | 2.4130 |
| $H_1$ | 0.8951 | -0.5482 | 2.2811 |
| $H_2$ | -0.8951 | -0.5482 | 2.2811 |
| $H_3$ | 0.0000 | 1.5066 | 3.5014 |
| $H_4$ | 0.8897 | 1.9711 | 2.0714 |
| $H_5$ | -0.8897 | 1.9711 | 2.0714 |

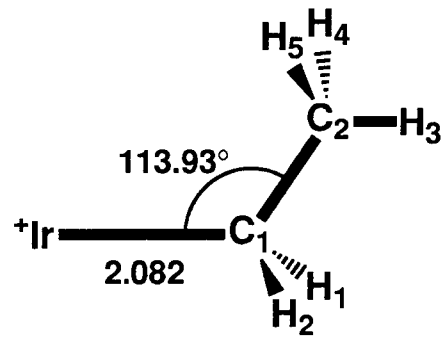


$C_s\ ^4A''\ IrC_2H_5^+$

| | | | |
|---|---|---|---|
| Ir | 0.0000 | 0.0000 | 0.0000 |
| $C_1$ | 0.0000 | 0.0000 | 2.0821 |
| $C_2$ | 0.0000 | 1.3878 | 2.6981 |
| $H_1$ | 0.8861 | -0.5773 | 2.3375 |
| $H_2$ | -0.8861 | -0.5773 | 2.3375 |
| $H_3$ | 0.0000 | 1.2704 | 3.7808 |
| $H_4$ | 0.8855 | 1.9584 | 2.4387 |
| $H_5$ | -0.8855 | 1.9584 | 2.4387 |

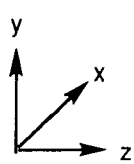


**Figure 3.** Geometries for ground states of $MC_2H_5^+$, for M = Co, Rh, and Ir. Cartesian coordiates are in Å.

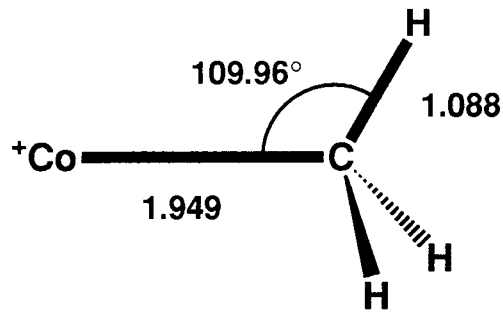


$^2E$

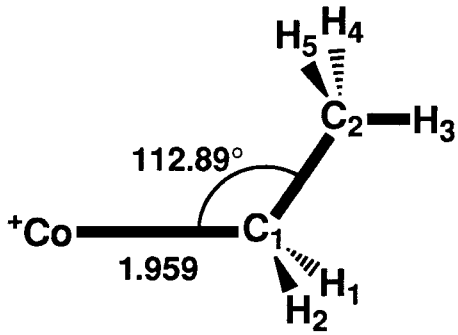


$C_s$ $^2A''$ $CoC_2H_5^+$

| | | | |
|---|---|---|---|
| Co | 0.0000 | 0.0000 | 0.0000 |
| $C_1$ | 0.0000 | 0.0000 | 1.9588 |
| $C_2$ | 0.0000 | 1.4108 | 2.5544 |
| $H_1$ | 0.8760 | -0.5628 | 2.2781 |
| $H_2$ | -0.8760 | -0.5628 | 2.2781 |
| $H_3$ | 0.0000 | 1.3542 | 3.6394 |
| $H_4$ | 0.8813 | 1.9782 | 2.2646 |
| $H_5$ | -0.8813 | 1.9782 | 2.2646 |

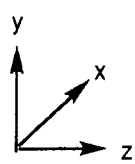


**Figure 4.** Geometries for the double excited states of $CoCH_3^+$ and $CoC_2H_5^+$. Cartesian coordiates are in Å.

### 3.3 Discussion

The first thing that should be noticed in this data is the significantly stronger bonds formed by $Ir^+$ as compared to $Co^+$ and $Rh^+$. The bond energies for $Co^+$ and $Rh^+$ are more or less comparable, but the bond energies for $Ir^+$ are on the order of 60% larger. As will be discussed, a number of disparate factors conspire to make $Ir^+$ ideal for forming covalent bonds.

The $M^+-C_2H_5$ results are also of interest since they have to date garnered little attention from either experiment or theory. While the $Rh^+-C_2H_5$ bond is 7.5 kcal/mol stronger than the $Rh^+-CH_3$ bond, the $M^+-CH_3$ and $M^+-C_2H_5$ bond strengths are comparable for M = Co and M = Ir. One obvious difference between the $Rh^+-C_2H_5$ bond and those of $Co^+$ and $Ir^+$ is the M−C−C angle, which is 7°−9° smaller for $Rh^+$ than for the other two metals. This suggests that a favorable interaction between the ion and the $\alpha$-methyl group may be responsible for the relatively strong $Rh^+-C_2H_5$ bond. Similar conclusions have been made to explain the 5.2 kcal/mol gain in stability for $ScC_3H_7^+$ as compared to $ScC_2H_5^+$.[12] In this case there is a clear coordination of the $\beta$-methyl group to the metal which increases the bond strength. Such interactions will be discussed in detail in Chapters IV and V.

Since the $M^+-H$ and $M^+-C$ bonds are similar in many ways, the remainder of this chapter will focus on the nature of the $M^+-H$ bond. When appropriate, unique features of the $M^+-C$ bonds will also be discussed. The purpose of this study is to separate extraneous influences on the $M^+-H$ and $M^+-C$ bonds from the intrinsic qualities of the bonds. These extraneous influences include promotion energies, exchange energy losses, and nonbonding interactions, factors which are easily modified by the presence of ligands on the metal.

### 3.3.1 Promotion energy

The difference in the spin of the ground state for the $Rh^+$ complexes (doublet) as compared to the $Co^+$ and $Ir^+$ complexes (quartet) is easily explained by consideration of the states used in forming the bonds. In the simplest model, the quartet state is derived from the $s^1d^7$ $^5$F state of the metal while the doublet state is derived from the $d^8$ $^3$F state of the metal. A covalent bond to the ligand is formed from the metal $s$ orbital in the quartet state (1)

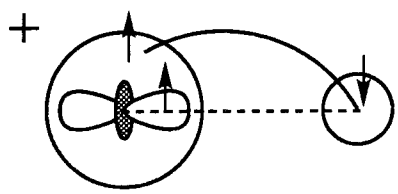

(1)

and from the metal $d_\sigma$ orbital in the doublet state (2).

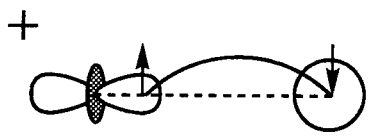

(2)

(For simplicity, only the valence $\sigma$ electrons are shown in these schemes.) Beyond the issue of whether or not the $s-$R bond is intrinsically stronger than the $d-$R bond, the accessibility of the $^3$F or $^5$F states can be a decisive factor in determining the ground state of the complex. For the $Co^+$ complexes, the ground states are all derived from the higher lying $^5$F state (9.9 kcal/mol above the $^3$F state) indicating that the $s$ bond is stronger than the $d$ bond. This is not too surprising given the difference in size of the $4s$ and $3d$ orbitals and the

**Table III.** Comparison of adiabatic and diabatic well depths for various $MR^+$ complexes, M = Co, Rh, and Ir, R = H, $CH_3$, $C_2H_5$.

| | Adiabatic $D_e$ | Diabatic $D_e$ |
|---|---|---|
| $CoH^+$ $^4\Phi$ | 48.7 | 58.6 |
| $RhH^+$ $^4\Phi$ | 29.7 | 78.8 |
| $IrH^+$ $^4\Sigma^-$ | 74.9 | 74.9 |
| $CoH^+$ $^2\Delta$ | 29.8 | 29.8 |
| $RhH^+$ $^2\Delta$ | 43.9 | 43.9 |
| $IrH^+$ $^2\Delta$ | 59.6 | 66.1 |
| $CoCH_3^+$ $^4A_2$ | 47.5 | 57.4 |
| $IrCH_3^+$ $^4A_2$ | 70.3 | 70.3 |
| $CoCH_3^+$ $^2E$ | 21.3 | 21.3 |
| $RhCH_3^+$ $^2E$ | 38.9 | 38.9 |
| $CoC_2H_5^+$ $^4A''$ | 45.8 | 55.7 |
| $IrC_2H_5^+$ $^4A''$ | 70.2 | 70.2 |
| $CoC_2H_5^+$ $^2A''$ | 24.0 | 24.0 |
| $RhC_2H_5^+$ $^2A''$ | 46.2 | 46.2 |

expected difference in the overlaps of the metal and ligand orbitals. The $Ir^+$ complexes are also all derived from the $^5F$ state. For this metal, the bonding state corresponds to the ground state of the metal. However, the $^3F-^5F$ promotion energy is 49.1 kcal/mol for $Rh^+$ and it is unlikely that the difference in the intrisic *s* and *d* bond strengths could be this large. Consequently, the ground states of the $Rh^+$ complexes are doublets derived from the $^3F$ state of the metal.

We have accounted for this promotion energy by considering the diabatic well depths of these complexes in Table III. These well depths reflect the strength of the bond with respect to the dominant bonding configuration on the metal.

With the exception noted below, it is apparant from this data that the trends in the bond strengths generally follows $Co^+ < Rh^+ < Ir^+$ in comparisons of similar states. Thus, it is the high $^3F$-$^5F$ promotion energy of $Rh^+$ which, in particular, leads to weaker bonds for this metal.

We should note that the diabatic bond strength for the $^4\Phi$ state of $RhH^+$ is artificially high. The wavefunction involves a significant contribution from the one-electron bonding configuration which can be described as the hydrogen electron high-spin coupled to the $d^8$ $^3F$ state of the metal (3).

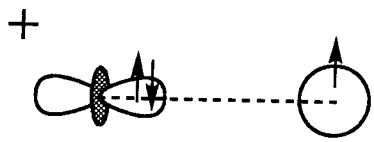

(3)

The strength of this interaction is derived from the ion-induced polarization of the charge on the H atom. The polarizability of the H atom is small (0.67 $Å^3$), but the short $Rh^+$–H bond distance (1.49 Å) leads to an interaction energy of ~23 kcal/mol. This type of ion-induced dipole interaction will be fully detailed in Chapters IV and V, but the magnitude of the interaction leads to a large weight for this bonding configuration in the quartet $RhH^+$ wavefunction. This is reflected in the *d* population of the metal of 7.48 electrons. Thus, the simple picture is invalid and the promotion energy is overestimated. Additional deviations from these simple pictures will be discussed in the next section.

### 3.3.2 S-D hybridization

A significant deviation from the simple bonding picture can be seen in the nature of the bonding orbitals which are depicted graphically in Figure 5 and quantitatively in Table IV. For the ground states of $MH^+$ and $MCH_3^+$, only the doublet $Rh^+$ complexes fit the simple *d* bond picture shown schematically in (2). On the other hand, the bonding in the $Co^+$ and $Ir^+$ complexes exhibit some important differences from the simple *s* bond picture shown schematically in (1).

The bonding in the $Ir^+$ complexes involves a mixture of *s* and *d* character which can be thought of as a resonance of an *s* bond (1) with a *d* bond (4)

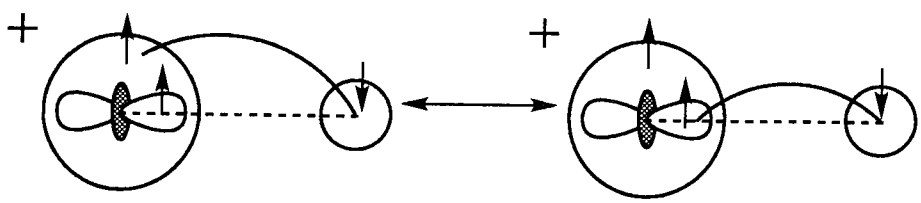

(4)

or more appropriately, as *sd* hybridization (5).

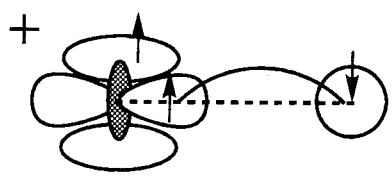

(5)

This *sd* hybridization leads to one orbital ($s + \lambda d_{z^2}$) which is polarized along the bond axis ($z$) and one orbital ($\lambda s - d_{z^2}$) which is polarized in the plane normal to the bond axis ($xy$). The advantages of this are twofold. (1) The orbital polarized in the $z$ direction has increased overlap with the ligand and

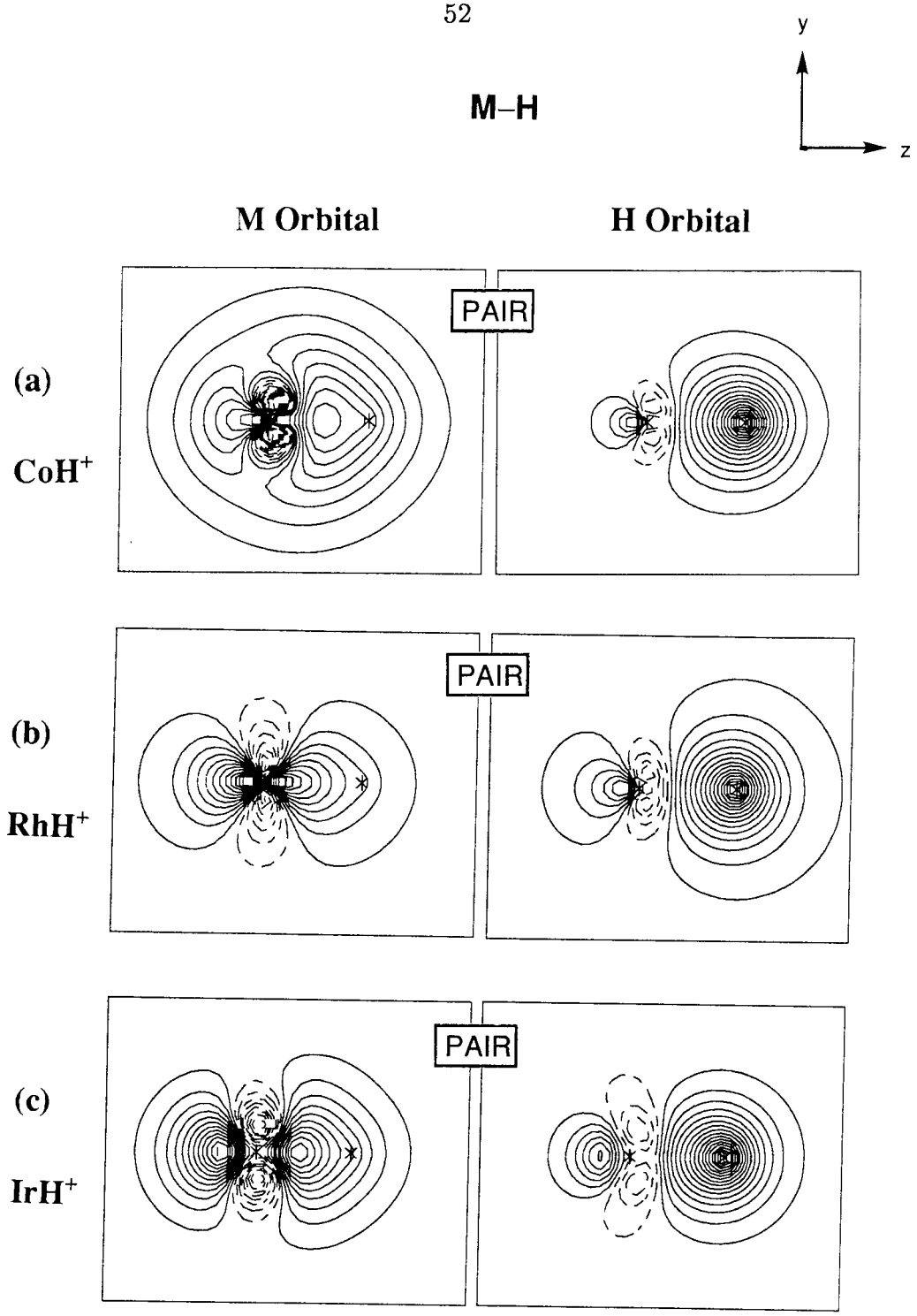


**Figure 5.** GVB-PP bonding orbitals for the ground states of $CoH^+$, $RhH^+$, and $IrH^+$. (a) The $Co^+$-H bond is derived predominantly from metal *s* character. (b) The $Rh^+$-H bond is derived predominantly from metal *d* character. (c) The $Ir^+$-H bond is derived from *sd* hybrid character.

**Table IV.** Hybridization in the GVB and MCPF bonding orbitals for the ground states of $MH^+$ and $MCH_3^+$, M = Co, Rh, and Ir. For the GVB-PP wavefunction, the combined composition of the two bond orbitals is given, but for the MCPF wavefunction, only the composition of the first natural orbital corresponding to the bond is given. The metal *s*, *p*, and *d* character as well as the ligand character are described in terms of percent of the total.

| | M *s* | M *p* | M *d* | R |
|---|---|---|---|---|
| $CoH^+$ GVB | 37.7 | 5.7 | 5.9 | 50.7 |
| $CoH^+$ MCPF | 24.1 | 5.2 | 28.4 | 42.3 |
| $CoCH_3^+$ GVB | 49.6 | 4.1 | 4.6 | 41.7 |
| $CoCH_3^+$ MCPF | 37.0 | 3.6 | 20.7 | 38.7 |
| $RhH^+$ GVB | 3.2 | 0.7 | 48.3 | 47.8 |
| $RhH^+$ MCPF | 4.7 | 2.4 | 52.5 | 40.4 |
| $RhCH_3^+$ GVB | 2.4 | 1.3 | 52.3 | 44.0 |
| $RhCH_3^+$ MCPF | 2.4 | 1.2 | 55.4 | 41.0 |
| $IrH^+$ GVB | 18.0 | 2.2 | 34.1 | 45.7 |
| $IrH^+$ MCPF | 16.7 | 4.2 | 43.7 | 35.4 |
| $IrCH_3^+$ GVB | 17.6 | 2.0 | 39.3 | 41.1 |
| $IrCH_3^+$ MCPF | 14.5 | 1.6 | 45.0 | 38.9 |

forms a stronger bond than either the pure *s* or pure *d* orbitals. (2) The non-bonding orbital polarized in the *xy* plane is less repulsive to the ligand than either the pure *s* or pure $d_{z^2}$ orbitals. For the case of $Ir^+$, the optimal mixture of *s* and *d* character in the bonding orbital appears to be about 70% *d* and 30% *sp* at the MCPF level (about 65% *d* and 35% *sp* at the GVB level). Such a mixture is consistent with previous analyses of the effectiveness of *sd* hybridization as a function of the $s/d$ ratio.[15]

Much of the effectiveness of *sd* hybridization rests on the similar size of the

$s$ and $d$ orbitals.[1] For the third row transtion metals, the lanthanide contraction leads to smaller $6s$ orbitals, 1.65 times the size of the $5d$ orbitals in the case of $Ir^+$. In contrast, the $4s$ orbital of $Co^+$ is 2.58 times the size of the $3d$ orbitals. $Rh^+$ is intermediate to these two metals with a $5s/4d$ ratio of 1.97:1. This leads us to conclude that $sd$ hybridization should be less effective in $Co^+$ than in $Ir^+$.

We have tested this hypothesis with a series of GVB-PP(5/5) calculations on the quartet states of $MH^+$ (M = Co, Rh, and Ir). As detailed in the appendix to this chapter, we were able to ensure that bonding was to the $s^1d^7$ configuration of the metal while varying the $s$ and $d$ character of the bonding and $\sigma$ non-bonding orbitals. Results are presented in Figures 6 and 7.

From Figure 6 it can be seen that $Rh^+$ and $Ir^+$ form strong $sd$ hybrid bonds to H, with an optimum hybridization of 60-70% $d$ character. In fact, the pure $s$ and pure $d$ bonds are unbound, reflecting the repulsion to the non-bonding $\sigma$ orbital which is either pure $d$ or pure $s$, respectively. For $Co^+$, the situation is markedly different. The optimal hybridization appears to be about 90% $s$ character and the bond strength decreases dramatically with increasing $d$ character. Again, this reflects to a large degree the repulsion to the non-bonding orbital as much as it does the intrinsic strength of the hybrid bond. That is, bonding to the large $4s$ orbital results in little repulsion to the small $3d$ orbital; however, bonding to the $3d$ orbital results in a large repulsion to the $4s$ orbital. This observation may have a profound impact on the chemistry of $Co^+$ when the metal is bound to multiple ligands. That is, it could be difficult for the metal to form a second covalent bond as rehybridization necessarily introduces more $d$ character into the bond and thereby weakens it. This should not be the case for either $Rh^+$ or $Ir^+$, where substantial rehybridization of the bonding orbitals can occur within the range of 30-80% $d$ character without an adverse effect on

the bond energy. This flexibility should make forming multiple bonds easier for $Rh^+$ and $Ir^+$ than for $Co^+$.

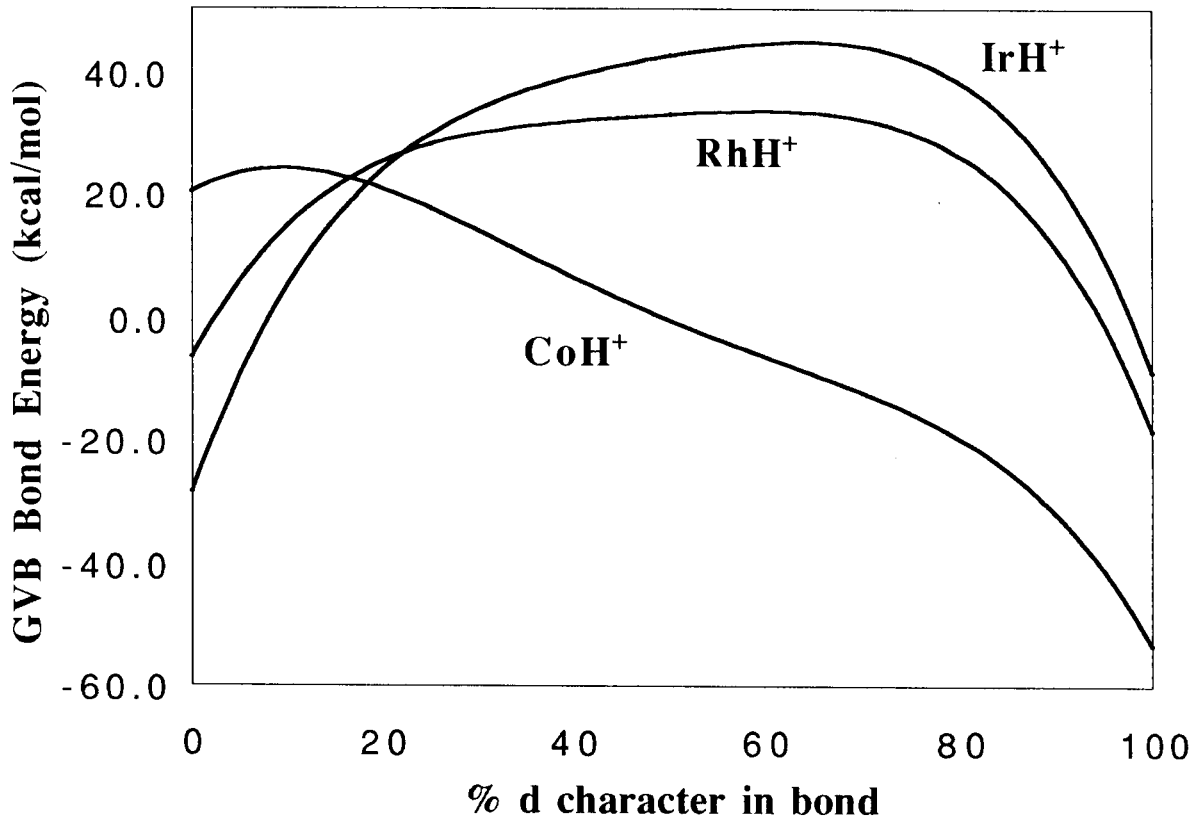


**Figure 6.** Diabatic bond energies for pure covalent bonds formed to H from the $^5F\ s^1d^7$ states of $Co^+$, $Rh^+$, and $Ir^+$ as a function of sd hybridization. Calculations were performed at the GVB-PP(5/5) level.

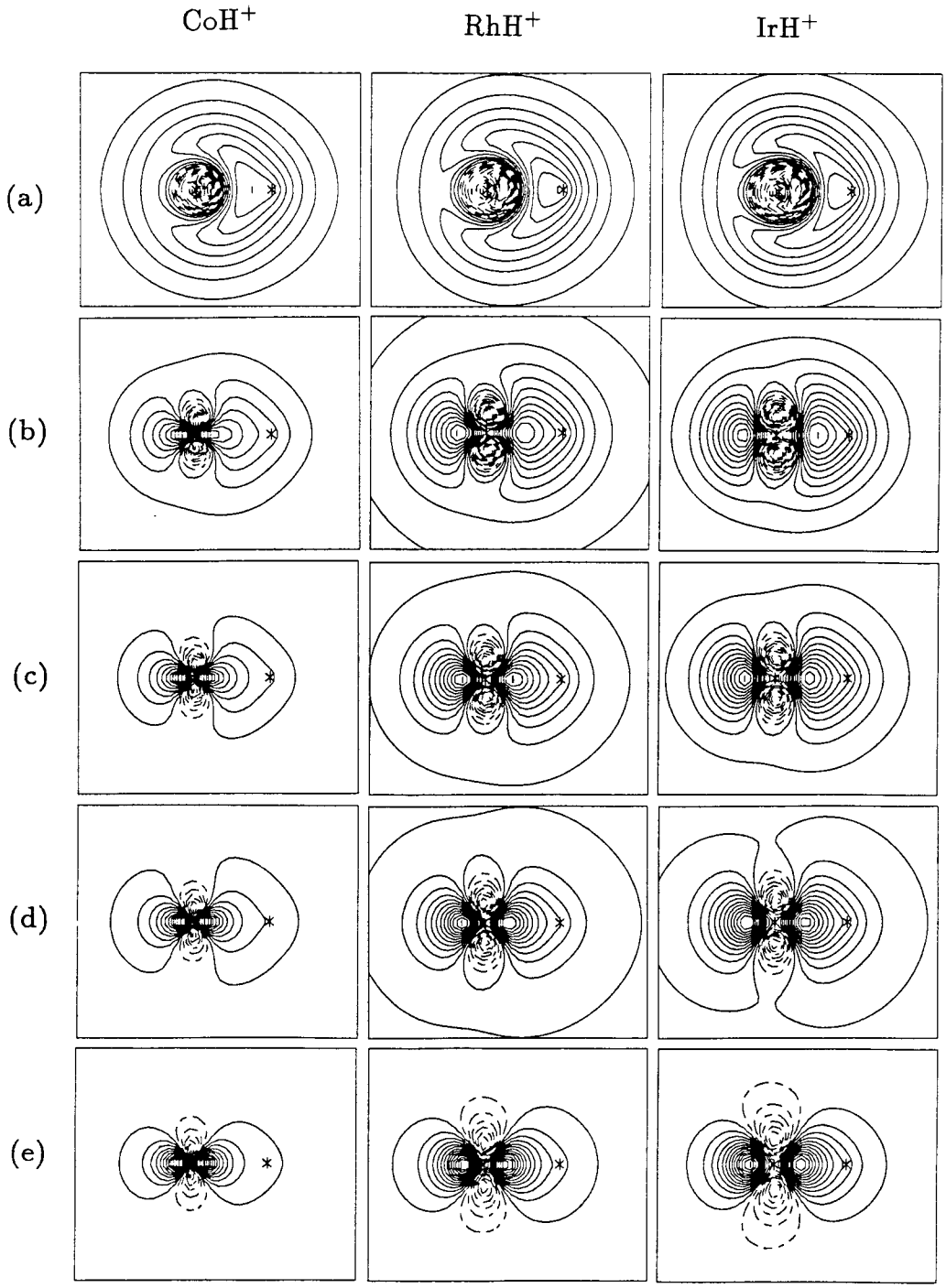


**Figure 7.** Plots of GVB-PP metal bonding orbitals for quartet $MH^+$ with varying *s* and *d* character. (a) 100% *s*, 0% *d*. (b) 75% *s*, 25% *d*. (c) 50% *s*, 50% *d*. (d) 25% *s*, 75% *d*. (e) 0% *s*, 100% *d*. Only (a) and (b) form strong bonds for $CoH^+$, while (b)-(d) form strong bonds for $RhH^+$ and $IrH^+$.

### 3.3.3 Other contributions to the bonding

One puzzle in this discussion is that at the MCPF level, the picture seems to change for $Co^+$ (Table IV). At the GVB level, the bonding in both $CoH^+$ and $CoCH_3^+$ is dominated by the $s$ orbital of the metal, fitting the simple picture of bonding to an $s^1d^7$ state (1). However, at the MCPF level, there is significant $d$ character in the bond (more so in the $Co^+-H$ bond than in the $Co^+-CH_3$ bond), suggesting that $sd$ hybridization becomes more favorable with the correlation of the non-bonding electrons. (Such a discrepancy in these two wavefunctions was noticed by Pettersson *et al.*[3]) No such discrepancy exists for the $Rh^+$ or $Ir^+$ complexes.

We find that the situation at the MCPF level only reflects to a small extent increased $sd$ hybridization of the type seen for $IrH^+$ and $IrCH_3^+$ (5). Instead, the situation is more like the $^4\Phi$ state of $RhH^+$ and reflects the introduction of resonance contributions such as the one-electron bond (3) and ligand to metal charge transfer (6).

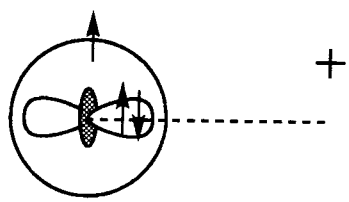


(6)

This conclusion is made based on data from a separate study on $CoCH_3^+$ in which it was found that only wavefunctions which produce an accurate description of the $^3F-^5F$ state splittings lead to the high $d$ contribution to the bonding seen in the MCPF calculations.[16] Wavefunctions which properly account for the spin-polarization in the bond (such as CASSCF, see next section) but still describe

the state splittings poorly lead to only small increases in the $d$ character (*i.e.*, through $sd$ hybridization) as compared to spin-restricted wavefunctions (such as GVB-PP). Thus, at the lower level wavefunctions where the $^5$F state is calculated to lie well below the $^3$F state, configurations with $d^8$ character such as (3) and (6) will not mix into the wavefuction and the bond will be dominated by $s$ character. At the higher level wavefunctions where the $^3$F state is properly lower in energy than the $^5$F state, an appropriate weight is given to these other configurations and more $d$ character is seen in the bonds.

While much of this discussion has been pedagogical in nature, it can be concluded that the $Co^+-H$ and $Co^+-C$ bonds are substantially weaker than the $Ir^+-H$ and $Ir^+-C$ in large part due to the issue of the effectiveness of $sd$ hybridization.

### 3.3.4 Exchange energy loss

An additional consideration which has bearing on promotion energies and on the relative strengths of $d$ bonds vs. $s$ bonds is the factor of exchange energy loss.[17] Exchange energy is the quantity behind Hund's rule and represents a favorable interaction between each pair of electrons of the same spin in an atom or molecule. This quantity is largest when the two interacting electrons are in close proximity, therefore intra-atomic exchange energy is of more importance than inter-atomic exchange energy in molecules. This intra-atomic exchange energy can be quite large in transition metals with tight $d$ orbitals (up to ~22 kcal/mol) and cannot be ignored.[18]

For a quintet $s^1d^7$ atom, there are 5 $\alpha$ spin $d$ electrons, 2 $\beta$ spin $d$ electrons, and 1 $\alpha$ spin $s$ electron. This leads to 5 exchange interactions between the $s$ electron and the same spin $d$ electrons ($5K_{sd}$), 10 exchange interactions among the $\alpha$ spin $d$ electrons ($5K_{dd}$), and 1 exchange interaction between the $\beta$ spin $d$ electrons ($1K_{dd}$) for a total of $5K_{sd}+11K_{dd}$. Similarly, for a triplet $d^8$ atom, there are 5 $\alpha$ spin $d$ electrons ($10K_{dd}$) and 3 $\beta$ spin $d$ electrons ($3K_{dd}$) for a total of $13K_{dd}$.

In forming a covalent bond to a ligand it is necessary to spin couple one of the metal (M) electrons with the ligand (R): $[\phi(M)\phi(R)+\phi(R)\phi(M)](\alpha\beta-\beta\alpha)$. As a result, the spin of the metal bonding electron is 50% $\alpha$ and 50% $\beta$ which alters the total exchange interactions on the metal. In bonding to the $s$ electron of the $s^1d^7$ state, the atomic exchange energy is $3.5K_{sd}+11K_{dd}$, a loss of $1.5K_{sd}$. In bonding to the $d$ electron of the $s^1d^7$ state, the atomic exchange energy is $4.5K_{sd}+10K_{dd}$, a loss of $0.5K_{sd}+1K_{dd}$. In bonding to the $d$ electron of the $d^8$ state, the atomic exchange energy is $12.5K_{dd}$, a loss of $0.5K_{dd}$.

**Table V.** Exchange energies ($K_{sd}$ and $K_{dd}$) for $Co^+$, $Rh^+$, and $Ir^+$ and exchange energy losses on bonding to an $s$ or $d$ orbital for the $s^1d^7$ state or a $d$ orbital for the $d^8$ state of these metals.

| | $K_{sd}$ | $K_{dd}$ | $s^1d^7(s)$ | $s^1d^7(d)$ | $d^8(d)$ |
|---|---|---|---|---|---|
| $Co^+$ [a] | 5 | 21 | 8 | 24 | 11 |
| $Rh^+$ [a] | 8 | 16 | 12 | 20 | 8 |
| $Ir^+$ [b] | 12 | 14 | 18 | 20 | 7 |

[a] Values based on Carter and Goddard.[18]

[b] Values based on numbers for $Re^+$ computed by Ohanessian and Goddard.[1] The $Ir^+$ numbers are expected to be similar.

In Table V, we give values of $K_{sd}$ and $K_{dd}$ for $Co^+$, $Rh^+$, and $Ir^+$, and indicate the exchange energy loss for the three cases detailed above. For the first row transition metals, there is a large difference in the values of $K_{sd}$ and $K_{dd}$. The tight $3d$ orbitals lead to large $d-d$ exchange (21 kcal/mol for $Co^+$), but the interaction of the $3d$ orbitals with the diffuse $4s$ orbital leads to a small $s-d$ exchange (5 kcal/mol). For $Rh^+$, the more diffuse $4d$ orbitals (as compared to the $3d$ orbitals) lead to a smaller $d-d$ exchange (16 kcal/mol) but a larger $s-d$ exchange (8 kcal/mol). For $Ir^+$, the similar size of the $6s$ and $5d$ orbitals leads to $d-d$ and $s-d$ exchanges which are comparable ($K_{sd}$=12 kcal/mol and $K_{dd}$=14 kcal/mol).

From the data in Table V it can be seen that bonding to either an $s$ orbital or a $d$ orbital in the $s^1d^7$ state of $Ir^+$ results in a similar loss of exchange energy. This suggests that for the quartet states of $IrH^+$, $IrCH_3^+$, and $IrC_2H_5^+$, the optimal hybridization of the $s$ and $d$ character in the bonding orbital should rest entirely on intrinsic properties and can be obtained without hindrances from the interactions of the bonding electrons with the non-bonding electrons. In contrast, the exchange energy loss in forming a bond to a $d$ orbital in the

$s^1d^7$ state of $Co^+$ is approximately three times as large as the loss in forming a bond to the $s$ orbital. Beyond the issue of the orbital size and the effectiveness of $sd$ hybridization, consideration of this exchange energy loss indicates that it is significantly more difficult to bond to a $d$ electron in this state. Removing this exchange interaction from the data in Figure 6 tends to shift the optimal hybridization toward increased $d$ character. This is a small effect, however, shifting the hybridization in $CoH^+$ from 90% $s$ to 85% $s$. As a consequence of this effect, wavefunctions which account for spin-polarization in the bond (where the metal bonding electron will tend to be more $\alpha$ spin and the ligand bonding electron will tend to be more $\beta$ spin) reclaim some of this lost exchange energy and lead to greater $d$ character in the bonding orbital than those that don't (such as CASSCF vs. GVB). Still, the increase in $d$ character is small, as indicated.

As a final note on this subject, it is generally useful to determine intrinsic bond strengths of metal ligand bonds by accounting for promotion energy and exchange energy loss. For instance, the $Rh^+ - H$ bond has a well depth of $D_e$=43.9 kcal/mol and an exchange energy loss of 8 kcal/mol. Thus, the intrinsic strength of the $Rh^+$–H bond is $D_e$=52 kcal/mol. We should warn the reader, however, that this effect as presented should not be taken as quantitative. Spin polarization of the bond can reclaim some of the lost exchange energy as mentioned and issues such as hybridization and mixing of states can make a proper accounting of $K_{sd}$ and $K_{dd}$ loss difficult. However, in qualitative terms this effect combined with promotion considerations dominates the trends in covalent bond energies across a given row of the transition series. It also has a strong influence on the strengths of subsequent covalent bonds to the metal.

### 3.3.5 Occupations of non-bonding $d$ orbitals

One remaining question which should be addressed is what factors determine the occupations of the non-bonding $d$ orbitals. Since in each of the cases studied here there are a number of options, why is one particular configuration of the $d$ electrons more favorable than another? According to ligand field theory, one would occupy these orbitals based on how much they were perturbed by the ligand. For the cases studied here, we would expect the repulsion to the ligands to follow the trend $d_\sigma > d_\pi > d_\delta$ for the quartet states and the trend $d_\pi > d_\delta$ for the doublet states. Thus, for $MH^+$, we would expect the $^4\Sigma^-$ state (with the $d_\sigma^1 d_\pi^2 d_\delta^4 s^1$ bonding configuration) and the $^2\Pi$ state (with the $d_\sigma^1 d_\pi^3 d_\delta^4$ bonding configuration) to be lowest lying for their respective spins. As we have seen, the $^4\Phi$ ground state of $CoH^+$ and the $^2\Delta$ ground state of $RhH^+$ are examples to the contrary. Moreover, the $^4\Sigma^-$ state of $IrH^+$ requires a multi-reference treatment and is dominantly derived from the $d_\sigma^1 d_\pi^4 d_\delta^2 s^1$ bonding configuration with only a minor contribution from the $d_\sigma^1 d_\pi^2 d_\delta^4 s^1$ bonding configuration. Even more peculiar, the $^4A_2$ states of $CoCH_3^+$ and $IrCH_3^+$ show significant hybridization of the $\pi$ and $\delta$ orbitals.

One aspect of the chemistry of highly unsaturated organometallic complexes that has received scant attention is the importance of intra-atomic repulsions (as opposed to inter-atomic repulsions) in determining the ground states of these complexes. We stress this point a great deal in this work since anything which helps the theorist decide *a priori* the ground state of the complex of interest (or at least narrows the choices) will reduce CPU waste. Much of the ensuing discussion on the effects of intra-atomic repulsions on the spectrum of states follows the work of Walch[19] and Schilling,[3b] but bears repeating.

**Table VI.** Couplings of electronic configurations necessary to obtain pure $^5$F and $^5$P states ($s^1d^7$). Configurations are designated by their singly occupied $d$ orbitals. The other $d$ orbitals are assumed to be doubly occupied and the $s$ orbital is assumed to be singly occupied.

| |
|---|
| $^5$F |
| $1(xz)(yz)(x^2-y^2)$ |
| $1(xz)(yz)(xy)$ |
| $\sqrt{\frac{4}{5}}(z^2)(x^2-y^2)(xy) - \sqrt{\frac{1}{5}}(z^2)(xz)(yz)$ |
| $\sqrt{\frac{1}{2}}(z^2)(xz)(x^2-y^2) - \sqrt{\frac{1}{2}}(z^2)(yz)(xy)$ |
| $\sqrt{\frac{1}{2}}(z^2)(xz)(xy) + \sqrt{\frac{1}{2}}(z^2)(yz)(x^2-y^2)$ |
| $\sqrt{\frac{2}{5}}(xz)(x^2-y^2)(xy) - \sqrt{\frac{3}{10}}(z^2)(xz)(xy) + \sqrt{\frac{3}{10}}(z^2)(yz)(x^2-y^2)$ |
| $\sqrt{\frac{2}{5}}(yz)(x^2-y^2)(xy) + \sqrt{\frac{3}{10}}(z^2)(xz)(x^2-y^2) + \sqrt{\frac{3}{10}}(z^2)(yz)(xy)$ |
| $^5$P |
| $\sqrt{\frac{4}{5}}(z^2)(xz)(yz) + \sqrt{\frac{1}{5}}(z^2)(x^2-y^2)(xy)$ |
| $\sqrt{\frac{3}{5}}(xz)(x^2-y^2)(xy) + \sqrt{\frac{1}{5}}(z^2)(xz)(xy) - \sqrt{\frac{1}{5}}(z^2)(yz)(x^2-y^2)$ |
| $\sqrt{\frac{3}{5}}(yz)(x^2-y^2)(xy) - \sqrt{\frac{1}{5}}(z^2)(xz)(x^2-y^2) - \sqrt{\frac{1}{5}}(z^2)(yz)(xy)$ |

**Table VII.** Couplings of electronic configurations necessary to obtain pure $^3$F and $^3$P states ($d^8$). Configurations are designated by their singly occupied $d$ orbitals. The other $d$ orbitals are assumed to be doubly occupied.

| |
|---|
| $^3$F |
| $1(z^2)(x^2-y^2)$ |
| $1(z^2)(xy)$ |
| $\sqrt{\frac{4}{5}}(xz)(yz)+\sqrt{\frac{1}{5}}(x^2-y^2)(xy)$ |
| $\sqrt{\frac{1}{2}}(xz)(x^2-y^2)+\sqrt{\frac{1}{2}}(yz)(xy)$ |
| $\sqrt{\frac{1}{2}}(xz)(xy)-\sqrt{\frac{1}{2}}(yz)(x^2-y^2)$ |
| $\sqrt{\frac{2}{5}}(z^2)(xz)-\sqrt{\frac{3}{10}}(xz)(x^2-y^2)+\sqrt{\frac{3}{10}}(yz)(xy)$ |
| $\sqrt{\frac{2}{5}}(z^2)(yz)+\sqrt{\frac{3}{10}}(xz)(xy)+\sqrt{\frac{3}{10}}(yz)(x^2-y^2)$ |
| $^3$P |
| $\sqrt{\frac{4}{5}}(x^2-y^2)(xy)-\sqrt{\frac{1}{5}}(xz)(yz)$ |
| $\sqrt{\frac{3}{5}}(z^2)(xz)+\sqrt{\frac{1}{5}}(xz)(x^2-y^2)-\sqrt{\frac{1}{5}}(yz)(xy)$ |
| $\sqrt{\frac{3}{5}}(z^2)(yz)-\sqrt{\frac{1}{5}}(xz)(xy)-\sqrt{\frac{1}{5}}(yz)(x^2-y^2)$ |

**Table VIII.** $s^1d^7$ and $d^8$ configurations in terms of $^5$F and $^5$P character and $^3$F and $^3$P character, respectively. Each configuration is specified by the singly occupied $d$ orbitals. The remaining $d$ orbitals are assumed doubly occupied and the $s$ orbital is assumed singly occupied in the $s^1d^7$ state.

| | |
|---|---|
| $s^1d^7$ | |
| $(xz)(yz)(x^2-y^2)$ | 100% $^5$F |
| $(xz)(yz)(xy)$ | 100% $^5$F |
| $(z^2)(xz)(x^2-y^2)$ | 80% $^5$F + 20% $^5$P |
| $(z^2)(xz)(xy)$ | 80% $^5$F + 20% $^5$P |
| $(z^2)(yz)(x^2-y^2)$ | 80% $^5$F + 20% $^5$P |
| $(z^2)(yz)(xy)$ | 80% $^5$F + 20% $^5$P |
| $(z^2)(x^2-y^2)(xy)$ | 80% $^5$F + 20% $^5$P |
| $(xz)(x^2-y^2)(xy)$ | 40% $^5$F + 60% $^5$P |
| $(yz)(x^2-y^2)(xy)$ | 40% $^5$F + 60% $^5$P |
| $(z^2)(xz)(yz)$ | 20% $^5$F + 80% $^5$P |
| $d^8$ | |
| $(z^2)(x^2-y^2)$ | 100% $^3$F |
| $(z^2)(xy)$ | 100% $^3$F |
| $(xz)(x^2-y^2)$ | 80% $^3$F + 20% $^3$P |
| $(xz)(xy)$ | 80% $^3$F + 20% $^3$P |
| $(yz)(x^2-y^2)$ | 80% $^3$F + 20% $^3$P |
| $(yz)(xy)$ | 80% $^3$F + 20% $^3$P |
| $(xz)(yz)$ | 80% $^3$F + 20% $^3$P |
| $(z^2)(xz)$ | 40% $^3$F + 60% $^3$P |
| $(z^2)(yz)$ | 40% $^3$F + 60% $^3$P |
| $(x^2-y^2)(xy)$ | 20% $^3$F + 80% $^3$P |

While it is adequate to pose the arguments on intra-atomic repulsions directly in terms of how repulsive a $d_\sigma$ orbital is to a $d_\pi$ or $d_\delta$ orbital, for instance, we find instead a more quantitative argument can be found in the atomic state splittings. A high spin $d^8$ configuration can couple the electrons into either the low-lying $^3$F state (7-fold degenerate) or the $^3$P excited state (3-fold degenerate). Similarly, a high spin $s^1d^7$ configuration can couple the electrons into either the low-lying $^5$F state (7-fold degenerate) or the $^5$P excited state (3-fold degenerate). These couplings are given in Tables VI and VII. Since most of these couplings are composed of linear combinations of configurations, this information can be deconvoluted to obtain a description of each individual configuration in terms of the pure atomic states. These are given in Table VIII. As can be seen from this data, only the $d^2_\sigma d^2_\pi d^3_\delta s^1$ configurations (where $\sigma = z^2$, $\pi = xz, yz$, $\delta = x^2 - y^2, xy$) are pure $^5$F and only the $d^1_\sigma d^4_\pi d^3_\delta$ configurations are pure $^3$F. The others have $^5$P or $^3$P components to them.

In the minimally or only moderately perturbed environments of these highly unsaturated organometallic complexes, the ground states are determined by trying to minimize the introduction of the atomic excited states into the wavefunction while adhering to certain constraints imposed by the ligands. On bonding to a ligand, the degeneracy of the metal orbitals will be broken and based on ligand field arguments some orbitals may be stabilized (increasing the likelihood that the orbitals are doubly occupied in the ground state) while others may be destabilized (increasing the likelihood that the orbitals are singly occupied in the ground state). In the case of $RhH^+$, the $d_{z^2}$ orbital is used in forming the bond so it is strictly singly occupied. Considering then the restrictions placed on the metal by having the $d_{z^2}$ orbital singly occupied, there are only two possible configurations of the non-bonding $d$ electrons which would give rise to a pure

$^3$F coupling on the $d^8$ metal. These configurations are

$$d^1_{z^2} d^2_{xz} d^2_{yz} d^1_{x^2-y^2} d^2_{xy}$$

and

$$d^1_{z^2} d^2_{xz} d^2_{yz} d^2_{x^2-y^2} d^1_{xy}$$

leading to a $^2\Delta$ state. All other configurations either introduce $^3$P character into the wavefunction or compromise the occupation of the $d_{z^2}$ orbital.

Similarly, given that the $d_{z^2}$ orbital has the largest overlap with the ligand in the quartet states of $MH^+$, it will be the most perturbed $d$ orbital and likely be singly occupied in the ground state. In order to achieve this without compromising the $^5$F coupling of the $s^1 d^7$ metal, the complex must be in either the $^4\Sigma^-$ state:

$$\sqrt{\frac{4}{5}} d^1_{z^2} d^2_{xz} d^2_{yz} d^1_{x^2-y^2} d^1_{xy} s^1 - \sqrt{\frac{1}{5}} d^1_{z^2} d^1_{xz} d^1_{yz} d^2_{x^2-y^2} d^2_{xy} s^1$$

or the $^4\Phi$ state:

$$\sqrt{\frac{1}{2}} d^1_{z^2} d^1_{xz} d^2_{yz} d^1_{x^2-y^2} d^2_{xy} s^1 - \sqrt{\frac{1}{2}} d^1_{z^2} d^2_{xz} d^1_{yz} d^2_{x^2-y^2} d^1_{xy} s^1$$

or

$$\sqrt{\frac{1}{2}} d^1_{z^2} d^1_{xz} d^2_{yz} d^2_{x^2-y^2} d^1_{xy} s^1 + \sqrt{\frac{1}{2}} d^1_{z^2} d^2_{xz} d^1_{yz} d^1_{x^2-y^2} d^2_{xy} s^1$$

(Note that in each of the above configurations, the $d_{z^2}$ orbital is singly occupied.) The only distinction between these two states is that the $^4\Sigma^-$ state has a higher occupation of the $d_\pi$ orbitals than the $^4\Phi$ state. This proves to be more repulsive in $CoH^+$ but more attractive in $IrH^+$, probably as a result of greater ligand to metal charge transfer in $IrH^+$; consequently, the ground state of $CoH^+$ is $^4\Phi$ and the ground state of $IrH^+$ is $^4\Sigma^-$.

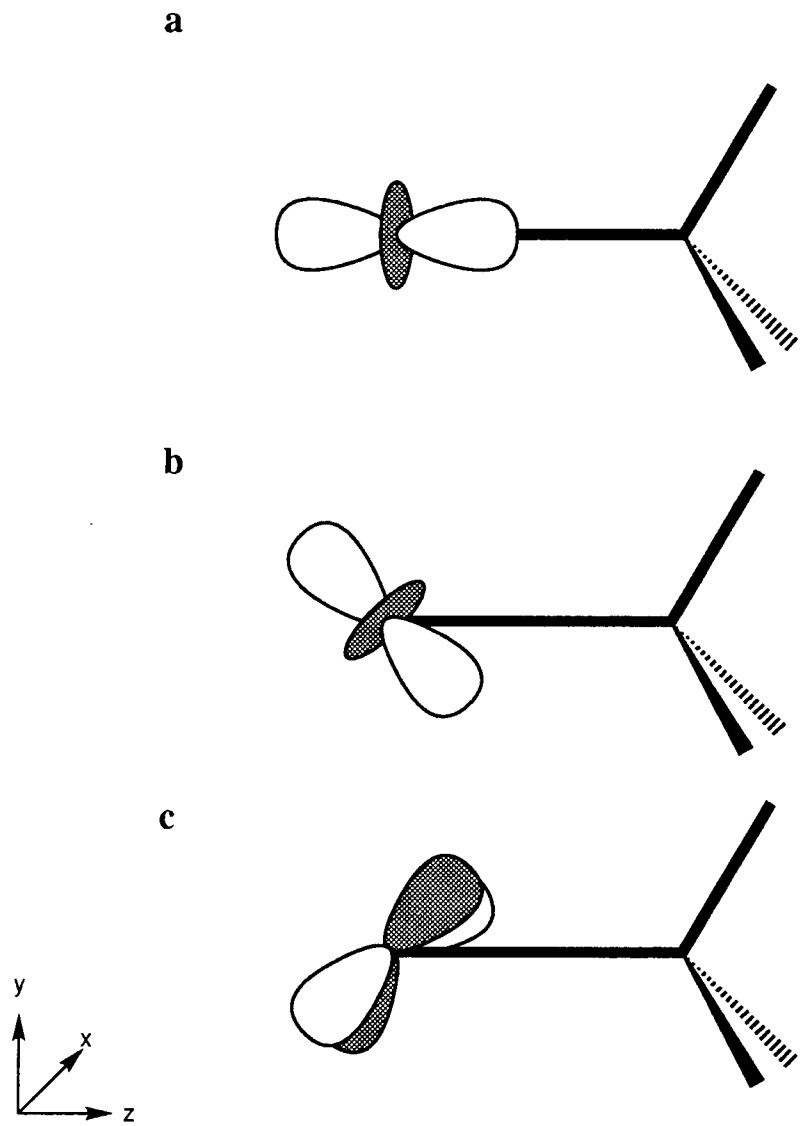


**Figure 8.** Example of orbital rotations to minimize metal-ligand repulsions while maintaining the optimal atomic couplings. The $d_\sigma$ orbital of $^4A_2$ $CoCH_3^+$ and $IrCH_3^+$ is singly occupied as expected (a). The remaining $d_\pi$ and $d_\delta$ orbitals hybridize to form orbitals with $\sigma$ (b) and $\delta$ (c) character offset from the principal axis by 54.74°. These orbitals are doubly occupied while the other orbitals resulting from hybridization are singly occupied.

In many cases, the optimal atomic coupling coincedent with the minimization of metal-ligand repulsions requires a rotation of the metal orbitals. This can be seen in the $^4A_2$ ground states of $CoCH_3^+$ and $IrCH_3^+$ and the analogous $^4A''$ states of $CoC_2H_5^+$ and $IrC_2H_5^+$. As expected, the $d_{z^2}$ orbital is singly occupied in the ground state. By ligand field arguments, the $d_\pi$ orbitals are the next most perturbed $d$ orbitals and the $d_\delta$ orbitals are the least perturbed. However, if one considers a rotation between the $d_\pi$ and $d_\delta$ orbitals, a more repulsive and a less repulsive set of $d$ orbitals will result. The $\pi$ and $\delta$ orbitals rehybridize as in Figure 8 such that the two doubly occupied (less repulsive) orbitals have characters which are $\sigma$-like and $\delta$-like, offset from the principal axis by an angle of 54.74°. Adjusting the axis of atomic symmetry by this angle, these doubly occupied $d'_{z^2}$ and $d'_{xy}$ orbitals are staggered with respect to the methyl C−H bonds and are the least repulsive to the ligand while leading to an effective $d'^2_{z^2} d'^1_{xz} d'^1_{yz} d'^1_{x^2-y^2} d'^2_{xy} s^1$ bonding configuration which is a pure $^5F$ coupling. (Note that the singly occupied $d$ orbitals of the metal represent a linear combination of the $d'_{yz}$, $d'_{xz}$ and $d'_{x^2-y^2}$ orbitals with respect to the new axis of atomic symmetry.) A very similar situation exists for the $C_{3v}$ geometry of $Co(CH_4)^+$ and further details of this phenomenon will be given in Chapter V.

## 3.4 Conclusions

We have considered the bonding in $MH^+$, $MCH_3^+$, and $MC_2H_5^+$, for M = Co, Rh, and Ir. While the nature of the $M^+-H$ and $M^+-C$ bond is similar for a given metal, there are important differences between the metals which result in bonds to $Ir^+$ which are ~60% stronger than those to $Co^+$ or $Rh^+$.

For each metal, the strongest bonds can be formed diabatically from the $s^1d^7$ $^5$F state. For $Ir^+$, this is the ground state. For the other two metals, the $d^8$ $^3$F state is the ground state. In the case of $Co^+$, however, the $^5$F state lies only 9.9 kcal/mol higher in energy and is easily accessible. This is not true for $Rh^+$, where a promotion energy of 49.1 kcal/mol is required to reach the $^5$F state. Consequently, the weaker bond formed from the $d^8$ configuration of the metal is actually lower in energy than that derived from the $s^1d^7$ configuration. Thus, the $MH^+$, $MCH_3^+$, and $MC_2H_5^+$ complexes each have quartet ground states for M = Co and Ir and doublet ground states for M = Rh.

Unlike $Rh^+$ and $Ir^+$, $Co^+$ does not lead to strong *sd* hybrid bonds from the $s^1d^7$ configuration. Whereas $IrH^+$ demonstrates a bonding orbital on the metal composed of 63% *d* character and 37% *sp* character (at the GVB level), the bonding orbital on the metal for $CoH^+$ is composed of 12% *d* character and 88% *sp* character. The dominance of *s* character in the bond stems from the fact that the 4*s* orbital is much larger than the 3*d* orbital, making *sd* hybridization an inefficient process for $Co^+$. At higher levels of theory (MCPF) more *d* character is mixed into the $Co^+-H$ and $Co^+-C$ bonds by mixing in resonance configurations involving bonding to the $d^8$ state. However, the ineffectiveness of *sd* hybridization in forming covalent bonds to $Co^+$ does not bode well for the formation of multiple bonds to this metal.

In sum, covalent bonding from $Ir^+$ is nearly ideal. This metal can form strong *sd* hybrid bonds (which $Co^+$ can't) directly from its $s^1d^7$ ground state (which $Rh^+$ can't). This is clearly reflected in the calculated bond strengths. Subtleties in the bonding arise from the interactions of the bonding electrons with the nonbonding electrons. These interactions include the loss of exchange energy and the electron-electron repulsions reflected in the atomic state couplings. Exchange energy is a wild card which can greatly alter the strength of a metal-ligand bond from its intrinsic value. As each ligand modifies the magnitude of this exchange energy, it is expected that successive ligand binding energies will be affected and, as a result, exhibit nonmonotonic behavior.

## Appendix

HF geometries optimizations for the quartet states of $MH^+$ were done in a point by point manner (fitting a quadratic to 3 points near the minimum). The wavefunction used had explicitly 1 electron in the $d_\sigma$ orbital and 6 electrons averaged over the remaining $d$ orbitals.

The determination of the GVB bond strength as a function of hybridization was done with the following procedure.

(1) Calculate the wavefunction for $s^1d^7$ $M^+$ + H at long distance using the orbital configuration described above.

(2) Make a series of linear combinationis of the $d_\sigma$ and $s$ orbitals to obtain the non-bonding orbital. These linear combinations are $1d_\sigma$, $\frac{\sqrt{3}}{2}d_\sigma - \frac{1}{2}s$, $\frac{1}{\sqrt{2}}d_\sigma - \frac{1}{\sqrt{2}}s$, $\frac{1}{2}d_\sigma - \frac{\sqrt{3}}{2}s$, $1s$.

(3) At the HF optimized geometry for the quartet state of $MH^+$, freeze the singly occupied non-bonding orbital from (2) and optimize all other orbitals at the GVB-PP(5/5) level.

By freezing the non-bonding orbital, hybridization has been restricted in the metal such that covalent bonding to the $s^1d^7$ state is guaranteed.

## References


(1) Ohanessian, G.; Goddard, W.A., III *Acc. Chem. Res.* **1990**, *23*, 386.

(2) (a) Schilling, J.B.; Goddard, W.A., III; Beauchamp, J.L. *J. Am. Chem. Soc.* **1986**, *108*, 582. (b) Schilling, J.B.; Goddard, W.A., III; Beauchamp, J.L. *J. Phys. Chem.* **1987**, *91*, 5616. (c) Schilling, J.B.; Goddard, W.A., III; Beauchamp, J.L. *J. Am. Chem. Soc.* bf 1987, *109*, 5565.

(3) Pettersson, L.G.M.; Bauschlicher, C.W., Jr.; Langhoff, S.R.; Partridge, H. *J. Chem. Phys.* **1987**, *87*, 481.

(4) (a) Alvarado-Swaisgood, A.E.; Harrison, J.F. *J. Phys. Chem.* **1988**, *92*, 2757. (b) Alvarado-Swaisgood, A.E.; Allison, J.; Harrison, J.F. *J. Am. Chem. Soc.* **1985**, *89*, 2517.

(5) Schilling, J.B.; Goddard, W.A., III; Beauchamp, J.L. *J. Am. Chem. Soc.* **1987**, *109*, 5573.

(6) Bauschlicher, C.W., Jr.; Langhoff, S.R.; Partridge, H.; Barnes, L.A. *J. Chem. Phys.* **1989**, *91*, 2399.

(7) Martinho Simões, J.A.; Beauchamp, J.L. Chem. Rev., **1990**, *90*, 629, and references therein.

(8) Armentrout, P.B.; Georgiadis, R. *Polyhedron* **1988**, *7*, 1573, and references therein.

(9) Elkind, J.L.; Armentrout, P.B. *J. Phys. Chem.* **1986**, *90*, 6576.

(10) Mandich, M.L.; Halle, L.F.; Beauchamp, J.L. *J. Am. Chem. Soc.* **1984**, *106*, 4403.

(11) (a) Sunderlin, L.S.; Armentrout, P.B. *Int. J. Mass Spectrom. Ion Processes* **1989**, *94*, 149. (b) Schultz, R.H.; Elkind, J.L.; Armentrout, P.B. *J. Am. Chem. Soc.* **1988**, *110*, 411. (c) Fisher, E.R.; Armentrout, P.B. *J. Am. Chem. Soc.* **1992**, *114*, 2039.

(12) Perry, J.K.; Goddard, W.A., III *J. Am. Chem. Soc.*, in press.

(13) Irikura, K.K.; Beauchamp, J.L. *J. Phys. Chem.* **1991**, *95*, 8344.

(14) Ohanessian, G.; Goddard, W.A., III, unpublished results.

(15) Steigerwald, M.L., Ph.D. thesis, California Institute of Technology, 1984.

(16) Perry, J.K.; Goddard, W.A., III; Ohanessian, G. *J. Chem. Phys.* **1992**, *97*, 7560.

(17) Goddard, W.A., III; Harding, L.B. *Ann. Rev. Phys. Chem.* **1978**, *29*, 363.

(18) Carter, E.A.; Goddard, W.A. *J. Phys. Chem.* **1988**, *92*, 5679.

(19) (a) Walch, S.P., Ph.D. thesis, California Institute of Technology, 1977. (b) Walch, S.P.; Bauschlicher, C.W., Jr. *J. Chem. Phys.* **1983**, *78*, 4597.

Chapter IV

# Complexation of $H_2$ with $Co^+$, $Rh^+$, and $Ir^+$

# Chapter IV

## Complexation of $H_2$ with $Co^+$, $Rh^+$, and $Ir^+$

### 4.1 Introduction

The characterization by theorists[1-9] and experimentalists[10-12] alike of the interaction of $H_2$ with atomic transition metal ions has produced a large body of data in the last few years. Such studies have led to quantitative measurements of $M^+-H$ and $M^+-H_2$ bond strengths. These studies have also been aimed at offering insight into oxidative addition and its reverse reaction, reductive elimination, two of the most important processes in catalysis.

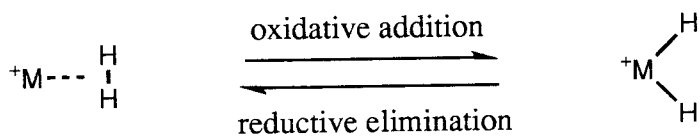


The community interested in obtaining these ion-$H_2$ potential energy surfaces widened appreciably with the discovery by Kubas *et al.*[13] in 1984 of organometallic complexes $[M(CO)_3(PR_3)_2(H_2)$, (M = Mo, W; R = Cy, *i*-Pr)] which possessed a previously unseen $\eta^2$ dihydrogen ligand rather than the more classical dihydride ligands. While such a complex had been regarded as an intermediate in the oxidative addition of $H_2$ to organometallic complexes, the finding that it could be stable was a landmark. It offered an illustration of how the energetics of oxidative addition and reductive elimination can be quite varied.

The role of the theorist has been to determine what factors contribute to the energetics controlling oxidative addition. For instance, Low and Goddard[14] showed that barriers for oxidative addition and reductive elimination in Pd and Pt complexes are lower for the H−H bond than they are for the C−H and C−C bonds (the C−C bond having the highest barriers). This does not reflect the trends in the overall thermochemistry for oxidative addition (the C−C bond is weaker than both the H−H bond and the C−H bond making the process of C−C oxidative addition more exothermic), but instead it reflects how the directionality of the ligand orbitals affects the stability of the transition state. The H 1*s* orbital is non-directional and this stabilizes the transition state since the H can form strong partial bonds to both the metal and the other ligand (either H or C). The C $sp^3$ hybrid orbital, on the other hand, is highly directional and this destabilizes the transition state since the C cannot form strong partial bonds to both the metal and the other ligand simultaneously. Thus, the barrier heights increase as H−H < C−H < C−C.

Less well understood, the nature of the metal is of even greater importance in determining the chemistry of oxidative addition. However, many of the electronic factors intrinsic to transition metals have not yet been clearly discussed in regard to their impact on this chemistry. Chief among these include the atomic state splittings and the relative strengths of *s*, *d*, and *sd* hybrid bonds. The interplay among these factors has produced a wide spectrum of chemistry observed for the bonding of $H_2$ to transition metal ions. Changes of spin, barriers to insertion, and double minima are just a few features that have been found on these potential energy surfaces, and we find that they can be readily explained by a careful consideration of the electronic structure of the metal ion.

In this chapter, we detail the chemistry of oxidation addition of $H_2$ to $Co^+$,

$Rh^+$, and $Ir^+$. In each case we consider the three lowest lying potential energy surfaces in detail. This offers a good example of the effect the atomic state splittings and atomic couplings can have on the chemistry of the metal. We should note that complexation of $H_2$ to $Co^+$ has been studied theoretically by Bauschlicher *et al.*[1] and our results for the energetics at the minimum are in quantitative agreement with theirs. These results are also in agreement with the experimental determination of the $Co^+-H_2$ complexation energy by Kemper and Bowers.[10] In addition, Balasubramanian and co-workers have obtained theoretical potential energy surfaces for a number of states of $RhH_2^+$ [2] and $IrH_2^+$ [3], and our results are in at least qualitative agreement.

## 4.2 Description of the bonding

### 4.2.1 The dihydrogen molecular complex

The initial interaction of the metal with $H_2$ is electrostatic, with the ion approaching the ligand perpendicular to the bond axis. This electrostatic attraction is dominated by the ion-induced dipole and charge-quadrupole interactions. The ion-induced dipole has the functional form

$$E_\alpha = \frac{1}{2}\alpha_\perp q^2 r^{-4}$$

where $q$ is the charge on the ion, $\alpha_\perp$ is the polarizability of $H_2$ perpendicular to the bond axis ($\alpha_\perp$=0.72 Å$^3$ [15]), and $r$ is the ion-molecule distance. The charge quadrupole has the functional form

$$E_\theta = \frac{1}{2}\theta q r^{-3}$$

where $\theta$ is the quadrupole moment of $H_2$ ($\theta$=+0.131 Å$^2$ [15]). A perpendicular ($C_{2v}$) approach of the ion to the bond axis is consistent with the positive quadrupole moment of $H_2$. A linear ($C_{\infty v}$) approach, on the other hand, leads to a repulsive ion-quadrupole interaction. The perpendicular approach also decreases the distance to the H−H center of mass ($r$) in comparison to the linear approach, increasing the ion-induced dipole as a result.

As this suggests, in order to maximize the attraction it is necessary to minimize the $M^+$−$H_2$ distance. In addition to the consideration of the $H_2$ orientation, minimization of the Pauli repulsion between the metal and $H_2$ is most important. Since the valence $s$ orbital is larger than the valence $d$ orbitals, and thus represents a greater repulsion to the ligand, the $d^8$ state of the metal forms a stronger bond than the $s^1d^7$ state. Since the ground states of $Co^+$

and $Rh^+$ are $^3F$ ($d^8$), it is clear that the lowest energy dihydrogen molecular complexes formed by these metals will be triplets derived from these states. For $Ir^+$, the ground state is $^5F$ ($s^1d^7$) with a 6.5 kcal/mol excitation energy to the $^3F$ ($d^8$) state. Thus, if the $^3F$ state forms an electrostatic bond to $H_2$ which is more than 6.5 kcal/mol stronger than that formed by the $^5F$ state, the ground state of the molecular complex will be a triplet as well. It is not clear without calculations if this will indeed be the case.

An additional consideration which also favors bonding to a $d^8$ state over bonding to an $s^1d^7$ state is the factor of charge transfer (Figure 1). This follows the Dewar-Chatt model[16] for bonding to alkenes (detailed in Chapter VIII). When coordinated perpendicular to the metal (the standard orientation is with the complex in the $yz$ plane with $z$ the principal axis), the $H_2$ bond ($\sigma_g$) acts as a two electron donor and lends charge to the *empty* $s$ orbital of the metal in $a_1$ symmetry (Figure 1$a$). This is accompanied by back-bonding involving charge transfer from the metal $d_{yz}$ to the empty $H_2$ antibonding orbital ($\sigma_u$) in $b_2$ symmetry (Figure 1$b$).

Since the metal is cationic, charge donation is expected to be more important than back-donation. However, back-donation should be most effective if the $d_{yz}$ orbital is doubly occupied rather than singly occupied. This is largely because of Hund's rule where the lowest energy states of metal atoms with between 5 and 10 $d$ electrons have all five $d$ orbitals with occupancies between 1 and 2 electrons. States which have empty $d$ orbitals are higher in energy. As a result, back-donation from a doubly occupied orbital of a cation in a $d^8$ configuration results in a dication in a $d^7$ configuration with two doubly occupied $d$ orbitals and three singly occupied $d$ orbitals–a favorable situation. Back-donation from a singly occupied orbital, however, results in a dication in a $d^7$ configuration with

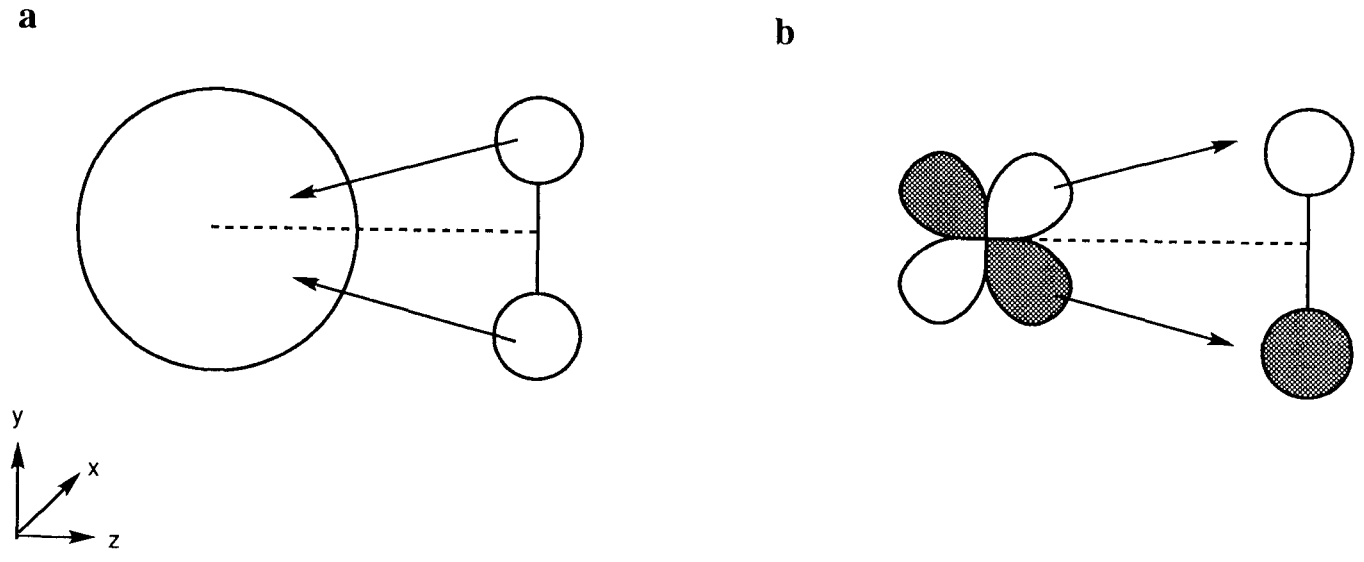


**Figure 1.** Charge transfer in $M(H_2)^+$ molecular complexes. (a) Donation from the $H_2$ $\sigma_g$ orbital to the empty *s* orbital of the metal in $a_1$ symmetry. (b) Back-donation from the metal $d_{yz}$ orbital to the empty $H_2$ $\sigma_u$ orbital in $b_2$ symmetry.

three doubly occupied $d$ orbitals, one singly occupied $d$ orbital, and one empty $d$ orbital–an unfavorable configuration. The situation is all the more favorable for back-donation from a doubly occupied orbital if one considers that this polarization of charge increases the exchange energy on the metal. The opposite is true with back-donation from a singly occupied orbital.

In sum, the $\eta^2$ dihydrogen molecular complex preferentially bonds to the metal ion in its $d^8$ configuration. The $b_2$ $d_{yz}$ orbital of the metal should be doubly occupied in order to maximize back-bonding. The occupations of the other $d$ orbitals should depend on their repulsion to the $H_2$ (*i.e.*, $d_{z^2} > d_{xz} > d_{x^2-y^2}$, $d_{xy}$). However, as was seen in Chapter III for the $MR^+$ species, the atomic coupling is an important factor in determining the occupations of non-bonding $d$ orbitals. As will be seen here, this is also the case for $M(H_2)^+$.

### 8.2.2 The dihydride complex

The bonding in the dihydride is shown schematically in Figure 2. For all three metals, the most favorable situation likely involves bonding to the $s^1d^7$ configuration (Figure 2*a*). Formation of two covalent bonds from the $s^1d^7$ configuration is best achieved through *sd* hybridization, where the $s+d_{yz}$ hybrid is directed toward one ligand and the $s-d_{yz}$ hybrid is directed toward the other. This leads to an H−M−H optimal angle of 90°. Since two of the metal orbitals are spin-paired to the ligands, the remaining two open shells of the metal lead to a ground state triplet for the insertion product. For $CoH_2^+$, this picture of *sd* hybridization is not quite correct and the nature of the problem will be detailed in Chapter VI. However, for the purposes of this investigation, the standard Molecular Orbital (MO) or Valence Bond (VB) pictures are adequate.

The bonding of two hydrogen atoms to the $s^1d^7$ state is an ideal situation for $Ir^+$ as *sd* hybridization has been shown to be particularly effective in $IrH^+$ and there is no promotion energy required to reach the bonding configuration. In fact, we can estimate the stability of the $IrH_2^+$ dihydride complex by using the bond energy for $IrH^+$ obtained in Chapter III and accounting for exchange energy losses. The $IrH^+$ bond is worth $D_e$=75 kcal/mol and the exchange energy loss associated with formation of this bond is approximately 19 kcal/mol ($K_{sd}$=12 kcal/mol and $K_{dd}$=14 kcal/mol and there is a loss of 1 $K_{sd}$ + $\frac{1}{2}$ $K_{dd}$ in the formation of an *sd* hybrid bond to an $s^1d^7$ state). This leads to an intrinsic bond strength of 94 kcal/mol. The exchange energy loss in $IrH_2^+$ is 32 kcal/mol (there is a loss of $\frac{3}{2}$ $K_{sd}$ + 1 $K_{dd}$ in the formation of one *s* bond and one *d* bond or two *sd* bonds). With an H−H bond energy of $D_e$=111 kcal/mol, we then expect $IrH_2^+$ to be stable by $D_e$=45 kcal/mol (2 × 94 − 32 − 111). A similar

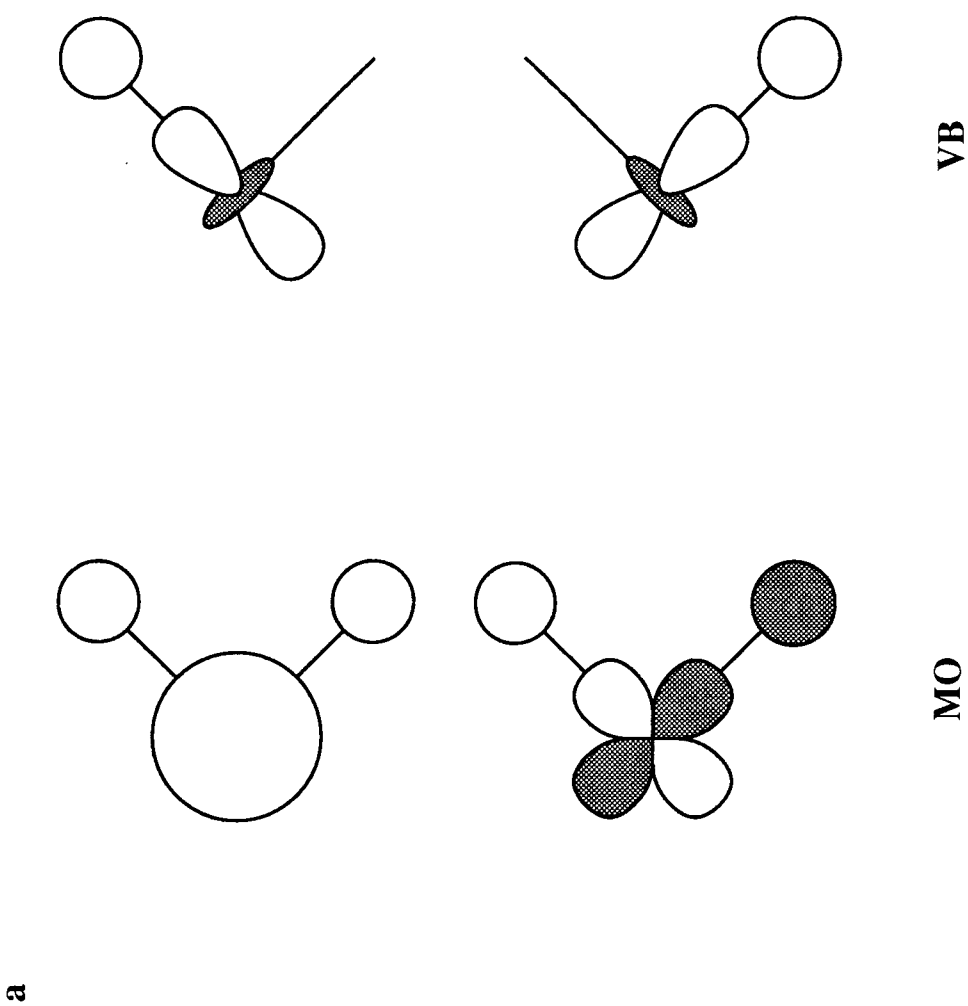
VB
MO
a

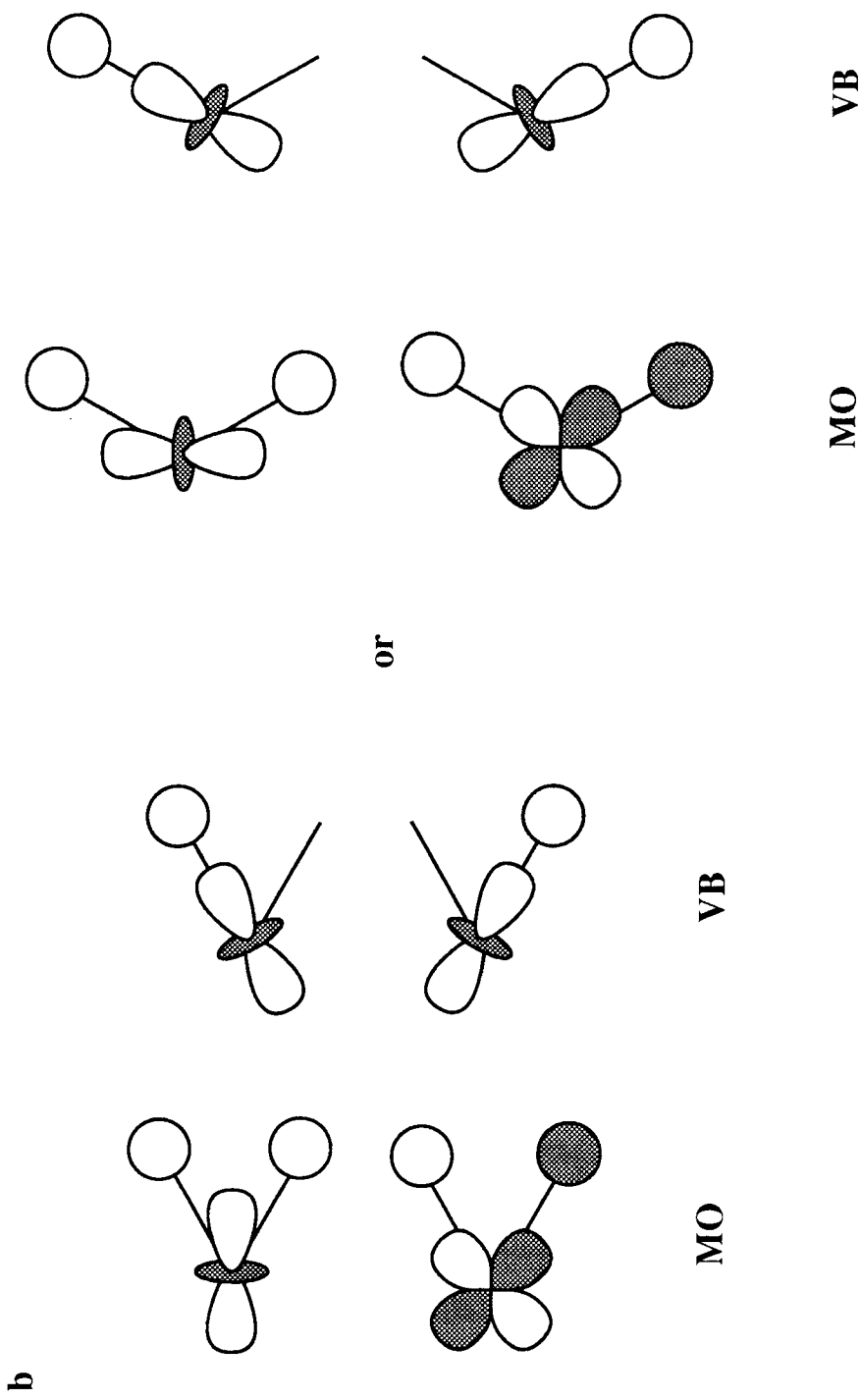
VB
MO
or
VB
MO
b

c

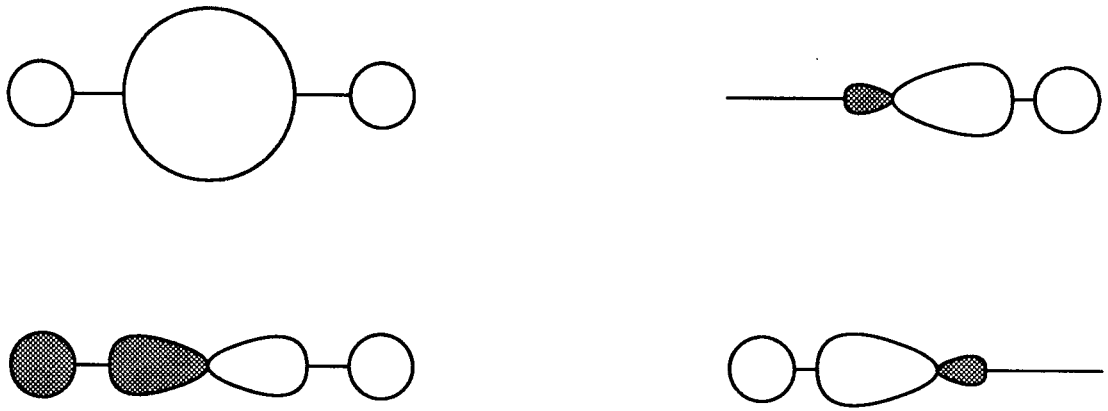

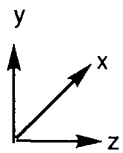


MO

VB

**Figure 2.** Bonding schemes in the $MH_2^+$ dihydride structures. (a) Bonding to an $s^1d^7$ state leads to *sd* hybridization. (b) Bonding to a $d^8$ state leads to *dd* hybridization. (c) Bonding to an $s^2d^6$ state leads to *sp* hybridization. Both Molecular Orbital (MO) and Valence Bond (VB) pictures are shown.

analysis for $CoH_2^+$ and $RhH_2^+$ suggests the insertion products are unbound. However, estimates for these numbers are not as reliable due to problems associated with rehybridization of the metal orbitals and the proper accounting of $K_{sd}$ loss vs. $K_{dd}$ loss.

Alternatively, bonding can also be achieved from the $d^8$ state through formation of pure $d$ bonds. This produces a singlet state. As was seen in Chapter III, however, these bonds are not as strong as the $sd$ hybrid bonds and of the three $MH_2^+$ complexes studied here, only $RhH_2^+$ is likely to have a singlet state of the dihydride which is competitive with the triplet states. This is a direct result of the 49.1 kcal/mol excitation energy associated with promotion to the $s^1d^7$ bonding configuration required in the formation of the triplet states.

The bonding to the $d^8$ configuration can be achieved through the formation of two $d_\sigma$ orbitals with an angle between them of either 54.74° or 125.26° (Figure 2*b*).[17] At these "magic" angles, a second orbital can be formed from the $d_{yz}$ and $d_{x^2-y^2}$ orbitals which has $d_\sigma$ character. The appropriate linear combination of these orbitals is

$$d'_\sigma = \sqrt{\frac{2}{3}}yz \pm \sqrt{\frac{1}{3}}(x^2 - y^2).$$

However, it should be recognized that such a state, while capable of forming the two strongest possible $d$ bonds, represents a mixture of the $^3$F and $^3$P states of the metal, as it can be considered $\frac{2}{3}$ $d_\sigma^1 d_\pi^3 d_\delta^4$ (which is 40% $^3$F and 60% $^3$P) and $\frac{1}{3}$ $d_\sigma^1 d_\pi^4 d_\delta^3$ (which is 100% $^3$F). Explicitly, this is then 60% $^3$F and 40% $^3$P. However, bonding to a pure $^3$F state entails formation of one bond to a $d_\sigma$ orbital and a second to a $d_\delta$ orbital at a bond angle of 90°. The $d_\delta$ bond is surely weaker and thus the relative strengths of $d_\sigma$ and $d_\delta$ bonds weighted against the partial $^3$F-$^3$P promotion determines whether the optimal H−M−H angle is closer to 54.74° or 125.26° or closer to 90°. Generally, this situation will have a tendency

to flatten the potential energy surface in the region between 60° and 120° but it can also lead to a double minimum.

As was done above for $IrH_2^+$, we can estimate the stability of the singlet state of $RhH_2^+$. From Chapter III, the doublet state of $RhH^+$ is bound by $D_e$=44 kcal/mol. Since this represents a pure $d$ bond, the intrinsic bond strength can be estimated at 52 kcal/mol ($K_{dd}$=16 kcal/mol and $\frac{1}{2}$ $K_{dd}$ is lost in bonding to the $d^8$ configuration). The promotion energy in forming a state which is 60% $^3$F and 40% $^3$P is 11 kcal/mol and a total of 8 kcal/mol is lost in exchange energy in $RhH_2^+$. Thus, the singlet state of the dihydride is unstable by 26 kcal/mol (2 $\times$ 52 − 11 − 8 − 111). While we do not consider the singlet potential energy surface here, we expect that a number of triplet states are lower lying.

Bonding to the $s^2d^6$ state of the metal could also be envisioned, leading to linear quintet dihydride structures (Figure 2$c$). Bonding is achieved through $sp$ hybrids as in $BeH_2$. However, the excitation energies to this state are so large (the $^3$F-$^5$D promotion energy is 116.0 kcal/mol for $Co^+$) that these quintet complexes should not be competitive and are not considered.

In summary, it is likely that the lowest lying dihydride structures are derived from the $^5$F $s^1d^7$ state of the metal. This involves bonding to the $a_1$ $s$ and $b_2$ $d_{yz}$ orbitals. The remaining six nonbonding $d$ electrons should be arranged so as to minimize repulsion to the ligands while best maintaining the atomic couplings. In the remainder of this chapter, we then consider the three lowest energy triplet surfaces in detail as a function of the H−M−H angle. This allows us to explore both the initial dihydrogen molecular complex and the product of oxidative addition, the dihydride complex, without involving the complication of a change of spin.

## 4.3 Results

We have performed MRCI+Q calculations on the $^3A_2$, $^3A_1$, and $^3B_1$ states of $CoH_2^+$, $RhH_2^+$, and $IrH_2^+$. Preliminary calculations on the $^3B_2$ and $^1A_1$ states of these complexes indicated they were higher in energy at geometries representative of both the dihydrogen molecular complex and the dihydride complex. These states were not investigated further. For $IrH_2^+$, we have also performed calculations on the four quintet states, $^5A_1$, $^5A_2$, $^5B_1$, and $^5B_2$, since these states correlate with the ground state of the metal. For each state studied, the minimum was rigorously optimized at the CI level in a point by point manner. Additional geometries were optimized as a function of the H−M−H angle. This required optimization of the M−H bond length for fixed angles of 50°, 70°, 90°, and 110° (for $IrH_2^+$, the angle of 30° was also investigated). Such a procedure provides a thorough picture of the process of oxidative addition for the three lowest energy states of the $MH_2^+$ complexes. The references used in the MRCI calculations for the three triplet states are given in Tables I-III.

Data on the minima for each state is presented in Figures 3-5. The entire potential energy curves encompassing the H−M−H angles from 0° to 110° are presented in Figures 6-8. Data on the quintet states of $IrH_2^+$ is given in Figure 9.

For each metal, the ground state of $MH_2^+$ is $^3A_2$. The reasons for this will be clarified in the next section. For $Co^+$ and $Rh^+$, insertion is an endothermic process with only the electrostatic dihydrogen molecular complexes forming bound minima. The lowest energy state of $CoH_2^+$ can insert into the $H_2$ bond up to an angle of 55° before crossing the threshold energy of the reactants. Similarly, $RhH_2^+$ can insert into the $H_2$ bond up to an angle of 50°. However, in

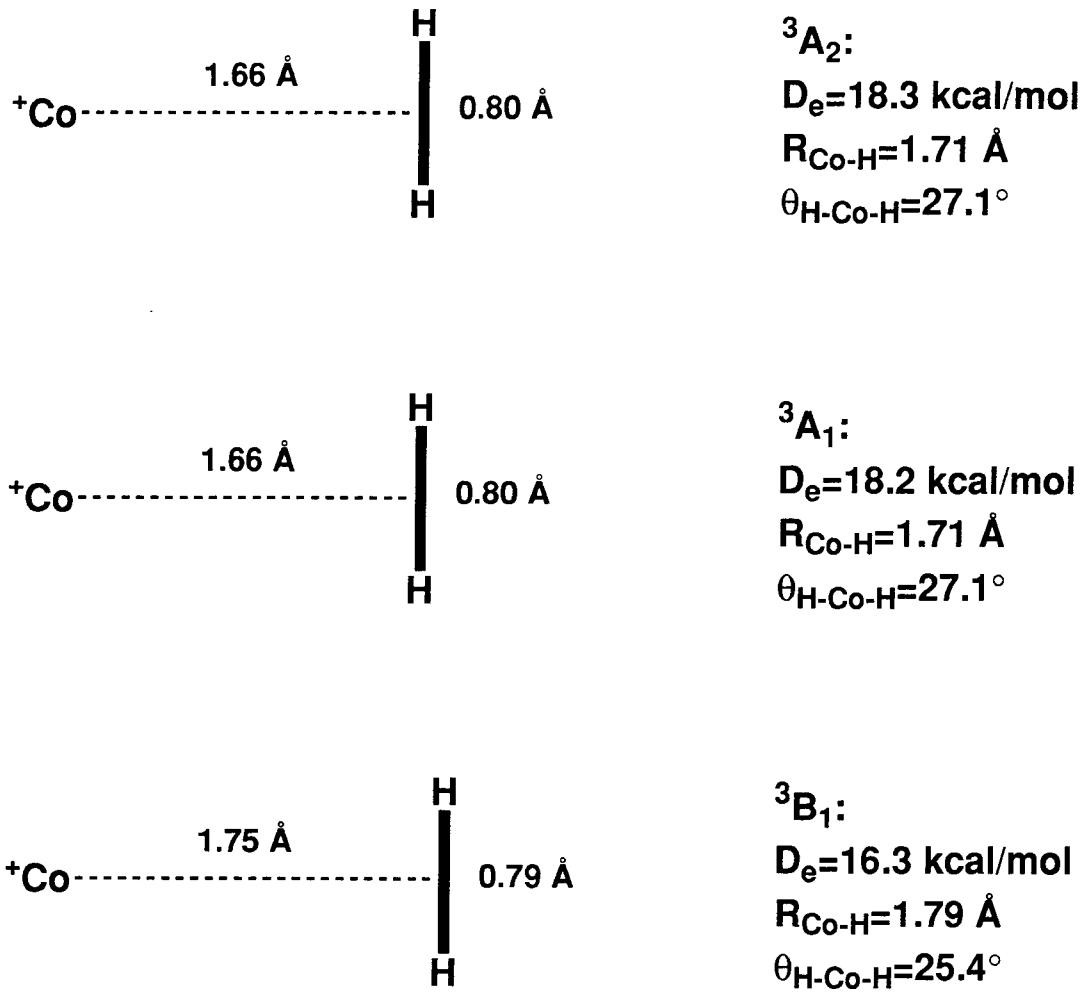


**Figure 3.** Bound minima for three states of $Co(H_2)^+$.

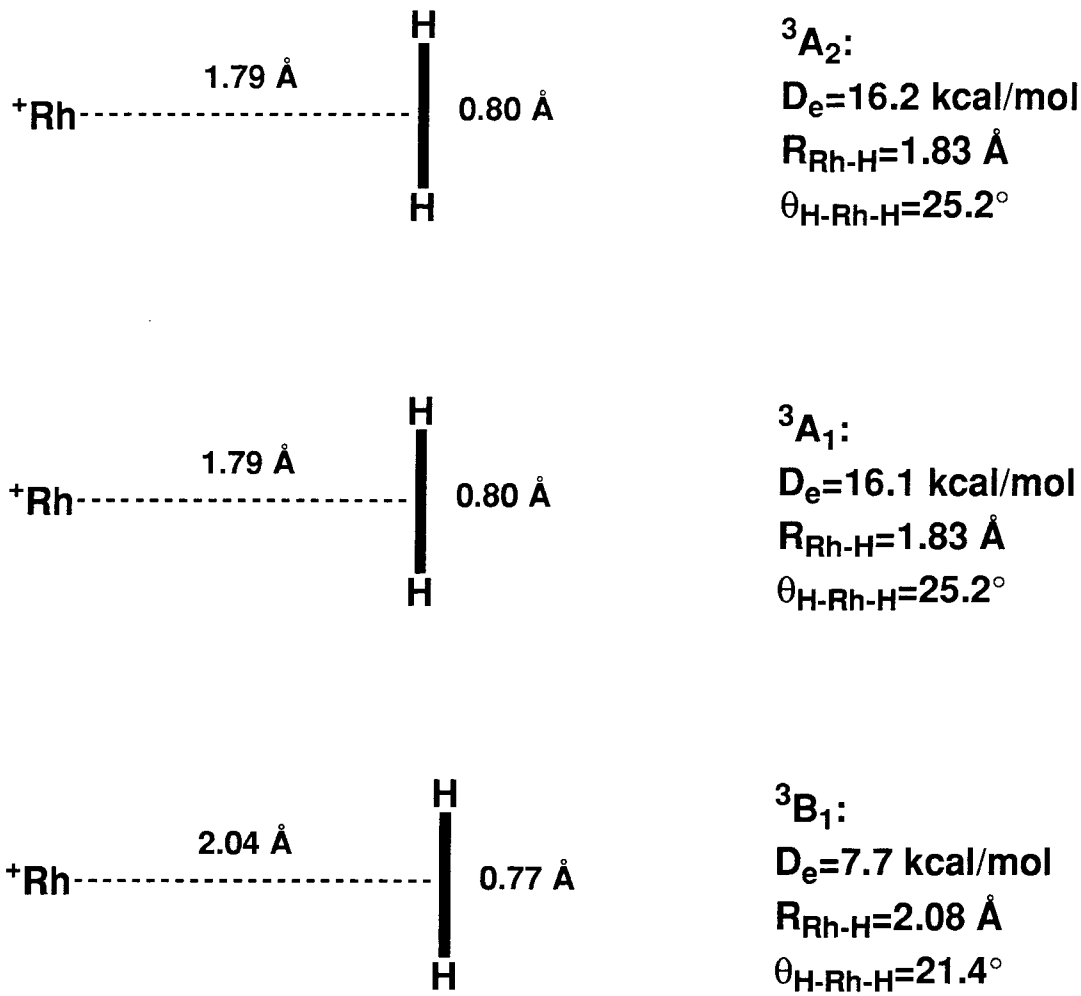


**Figure 4.** Bound minima for three states of $Rh(H_2)^+$.

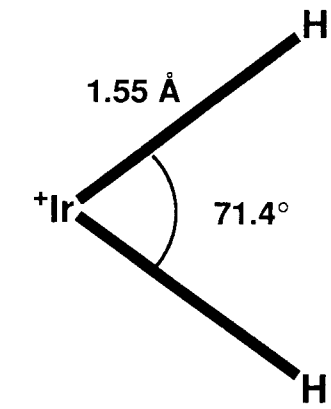


$^3A_2$:
$D_e$=41.3 kcal/mol
$R_{Ir\text{-}H_2}$=1.26 Å
$R_{H\text{-}H}$=1.81 Å

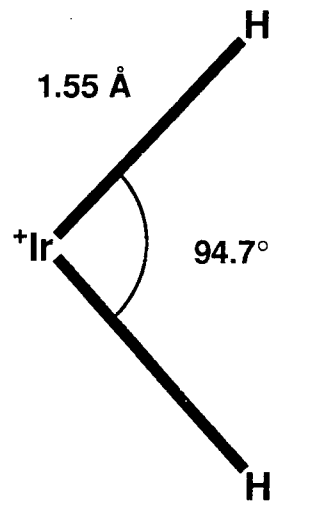


$^3B_1$:
$D_e$=37.6 kcal/mol
$R_{Ir\text{-}H_2}$=1.05 Å
$R_{H\text{-}H}$=2.28 Å

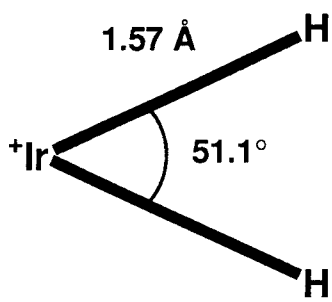


$^3A_1$:
$D_e$=35.6 kcal/mol
$R_{Ir\text{-}H_2}$=1.42 Å
$R_{H\text{-}H}$=1.35 Å

**Figure 5.** Bound minima for three states of $IrH_2^+$.

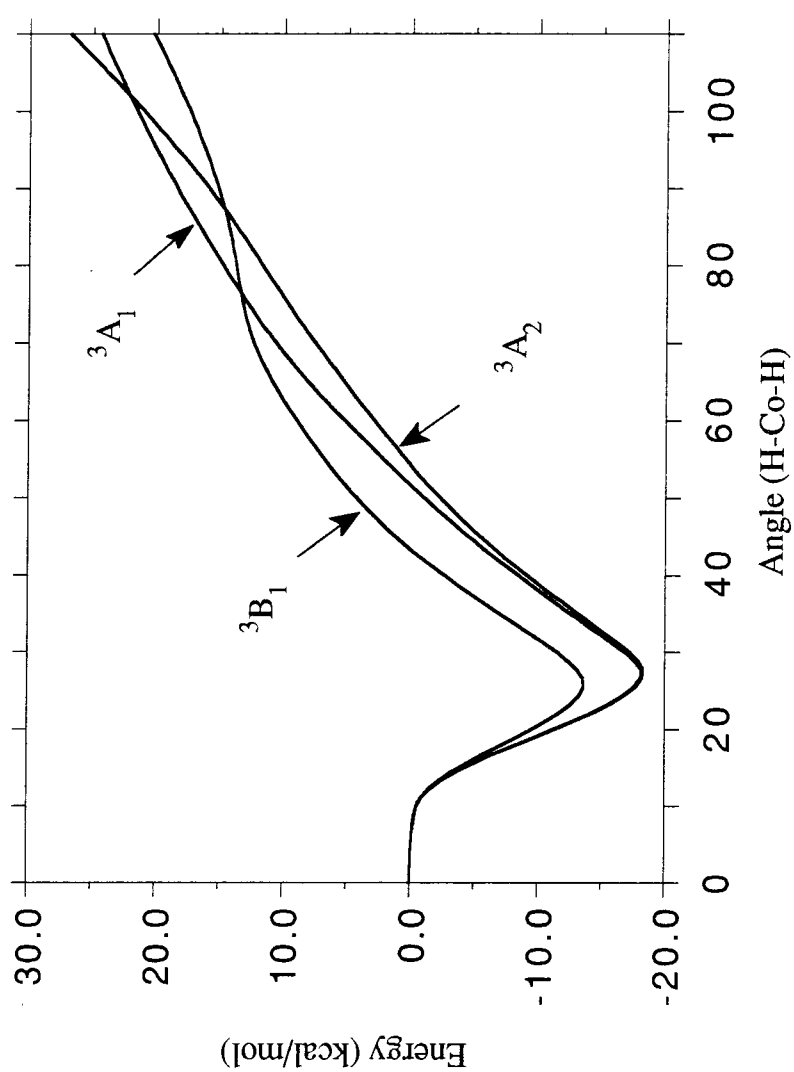


**Figure 6.** Potential energy curves for the three lowest energy states of $CoH_2^+$ as a function of the H-Co-H angle.

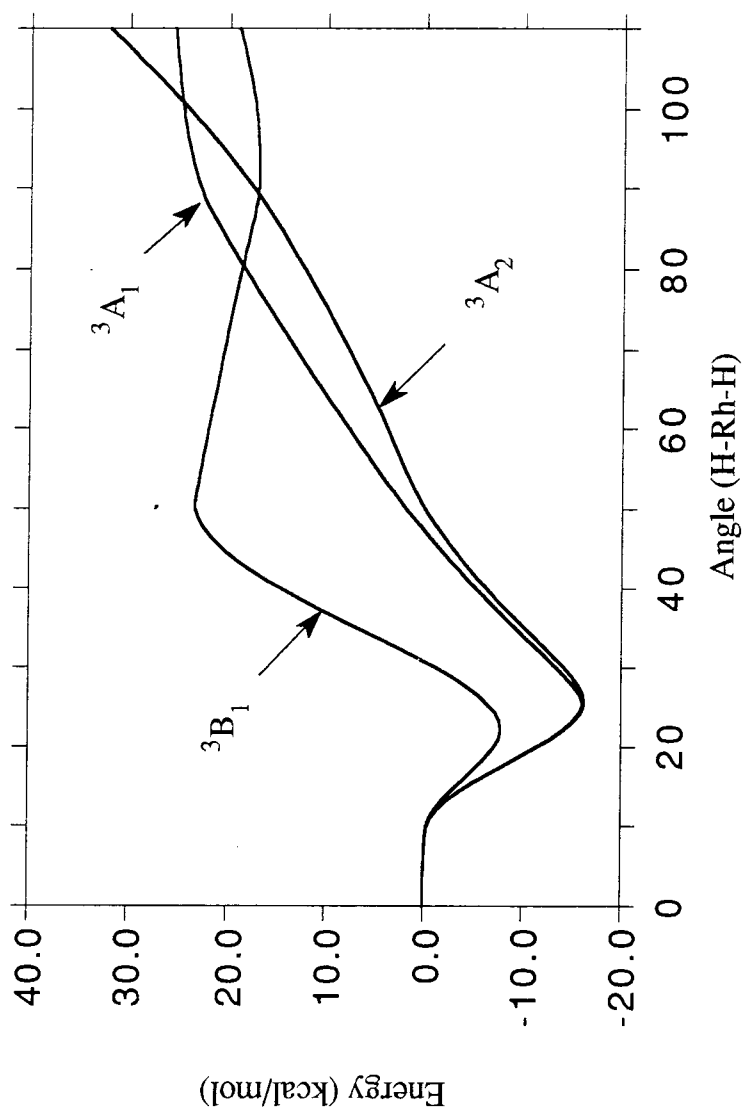


**Figure 7.** Potential energy curves for the three lowest energy states of $RhH_2^+$ as a function of the H-Rh-H angle.

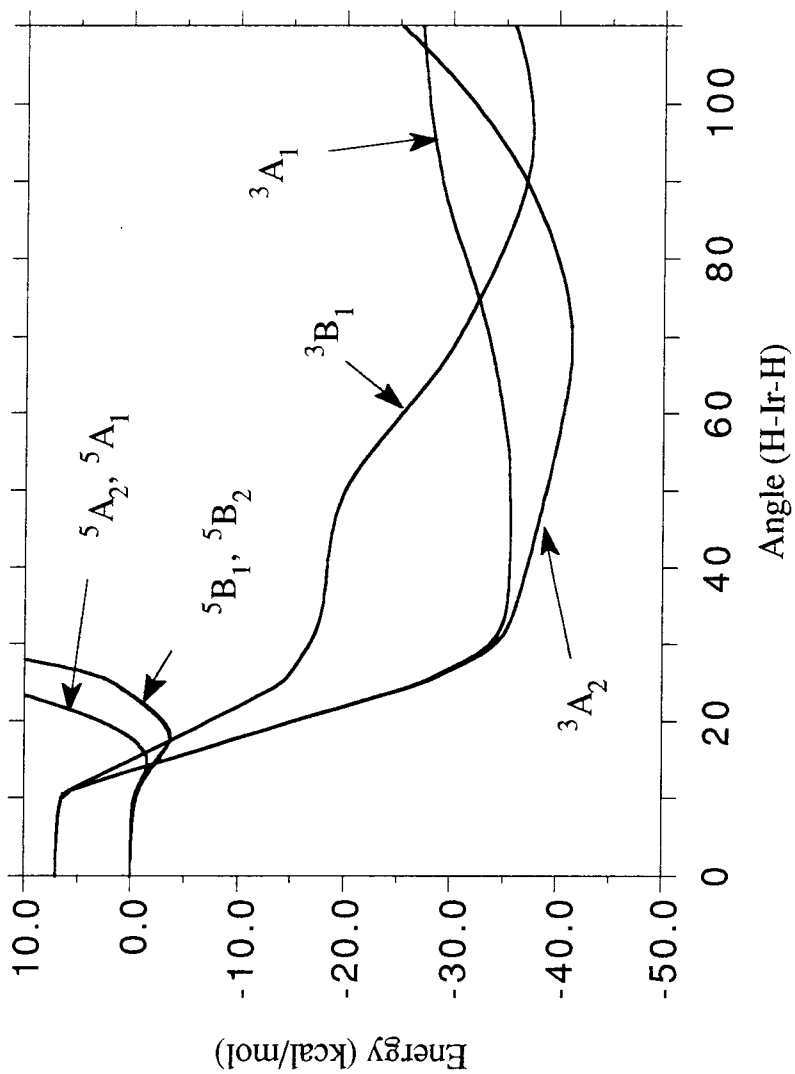


**Figure 8.** Potential energy curves for the three lowest energy states of $IrH_2^+$ as a function of the H-Ir-H angle. The four weakly bound quintet states are also shown.

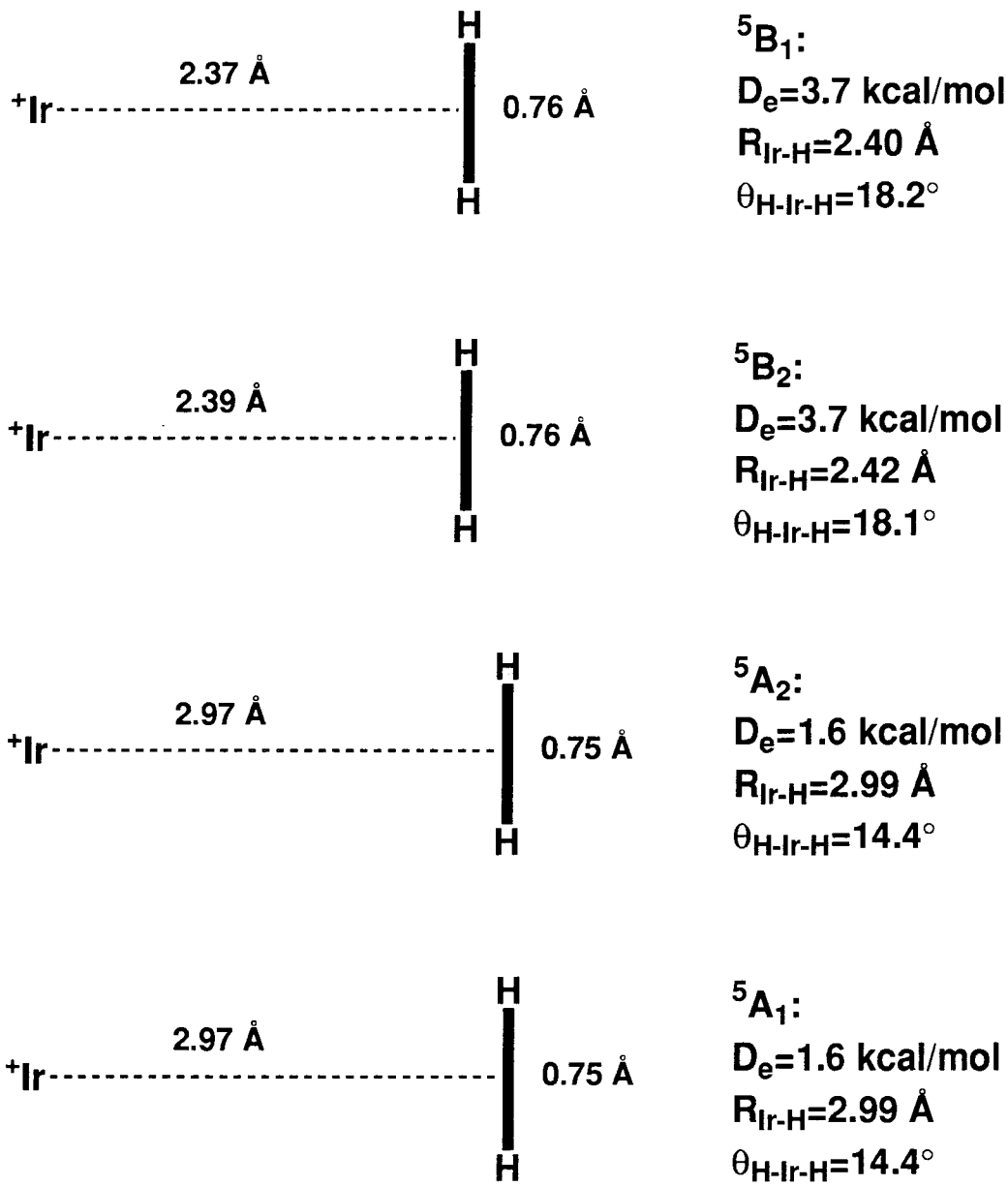


**Figure 9.** Quintet states of $Ir(H)_2^+$.

**Table I.** Configurations used as references in the MRCI calculations on the $^3A_2$ states of $MH_2^+$. $s$ and $p$ semi-core orbitals are designated as $1a_1$ $s$, $2a_1$ $p_z$, $1b_1$ $p_x$, and $1b_2$ $p_y$. The last configuration listed was used only for $RhH_2^+$.

| $3a_1$ $d_{x^2-y^2}$ | $2b_1$ $d_{xz}$ | $4a_1$ M-H H-H | $2b_2$ M-H $d_{yz}$ | $5a_1$ $d_{z^2}$ | $1a_2$ $d_{xy}$ | $3b_2$ M-H* H-H* | $6a_1$ M-H* $s$ |
|---|---|---|---|---|---|---|---|
| 2 | 2 | 2 | 2 | 1 | 1 | 0 | 0 |
| 2 | 2 | 2 | 0 | 1 | 1 | 2 | 0 |
| 2 | 2 | 0 | 2 | 1 | 1 | 2 | 0 |
| 2 | 2 | 0 | 2 | 1 | 1 | 0 | 2 |
| 2 | 2 | 1 | 1 | 1 | 1 | 1 | 1 |
| 2 | 2 | 2 | 1 | 1 | 1 | 1 | 0 |
| 2 | 2 | 1 | 2 | 1 | 1 | 0 | 1 |
| 2 | 2 | 1 | 1 | 2 | 1 | 1 | 0 |

**Table II.** Configurations used as references in the MRCI calculations on the $^3A_1$ states of $MH_2^+$. $s$ and $p$ semi-core orbitals are designated as $1a_1$ $s$, $2a_1$ $p_z$, $1b_1$ $p_x$, and $1b_2$ $p_y$. The last configuration listed was used only for $RhH_2^+$.

| $2b_1$ $d_{xz}$ | $1a_2$ $d_{xy}$ | $3a_1$ M-H H-H | $2b_2$ M-H $d_{yz}$ | $4a_1$ $d_{z^2}$ | $5a_1$ $d_{x^2-y^2}$ | $3b_2$ M-H* H-H* | $6a_1$ M-H* $s$ |
|---|---|---|---|---|---|---|---|
| 2 | 2 | 2 | 2 | 1 | 1 | 0 | 0 |
| 2 | 2 | 2 | 0 | 1 | 1 | 2 | 0 |
| 2 | 2 | 0 | 2 | 1 | 1 | 2 | 0 |
| 2 | 2 | 0 | 2 | 1 | 1 | 0 | 2 |
| 2 | 2 | 1 | 1 | 1 | 1 | 1 | 1 |
| 2 | 2 | 2 | 1 | 1 | 1 | 1 | 0 |
| 2 | 2 | 1 | 2 | 1 | 1 | 0 | 1 |
| 2 | 2 | 1 | 1 | 2 | 1 | 1 | 0 |

**Table III.** Configurations used as references in the MRCI calculations on the $^3B_1$ states of $MH_2^+$. $s$ and $p$ semi-core orbitals are designated as $1a_1$ $s$, $2a_1$ $p_z$, $1b_1$ $p_x$, and $1b_2$ $p_y$. The last configuration listed was used only for $RhH_2^+$.

| $3a_1$ $d_{x^2-z^2}$ | $1a_2$ $d_{xy}$ | $4a_1$ M-H H-H | $2b_2$ M-H $d_{yz}$ | $5a_1$ $d_{y^2}$ | $2b_1$ $d_{xz}$ | $3b_2$ M-H* H-H* | $6a_1$ M-H* $s$ |
|---|---|---|---|---|---|---|---|
| 2 | 2 | 2 | 2 | 1 | 1 | 0 | 0 |
| 2 | 2 | 2 | 0 | 1 | 1 | 2 | 0 |
| 2 | 2 | 0 | 2 | 1 | 1 | 2 | 0 |
| 2 | 2 | 0 | 2 | 1 | 1 | 0 | 2 |
| 2 | 2 | 1 | 1 | 1 | 1 | 1 | 1 |
| 2 | 2 | 2 | 1 | 1 | 1 | 1 | 0 |
| 2 | 2 | 1 | 2 | 1 | 1 | 0 | 1 |
| 2 | 2 | 1 | 1 | 2 | 1 | 1 | 0 |

neither case is insertion stable with respect to the molecular complex, and of the six total states for these two complexes, only the $^3B_1$ state of $RhH_2^+$ forms a metastable dihydride structure, and this is unbound by 17 kcal/mol. The barrier for reductive elimination of $H_2$ from this state is 6 kcal/mol with respect to the dihydride. For the two other states of $RhH_2^+$ and all three states of $CoH_2^+$, there is no barrier to reductive elimination of $H_2$ from geometries consistent with a dihydride.

In contrast, for $Ir^+$, insertion is strongly exothermic for all three triplet states. The $^3A_1$ state inserts to the smallest angle minimum ($\theta_{H-Ir-H}$=51.1°), with the $^3A_2$ state leading to a minimum at an angle of 71.4° and the $^3B_1$ state leading to a minimum at an angle of 94.7°. In no case is there a barrier to oxidative addition, although the $^3B_1$ state exhibits a plateau in the region between 30° and 50°. The quintet states form only weakly bound electrostatic minima

and the triplet states are expected to cross these states below the threshold energy. With the strong spin-orbit coupling of the third row metal, the change of spin is expected to be facile and insertion should occur from the ground state of $Ir^+$.

While it is perhaps not too surprising, based on the $M^+-H$ bond strengths, that insertion is exothermic for $Ir^+$ but endothermic for $Co^+$ and $Rh^+$, the well depths for the molecular complexes of $Co(H_2)^+$ and $Rh(H_2)^+$ are deeper than anticipated. This will be discussed in the next section, as will the factors leading to the ordering of the states at various points along the potential energy curves and the factors leading to the optimal $IrH_2^+$ geometries.

## 4.4 Discussion

Since our estimated value for the stability of the $IrH_2^+$ complex was 45 kcal/mol, in excellent agreement with the calculated exothermicity of $\grave{D}_e$=41.3 kcal/mol, it is clear that the trend in the energetics for the dihydride structures is closely related to the $M^+-H$ bond strengths for this metal. For the dihydrogen molecular complexes of the other two metals, it is then reasonable to ask to what extent the electrostatic components of the ion-induced dipole and ion-quadrupole contribute to the bond energy. This is assessed in Table IV. For both $CoH_2^+$ and $RhH_2^+$, the electrostatic interactions calculated at the optimum geometries are in good agreement with the MRCI bond energies (assuming a charge on the metal of +1.0 e.s.u.). In particular, approximately $\frac{3}{4}$ of the bond energy is derived from the charge-induced dipole. This is perhaps surprising given the relatively low polarizability of $H_2$. However, it is the balance of the electrostatic attractions with the Pauli repulsion which determines the bond strength, and the proximity of the molecule to the ion in these cases leads to a strong interaction.

It is reasonable to assume that since the bonding is electrostatic in origin it would be well described at the HF level of theory. As can be seen in Table V, this is not the case. The HF level can account for less than half the bond energy in the $^3A_2$ state of $Co(H_2)^+$. This is largely because the $Co-H_2$ bond length is ~0.3 Å too long. At the optimum HF geometry, the ion-induced dipole is worth 8.4 kcal/mol and the ion-quadrupole is worth 3.0 kcal/mol, for a total estimated bond energy of 11.4 kcal/mol. This can be compared to the calculated bond energy of $D_e$=8.1 kcal/mol. While HF could underestimate the electrostatic contributions to the bonding and thereby lead to a longer bond length,

**Table IV.** Electrostatic components to the bonding in $Co(H_2)^+$ and $Rh(H_2)^+$, calculated at the optimum geometries for the $^3A_2$, $^3A_1$, and $^3B_1$ states, and compared to the MRCI+Q bond energy (in kcal/mol).

| | $Co(H_2)^+$ | | | $Rh(H_2)^+$ | | |
|---|---|---|---|---|---|---|
| | $^3A_2$ | $^3A_1$ | $^3B_1$ | $^3A_2$ | $^3A_1$ | $^3B_1$ |
| $E_\alpha$ | 15.7 | 15.7 | 12.7 | 11.6 | 11.6 | 6.9 |
| $E_\theta$ | 4.8 | 4.8 | 4.1 | 3.8 | 3.8 | 2.6 |
| $E_{Total}$ | 20.5 | 20.5 | 16.8 | 15.4 | 15.4 | 9.5 |
| $D_e$ | 18.3 | 18.2 | 16.3 | 16.2 | 16.1 | 7.7 |

**Table V.** Comparison of HF, MCPF, and MRCI+Q properties for the $^3A_2$ state of $Co(H_2)^+$.

| | HF | MCPF | MRCI+Q |
|---|---|---|---|
| $D_e$ (kcal/mol) | 8.1 | 17.2 | 18.3 |
| $r_e$ (Co–$H_2$, Å) | 1.94 | 1.69 | 1.66 |
| $r_e$ (H–H, Å) | 0.75 | 0.79 | 0.80 |
| $\omega_e$ (Co–$H_2$, $cm^{-1}$) | 560 | 902 | 909 |
| $\omega_e$ (H–H, $cm^{-1}$) | 4340 | 3710 | 3580 |
| $\mu$ (D) [a] | +0.714 | +0.323 | +0.384 |

[a] The dipole moment was calculated with the $Co^+$ at the origin. The positive sign indicates charge transfer from $H_2$ to the $Co^+$.

the dominant reason for the longer bond length (and consequently weaker bond) is due to a repulsion between the ion and $H_2$ which is reduced at the CI level.

Reduction in repulsion is achieved through charge donation and back-donation. In a comparison of properties of the HF and MRCI wavefunctions at the MRCI optimum geometry, it is clear that HF underestimates the extent of back-donation, leading to a Mulliken population for the $3d$ shell of 7.980 electrons compared to 7.932 electrons at the CI level. The reduced back-donation is further evidenced by the dipole moment, which is too large at the HF level (+0.489 compared to +0.384 D), reflecting a situation in which the balance of charge transfer is weighted too heavily in favor of donation from ligand to metal. This leads to too large a positive charge on the $H_2$ which is repulsive to the metal ion. The CI level is able to properly account for the back-donation, perhaps because the method can describe the spin-polarization of the $d_{yz}$ charge, threreby increasing the exchange energy on the metal and making charge transfer more favorable.

From Table VI, another influence on the bond lengths, and thus the bond strengths, can be seen in the complete Mulliken population analysis for the metal orbitals of these complexes. There is a great deal of information in this table, from which an understanding of the ordering of states for the molecular complex can be obtained, as well as an understanding of the geometries of the dihydride complexes of $IrH_2^+$ and the curve crossings for all three metals. In regard to the dihydrogen molecular complexes, one should consider the occupations of the $d$ orbitals. From the description of back-bonding given previously, the $b_2$ $d_{yz}$ orbital should be doubly occupied in all states. It is then reasonable to assume that among the other $d$ orbitals, the repulsion to the ligand follows the trend $d_{z^2} >> d_{xz} > d_{x^2-y^2}$, $d_{xy}$. For $Co(H_2)^+$ and $Rh(H_2)^+$, the $d_{z^2}$ orbital has an

**Table VI.** Mulliken population analysis for the metal orbitals of the $^3A_2$, $^3A_1$, and $^3B_1$ minima of $MH_2^+$, M = Co, Rh, and Ir.

| | $Co(H_2)^+$ | | |
|---|---|---|---|
| | $^3A_2$ | $^3A_1$ | $^3B_1$ |
| $s$ | 0.141 | 0.141 | 0.145 |
| $p$ | 0.124 | 0.124 | 0.116 |
| $d$ | 7.932 | 7.933 | 7.909 |
| $d_{z^2}$ | 1.028 | 1.027 | 1.715 |
| $d_{yz}$ | 1.929 | 1.930 | 1.948 |
| $d_{xz}$ | 1.986 | 1.986 | 0.997 |
| $d_{x^2-y^2}$ | 1.990 | 0.998 | 1.256 |
| $d_{xy}$ | 0.998 | 1.992 | 1.992 |
| | $Rh(H_2)^+$ | | |
| | $^3A_2$ | $^3A_1$ | $^3B_1$ |
| $s$ | 0.136 | 0.136 | 0.091 |
| $p$ | 0.100 | 0.100 | 0.084 |
| $d$ | 7.909 | 7.909 | 7.908 |
| $d_{z^2}$ | 1.036 | 1.034 | 1.658 |
| $d_{yz}$ | 1.919 | 1.920 | 1.958 |
| $d_{xz}$ | 1.976 | 1.976 | 0.993 |
| $d_{x^2-y^2}$ | 1.983 | 0.995 | 1.314 |
| $d_{xy}$ | 0.995 | 1.984 | 1.984 |
| | $Ir(H_2)^+$ | | |
| | $^3A_2$ | $^3A_1$ | $^3B_1$ |
| $s$ | 0.846 | 0.696 | 0.891 |
| $p$ | 0.156 | 0.149 | 0.141 |
| $d$ | 7.391 | 7.499 | 7.304 |
| $d_{z^2}$ | 1.400 | 1.083 | 1.932 |
| $d_{yz}$ | 1.333 | 1.488 | 1.250 |
| $d_{xz}$ | 1.969 | 1.959 | 0.992 |
| $d_{x^2-y^2}$ | 1.697 | 0.994 | 1.160 |
| $d_{xy}$ | 0.992 | 1.975 | 1.970 |

occupancy near 1.0 electron for the $^3A_2$ and $^3A_1$ states. However, for the $^3B_1$ state, the occupation of the $d_{z^2}$ orbital is ~1.7 electrons. Thus, it is easy to see that the increased repulsion along the $z$ axis results in a longer bond length for this state and a weaker bond.

The problem at hand is then to understand why the occupation of the $d_{z^2}$ orbital is higher for the $^3B_1$ state than for the other two. The reason behind this involes the subtlety of atomic couplings outlined in Chapter III. Given the restriction that the $b_2$ $d_{yz}$ orbital should be doubly occupied in order to maximize back-bonding, the occupations of the remaining $d$ orbitals are limited if a pure $^3F$ state is to be achieved. For the $^3A_2$ state, the configuration,

$$(a_1 d_{x^2-y^2})^2 (b_1 d_{xz})^2 (b_2 d_{yz})^2 (a_1 d_{z^2})^1 (a_2 d_{xy})^1,$$

satisfies these conditions while having the repulsive $d_{z^2}$ orbital singly occupied. For the $^3A_1$ state, the situation is similar with the configuration,

$$(a_2 d_{xy})^2 (b_1 d_{xz})^2 (b_2 d_{yz})^2 (a_1 d_{z^2})^1 (a_1 d_{x^2-y^2})^1.$$

However, with the $^3B_1$ state, the only way to satisfy the restriction of having the $d_{yz}$ orbital doubly occupied while maintaining the $^3F$ coupling of the metal is to effectively rotate the $\sigma$ axis of the metal atom by 90° such that the $d_{y^2}$ orbital is then the $\sigma$ orbital and the $d_{x^2-z^2}$ and $d_{xz}$ orbitals are $\delta$ orbitals. Such a rotation of the orbitals is valid under the $C_{2v}$ symmetry of the $MH_2^+$ complexes. Thus, the configuration,

$$(a_1 d_{x^2-z^2})^2 (a_2 d_{xy})^2 (b_2 d_{yz})^2 (a_1 d_{y^2})^1 (b_1 d_{xz})^1,$$

characterizes the metal in the $^3B_1$ state of the dihydrogen complexes and the increased occupation of the $z^2$ component as a result leads to increased repulsion.

The only other alternatives for the $^3B_1$ state are to singly occupy the $d_{z^2}$ orbital and either: (1) reduce the occupation of the $d_{yz}$ orbital in a multi-configurational description of the pure $^3F$ state, or (2) introduce $^3P$ character into the wavefunction. Neither of these options appears to be a viable alternative. Such considerations explain why the $^3B_2$ state is not competitive with the other triplets. In this state, either the $d_{yz}$ orbital will have an occupation of less than 2 electrons or significant $^3P$ character will be mixed into the wavefunction. The weakness of this bond in particular then underscores the importance of back-bonding in these dihydrogen molecular complexes.

A similar analysis can be made for states of the dihydrides of $IrH_2^+$. In the simple view of the bonding on the triplet surfaces, as the H−Ir−H angle increases, donation of charge to the $s$ orbital increases as does back-donation of charge from the $d_{yz}$ orbital. (In the extreme, this converts the $d^8$ configuration of the metal, with an empty $s$ orbital and a doubly occupied $d_{yz}$ orbital, to the $s^1d^7$ configuration, with a singly occupied $s$ orbital and a singly occupied $d_{yz}$ orbital.) For the dihydride, two covalent bonds are formed to the hydrogens using these orbitals. Looking at the coupling on the metal atom, given the restriction that the $b_2$ $d_{yz}$ orbital should then be *singly* occupied, it is necessary to determine what orbital configurations lead to a pure $^5F$ state of the metal.

For the $^3A_2$ state of $IrH_2^+$, such a configuration is

$$(a_1 d_{y^2})^2 (b_1 d_{xz})^2 (a_1 d_{x^2-z^2})^1 (b_2 d_{yz})^1 (a_2 d_{xy})^1 (a_1 s)^1,$$

with the $d_{y^2}$ orbital doubly occupied. For the $^3B_1$ state, such a configuration is

$$(a_1 d_{z^2})^2 (a_2 d_{xy})^2 (a_1 d_{x^2-y^2})^1 (b_1 d_{xz})^1 (b_2 d_{yz})^1 (a_1 s)^1,$$

with the $d_{z^2}$ orbital doubly occupied. These occupations can be verified by inspection of the Mulliken population data presented in Table VI. For the $^3A_2$

state, the occupations of the $d_{z^2}$ and $d_{x^2-y^2}$ orbitals are 1.4 and 1.7 electrons, respectively, suggesting extensive hybridization of the $d_{z^2}$ and $d_{x^2-y^2}$ orbitals (*i.e.*, a reorientation of the atomic $\sigma$ axis). For the $^3B_2$ state, the occupations of the $d_{z^2}$ and $d_{x^2-y^2}$ orbitals are 1.9 and 1.2 electrons, respectively, suggesting little hybridization between these orbitals.

It should be recognized that at the H−M−H angle of 90°, the $y^2$ component is equally as repulsive to the two hydrogens as the $z^2$ component. With this in mind, it can be seen that the $^3A_2$ state (with the doubly occupied $d_{y^2}$ orbital) should have an optimum angle less than 90° while the $^3B_1$ state (with the doubly occupied $d_{z^2}$ orbital) should have an optimum angle greater than 90°. Moreover, the two states should cross in the vicinity of 90°. As can be seen in Figures 5 and 8, the optimal angle for the $^3A_2$ state is 71.4° and the optimal angle for the $^3B_1$ state is 94.7° and the two curves cross at 90°. In both cases, the optimal angle is shifted more acutely by mixing in the resonance of the $d^8$ molecular complex.

For $CoH_2^+$ and $RhH_2^+$, the $^3A_2$ and $^3B_1$ curves also cross in the vicinity of 90° for identical reasons (Figures 6 and 7). Furthermore, it should be noted that, as the H−M−H angle decreases for the $^3B_1$ state, repulsion to the doubly occupied $d_{z^2}$ orbital increases. This is the origin of the barrier on the $^3B_1$ curve for $RhH_2^+$ (Figure 7).

Finally, for the $^3A_1$ state of $IrH_2^+$, no pure $^5F$ state can be formed subject to the restriction that the $b_2$ $d_{yz}$ orbital be singly occupied. Consequently, the configuration,

$$(a_2 d_{xy})^2 (b_1 d_{xz})^2 (a_1 d_{z^2})^1 (a_1 d_{x^2-y^2})^1 (b_2 d_{yz})^1 (a_1 s)^1,$$

is 80% $^3F$ and 20% $^3P$, and the $^3A_1$ state is destabilized relative to the $^3A_2$

and $^3B_1$ states upon insertion. As a result, this state mixes in more of the $d^8$ molecular complex resonance than the other two states and the optimal angle is acute at 51.1°. Note that for all three metal complexes, the $^3A_2$ and $^3A_1$ states cross at an angle between 100° and 110°. This is because repulsion to the doubly occupied $d_{y^2}$ orbital rises rapidly in the $^3A_2$ state for angles greater than 90°. This is not an issue for the $^3A_1$ state, where the $z^2$ and $y^2$ components have equal occupations, and thus the curve rises more slowly in this region.

## 4.5 Conclusions

We have examined the three lowest lying potential energy surfaces of $CoH_2^+$, $RhH_2^+$, and $IrH_2^+$. Only in the case of $IrH_2^+$ do we find insertion into the H−H bond to be an exothermic (and barrierless) process. This is a direct result of the strong $IrH^+$ bond detailed in Chapter III. This oxidative addition requires a change of spin from quintet to triplet and we find the curve crossing to occur at a relatively long Ir−$H_2$ distance. We expect that the strong spin-orbit coupling of the third row transition metal will make this change of spin quite efficient.

For $CoH_2^+$ and $RhH_2^+$, insertion into the H−H bond is endothermic and only the dihydrogen molecular complexes are stable. While the bonding in these complexes is dominated by the electrostatic interactions of an ion-induced polarization and an ion-quadrupole, the influence of charge donation and back-donation cannot be ignored. This charge transfer serves to reduce the M−$H_2$ distance and thereby increase the electrostatic attraction.

A careful analysis of the wavefunctions for the $^3A_2$, $^3A_1$, and $^3B_1$ states of these complexes reveals the importance of maintaining the appropriate atomic coupling in regards to the ordering of these states. In the molecular complex limit, bonding is to the $d^8$ configuration of the ion. The $^3F$ coupling of the metal then leads to a favorable configuration of electrons in the $^3A_2$ and $^3A_1$ states but a more repulsive configuration in the $^3B_1$ state. In the dihydride limit, bonding is instead to the $s^1d^7$ configuration of the ion. The $^5F$ coupling of the metal then leads to a favorable configuration of electrons in the $^3A_2$ state for an H−M−H angle less than 90° and a favorable configuration of electrons in the $^3B_1$ state for an H−M−H angle greater than 90°. For the $^3A_1$ state, considerable mixing of the $^5P$ atomic coupling into the wavefunction is seen and the state is higher

in energy than the other two states in the vicinity of 90°.

This simple model of oxidative addition bodes well for alkane activation by $Ir^+$, where C–H and C–C insertions should be important, if not rate determining, processes. For $Co^+$ and $Rh^+$, it appears that oxidative addition is unfavorable and alkane activation should be more difficult with these metals.

## Appendix

Standard procedures were used for the calculations presented in this chapter. Note, however, that the two $p$ polarization functions used on the hydrogens had exponents of 1.4 and 0.5, optimized at the HFSD level for $H_2$.

**References**

(1) Bauschlicher, C.W.; Partridge, H.; Langhoff, S.R. *J. Phys. Chem.* **1992**, *96*, 2475.

(2) Das, K.K.; Balasubramanian, K. *J. Phys. Chem.* **1992**, *95*, 6880.

(3) Balasubramanian, K.; Dai, D. *J. Chem. Phys.* **1990**, *93*, 7243.

(4) Zhang, H.; Balasubramanian, K. *J. Phys. Chem.*, **1992**, *96*, 6981.

(5) (a) Alvarado-Swaisgood, A.E.; Harrison, J.F. *J. Phys. Chem.* **1985**, *89*, 5198. (b) Rappe; A.K.; Upton, T.H. *J. Chem. Phys.* **1986**, *85*, 4400.

(6) Mavridis; A.; Harrison, J.F. *J. Chem. Soc. Faraday Trans. 2* **1989**, *85*, 1391.

(7) (a) Schilling, J.B.; Goddard, W.A., III; Beauchamp, J.L. *J. Phys. Chem.* **1987**, *91*, 4470. (b) Rivera, M.; Harrison, J.F.; Alvarado-Swaisgood, A. *J. Phys. Chem.* **1990**, *94*, 6969.

(8) (a) Das, K.K.; Balasubramanian, K. *J. Chem. Phys.* **1989**, *91*, 2433. (b) Das, K.K.; Balasubramanian, K. *J. Chem. Phys.* **1989**, *91*, 6254. (c) Das, K.K.; Balasubramanian, K. *J. Chem. Phys.* **1990**, *92*, 6697. (d) Knight, L.B.; Cobranchi, S.T.; Herlong, J.; Kirk, T.; Balasubramanian, K.; Das, K.K. *J. Chem. Phys.* **1990**, *92*, 2721.

(9) (a) Dai, D.; Balasubramanian, K. *Chem. Phys. Lett.* **1991**, *185*, 165. (b) Das, K.K.; Balasubramanian, K. *J. Chem. Phys.* **1991**, *94*, 3722.

(10) Kemper, P.R.; Bushnell, J.; von Helden, G.; Bowers, M.T. *J. Phys. Chem.* **1993**, *97*, 52.

(11) (a) Elkind, J.L.; Armentrout, P.B. *J. Am. Chem. Soc.* **1986** *108*, 2765. (b) Georgiadis, R.; Armentrout, P.B. *J. Phys. Chem.* **1988**, *92*, 7060. (c) Elkind, J.L.; Sunderlin, L.S.; Armentrout, P.B. *J. Phys. Chem.* **1989**, *93*, 3151. (d) Tolbert, M.A.; Beauchamp, J.L. *J. Am. Chem. Soc.* **1984**, *106*, 8117. (e) Elkind, J.L.; Armentrout, P.B. *Int. J. Mass Spectrom. Ion Processes* **1988**, *83*, 259. (f) Elkind, J.L.; Armentrout, P.B. *J. Phys. Chem.* **1985**, *89*, 5626. (g) Elkind, J.L.; Armentrout, P.B. *J. Chem. Phys.* **1987**, *86*, 1868. (h) Elkind, J.L.; Armentrout, P.B. *J. Chem. Phys.* **1986**, *84*, 4862. (i) Elkind, J.L.; Armentrout, P.B. *J. Phys. Chem.* **1986**, *90*, 5736. (j) Halle, L.F.; Klein, F.S.; Beauchamp, J.L. *J. Am. Chem. Soc.* **1984**, *106*, 2543. (k) Armentrout, P.B.; Beauchamp,

J.L. *J. Am. Chem. Soc.* **1981**, *103*, 784. (l) Elkind, J.L.; Armentrout, P.B. *J. Phys. Chem.* **1986**, *90*, 6576. (m) Armentrout, P.B.; Beauchamp, J.L. *Chem. Phys.* **1980**, *50*, 37.

(12) (a) Elkind, J.L.; Armentrout, P.B. *Inorg. Chem.* **1986**, *25*, 1078. (b) Mandich, M.L.; Halle, L.F.; Beauchamp, J.L. *J. Am. Chem. Soc.* **1984**, *106*, 4403.

(13) Kubas, G.J.; Ryan, R.R.; Swanson, B.I.; Vergamini, P.J.; Wasserman, H.J. *J. Am. Chem. Soc.* **1984**, *106*, 451.

(14) Low, J.J.; Goddard, W.A., III *Organometallics* **1986**, *5*, 609.

(15) Davies, D.W. *Theory of the Electric and Magnetic Properties of Molecules*; Wiley: New York, 1967.

(16) Crabtree, R.H. *The Organometallic Chemistry of the Transition Metals*; Wiley: New York, 1988, Chap. 5.

(17) (a) Pauling, L. *The Nature of the Chemical Bond, Ed. 3*; Cornell Univ.: Ithaca, N.Y., 1960, p. 152. (b) Rappe; A.K., Ph.D. thesis, California Institute of Technology, 1981.

Chapter V

# Molecular Complexes of Transition Metal Cations with Small Alkanes

# Chapter V

# Molecular Complexes of Transition Metal Cations with Small Alkanes

## 5.1 Introduction

There are two principal motivations for studying ion-molecule complexes. The first is to understand the nature of solvation. The second is to understand how M(alkane)$^+$ complexes function as precursors to activation of C−C and C−H bonds. The effect of spin and geometric coordination on complexation energies is particularly important to discussions of both of these topics. For instance, of principal concern to the issue of solvation is the variation in sequential bond energies of M(alkane)$_x^+$ species. The key to understanding this problem is the determination of how one ligand alters the electronic structure of the metal ion and thereby affects the complexation energy of the next ligand. As to the role of M(alkane)$^+$ complexes as precursors to alkane activation, it is desirable to know how these cluster well depths vary as a function of alkane size. Experiments have found that $Co^+$ is unreactive toward $CH_4$ and $C_2H_6$, slowly eliminates $H_2$ and $CH_4$ from $C_3H_8$, and rapidly eliminates these same products from $n$-$C_4H_{10}$[1,2] and it is generally believed that this trend, which is illustrated in Figure 1 for $Co^+$ reacting with $C_2H_6$ and $C_3H_8$, is due at least in part to the increasing strength of the predissociation molecular complex.[3] As the first step along the reaction pathway involves oxidative addition to a C−H bond, it is assumed that the barrier to insertion is relatively constant for all alkanes. It is then the depth of the well for the molecular complex which determines whether the barrier lies above or below the dissociation threshold.

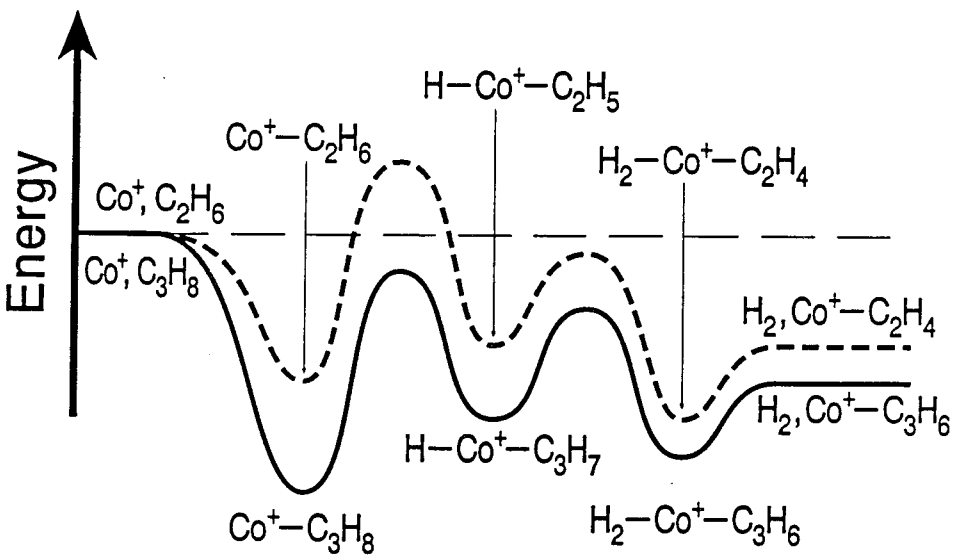


**Figure 1.** Schematic potential energy surfaces for the dehydrogenation of ethane (dashed line) and propane (solid line) by $Co^+$. While both exothermic, the deeper well for the initial molecular complex of $Co(C_3H_8)^+$ "pulls" the C–H activation barrier down below the threshold energy, allowing the reaction to proceed. The more shallow well for the $Co(C_2H_6)^+$ complex leads to a C–H activation barrier which is above the threshold energy and thus bars reaction.

Thus, $Co(C_2H_6)^+$ may not have enough energy to overcome the barrier to insertion, but $Co(C_3H_8)^+$ does. Whether these assumptions are valid or not, it is clear that a detailed understanding of these ion-molecule complexes is vital to understanding the chemistry of alkane dehydrogenation and demethanation.

While the ability of experiment to characterize these ion-molecule clusters has mostly been limited to the determination of complexation energies, the accuracy of the methods has improved greatly in the last few years. To a large extent, much of the confusion regarding the isomeric form of species being studied (such as a dimethyl complex vs. an ion-ethane complex) has been eliminated in the more recent studies. Among these recent studies, gas-phase equilibrium measurements by Bowers and co-workers[4] led to complexation energies for $Co^+$ with $CH_4$ and $C_2H_6$. These bond energies were found to be 22.9±0.7 and 28.0±1.1 kcal/mol, respectively. Armentrout[5] has also investigated these bond strengths with the technique of threshold collisional activation (TCA) obtaining values of 21.4±1.2 and 24.0±0.7, respectively. The Armentrout group also reported a BDE of 30.9±1.4 kcal/mol for $Co(C_3H_8)^+$. These dissociation energies are notably higher than those obtained for $Fe(CH_4)^+$,[6] $Fe(C_2H_6)^+$,[7] and $Fe(C_3H_8)^+$,[8] which are 13.7±0.8, 15.3±1.4, and 19±2, respectively. This discrepancy is believed to be due to the difference in the ground states of $Co^+$ and $Fe^+$: $Co^+$ is $d^8$ and $Fe^+$ is $s^1d^6$.

Both the Bowers and Armentrout groups have also obtained data on the BDE's for complexation of multiple ligands to a single ion. In particular, they found that the $(CH_4)Co^+-CH_4$ bond is about 2 kcal/mol stronger than the $Co^+-CH_4$ bond.[4,5] In contrast, for $Co(C_2H_6)_2^+$, Bowers *et al.*[4] found that the second bond was weaker than the first by about 1 kcal/mol. For $Fe(CH_4)_2^+$, Armentrout *et al.*[6] found that the second bond is nearly 10 kcal/mol stronger

than the first and it has been argued that this reflects a change of spin on the metal. However, it is not clear whether this spin change occurs upon formation of the first bond or the second and questions about whether diabatic or adiabatic bond energies are being measured remain.

Theory has had much to say about the bonding of molecular hydrogen to transition metals (Chapter IV), but considerably less has been said on the bonding of alkanes. Of the few studies that exist in the literature, Rosi *et al.*[9] looked at complexation of ethane to several metal cations ($Cu^+$, $Ag^+$, $Cr^+$, and $Mo^+$) in their study of the dimethyl complexes of the first- and second-row transition metals. They identified two coordination sites: one possessing $C_2$ symmetry (favored by $Cu^+$) and one in which the metal is coordinated to two C−H bonds in $C_s$ symmetry (favored by $Ag^+$). Berthier *et al.*[10] studied the complexation of $CH_4$ to $Cu^+$ and Hill, Freiser, and Bauschlicher[11] looked at the bonding of $Cu^+$, $Y^{2+}$, and $Sc^{2+}$ to a number of hydrocarbons. In both of these studies, $Cu^+$ was found to coordinate to $CH_4$ in a $C_{3v}$ geometry, but recent calculations have found the $C_{2v}$ geometry to be more favorable.[12]

Thus, the bonding of transition metal ions to small alkanes has yet to be fully characterized. Theory can offer a great deal of insight into this problem and, in this chapter, we present results of MCPF calculations on $M(CH_4)^+$, $M(CH_4)_2^+$, $M(C_2H_6)^+$, and $M(C_3H_8)^+$ (M=Co, Rh, Ir, and Fe), analyzing the nature of the ion-alkane bond and verifying the accuracy of the existing experimental data for $Co^+$ and $Fe^+$. Most of the emphasis will be placed on the results for $Co^+$, which were used by Bowers and co-workers[4] to refine the analysis of their experimental data. These results were published previously in a similar form.[13] Results for $Rh^+$, $Ir^+$, and $Fe^+$ serve as a comparison between transition metals of different rows and columns in the periodic table and only hint at the

wide variation in properties of these clusters which could be observed in a study of the complete transition series.

## 5.2 Summary of the Bonding

The ion-methane bond strength is derived almost entirely of an ion-induced polarization. As discussed in Chapter IV, this quantity has the functional form

$$E_\alpha = \frac{1}{2}\alpha q^2 r^{-4}$$

where $q$ is the charge on the ion, $\alpha$ is the polarizability of the ligand, and $r$ is the ion-molecule distance. The polarizability of $CH_4$ ($\alpha$=2.59 Å$^3$) is quite a bit larger than that of $H_2$ ($\alpha$=0.80 Å$^3$)[14] which increases $E_\alpha$. At the same time $CH_4$ is a bulkier ligand than $H_2$ which increases $r$ and thus decreases $E_\alpha$. As a result, the $M^+-CH_4$ bond strengths are nearly the same as the $M^+-H_2$ bond strengths in many cases.

For the larger alkanes ($C_2H_6$ and $C_3H_8$) there is also the element of the ion-dipole

$$E_\mu = a\mu q r^{-2}$$

and/or ion-quadrupole

$$E_\theta = b\theta q r^{-3}$$

interactions, where $\mu$ is the dipole moment and $\theta$ is the quadrupole moment of the molecule, and $a$ and $b$ are functions of the angle of approach of the ion to the molecule. As with $M(H_2)^+$, however, these interaction energies are of secondary importance when compared to the ion-induced polarization.

Further consideration should also be given to the element of charge transfer. Since the electronegativity of these transition metal cations is generally higher than the electronegativity of the alkanes (the IP of $Co^+$ is 17.06 eV[15] and the IP of $CH_4$ is 12.70 eV[16]), ligand to metal donation dominates. Thus, the balance between the Pauli repulsion of the ion and ligand and the electrostatic interactions between them then determines the bond strength.

The reduction of Pauli repulsion is perhaps the most important element which makes transition metal ion molecular complexes interesting. While orbital size is a primary consideration in the determination of the ion-alkane bond length, other factors such as $d$ orbital occupations and $sd$ hybridization can reduce this distance and thereby increase the ion-induced dipole and other attractive electrostatic interactions. In particular, we find that the optimal arrangement of electrons on the metal to minimize Pauli repulsion (and also maximize ligand to metal charge transfer) depends largely on atomic state splittings. Consequently, non-monotonic behavior in $M^+-$alkane bond strengths across a transition series row or non-monotonic behavior in successive $M^+-$alkane bond strengths can be observed.

The most effective means of reducing Pauli repulsion between the metal and ligand is by having the most respulsive metal orbitals empty or only partially occupied. We should also note that the orbitals which are most repulsive to the ligand are usually the ones which are best able to accept charge from the ligand, so having these orbitals empty or only partially occupied will increase the degree of charge transfer. Thus, since the valence $s$ orbital is larger and more repulsive then the valence $d$ orbitals, a metal with an occupied $s$ orbital will generally lead to a diabatic bond strength which is weaker than a metal with an empty $s$ orbital. This is also true of orbitals within the $d$ shell, where for $Co(H_2)^+$ (Chapter IV), the $d_{z^2}$ was most repulsive to the ligand and was singly occupied in the ground state. However, as was also seen in Chapter IV, state splittings and atomic couplings must be kept in mind. Singly occupying the two most repulsive $3d$ orbitals of $d^8$ $Co^+$, for instance, may not lead to the ground state. Instead, singly occupying the one orbital which is most repulsive to the ligand and singly occupying its $\sigma - \delta$ complement to produce a pure $^3F$

coupling is more often the rule.

A second means of reducing Pauli repulsion is through $sd$ hybridization. As discussed for the metal alkyls (Chapter III), $sd$ hybridization is most effective when the orbitals are of a similar size and similar energy. However, in these ion-alkane clusters, even the hybridization of $4s$ and $3d$ orbitals of $Co^+$, which is inefficient in forming covalent bonds, is effective in reducing Pauli repulsion to the ligand. Consequently, it is often the case that the most repulsive $d_{z^2}$ orbital is doubly occupied on the metal. This orbital hybridizes with the $s$ to form a $d_{z^2} - \lambda s$ orbital which is polarized in the $x$ and $y$ directions and is less repulsive to the ligand. Blomberg *et al.*[17] noted that this hybridization has the effect of deshielding the metal nucleus from the methane, thereby increasing the electrostatic components of the bond. We also note that this hybridization leaves the empty $s + \lambda d_{z^2}$ orbital polarized along the $z$ axis, increasing the metal's ability to accept charge from the ligand.

As with much of transition metal chemistry, each ion-alkane interaction is unique. However, with these simple rules, much of the nature of these clusters can be explained. For each complex considered in this chapter, we detail how these effects combine to lead to the calculated ground state geometry and electronic configuration. Many of the illustrated differences between the various metals are subtle, but ultimately a clear picture emerges as to how these ion-alkane clusters are formed.

## 5.3 $M(CH_4)^+$

### 5.3.1 $Co(CH_4)^+$

Results for the complexation of $CH_4$ to $Co^+$ are presented in Table I and Figure 2. Such complexation is not without precedent and has been identified as a precursor to insertion into a methane C−H bond (oxidative addition) by both bare[17,18] and ligated[19,20] metals. The ground state of the cluster is derived from the $^3F$ ground state of the metal ion and we find $D_e$=21.4 kcal/mol in excellent agreement with the experimental values of $D_0^\circ$=22.9±0.7[4] and 21.4±1.2 kcal/mol.[5] The $\eta^2$ $C_{2v}$ geometry (with coordination of the metal to two H atoms, 2*a*) is slightly more stable than the $\eta^3$ $C_{3v}$ geometry (with coordination of the metal to three H atoms, 2*b*). Maitre and Bauschlicher[12] have also found the $\eta^2$ geometry to be the most favorable structure for $Cu(CH_4)^+$ in the most recent and most accurate calculations on that cluster. As already discussed, the bonding in $Co(CH_4)^+$ is largely electrostatic, dominated by charge-induced polarization. Other effects, such as charge transfer, are also important and these are detailed in the ensuing discussion.

The triplet ground state of the $\eta^2$ $C_{2v}$ complex has a $Co^+$ configuration of

$$(a_1 d_{y^2-z^2})^2 (a_2 d_{xy})^2 (b_1 d_{xz})^2 (a_1 d_{x^2})^1 (b_2 d_{yz})^1$$

where the two C−H bonds coordinated to the $Co^+$ are in the $yz$ plane and $z$ is the principal axis. This leads to a $^3B_2$ state. Careful analysis of the $Co(CH_4)^+$ MCPF natural orbitals (including a study of the Mulliken populations given in Table II) suggests that there is charge transfer from the $CH_4$ to the metal from both the $a_1$ and $b_2$ symmetries with no evidence of backbonding. While $H_2$ is a *two*-electron donor (with some $\pi$ acid character), $\eta^2$-$CH_4$ is a *four*-electron

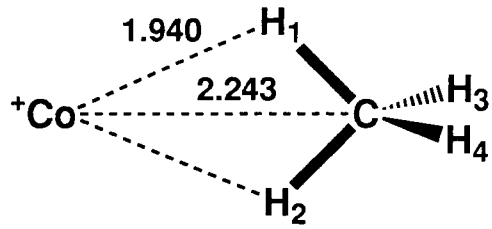


$\eta^2$ $C_{2v}$ $^3B_2$

| | | | |
|---|---|---|---|
| Co | 0.0000 | 0.0000 | 0.0000 |
| C | 0.0000 | 0.0000 | 2.2430 |
| $H_1$ | 0.0000 | 0.9524 | 1.6906 |
| $H_2$ | 0.0000 | -0.9524 | 1.6906 |
| $H_3$ | 0.8890 | 0.0000 | 2.8597 |
| $H_4$ | -0.8890 | 0.0000 | 2.8597 |

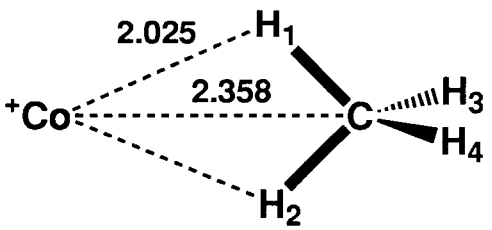


$\eta^2$ $C_{2v}$ $^3A_2$

| | | | |
|---|---|---|---|
| Co | 0.0000 | 0.0000 | 0.0000 |
| C | 0.0000 | 0.0000 | 2.3580 |
| $H_1$ | 0.0000 | 0.9389 | 1.7945 |
| $H_2$ | 0.0000 | -0.9389 | 1.7945 |
| $H_3$ | 0.8906 | 0.0000 | 2.9714 |
| $H_4$ | -0.8906 | 0.0000 | 2.9714 |

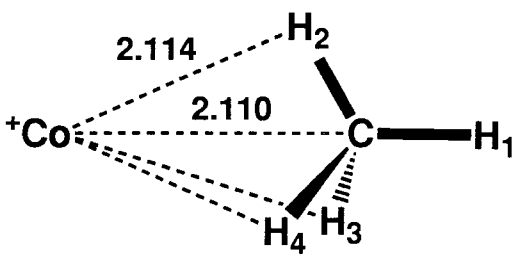


$\eta^3$ $C_{3v}$ $^3A_2$

| | | | |
|---|---|---|---|
| Co | 0.0000 | 0.0000 | 0.0000 |
| C | 0.0000 | 0.0000 | 2.1100 |
| $H_1$ | 0.0000 | 0.0000 | 3.1902 |
| $H_2$ | 0.0000 | 1.0590 | 1.8300 |
| $H_3$ | 0.9171 | -0.5295 | 1.8300 |
| $H_4$ | -0.9171 | -0.5295 | 1.8300 |

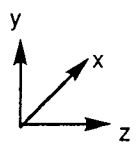


**Figure 2.** Geometries for three states of $Co(CH_4)^+$. Cartesian coordinates in Å.

**Table I.** Properties of $Co(CH_4)^+$.

| | $\eta^2$ $C_{2v}$ $^3B_2$ | $\eta^2$ $C_{2v}$ $^3A_2$ | $\eta^3$ $C_{3v}$ $^3A_2$ |
|---|---|---|---|
| $D_e$ (kcal/mol)[a] | 21.4 | 18.0 | 20.1 |
| $D_e$ (unrelaxed)[b] | 19.5 | 16.8 | 19.0 |
| $\omega_e$ (Co–C, $cm^{-1}$) | 343 | 314 | 340 |
| $r_e$ (Co–C, Å) | 2.24 | 2.36 | 2.11 |
| $r_e$ (Co–H) | 1.94 | 2.03 | 2.11 |
| $E_\alpha^c$ | 17.7 | 14.9 | 18.2 |
| $r_\alpha^d$ | 2.22 | 2.32 | 2.20 |
| $3d$ population | 7.88 | 7.96 | 7.86 |
| $\mu$ (D) | +2.18 | +2.05 | +2.35 |
| charge on Co | +0.66 | +0.74 | +0.68 |

[a] The experimental values are $D_0^\circ$=22.9±0.7[4] and 21.4±1.2 kcal/mol.[5]
[b] See appendix.
[c] Contribution to the energy from the charge-induced dipole.
[d] $r_\alpha$ is used to compute the charge-induced dipole. See appendix.

**Table II.** Valence Mulliken populations of $Co^+$ in $Co(CH_4)^+$.

| | $\eta^2$ $C_{2v}$ $^3B_2$ | $\eta^2$ $C_{2v}$ $^3A_2$ | $\eta^3$ $C_{3v}$ $^3A_2$ |
|---|---|---|---|
| $a_1/a_1$ $4s$ | 0.287 | 0.151 | 0.275 |
| $b_1/e(a')$ $4p_x$ | 0.008 | 0.006 | 0.028 |
| $b_2/e(a'')$ $4p_y$ | 0.031 | 0.026 | 0.028 |
| $a_1/a_1$ $4p_z$ | 0.110 | 0.093 | 0.092 |
| $a_1/a_1$ $4d_{z^2}$ | 1.633 | 1.009 | 1.852 |
| $b_1/e(a')$ $3d_{xz}$ | 1.980 | 1.982 | 1.323 |
| $b_2/e(a'')$ $3d_{yz}$ | 1.023 | 1.988 | 1.323 |
| $a_1/e(a')$ $3d_{x^2-y^2}$ | 1.258 | 1.984 | 1.682 |
| $a_2/e(a'')$ $3d_{xy}$ | 1.986 | 0.998 | 1.682 |

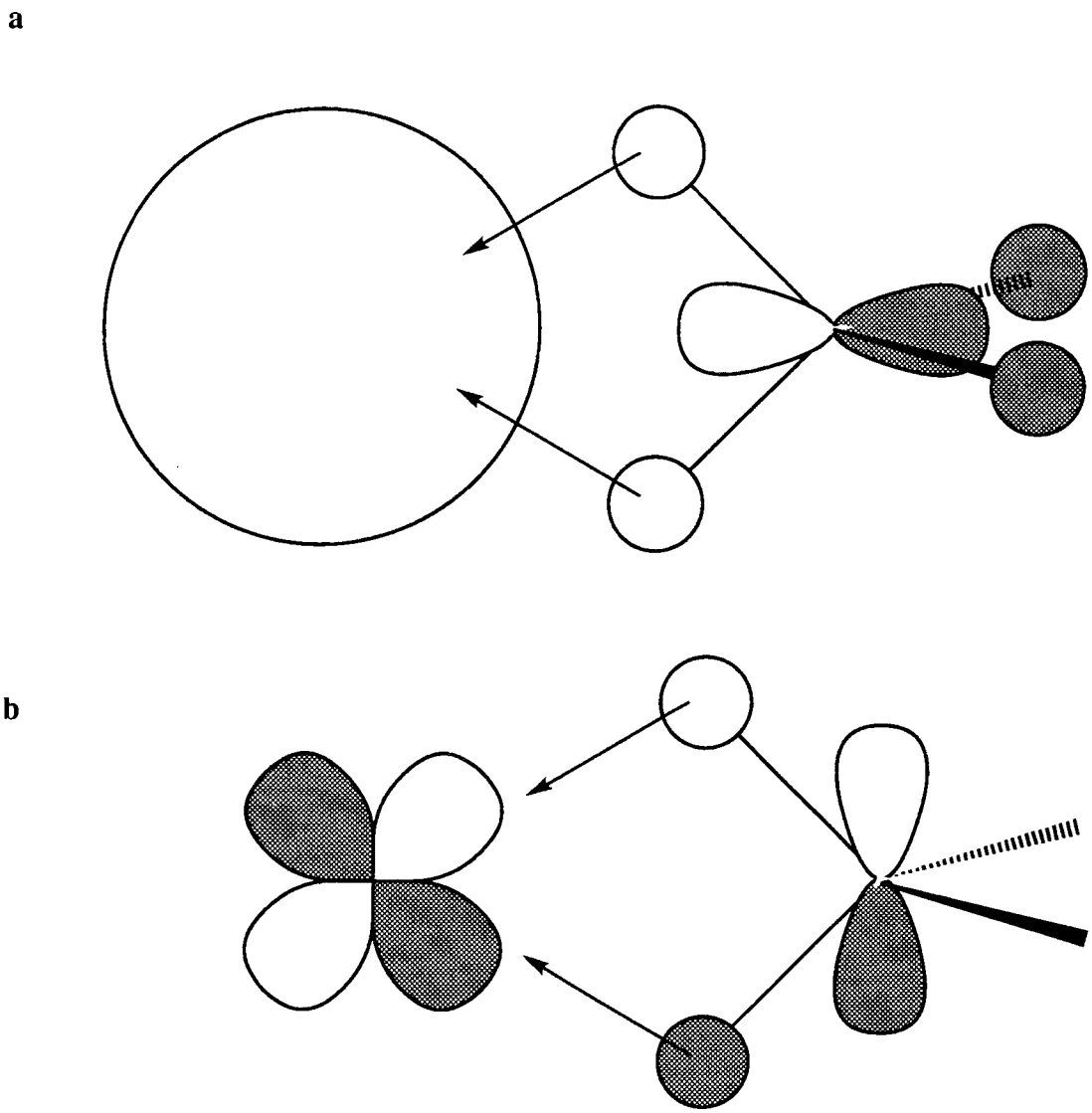


**Figure 3.** Charge donation from $CH_4$ orbitals to $Co^+$ orbitals for the $C_{2v}$ $^3B_2$ state. (a) Charge donation in $a_1$ symmetry into the empty $4s$ orbital. (b) Charge donation in $b_2$ symmetry into the singly occupied $3d_{yz}$ orbital.

donor. This is illustrated in Figure 3. The two C−H bonds coordinated to the metal transform under the $a_1$ and $b_2$ irreducible representations, and it is these orbitals which donate charge to the metal. As expected, charge transfer is dominantly from the $CH_4$ $3a_1$ orbital into the empty $Co^+$ $a_1$ $4s$ and $4p_z$ orbitals. The charge transfer in $b_2$ symmetry is into the empty $Co^+$ $b_2$ $4p_y$ orbital and partially occupied $Co^+$ $b_2$ $3d_{yz}$ orbital but is significantly smaller ($\sim$0.07 electron in $b_2$ symmetry vs. $\sim$0.3 electron in $a_1$ symmetry). Thus, with this charge transfer in $b_2$ symmetry, the $d_{yz}$ is singly, rather than doubly, occupied. It should be kept in mind, however, that the dominant effect of having this orbital singly occupied may be to reduce Pauli repulsion to the C−H bonds.

Since the $d_{yz}$ orbital is singly occupied, the $d_{x^2}$ orbital is also singly occupied in order to maintain the $^3F$ character of the metal (Chapter III). Among the doubly occupied orbitals, the repulsive $d_{y^2-z^2}$ is found to hybridize with the $4s$. The $d$ orbital is thus polarized along the $y$ axis, reducing its repulsion to the ligand along the $z$ direction.

As in $Co(H_2)^+$, one might have expected the $a_1$ $d_{z^2}$ orbital to be the most repulsive to the methane and, thus, the most likely to be singly occupied. Hence, we also considered in detail the $^3A_2$ state with the $Co^+$ configuration:

$$(b_2 d_{yz})^2 (b_1 d_{xz})^2 (a_1 d_{x^2-y^2})^2 (a_1 d_{z^2})^1 (a_2 d_{xy})^1$$

In this state, the $a_2$ $d_{xy}$ orbital is also singly occupied, as in $Co(H_2)^+$. The bond was found to be worth 18.0 kcal/mol which is 3.4 kcal/mol weaker than the $^3B_2$ ground state. Additionally, the Co−C distance is $\sim$0.1 Å longer (2.36 Å) and the Co−$CH_4$ stretch is smaller (314 $cm^{-1}$) than for the $^3B_2$ state. While charge donation occurs from the $CH_4$ $3a_1$ orbital into the Co $4s$, the $a_2$ $d_{xy}$ orbital is not suitable for accepting charge and does little to reduce Pauli repulsion to the

ligand. Furthermore, there is no evidence for back-bonding similar to that of $Co(H_2)^+$ and the *sd* hybridization is smaller (as is reflected in the total *s* and *d* populations of Tables I and II). Unlike hybridization of a *doubly* occupied $3d$ orbital with the empty $4s$ orbital, which involves a mixture of the ground state of $Co^+$ ($a\ ^3F\ d^8$) with the low-lying $b\ ^3F\ s^1d^7$ state, hybridization of a *singly* occupied $d_{z^2}$ orbital with the empty $4s$ orbital involves a mixture of the ground state of $Co^+$ with the highly excited $c\ ^3P\ s^1d^7$ state. These effects appear to be strong enough in $Co(CH_4)^+$ to make the $^3B_2$ state lower in energy than the $^3A_2$ state.

For the $\eta^3$ $C_{3v}$ structure, a similar situation exists. In this case, the methane is a *six*-electron donor with the three C–H bonds transforming under the $a_1$, $e(a')$, and $e(a'')$ symmetries. The behavior of the $Co^+$ as an acceptor is, however, somewhat unusual. Again, with $z$ the principal axis, the $d_{z^2}$ orbital is doubly occupied and hybridizes with the empty $4s$ to reduce repulsion and polarize the charge-accepting $4s$ orbital in the $z$ direction. The additional metal orbitals are linear combinations of the $d_\pi$ and $d_\delta$ orbitals, such that the two that are singly occupied possess approximately $\sigma$ and $\delta$ character offset from the $z$ axis by an angle of 54.74°. This "magic angle" produces a second $d_\sigma$ orbital[21] from

$$d'_\sigma = \sqrt{\frac{2}{3}}yz + \sqrt{\frac{1}{3}}(x^2 - y^2)$$

and a $d_\delta$ orbital with respect to this from

$$d'_\delta = \sqrt{\frac{2}{3}}xz - \sqrt{\frac{1}{3}}xy.$$

The $\sigma$-$\delta$ character of the singly occupied orbitals ensures that the metal is in its $^3F$ state and the angle of rotation is most ideal for reducing Pauli repulsion to the ligand. It also allows for charge transfer as indicated in Figure 4. As

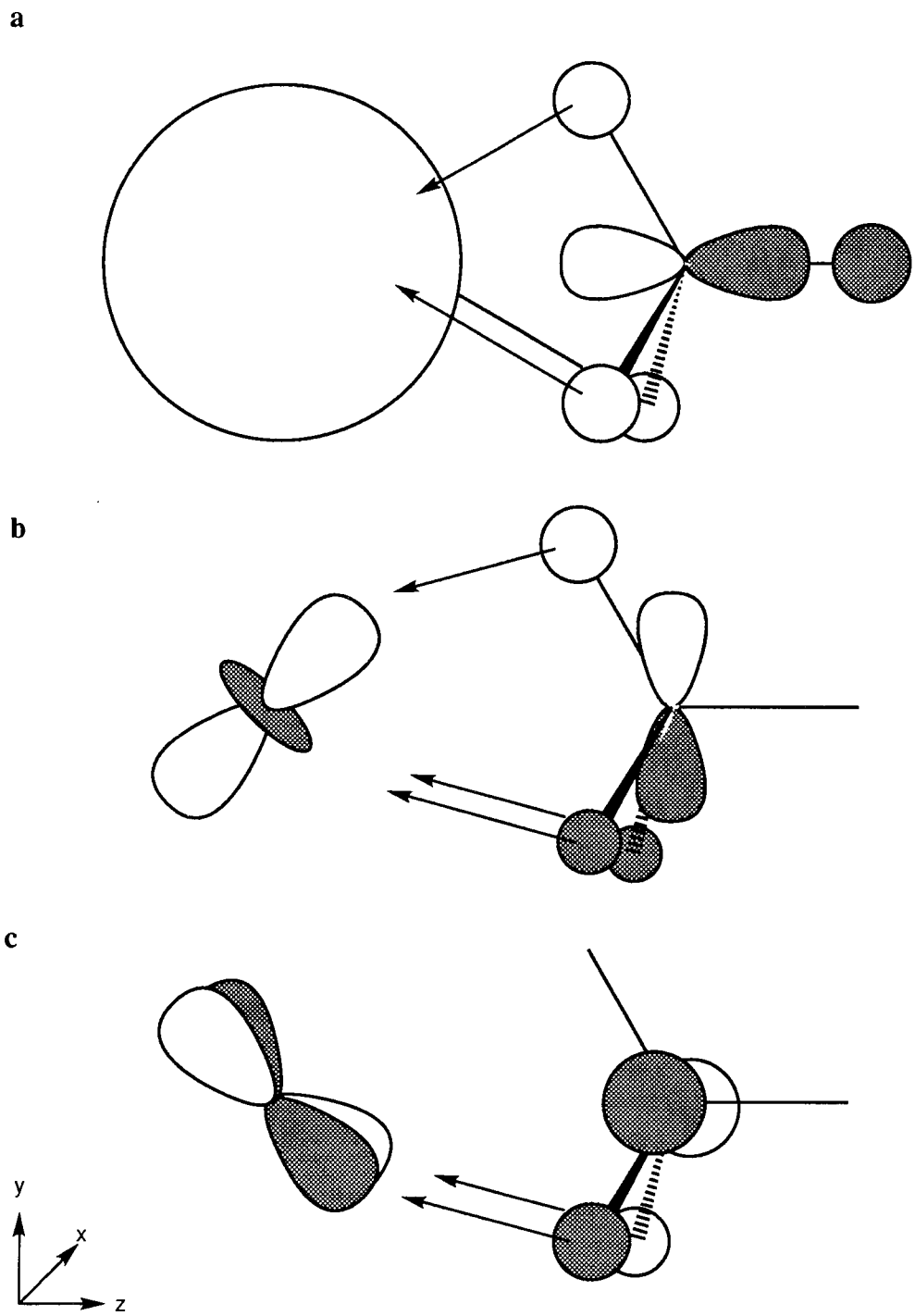


**Figure 4.** Charge donation from $CH_4$ orbitals to $Co^+$ orbitals for the $C_{3v}$ $^3A_2$ state. (a) Charge donation in $a_1$ symmetry into the empty 4*s* orbital. (b) Charge donation in *e(a')* symmetry into the singly occupied $3d_\sigma$ orbital. (c) Charge donation in *e(a")* symmetry into the singly occupied $3d_\delta$ orbital.

expected, this charge transfer occurs from the $CH_4$ $3a_1$ orbital into the metal $4s$ [hybridized with the $d_{z^2}$ $(4a)$]. But in addition, charge is donated into the two singly occupied orbitals of the metal: from the $CH_4$ $e(a')$ into the $d'_\sigma$ orbital $(4b)$ and from the $CH_4$ $e(a'')$ into the $d'_\delta$ orbital $(4c)$. In sum, $\eta^3$-$CH_4$ is like a tridentate ligand coordinated facially to the $Co^+$.

It should be emphasized that the strength of the $Co^+-CH_4$ bond is primarily due to charge-induced polarization. However, estimates of the contribution to the bond energy from this effect (see appendix) suggest that the $\eta^3$ conformation should be slightly lower in energy than the $\eta^2$ conformation ($E_\alpha$=18.2 vs. $E_\alpha$=17.7 kcal/mol, respectively). Consideration of other factors, such as Pauli repulsion, charge transfer from the $CH_4$ to the $Co^+$, and polarization of the nonbonding orbitals on the metal may be responsible for the reversal of ordering of these two states. The fact that $Cu(CH_4)^+$ (reference 12) is also $\eta^2$ suggests something more intrinsic than the $d$ occupations is responsible, as the $d^{10}$ closed shell of $Cu^+$ introduces no biases toward one geometry or the other as could be the case for $d^8$ $Co^+$. The fact that the $Cu^+-CH_4$ bond strength [21.4 kcal/mol at the CCSD(T) level][12] is identical to the $Co^+-CH_4$ bond strength is fortuitous, however. The general trend should be an increase in the complexation energy for $d^n$ transition metals as we move to the right in the periodic table (*i.e.*, $Cr^+ < Co^+ < Ni^+ < Cu^+$) following the trend of decreasing ion size and, thus, decreasing ion-molecule distance. On the other hand, metals such as $Co^+$ and $Ni^+$ have an advantage over metals such as $Cr^+$ and $Cu^+$ in that more freedom to orient the open-shell electrons to minimize repulsive interactions exists and greater $sd$ hybridization occurs, as was seen in the comparison of the $^3B_2$ and $^3A_2$ states of $Co(CH_4)^+$.

### 5.3.2 $Rh(CH_4)^+$

For $Rh(CH_4)^+$, the $\eta^2$ $C_{2v}$ geometry is also more favorable than the $\eta^3$ $C_{3v}$ geometry (see Table III and Figure 5). However, an important distinction from $Co(CH_4)^+$ is that the $\eta^2$ $^3A_2$ state is more strongly bound than the $^3B_2$ state. The difference in energy is only 0.3 kcal/mol, but this still respresents a reversal of the ordering of these states for the two metals. Similarly, the lowest energy $\eta^3$ $^3E$ ground state is analagous to the $\eta^2$ $^3A_2$ state with $d_{z^2}$ and $d_{xy}$ (or $d_{x^2-y^2}$) holes rather than the "magic angle" holes of the $\eta^3$ $Co(CH_4)^+$ system. We trace the favorability of these states in the $Rh^+$ complex to the high energy of the $5s$ orbital. With an excitation energy of 49.1 kcal/mol from the $d^8$ $^3F$ ground state to the $s^1d^7$ $^5F$ state, $sd$ hybridization is significantly more difficult to achieve than in the $Co^+$ complex, where the excitation energy from the $d^8$ state to the $s^1d^7$ state is only 9.9 kcal/mol. While $sd$ hybridization in $Rh^+$ may be expected to be more efficient in reducing repulsion to the ligand by virtue of the more similar sizes of the $5s$ and $4d$ orbitals as compared to the $4s$ and $3d$ orbitals of $Co^+$ (see Chapter III), the inaccessibility of the $5s$ orbital in $Rh^+$ ensures that this hybridization will be minimal with such a small purturbative force as a $CH_4$ ligand. The lack of significant $sd$ hybridization is reflected in the constancy of the $4d$ population for various states and geometries of $Rh(CH_4)^+$, as seen in Table III. Consequently, the best way for $Rh^+$ to reduce Pauli repulsion to the $CH_4$ is not by $sd$ hybridization (as in the $\eta^2$ $^3B_2$ state) but by singly occupying the $d_{z^2}$ orbital. Therefore, the $\eta^2$ $^3A_2$ state and its $\eta^3$ analogue are most favorable.

It should be noted that the $Rh^+-CH_4$ bond is weaker than the $Co^+-CH_4$ bond by 7 kcal/mol due to the fact that the $4d$ orbitals of $Rh^+$ are larger than the $3d$ orbitals of $Co^+$, increasing the $M^+-CH_4$ distance by 0.3-0.4 Å.

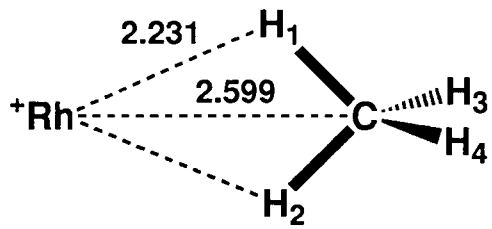


$\eta^2$ $C_{2v}$ $^3A_2$

| | | | |
|---|---|---|---|
| Rh | 0.0000 | 0.0000 | 0.0000 |
| C | 0.0000 | 0.0000 | 2.5990 |
| $H_1$ | 0.0000 | 0.9335 | 2.0263 |
| $H_2$ | 0.0000 | -0.9335 | 2.0263 |
| $H_3$ | 0.8903 | 0.0000 | 3.2102 |
| $H_4$ | -0.8903 | 0.0000 | 3.2102 |

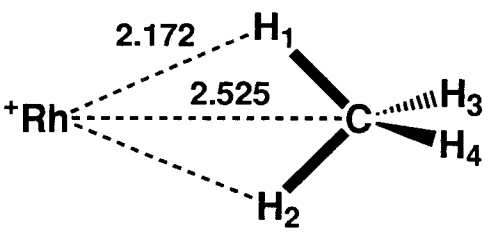


$\eta^2$ $C_{2v}$ $^3B_2$

| | | | |
|---|---|---|---|
| Rh | 0.0000 | 0.0000 | 0.0000 |
| C | 0.0000 | 0.0000 | 2.5250 |
| $H_1$ | 0.0000 | 0.9424 | 1.9567 |
| $H_2$ | 0.0000 | -0.9424 | 1.9567 |
| $H_3$ | 0.8894 | 0.0000 | 3.1364 |
| $H_4$ | -0.8894 | 0.0000 | 3.1364 |

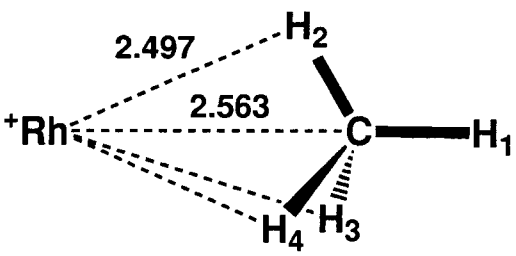


$\eta^3$ $C_{3v}$ $^3E$

| | | | |
|---|---|---|---|
| Rh | 0.0000 | 0.0000 | 0.0000 |
| C | 0.0000 | 0.0000 | 2.5630 |
| $H_1$ | 0.0000 | 0.0000 | 3.6448 |
| $H_2$ | 0.0000 | 1.0469 | 2.2670 |
| $H_3$ | 0.9067 | -0.5235 | 2.2670 |
| $H_4$ | -0.9067 | -0.5235 | 2.2670 |

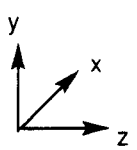


**Figure 5.** Geometries for three states of $Rh(CH_4)^+$. Cartesian coordinates in Å.

**Table III.** Properties of $Rh(CH_4)^+$.

| | $\eta^2$ $C_{2v}$ $^3A_2$ | $\eta^2$ $C_{2v}$ $^3B_2$ | $\eta^3$ $C_{3v}$ $^3E$ |
|---|---|---|---|
| $D_e$ (kcal/mol) | 14.4 | 14.1 | 12.1 |
| $D_e$ (unrelaxed) | 13.3 | 12.8 | 11.2 |
| $\omega_e$ (Rh–C, $cm^{-1}$) | 261 | 245 | 236 |
| $r_e$ (Rh–C, Å) | 2.60 | 2.53 | 2.56 |
| $r_e$ (Rh–H) | 2.23 | 2.17 | 2.50 |
| $E_\alpha$ | 10.2 | 11.4 | 9.1 |
| $r_\alpha$ | 2.55 | 2.48 | 2.62 |
| $4d$ population | 7.92 | 7.92 | 7.92 |
| $\mu$ (D) | +2.01 | +2.26 | +2.03 |
| charge on Rh | +0.83 | +0.77 | +0.90 |

The increased bond distance is then reflected in the magnitude of the charge-induced polarization which is, for instance, 11.4 kcal/mol for the $\eta^2$ $^3B_2$ state of $Rh(CH_4)^+$ compared to 17.7 kcal/mol for the same state of $Co(CH_4)^+$.

The fact that both of the $\eta^2$ and $\eta^3$ ground states have $d_\sigma$ and $d_\delta$ holes and the $\eta^2$ state is energetically favorable reinforces the argument [based on $Cu(CH_4)^+$] that there is an intrinsic bias for these metals to bond to $CH_4$ in the $\eta^2$ conformation. As with $Cu^+$, the arrangement of the electrons on $Rh^+$ offers no biases to the $CH_4$ as to its orientation. It can be argued that the $^3B_2$ state favors the $\eta^2$ conformation over the $\eta^3$ conformation because repulsion is more effectively reduced and charge transfer enhanced by singly occupying the $d_{yz}$ orbital. However, this is not true of the $^3A_2$ state so there seems to be a tendency for these transition metal–$CH_4$ complexes toward a $C_{2v}$ geometry.

### 5.3.3 $Ir(CH_4)^+$

Based on the above arguments we would expect that the $\eta^2$ $^3B_2$ state of $Ir(CH_4)^+$ would be the lowest energy triplet. This is indeed the case (see Table IV and Figure 6). Since the $s^1d^7$ $^5F$ state is the ground state of $Ir^+$, the problem of accessibility of the valence $s$ orbital for $sd$ hybridization is clearly not an issue. Moreover, since the $6s$ and $5d$ orbitals are closer in size than the $4s$ and $3d$ orbitals, we would expect $sd$ hybridization to be significantly more effective in the third row metals than in the first (see Chapter III). Consequently, the high polarizability of the $Ir^+$ orbitals is largely responsible for the relatively strong diabatic dissociation energy of $Ir(CH_4)^+$.

With respect to the $^5F$ ground state of $Ir^+$, the $^3B_2$ state of $Ir(CH_4)^+$ is bound by $D_e$=20.6 kcal/mol. The diabatic well depth is $D_e$=27.2 kcal/mol, 5.8 kcal/mol stronger than the $^3B_2$ $Co^+-CH_4$ bond. This increase in the bond strength occurs despite the fact that the $M-CH_4$ distance is slightly larger (by 0.06 Å) reducing the magnitude of the charge-induced dipole (15.5 vs. 17.7 kcal/mol). However, with $sd$ hybridization (and, in fact, $pd$ hybridization) being more effective in $Ir^+$ than $Co^+$, Pauli repulsion is more easily reduced and, more importantly, the effective charge of the ion is increased as the electron density is polarized away from the $CH_4$ ligand. Other factors such as charge transfer may also strengthen the bond as the electronegativity of $Ir^+$ is larger than that of $Co^+$, enhancing the effect.

Since the ground state of $Ir^+$ is $s^1d^7$ $^5F$, unlike $Co^+$ and $Rh^+$, there is an issue of whether the quintet states of $Ir(CH_4)^+$ are lower in energy than the triplet states. It is easily argued that these states should be more weakly bound in comparison to the triplet diabatic well depths since the occupied $6s$ orbital

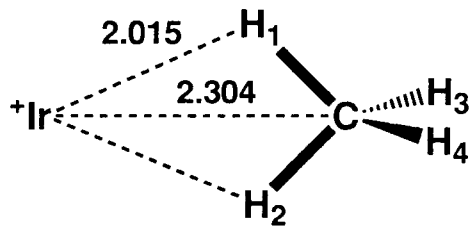


$\eta^2$ $C_{2v}$ $^3B_2$

| | | | |
|---|---|---|---|
| Ir | 0.0000 | 0.0000 | 0.0000 |
| C | 0.0000 | 0.0000 | 2.3040 |
| $H_1$ | 0.0000 | 0.9780 | 1.7620 |
| $H_2$ | 0.0000 | -0.9780 | 1.7620 |
| $H_3$ | 0.8960 | 0.0000 | 2.9093 |
| $H_4$ | -0.8960 | 0.0000 | 2.9093 |

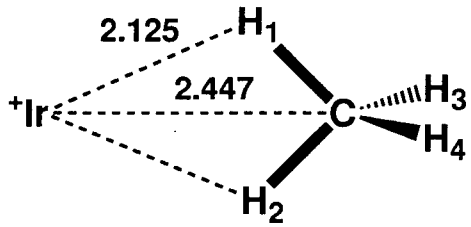


$\eta^2$ $C_{2v}$ $^3A_2$

| | | | |
|---|---|---|---|
| Ir | 0.0000 | 0.0000 | 0.0000 |
| C | 0.0000 | 0.0000 | 2.4470 |
| $H_1$ | 0.0000 | 0.9546 | 1.8982 |
| $H_2$ | 0.0000 | -0.9546 | 1.8982 |
| $H_3$ | 0.8959 | 0.0000 | 3.0514 |
| $H_4$ | -0.8959 | 0.0000 | 3.0514 |

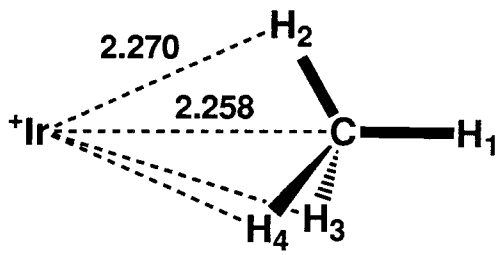


$\eta^3$ $C_{3v}$ $^3A_2$

| | | | |
|---|---|---|---|
| Ir | 0.0000 | 0.0000 | 0.0000 |
| C | 0.0000 | 0.0000 | 2.2580 |
| $H_1$ | 0.0000 | 0.0000 | 3.3437 |
| $H_2$ | 0.0000 | 1.0701 | 2.0018 |
| $H_3$ | 0.9267 | -0.5350 | 2.0018 |
| $H_4$ | -0.9267 | -0.5350 | 2.0018 |

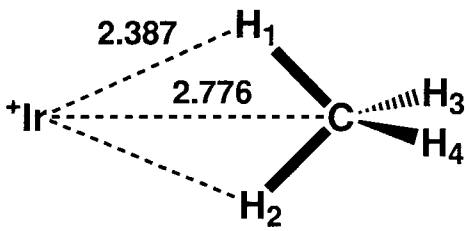


$\eta^2$ $C_{2v}$ $^5B_1$

| | | | |
|---|---|---|---|
| Ir | 0.0000 | 0.0000 | 0.0000 |
| C | 0.0000 | 0.0000 | 2.7760 |
| $H_1$ | 0.0000 | 0.9314 | 2.1978 |
| $H_2$ | 0.0000 | -0.9314 | 2.1978 |
| $H_3$ | 0.8899 | 0.0000 | 3.3896 |
| $H_4$ | -0.8899 | 0.0000 | 3.3896 |

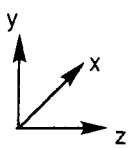


**Figure 6.** Geometries for four states of $Ir(CH_4)^+$. Cartesian coordinates in Å.

**Table IV.** Properties of $Ir(CH_4)^+$.

| | $\eta^2$ $C_{2v}$ $^3B_2$ | $\eta^2$ $C_{2v}$ $^3A_2$ | $\eta^3$ $C_{3v}$ $^3A_2$ | $\eta^2$ $C_{2v}$ $^5B_1$ |
|---|---|---|---|---|
| $D_e$ (kcal/mol)[a] | 20.6 | 16.6 | 14.2 | 8.9 |
| $D_e$ (unrelaxed) | 17.0 | 14.2 | 11.8 | 8.2 |
| $D_e$ (diabatic) | 27.1 | 23.1 | 20.7 | 8.9 |
| $\omega_e$ (Ir−C, $cm^{-1}$) | 349 | 290 | 286 | 186 |
| $r_e$ (Ir−C, Å) | 2.30 | 2.45 | 2.26 | 2.78 |
| $r_e$ (Ir−H) | 2.02 | 2.13 | 2.27 | 2.39 |
| $E_\alpha$ | 15.5 | 12.5 | 13.7 | 7.9 |
| $r_\alpha$ | 2.30 | 2.42 | 2.37 | 2.72 |
| $5d$ population | 7.75 | 7.84 | 7.73 | 6.99 |
| $\mu$ (D) | +2.92 | +2.64 | +3.16 | +3.22 |
| charge on Ir | +0.61 | +0.67 | +0.68 | +0.74 |

[a] Energies are with respect to the $^5F$ ground state of $Ir^+$ which is calculated to be 6.5 kcal/mol lower in energy than the $^3F$ state.

is larger than the $5d$ orbitals, increasing the bond length due to Pauli repulsion. However, it is not clear whether these quintet bond strengths are more than 6.5 kcal/mol weaker than the most strongly bound triplet (this is the calculated $^5F-^3F$ excitation energy for $Ir^+$). One factor working in favor of the quintet states is the high polarizability of the valence $s$ electron. Hybridization with the $6p$ orbital polarizes the $6s$ electron away from the ligand, increasing the effective charge of the ion. This is reflected in the larger dipole moment for this state. We calculate that the $\eta^2$ $^5B_1$ state, with the metal valence orbital occupations of

$$(a_1 d_{x^2})^2 (b_1 d_{xz})^2 (a_1 d_{y^2-z^2})^1 (b_2 d_{yz})^1 (a_2 d_{xy})^1 (a_1 s)^1$$

is only bound by $D_e$=8.9 kcal/mol. While not detailed here, the $\eta^3$ quintet state is even more weakly bound. We note that since spin-orbit coupling is so strong

with this heavy metal, we expect that a spin change upon clustering is a facile process.

### 5.3.4 $Fe(CH_4)^+$

A first row metal which is similar to $Ir^+$ in many ways is $Fe^+$. It has a ground state of $s^1d^6$ $^6$D, 5.7 kcal/mol below the $d^7$ $^4$F state. The bonding of $CH_4$ to this metal has been studied experimentally and we consider this cluster here because of the questions surrounding the spin of the ground state.

Based on collision induced dissociation (CID) data for the successive $Fe(CH_4)_x^+$ binding energies[6] and data for ligand exchange,[22] it has been argued that the ground state of $Fe(CH_4)^+$ is sextet with a bond energy of $D_0^\circ$=13.7±0.8 kcal/mol. The interpretation of these experiments, however, can be quite difficult and often rests on assumptions made about related systems. We instead find that the ground state is quartet with a bond energy of $D_e$=12.9 kcal/mol (see Table V and Figure 7). The lowest energy sextet state is bound by only $D_e$=9.1 kcal/mol. As we might have expected the quartet $Fe^+-CH_4$ diabatic bond strength to be comparable to that of triplet $Co^+-CH_4$, we would then have predicted an adiabatic bond strength for quartet $Fe^+-CH_4$ of $D_e$ ~15.7 kcal/mol (21.4 - 5.7). The true bond strength is about 3 kcal/mol smaller than this, perhaps reflecting the larger size of the metal ion or a less optimal arrangement of the metal valence electrons.

With a quartet ground state, a comparison to experiment is only meaningful if adiabatic bond strengths are being measured. It is difficult to assess whether this is the case for $Fe(CH_4)^+$. The spin-allowed product of the CID of quartet $Fe(CH_4)^+$ with Xe is $^4$F $Fe^+$ + $CH_4$, but a spin transition to the $^6$D state of $Fe^+$ cannot be ruled out. Indeed, it is likely that a mixture of $^4$F and $^6$D states are being formed such that the experimentally measured threshold represents a quantity intermediate to the adiabatic and diabatic bond strengths. Since our

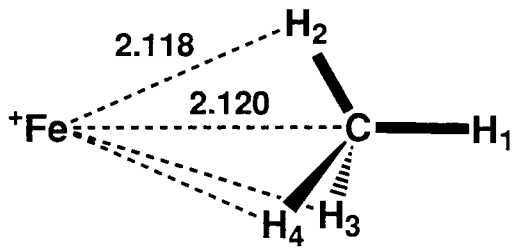


$\eta^3 C_{3v}\ ^4E$

| | | | |
|---|---|---|---|
| Fe | 0.0000 | 0.0000 | 0.0000 |
| C | 0.0000 | 0.0000 | 2.1200 |
| $H_1$ | 0.0000 | 0.0000 | 3.2010 |
| $H_2$ | 0.0000 | 1.0583 | 1.8346 |
| $H_3$ | 0.9165 | -0.5292 | 1.8346 |
| $H_4$ | -0.9165 | -0.5292 | 1.8346 |

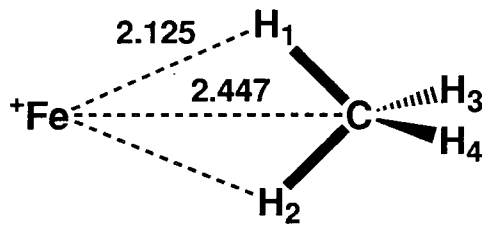


$\eta^2 C_{2v}\ ^4B_1$

| | | | |
|---|---|---|---|
| Fe | 0.0000 | 0.0000 | 0.0000 |
| C | 0.0000 | 0.0000 | 2.3020 |
| $H_1$ | 0.0000 | 0.9476 | 1.7441 |
| $H_2$ | 0.0000 | -0.9476 | 1.7441 |
| $H_3$ | 0.8882 | 0.0000 | 2.9155 |
| $H_4$ | -0.8882 | 0.0000 | 2.9155 |

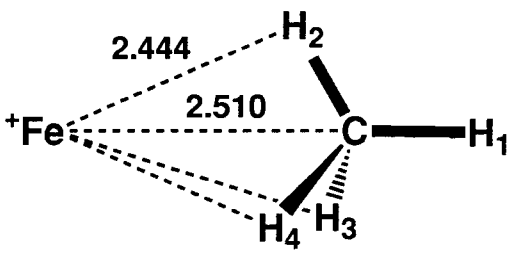


$\eta^3 C_{3v}\ ^6E$

| | | | |
|---|---|---|---|
| Fe | 0.0000 | 0.0000 | 0.0000 |
| C | 0.0000 | 0.0000 | 2.5100 |
| $H_1$ | 0.0000 | 0.0000 | 3.5922 |
| $H_2$ | 0.0000 | 1.0495 | 2.2074 |
| $H_3$ | 0.9089 | -0.5248 | 2.2074 |
| $H_4$ | -0.9089 | -0.5248 | 2.2074 |

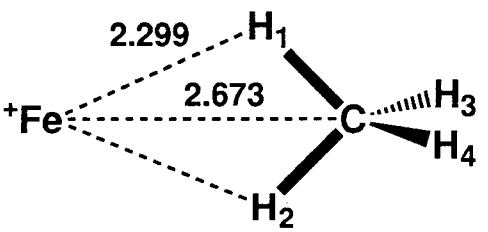


$\eta^2 C_{2v}\ ^6A_1$

| | | | |
|---|---|---|---|
| Fe | 0.0000 | 0.0000 | 0.0000 |
| C | 0.0000 | 0.0000 | 2.6730 |
| $H_1$ | 0.0000 | 0.8904 | 2.1005 |
| $H_2$ | 0.0000 | -0.8904 | 2.1005 |
| $H_3$ | 0.9334 | 0.0000 | 3.2843 |
| $H_4$ | -0.9334 | 0.0000 | 3.2843 |

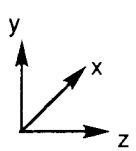


**Figure 7.** Geometries for four states of $Fe(CH_4)^+$. Cartesian coordinates in Å.

**Table V.** Properties of $Fe(CH_4)^+$.

| | $\eta^3$ $C_{3v}$ $^4$E | $\eta^2$ $C_{2v}$ $^4$B$_1$ | $\eta^3$ $C_{3v}$ $^6$E | $\eta^2$ $C_{2v}$ $^6$A$_1$ |
|---|---|---|---|---|
| $D_e$ (kcal/mol)[a] | 12.9 | 12.7 | 9.1 | 8.5 |
| $D_e$ (unrelaxed)[a] | 11.9 | 11.2 | 8.5 | 7.8 |
| $D_e$ (diabatic)[b] | 20.7 | 19.5 | 9.1 | 8.5 |
| $\omega_e$ (Fe–C, cm$^{-1}$) | 358 | 318 | 196 | 195 |
| $r_e$ (Fe–C, Å) | 2.12 | 2.30 | 2.51 | 2.67 |
| $r_e$ (Fe–H) | 2.12 | 2.01 | 2.44 | 2.30 |
| $E_\alpha$ | 17.9 | 15.6 | 9.9 | 9.1 |
| $r_\alpha$ | 2.21 | 2.29 | 2.57 | 2.62 |
| 3d population | 6.77 | 6.88 | 6.03 | 6.03 |
| $\mu$ (D) | +2.23 | +2.01 | +3.62 | +3.49 |
| charge on Fe+ | +0.72 | +0.71 | +0.79 | +0.76 |

[a] Energies are with respect to the $^6$D ground state of $Fe^+$ which is experimentally 5.7 kcal/mol lower in energy than the $^4$F state (14.7 kcal/mol, calculated). Energies for the quartet states include an empirical correction to account for the error in the $^6$D-$^4$F state splitting (see Chapter II). The experimental complexation energy is $D_0^\circ$=13.7±0.8 kcal/mol.[6]

[b] Calculated diabatic dissociation energies without empirical corrections.

results compare well to experiment, we conclude that the ground state is in fact quartet and that the adiabatic bond strength is (dominantly) being measured.

Unlike the other transition metal–methane complexes studied here and elsewhere[12], we find the lowest energy structures of $Fe(CH_4)^+$ to be $\eta^3$ (for both the quartet and sextet states). The energy differences between the $\eta^3$ and $\eta^2$ configurations is, however, small (0.2 kcal/mol for the quartet and 0.6 kcal/mol for the sextet). The ground state is $\eta^3$ $C_{3v}$ $^3$E with the $Fe^+$ electron configuration of

$$(a_1 d_{z^2})^2 (e(a'')d_{xy})^2 (e(a')d_{xz})^1 (e(a'')d_{yz})^1 (e(a')d_{x^2-y^2})^1$$

or equivalently

$$(a_1 d_{z^2})^2 (e(a')d_{x^2-y^2})^2 (e(a')d_{xz})^1 (e(a'')d_{yz})^1 (e(a'')d_{xy})^1$$

and it is bound by $D_e$=12.9 kcal/mol. For a $d^7$ configuration, doubly occupying $d_\sigma$ and $d_\delta$ orbitals and singly occupying the other $d_\delta$ and both $d_\pi$ orbitals ensures a $^4$F coupling on the metal. Consequently, the two singly occupied $d_\pi$ are capable of accepting charge from the ligand and the doubly occupied $a_1$ $d_\sigma$ orbital hybridizes with the $4s$ to reduce repulsion to the $CH_4$. Like $Ir^+$, $sd$ hybridization is easier for $Fe^+$ than for $Co^+$ or $Rh^+$ since the ground state of the metal is $s^1d^6$, ensuring that the $4s$ orbital is accessible.

The lowest energy quartet $C_{2v}$ state is $^4B_1$ with the $Fe^+$ valence electron configuration of

$$(a_1 d_{y^2})^2 (b_1 d_{xz})^2 (a_1 d_{x^2-z^2})^1 (b_2 d_{yz})^1 (a_2 d_{xy})^1.$$

It is bound by $D_e$=12.7 kcal/mol. In this case, the less repulsive $d_{y^2}$ orbital is doubly occupied rather than the $d_{z^2}$ orbital. As a result, the $b_1$ $d_{xz}$ orbital is also doubly occupied. The $^4A_2$ state, derived from doubly occupying the $a_1$ $d_{z^2}$ and $a_2$ $d_{xy}$ orbitals, is only $\sim$1 kcal/mol weaker than the $^4B_1$ state due to $sd$ hybridization reducing the repulsion of the $d_{z^2}$ orbital. The $d_{x^2}$ orbital may be even less repulsive than the $d_{y^2}$ orbital, but doubly occupying this orbital would also require doubly occupyinig the $b_2$ $d_{yz}$ orbital which is clearly unfavorable.

The electronic configurations of the $\eta^3$ and $\eta^2$ structures for the sextet state of $Fe(CH_4)^+$ are similar. Both have the valence orbital occupations of

$$(d_{x^2-y^2})^2 (d_{z^2})^1 (d_{xz})^1 (d_{yz})^1 (d_{xy})^1 (a_1 s)^1$$

where, for the $C_{3v}$ geometry the configuration

$$(d_{xy})^2 (d_{z^2})^1 (d_{xz})^1 (d_{yz})^1 (d_{x^2-y^2})^1 (a_1 s)^1$$

is degenerate. As was explained in Chapter IV for $Co(H_2)^+$, these two configurations are not degenerate for the $C_{2v}$ geometry and the $^6A_1$ state is more

favorable than the $^6A_2$ state due to the gain in flexibility in the $^6A_1$ state by having one of the $a_1$ $3d$ orbitals singly occupied and the other doubly occupied. In both geometries it is clear that the least repulsive orbital to the $CH_4$ is a $d_\delta$ orbital. Since there are no biases in an $s^1d^6$ configuration in regard to the occupations of the $d$ orbitals, the least repulsive is then doubly occupied in the cluster.

## 5.4 $M(CH_4)_2^+$

### 5.4.1 $Co(CH_4)_2^+$

To understand solvation, it is necessary to determine how the presence of one ligand on a metal can affect the energetics of another. Both the Bowers[4] and Armentrout[5] groups have looked at the bonding of multiple methanes to $Co^+$ and both find that the second bond is stronger than the first by 1.9 kcal/mol ($D_0^\circ$=22.9±0.7 vs. $D_0^\circ$=24.8±0.8 kcal/mol[4] and $D_0^\circ$=21.4±1.2 vs. $D_0^\circ$=23.1±1.2 kcal/mol[5]). In addition, Armentrout finds the third bond to be significantly weaker ($D_0^\circ$=9.7±1.2 kcal/mol) but the fourth bond to be only moderately weaker ($D_0^\circ$=16.6±2.3 kcal/mol). In conjunction with these experiments, we have done calculations on $Co(CH_4)_2^+$ and, in agreement with these studies, we find the second $CH_4$ to bond more strongly than the first by 1.7 kcal/mol ($D_e$=21.4 vs. $D_e$=23.1 kcal/mol). The results of these calcualtions are given in Table VI and Figure 8.

The ground state involves $\eta^2$ coordination of both methanes to the metal with a C−Co−C angle of 180°. Contrary to the results of Bauschlicher *et al.*[23] for $Co(H_2)_2^+$, in which the $H_2$ ligands were found to be *staggered* in a $D_{2d}$ conformation, we find the four C−H bonds coordinated to the metal to be *eclipsed* in a $D_{2h}$ geometry. More surprisingly, the difference in energy between the $D_{2h}$ and $D_{2d}$ conformations is quite large for $Co(CH_4)_2^+$ (~6 kcal/mol) compared to the difference in energy between the $D_{2d}$ and $D_{2h}$ conformations of $Co(H_2)_2^+$ (1.4 kcal/mol).[20]

When one considers that $H_2$ is a $\sigma$-donor, $\pi$-acceptor but $CH_4$ is a four-electron donor, the reasons for the marked difference between $Co(CH_4)_2^+$ and $Co(H_2)_2^+$ become clear. The bonding in the $D_{2h}$ ground state of $Co(CH_4)_2^+$ (see

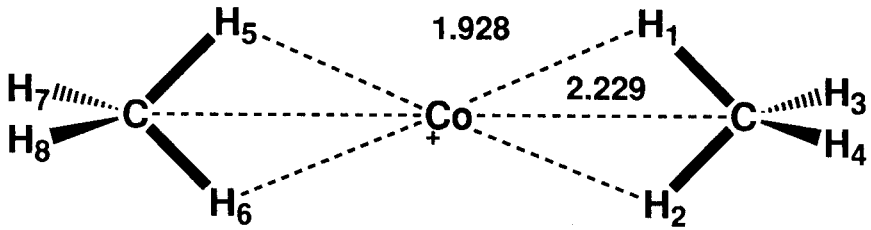


## $\eta^2$ $D_{2h}$ $^3B_{3g}$

| | | | |
|---|---|---|---|
| Co | 0.0000 | 0.0000 | 0.0000 |
| $C_1$ | 0.0000 | 0.0000 | 2.2290 |
| $C_2$ | 0.0000 | 0.0000 | -2.2290 |
| $H_1$ | 0.0000 | 0.9531 | 1.6759 |
| $H_2$ | 0.0000 | -0.9531 | 1.6759 |
| $H_3$ | 0.8859 | 0.0000 | 2.8471 |
| $H_4$ | -0.8859 | 0.0000 | 2.8471 |
| $H_5$ | 0.0000 | 0.9531 | -1.6759 |
| $H_6$ | 0.0000 | -0.9531 | -1.6759 |
| $H_7$ | 0.8859 | 0.0000 | -2.8471 |
| $H_8$ | -0.8859 | 0.0000 | -2.8471 |

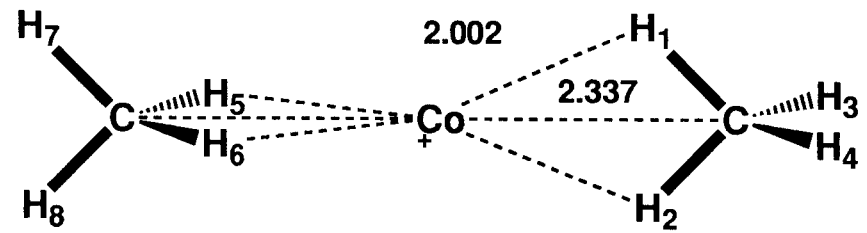


## $\eta^2$ $D_{2d}$ $^3B_2$

| | | | |
|---|---|---|---|
| Co | 0.0000 | 0.0000 | 0.0000 |
| $C_1$ | 0.0000 | 0.0000 | 2.3370 |
| $C_2$ | 0.0000 | 0.0000 | -2.3370 |
| $H_1$ | 0.0000 | 0.9359 | 1.7693 |
| $H_2$ | 0.0000 | -0.9359 | 1.7693 |
| $H_3$ | 0.8868 | 0.0000 | 2.9518 |
| $H_4$ | -0.8868 | 0.0000 | 2.9538 |
| $H_5$ | 0.9359 | 0.0000 | -1.7693 |
| $H_6$ | -0.9359 | 0.0000 | -1.7693 |
| $H_7$ | 0.0000 | 0.8868 | -2.9518 |
| $H_8$ | 0.0000 | -0.8868 | -2.9518 |

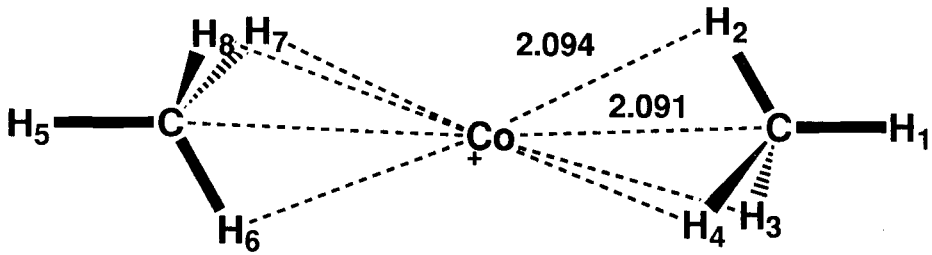


$\eta^3 D_{3d}\ ^4A_{2g}$

| | | | |
|---|---|---|---|
| Co | 0.0000 | 0.0000 | 0.0000 |
| $C_1$ | 0.0000 | 0.0000 | 2.0910 |
| $C_2$ | 0.0000 | 0.0000 | -2.0910 |
| $H_1$ | 0.0000 | 0.0000 | 3.1717 |
| $H_2$ | 0.0000 | 1.0583 | 1.8067 |
| $H_3$ | 0.9165 | -0.5291 | 1.8067 |
| $H_4$ | -0.9165 | -0.5291 | 1.8067 |
| $H_5$ | 0.0000 | 0.0000 | -3.1717 |
| $H_6$ | 0.0000 | -1.0583 | -1.8067 |
| $H_7$ | 0.9165 | 0.5291 | -1.8067 |
| $H_8$ | -0.9165 | 0.5291 | -1.8067 |

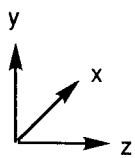


**Figure 8.** Geometries for three states of $Co(CH_4)_2^+$. Cartesian coordinates in Å.

**Table VI.** Properties of $Co(CH_4)_2^+$.

| | $\eta^2$ $D_{2h}$ $^3B_{3g}$ | $\eta^2$ $D_{2d}$ $^3B_2$ | $\eta^3$ $D_{3d}$ $^3A_{2g}$ |
|---|---|---|---|
| $D_e^a$ (kcal/mol) | 23.1 | 14.8 | 21.4 |
| $D_e$ (unrelaxed) | 21.4 | 14.4 | 21.2 |
| $\omega_e$ (sym C–Co–C, $cm^{-1}$) | 318 | 293 | 322 |
| $r_e$ (Co–C, Å) | 2.23 | 2.34 | 2.09 |
| $r_e$ (Co–H) | 1.93 | 2.00 | 2.09 |
| $E_\alpha^b$ | 18.3 | 13.3 | 20.0 |
| $r_\alpha$ | 2.21 | 2.30 | 2.19 |
| $3d$ population | 7.83 | 7.94 | 7.82 |
| charge on Co | +0.43 | +0.51 | +0.48 |

[a] The experimental values are $D_0^\circ$=24.8±0.8[4] and 23.3±1.2 kcal/mol.[5] The zero-point correction is estimated to be 0.7 kcal/mol.
[b] $E_\alpha$ is given as the total contribution of charge-induced polarization to the energy of $Co(CH_4)_2^+$ − 17.7 kcal/mol (the contribution of charge-induced polarization to the energy of $C_{2v}$ $Co(CH_4)^+$.

Figure 9) is no different in concept from that of $\eta^2$ $C_{2v}$ $Co(CH_4)^+$. The $Co^+$ configuration is still

$$(a_g d_{y^2-z^2})^2 (b_{1g} d_{xy})^2 (b_{2g} d_{xz})^2 (a_g d_{x^2})^1 (b_{3g} d_{yz})^1.$$

(Again, $z$ is the principal axis and the four C–H bonds coordinated to the metal are in the $yz$ plane.) This leads to a $^3B_{3g}$ ground state. The empty $4s$ and the singly occupied $d_{yz}$ orbitals of $Co^+$ accept charge from the two methanes. This requires that the coordinating C–H bonds of both methanes be in the $yz$ plane, leading to the eclipsed $D_{2h}$ geometry of $Co(CH_4)_2^+$.

The increase in bond energy for the second methane is then due to the hybridization of the $d_{y^2-z^2}$ and $4s$ orbitals. There is some cost in energy associated with this hybridization, and it is largely accounted for in the complexation of

the first methane. As the hybridization is already appropriate for complexation of a second methane (in the $D_{2h}$ geometry), the second bond energy is larger. A comparison of the $3d$ populations for the ground states of $Co(CH_4)^+$ and $Co(CH_4)_2^+$ in fact suggest that $sd$ hybridization has increased slightly with complexation of the second methane. This would further deshield the metal nucleus and reduce Pauli repulsion, increasing the strength of each $Co^+-CH_4$ bond.

For the $D_{2d}$ geometry, the $^3B_2$ state with the $d_{z^2}$ and $d_{xy}$ orbitals singly occupied was studied in detail at the MCPF level (the $^3B_1$ state with $d_{z^2}$ and $d_{x^2-y^2}$ holes is essentially degenerate). The $d_\delta$ orbital is not of a symmetry appropriate for accepting charge from the ligands, and having it singly occupied does little to reduce Pauli repulsion. Thus, the advantages of bonding present in the $D_{2h}$ geometry are lost and the bond is weaker by 8.3 kcal/mol.

However, a second state for this $D_{2d}$ geometry was found to be lower in energy. Unfortunately it requires a multi-reference treatment and the single-reference MCPF method is inadequate to describe it. While not as quantitative as MCPF calculations in general, we did SDCI+Q calculations (multi-reference when appropriate) on a number of different states for the four principal geometries ($D_{2h}$, $D_{2d}$, $D_{3d}$, and $D_{3h}$). These calculations were large (over 2,000,000 spin eigenfunctions in some cases) so no geometry optimizations were done. In the single reference cases, the MCPF geometries were used. In the multi-reference cases, the geometries were approximated based on the MCPF geometries of other states. The results of these calculations are detailed in Table VII.

The lowest energy $D_{2d}$ state, illustrated in Figure 10, is $^3A_2$ with a dominant configuration which has $d_{xz}$ and $d_{yz}$ holes and a secondary configuration which has $d_{x^2-y^2}$ and $d_{xy}$ holes to maintain the $^3F$ coupling of the metal. This state basically represents a compromise in which the $d_\pi$ orbitals have occupa-

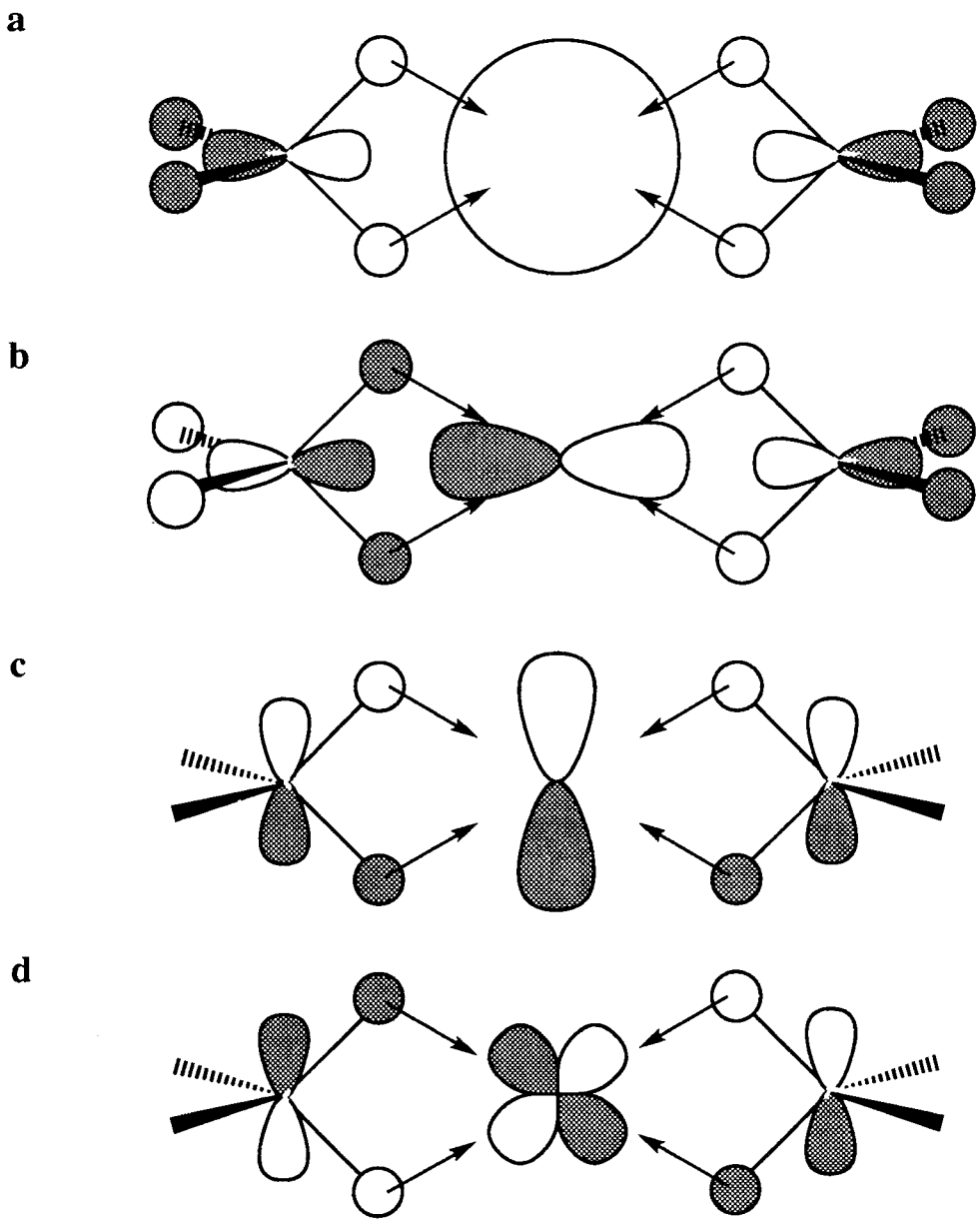


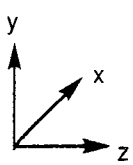


**Figure 9.** Charge donation from $CH_4$ orbitals to $Co^+$ orbitals for the $^3B_{3g}$ state of $D_{2h}$ $Co(CH_4)_2^+$. (a) Charge donation in $a_g$ symmetry into the empty $4s$ orbital. (b) Charge donation in $b_{1u}$ symmetry into the empty $4p_z$ orbital. (c) Charge donation in $b_{2u}$ symmetry into the empty $4p_y$ orbital. (d) Charge donation in $b_{3g}$ symmetry into the singly occupied $3d_{yz}$ orbital.

**Table VII.** SDCI+Q second bond strengths of $Co(CH_4)_2^+$.

| geometry | state | holes | SDCI | MCPF[a] |
|---|---|---|---|---|
| $D_{2h}$ | $^3B_{3g}$ | $x^2/yz$ | 21.3 | 23.1 |
| $D_{3d}$ | $^3A_{2g}$ | $\sigma'/\delta'$ | 19.2 | 21.4 |
| $D_{2h}$ | $^3B_{2g}$ | $yz/xy, xz/x^2-z^2$ | 19.1 | (20.7) |
| $D_{3h}$ | $^3A_2'$ | $xz/yz, xy/x^2-y^2$ | 18.2 | (20.3) |
| $D_{2h}$ | $^3B_{1g}$ | $xz/yz, xy/x^2-y^2$ | 17.2 | (19.2) |
| $D_{2d}$ | $^3A_2$ | $xz/yz, xy/x^2-y^2$ | 15.6 | (17.4) |
| $D_{2d}$ | $^3B_2$ | $z^2/xy$ | 15.2 | 14.8 |

[a] Numbers in parenthesis are estimated by scaling the SDCI bond energy based on the error in either the $D_{3d}$ $^3A_{2g}$ state or the $D_{2h}$ $^3B_{3g}$ state, depending on which is more appropriate.

tions between one and two electrons. This is not as optimal as the $D_{2h}$ ground state but it is better than the $D_{2d}$ $^3B_2$ state in which both $d_\pi$ orbitals have occupations of two electrons. Based on the underestimation of the bond strengths at the SDCI+Q level as compared to the MCPF level for the most similar single configuration state ($D_{3d}$ $^3A_{2g}$, to be described below), we estimate the second bond in the $D_{2d}$ $^3A_2$ state of $Co(CH_4)_2^+$ to be worth $D_e$ ~17.4 kcal/mol. This is still 5.7 kcal/mol weaker than the $D_{2h}$ bond.

There is also a state in $D_{2h}$ symmetry which is very similar to the state just described for $D_{2d}$ symmetry. It requires two configurations as well to be described properly (these configurations having $\pi - \pi$ and $\delta - \delta$ holes). This state is estimated to be ~3.9 kcal/mol above the ground state or ~1.8 kcal/mol below the comparable $D_{2d}$ state. The fact that it is lower in energy than the $D_{2d}$ state suggests that it is better to donate charge from the two $CH_4$ ligands into a single $3d$ orbital than into different $3d$ orbitals. The argument for this is analogous to that made for backdonation from either one or two singly occupied

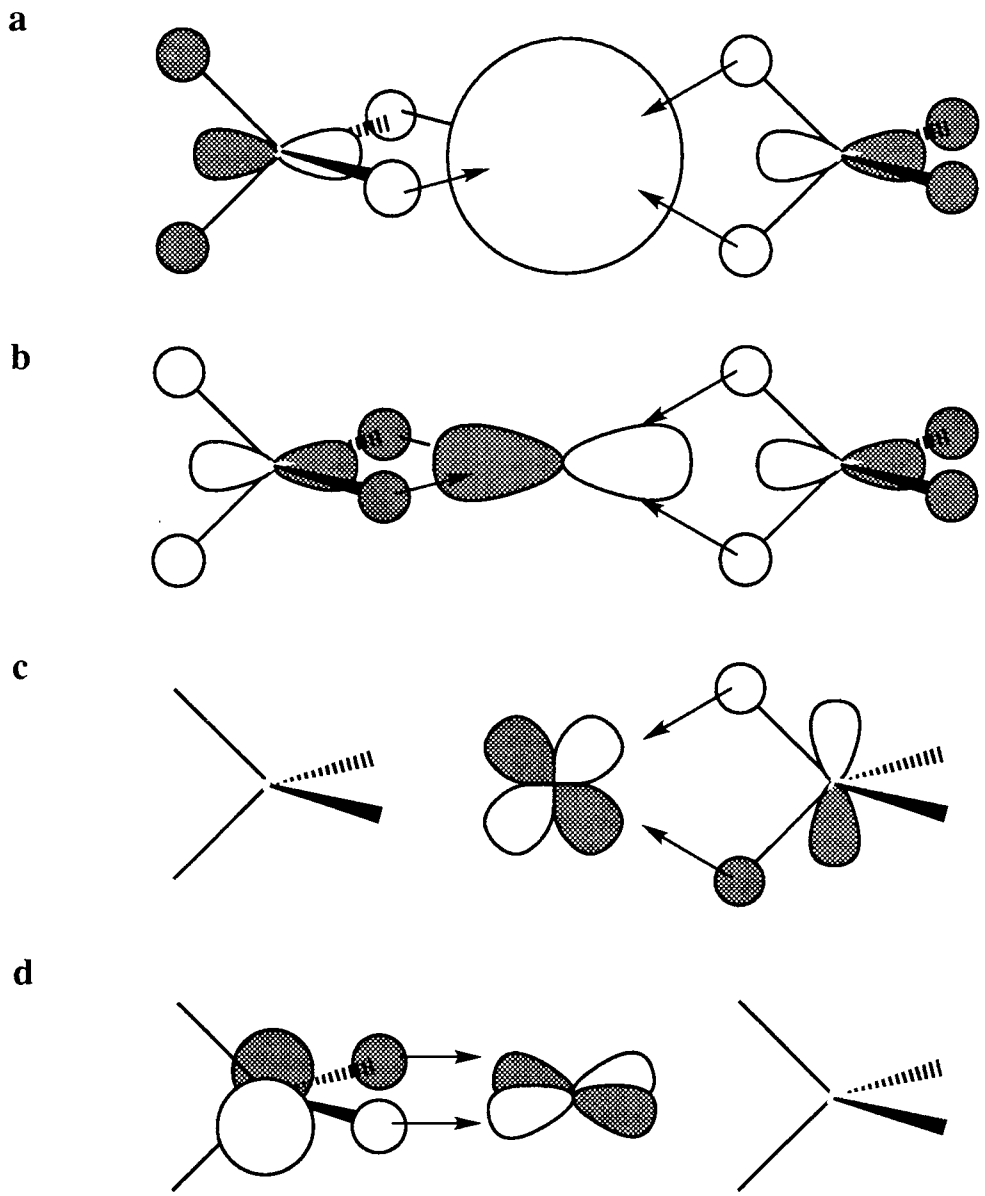


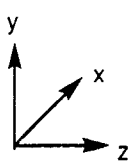


**Figure10.** Charge donation from $CH_4$ orbitals to $Co^+$ orbitals for the $^3A_2$ state of $D_{2d}Co(CH_4)_2^+$. (a) Charge donation in $a_1$ symmetry into the empty $4s$ orbital. (b) Charge donation in $b_2$ symmetry into the empty $4p_z$ orbital. (c) Charge donation in *e(a')* symmetry into partially occupied $3d_{yz}$ orbital. (d) Charge donation in *e(a")* symmetry into the partially occupied $3d_{xz}$ orbital.

orbitals in $V(H_2)_2^+$.[12] In this case, the eclipsed conformation was also found to be more stable than the staggered and Maitre and Bauschlicher suggested that the greater loss of $3d-3d$ exchange energy in backdonation of charge from two singly occupied $3d$ orbitals as compared to backdonation from only one was responsible. The reverse situation, $CH_4$ donation of charge into singly occupied $3d$ orbitals, would use the same reasoning. Consequently, for these comparable states of $Co(CH_4)_2^+$, the eclipsed conformation is more favorable than the staggered.

In contrast, for $Co(H_2)_2^+$, illustrated in Figure 11, the opposite situation exists and the staggered geometry is lower in energy than the eclipsed.[23] In this case, Bauschlicher *et al.* argue that it is better to have backbonding from two different doubly occupied $3d_\pi$ orbitals than only one, a fact which would favor the staggered geometry over the eclipsed geometry. More to the point, in the $D_{2d}$ geometry, one $d_\pi$ orbital is polarized toward the first $H_2$ molecule and the other $d_\pi$ orbital is polarized toward the second. Since the orbitals in question are doubly occupied, exchange energy will likely increase rather than decrease with backdonation. Still, these differences are subtle compared to the difference between the $D_{2h}$ ground state and the $D_{2d}$ excited state of $Co(CH_4)_2^+$.

We have also examined coordination of a second methane in the $\eta^3$ conformation. In this case, we find the bonds to be *staggered* in a $D_{3d}$ geometry. The bond is worth 21.4 kcal/mol with respect to $CH_4$ + $C_{2v}$ $Co(CH_4)^+$, 1.7 kcal/mol weaker than the $D_{2h}$ ground state. The fact that the methanes are staggered is consistent with the description of the $\eta^3$ $C_{3v}$ $Co(CH_4)^+$ bond as already detailed (see Figure 12). The singly occupied $d'_\sigma$ and $d'_\delta$ orbitals (off the principal axis by 54.74°) lead to the greatest reduction in Pauli repulsion if the six coordinated C−H bonds are in a pseudo-octahedral (trigonally distorted) arrangement.

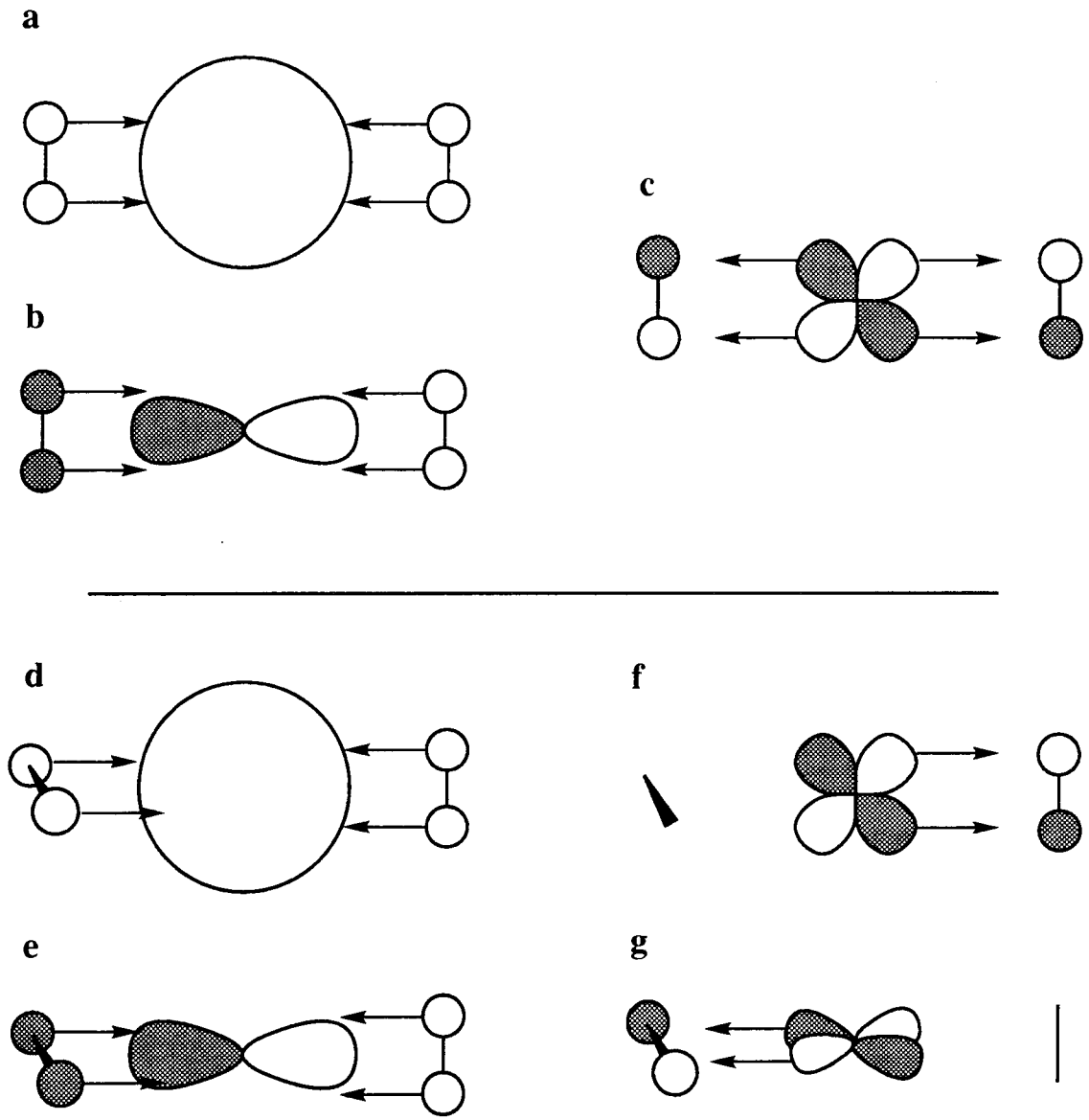


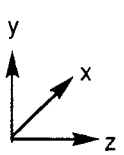


**Figure 11.** Charge donation and backdonation in $Co(H_2)_2^+$ for both the $^3B_{1g}$ $D_{2h}$ (a-c) and $^3B_2$ $D_{2d}$ states (d-g). (a) Donation from $H_2 a_g$ orbital into empty $4s$. (b) Donation from $H_2$ $b_{1u}$ orbital into empty $4p_z$. (c) Backdonation from doubly occupied $3d_{yz}$ into empty $H_2$ $b_{3g}$ orbital. (d) Donation from $H_2$ $a_1$ orbital into empty $4s$. (e) Donation from $H_2$ $b_2$ orbital into empty $4p_z$. (f) Backdonation from doubly occupied $3d_{yz}$ into empty $H_2$ $e(a')$ orbital. (g) Backdonation from doubly occupied $3d_{xz}$ into empty $H_2$ $e(a'')$ orbital. See references 12 and 23.

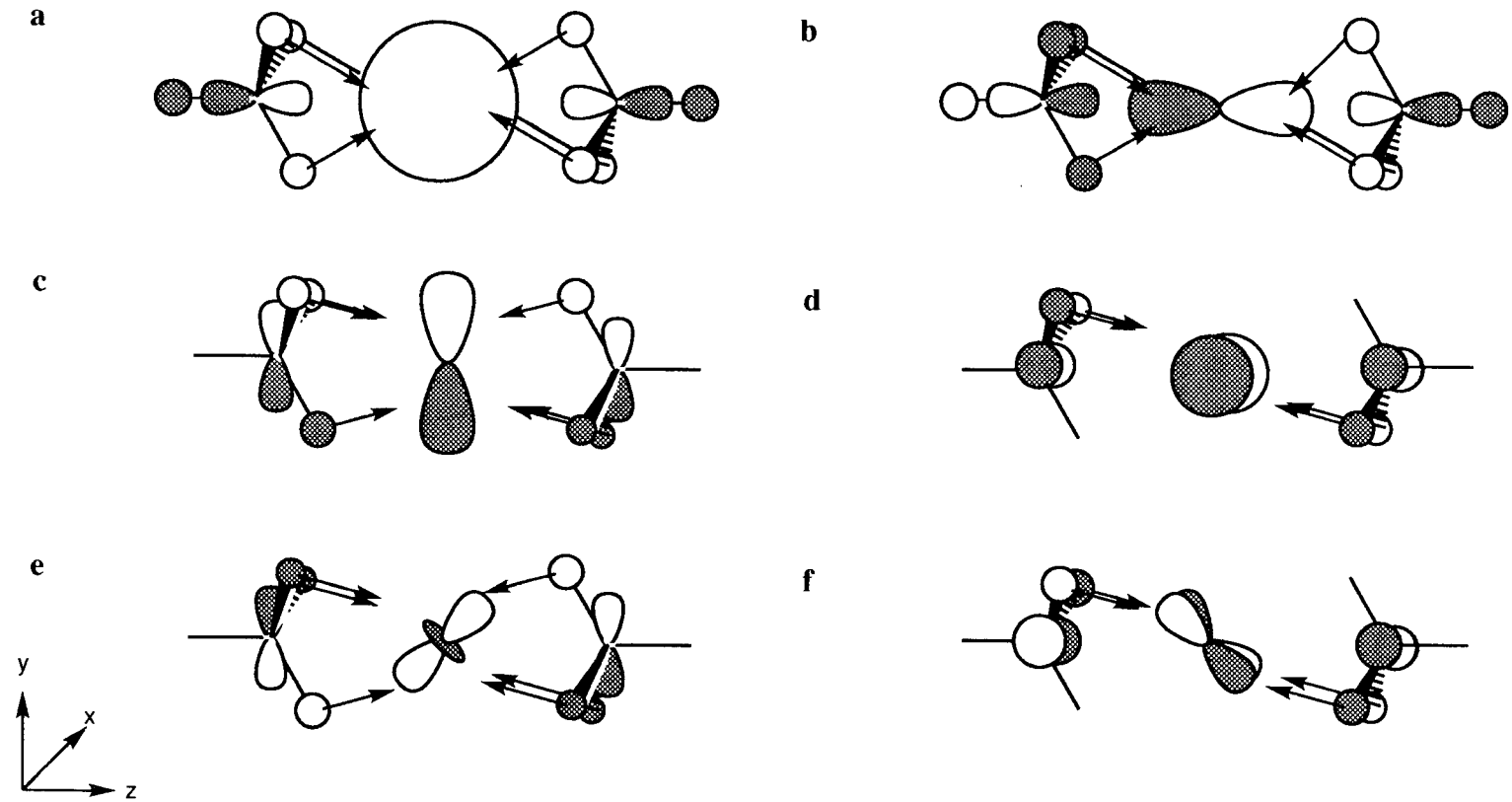


**Figure 12.** Charge donation from $CH_4$ orbitals to $Co^+$ orbitals for the $D_{3d}$ $^3A_{2g}$ state of $Co(CH_4)_2^+$. (a) Charge donation in $a_{1g}$ symmetry into the empty $4s$. (b) Charge donation in $a_{2u}$ symmetry into the empty $4p_z$. (c) Charge donation in $e_u(a')$ symmetry into the empty $4p_y$. (d) Charge donation in $e_u(a'')$ symmetry into the empty $4p_x$. (e) Charge donation in $e_g(a')$ symmetry into the singly occupied $3d_\sigma$. (f) Charge donation in $e_g(a'')$ symmetry into the singly occupied $3d_\delta$.

In the case of the $D_{3h}$ geometry, the lowest energy state is again described by two configurations having $\pi-\pi$ and $\delta-\delta$ holes. Using the optimized geometry of the $D_{3d}$ state and rotating one of the methanes by 60° about the principal axis, an SDCI+Q energy was calculated. Based on this energy, we estimate an energy comparable to the MCPF level to be $D_e$ ~20.3 kcal/mol, 1.1 kcal/mol weaker than the $D_{3d}$ state.

### 5.4.2 $Rh(CH_4)_2^+$

The most important difference between the $Rh(CH_4)_x^+$ clusters and the $Co(CH_4)_x^+$ clusters is the relative lack of *sd* hybridization for $Rh^+$. Like $Co(CH_4)_2^+$, the ground state of $Rh(CH_4)_2^+$ is $D_{2h}$ $^3B_{3g}$ with $d_{yz}$ and $d_{x^2}$ holes and the $(CH_4)Rh^+-CH_4$ bond is worth $D_e$=15.4 kcal/mol (see Table VIII and Figure 13). The $^3B_{1g}$ state, which is analogous to the ground state of $Rh(CH_4)^+$ with $d_{z^2}$ and $d_{xy}$ holes, is only 1.8 kcal/mol higher in energy. The 4*d* population for the ground state (7.88 electrons) is slightly smaller than the 7.92 electrons for $Rh(CH_4)^+$, indicative of a small increase in *sd* hybridization. Since the promotion energy for *sd* hybridization is diffused over two metal-ligand bonds rather than just one and thereby effectively reduced by half for each bond, the hybridization is more favorable. Still, the *d* population is higher than it is in $Co(CH_4)_2^+$ (7.83 electrons).

Perhaps more interesting is the comparison of the $D_{2h}$ $^3B_{1g}$ and $D_{2d}$ $^3B_1$ (or $^3B_2$) states of $Rh(CH_4)_2^+$. Both of these states are derived from the $^3A_2$ state of $Rh(CH_4)^+$, with $d_\sigma$ and $d_\delta$ holes. Since the orbital occupations do not suggest a preference for either a staggered or eclipsed geometry and *sd* hybridization does not play a role, the two geometries are expected to have very similar characteristics. In fact, as seen in Table VIII, they are virtually identical in regard to both geometry and energetics. While not determined explicitly, a similar situation likely exists for the lowest lying states of the $D_{3d}$ staggered and $D_{3h}$ eclipsed forms of the $\eta^3$ conformer.

Thus, as a result of minimal *sd* hybridization in $Rh^+$, the difference in energy between the lowest lying states of the $D_{2h}$ and $D_{2d}$ conformers of $Rh(CH_4)_2^+$ is only 1.8 kcal/mol compared to ~5.7 kcal/mol for $Co(CH_4)_2^+$ where there is

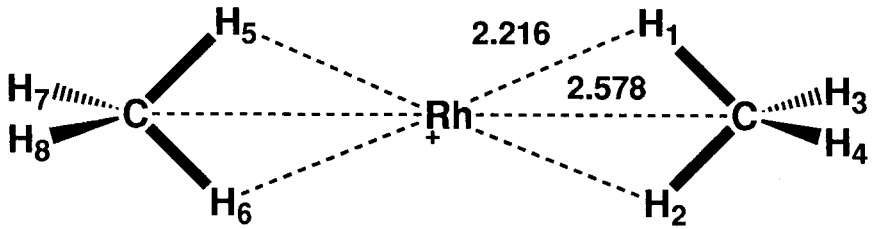


## $\eta^2$ $D_{2h}$ $^3B_{1g}$

| | | | |
|---|---|---|---|
| Rh | 0.0000 | 0.0000 | 0.0000 |
| $C_1$ | 0.0000 | 0.0000 | 2.5780 |
| $C_2$ | 0.0000 | 0.0000 | -2.5780 |
| $H_1$ | 0.0000 | 0.9351 | 2.0093 |
| $H_2$ | 0.0000 | -0.9351 | 2.0093 |
| $H_3$ | 0.8888 | 0.0000 | 3.1910 |
| $H_4$ | -0.8888 | 0.0000 | 3.1910 |
| $H_5$ | 0.0000 | 0.9351 | -2.0093 |
| $H_6$ | 0.0000 | -0.9351 | -2.0093 |
| $H_7$ | 0.8888 | 0.0000 | -3.1910 |
| $H_8$ | -0.8888 | 0.0000 | -3.1910 |

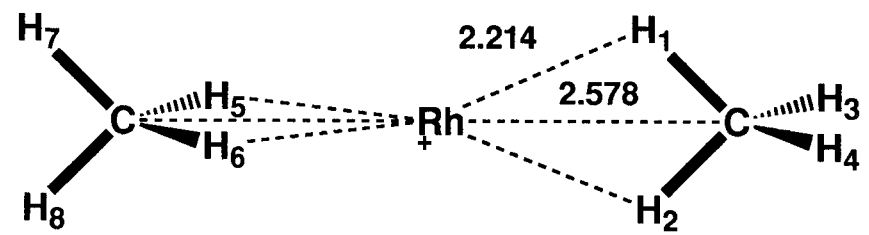


## $\eta^2$ $D_{2d}$ $^3B_1$

| | | | |
|---|---|---|---|
| Rh | 0.0000 | 0.0000 | 0.0000 |
| $C_1$ | 0.0000 | 0.0000 | 2.5780 |
| $C_2$ | 0.0000 | 0.0000 | -2.5780 |
| $H_1$ | 0.0000 | 0.9324 | 2.0079 |
| $H_2$ | 0.0000 | -0.9324 | 2.0079 |
| $H_3$ | 0.8898 | 0.0000 | 3.1912 |
| $H_4$ | -0.8898 | 0.0000 | 3.1912 |
| $H_5$ | 0.9324 | 0.0000 | -2.0079 |
| $H_6$ | -0.9324 | 0.0000 | -2.0079 |
| $H_7$ | 0.0000 | 0.8898 | -3.1912 |
| $H_8$ | 0.0000 | -0.8898 | -3.1912 |

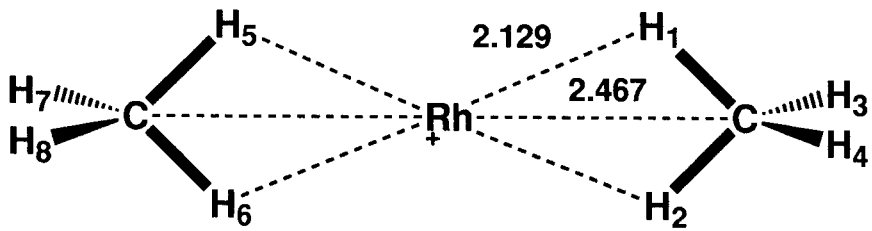


$\eta^2$ $D_{2h}$ $^3B_{3g}$

| | | | |
|---|---|---|---|
| Rh | 0.0000 | 0.0000 | 0.0000 |
| $C_1$ | 0.0000 | 0.0000 | 2.4670 |
| $C_2$ | 0.0000 | 0.0000 | -2.4670 |
| $H_1$ | 0.0000 | 0.9461 | 1.9070 |
| $H_2$ | 0.0000 | -0.9461 | 1.9070 |
| $H_3$ | 0.8910 | 0.0000 | 3.0792 |
| $H_4$ | -0.8910 | 0.0000 | 3.0792 |
| $H_5$ | 0.0000 | 0.9461 | -1.9070 |
| $H_6$ | 0.0000 | -0.9461 | -1.9070 |
| $H_7$ | 0.8910 | 0.0000 | -3.0792 |
| $H_8$ | -0.8910 | 0.0000 | -3.0792 |

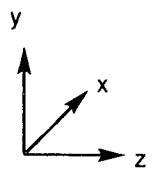


**Figure 13.** Geometries of three states of $Rh(CH_4)_2^+$. Cartesian coordiantes are in Å.

**Table VIII.** Properties of $Rh(CH_4)_2^+$.

| | $\eta^2$ $D_{2h}$ $^3B_{3g}$ | $\eta^2$ $D_{2h}$ $^3B_{1g}$ | $\eta^2$ $D_{2d}$ $^3B_1$[a] |
|---|---|---|---|
| $D_e$ (kcal/mol) | 15.4 | 13.6 | 13.6 |
| $D_e$ (unrelaxed) | 13.8 | 12.7 | 12.8 |
| $\omega_e$ (sym C–Rh–C, $cm^{-1}$) | 244 | 249 | 250 |
| $r_e$ (Rh–C, Å) | 2.47 | 2.58 | 2.58 |
| $r_e$ (Rh–H) | 2.13 | 2.22 | 2.21 |
| $E_\alpha^b$ | 14.4 | 10.8 | 10.9 |
| $r_\alpha$ | 2.43 | 2.53 | 2.53 |
| $4d$ population | 7.88 | 7.90 | |
| charge on Rh | +0.51 | +0.62 | |

[a] For technical reasons we were unable to obtain the $4d$ populations and the Rh charge for the $D_{2d}$ $^3B_1$ state. We anticipate that these numbers are identical to those of the $D_{2h}$ $^3B_{1g}$ state.
[b] $E_\alpha$ is given as the total contribution of charge-induced polarization to the energy of $Rh(CH_4)_2^+$ – 10.2 kcal/mol (the contribution of charge-induced polarization to the energy of $C_{2v}$ $Rh(CH_4)^+$.

more extensive *sd* hybridization.

### 5.4.3 $Fe(CH_4)_2^+$

We have considered only one state of $Fe(CH_4)_2^+$ (see Table IX and Figure 14). This is the $\eta^3$ $D_{3d}$ $^4E_g$ state with the $d_{z^2}$ and $d_{xy}$ orbitals of the metal doubly occupied as in the ground state of $Fe(CH_4)^+$. We assume that the sextet state of $Fe(CH_4)_2^+$ is only weakly bound. Since the first $CH_4$ strongly polarizes the $4s$ electron away from the ligand, a second $CH_4$ would be repelled upon bonding at an angle of 180°.

The motivation for these calculations was largely as a means to verify the nature of the $Fe(CH_4)^+$ ground state. As there is some question as to whether adiabatic or diabatic bond energies are being measured for $Fe^+ + CH_4$, a comparison between our calculated second bond strength and the experimental value may help render a conclusion on this matter. In excellent agreement with experiment, we find a dissociation energy of $D_e$=22.7 kcal/mol (compared to Armentrout's value of $D_0^\circ$=23.3±1.0 kcal/mol[6]). [Note that since the extent of *sd* hybridization is approximately the same in $Fe(CH_4)_2^+$ as in $Fe(CH_4)^+$, there is no need to empirically correct the dissociation energy for the error in the state splittings.] As both calculated *adiabatic* first and second bond energies compare well to experiment, we conclude that adiabatic dissociation energies are being measured. The accuracy of the calculations is further supported by the calculations on the $Co^+$ clusters which also compared well with experiment.

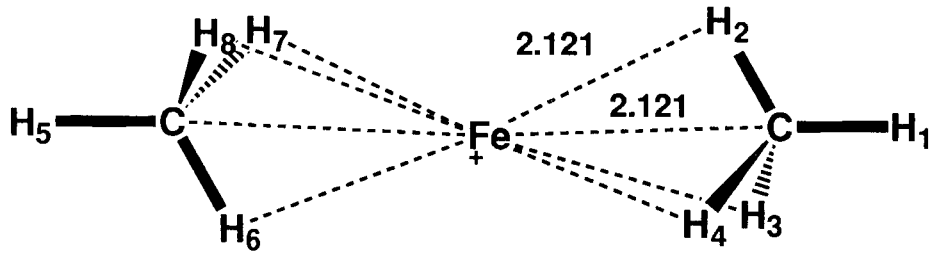


$\eta^3$ $D_{3d}$ $^4E_g$

| | | | |
|---|---|---|---|
| Fe | 0.0000 | 0.0000 | 0.0000 |
| $C_1$ | 0.0000 | 0.0000 | 2.1210 |
| $C_2$ | 0.0000 | 0.0000 | -2.1210 |
| $H_1$ | 0.0000 | 0.0000 | 3.2012 |
| $H_2$ | 0.0000 | 1.0595 | 1.8374 |
| $H_3$ | 0.9175 | -0.5297 | 1.8374 |
| $H_4$ | -0.9175 | -0.5297 | 1.8374 |
| $H_5$ | 0.0000 | 0.0000 | -3.2012 |
| $H_6$ | 0.0000 | -1.0595 | -1.8374 |
| $H_7$ | 0.9175 | 0.5297 | -1.8374 |
| $H_8$ | -0.9175 | 0.5297 | -1.8374 |

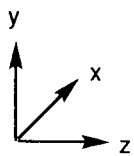


**Figure 14.** Geometries for one state of $Fe(CH_4)_2^+$. Cartesian coordinates in Å.

**Table IX.** Properties of $Fe(CH_4)_2^+$.

| | $\eta^3$ $D_{3d}$ $^3E_g$ |
|---|---|
| $D_e$ (kcal/mol)[a] | 22.7 |
| $D_e$ (unrelaxed) | 20.8 |
| $\omega_e$ (sym C–Fe–C, $cm^{-1}$) | 333 |
| $r_e$ (Fe–C, Å) | 2.12 |
| $r_e$ (Fe–H) | 2.12 |
| $E_\alpha^b$ | 17.8 |
| $r_\alpha$ | 2.22 |
| $3d$ population | 6.74 |
| charge on Fe | +0.60 |

[a] The experimental bond strength is $D_0^\circ$=23.3±1.0 kcal/mol.
[b] $E_\alpha$ is given as the total contribution of charge-induced polarization to the energy of $Fe(CH_4)_2^+$ − 17.8 kcal/mol (the contribution of charge-induced polarization to the energy of $C_{2v}$ $Fe(CH_4)^+$.

## 5.5 $M(C_2H_6)^+$

### 5.5.1 $Co(C_2H_6)^+$

The potential energy surface for $Co(C_2H_6)^+$ is quite flat. Four different coordination sites (Figure 15) were investigated with the difference in BDE's being $\leq$1.4 kcal/mol (see Table X). These structures are

(a) coordination of the $Co^+$ to three hydrogen atoms bound to different carbon atoms ($\eta^3$ $C_s$), worth $D_e$=25.0 kcal/mol,

(b) coordination of the $Co^+$ to two hydrogen atoms bound to different carbon atoms ($\eta^2$ $C_2$), worth $D_e$=24.9 kcal/mol,

(c) coordination of the $Co^+$ to two hydrogen atoms bound to the same carbon atom ($\eta^2$ $C_s$), worth $D_e$=24.7 kcal/mol, and

(d) coordination of the $Co^+$ to three hydrogen atoms bound to the same carbond atom ($\eta^3$ $C_{3v}$), worth $D_e$=23.6 kcal/mol.

The calculated complexation energy of $D_e$=25.0 kcal/mol can be compared to the experimental values of $D_0^\circ$=28.0$\pm$1.1[4] and $D_0^\circ$=24.0$\pm$0.7 kcal/mol.[5]

While it would superficially appear that the two geometries which describe coordination of the $Co^+$ to two carbons, in $C_2$ and $C_s$ symmetries, should have properties comparable to that of $Co(H_2)^+$ (*i.e.*, coordination to the C$-$C or H$-$H bond, see Chapter IV), the bonding is more consistently described as coordination to C$-$H bonds. The lowest energy $C_s$ structure should be considered as an $\eta^3$ coordination to one C$-$H bond on one carbon and to two C$-$H bonds on the other while the $C_2$ structure should be considered as an $\eta^2$ coordination to one C$-$H bond on each of the two carbons. A number of points lead us to this conclusion:

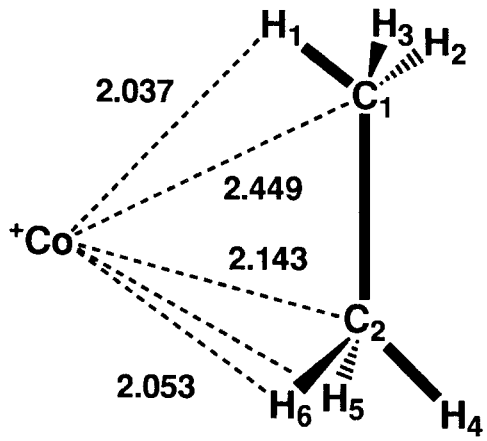


## $\eta^3$ $C_s$ $^3A''$

| | | | |
|---|---|---|---|
| Co | 0.0000 | -0.4562 | -2.1200 |
| $C_1$ | 0.0000 | 0.7692 | 0.0000 |
| $C_2$ | 0.0000 | -0.7692 | 0.0000 |
| $H_1$ | 0.0000 | 1.2414 | -0.9947 |
| $H_2$ | 0.8826 | 1.1464 | 0.4947 |
| $H_3$ | -0.8826 | 1.1464 | 0.4947 |
| $H_4$ | 0.0000 | -1.1579 | 1.0011 |
| $H_5$ | 0.9061 | -1.2082 | -0.4379 |
| $H_6$ | -0.9061 | -1.2082 | -0.4379 |

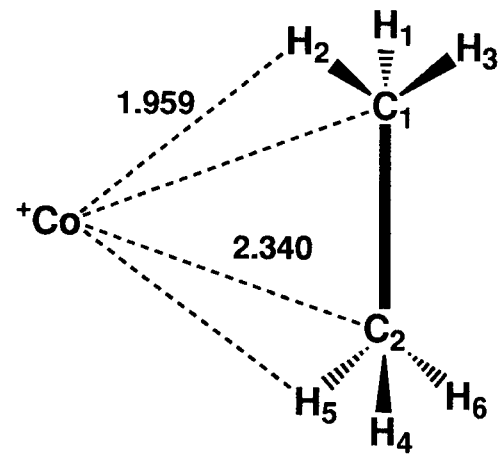


## $\eta^2$ $C_2$ $^3B$

| | | | |
|---|---|---|---|
| Co | 0.0000 | 0.0000 | -2.2100 |
| $C_1$ | 0.0000 | 0.7683 | 0.0000 |
| $C_2$ | 0.0000 | -0.7683 | 0.0000 |
| $H_1$ | 1.0010 | 1.1786 | 0.0260 |
| $H_2$ | -0.5643 | 1.2556 | -0.8162 |
| $H_3$ | -0.5255 | 1.1231 | 0.8764 |
| $H_4$ | -1.0010 | -1.1786 | 0.0260 |
| $H_5$ | 0.5643 | -1.2556 | -0.8162 |
| $H_6$ | 0.5255 | -1.1231 | 0.8764 |

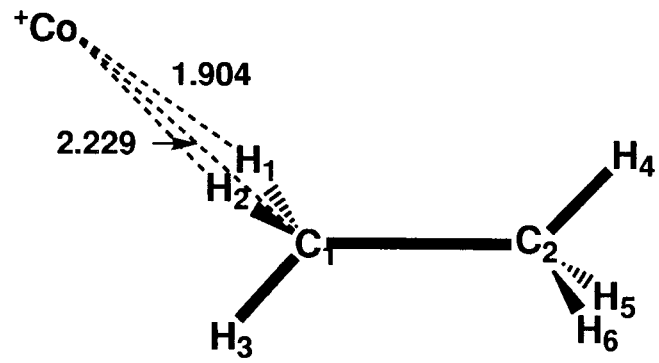


$\eta^2$ $C_s$ $^3A''$

| | | | |
|---|---|---|---|
| Co | 0.0000 | 1.7612 | -1.3662 |
| $C_1$ | 0.0000 | 0.0000 | 0.0000 |
| $C_2$ | 0.0000 | 0.0057 | 1.5316 |
| $H_1$ | 0.9454 | 0.4529 | -0.3570 |
| $H_2$ | -0.9454 | 0.4529 | -0.3570 |
| $H_3$ | 0.0000 | -1.0020 | -0.4097 |
| $H_4$ | 0.0000 | 1.0150 | 1.9276 |
| $H_5$ | 0.8777 | -0.5069 | 1.9066 |
| $H_6$ | -0.8777 | -0.5069 | 1.9066 |

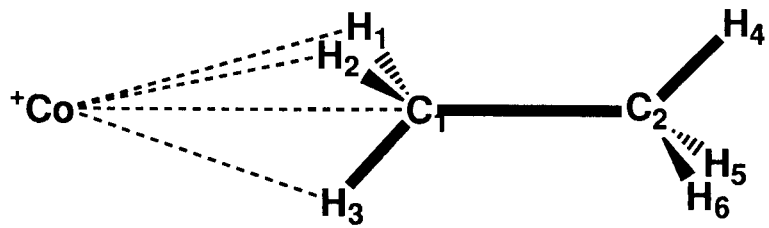


$\eta^3$ $C_{3v}$ $^3A_2$

| | | | |
|---|---|---|---|
| Co | 0.0000 | 0.0000 | -2.0880 |
| $C_1$ | 0.0000 | 0.0000 | 0.0000 |
| $C_2$ | 0.0000 | 0.0000 | 1.5394 |
| $H_1$ | 0.9097 | 0.5252 | -0.3270 |
| $H_2$ | -0.9097 | 0.5252 | -0.3270 |
| $H_3$ | 0.0000 | -1.0504 | -0.3270 |
| $H_4$ | 0.0000 | 1.0156 | 1.9114 |
| $H_5$ | 0.8795 | -0.5078 | 1.9114 |
| $H_6$ | -0.8795 | -0.5078 | 1.9114 |

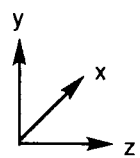


**Figure 15.** Geometries of four states of $Co(C_2H_6)^+$. Cartesian coordinates are in Å.

**Table X.** Properties of $Co(C_2H_6)^+$.

| | $\eta^3$ $C_s$ $^3A''$ | $\eta^2$ $C_2$ $^3B$ | $\eta^2$ $C_s$ $^3A''$ | $\eta^3$ $C_{3v}$ $^3A_2$ |
|---|---|---|---|---|
| $D_e$ (kcal/mol)[a] | 25.0 | 24.9 | 24.7 | 23.6 |
| $D_e$ (unrelaxed) | 23.6 | 22.8 | 22.6 | 22.4 |
| $\omega_e$ (Co–C, $cm^{-1}$) | | 261 | 286 | 288 |
| $r_e$ (Co–$C_1$, Å) | 2.14 | 2.34 | 2.23 | 2.09 |
| $r_e$ (Co–$C_2$, Å) | 2.45 | 2.34 | 3.39 | 3.63 |
| $r_e$ (Co–H) | 2.05, 2.04[b] | 1.96 | 1.90 | 2.05 |
| $E_\alpha$ | 25.5 | 23.8 | 21.3 | 22.1 |
| $r_\alpha$ | 2.32 | 2.36 | 2.43 | 2.40 |
| $3d$ population | 7.90 | 7.93 | 7.88 | 7.86 |
| $\mu$ (D) | +3.037 | +2.923 | +2.989 | +3.327 |
| charge on Co | +0.61 | +0.67 | +0.62 | +0.63 |

[a] The experimental values are $D_0^\circ$=28.0±1.1[4] and 24.0±0.7 kcal/mol.[5]
[b] The first number is the distance from the $Co^+$ to the two closest H atoms bound to $C_1$ and the second is the distance to the closest H atom bound to $C_2$.

(1) The Co–H bond distances are comparable to what they are in $Co(CH_4)^+$.

(2) The $Co^+$ is approximately equidistant from the three hydrogens in the $\eta^3$ $C_s$ geometry of $Co(C_2H_6)^+$ but is significantly closer to one of the carbons than the other ($r_e$(Co–C)=2.14 vs. 2.45Å).

(3) The $\eta^3$ $C_s$ electronic configuration of $Co(C_2H_6)^+$ is consistent with our arguments for bonding in $\eta^3$ $Co(CH_4)^+$.

(4) The $\eta^2$ $C_2$ electronic configuration is consistent with our arguments for bonding in $\eta^2$ $Co(CH_4)^+$.

These last two points are perhaps most convincing. For the $\eta^3$ $C_s$ structure, there is a singly occupied $d'_\sigma$ orbital directed toward the in-plane C–H bond and a singly occupied $d'_\delta$ orbital directed toward the two out-of-plane C–H bonds on

the other carbon. Both of these orbitals accept charge from the ethane, as does the $4s$ orbital. A second $d_\sigma$ orbital, offset from the $d'_\sigma$ orbital by $\sim$54.74°, is doubly occupied and is directed toward the C−C bond, hybridizing with the $4s$ to reduce repulsion. For the $\eta^2$ $C_2$ structure, a $d_\pi$ orbital, approximately in the H−Co−H plane, is singly occupied and accepts charge from the ligand as in the $^3B_2$ ground state of $Co(CH_4)^+$. In contrast, if $Co^+$ were to strictly coordinate to the C−C bond it would likely possess $d_{z^2}$ and $d_{xy}$ holes (with the C−Co−C backbone in the $yz$ plane and $z$ the $C_2$ axis of rotation), as in the ground state of $Co(H_2)^+$. Such a state would have a doubly occupied $d_{yz}$ orbital capable of backbonding to the C−C bond, resulting in a molecular complex suitable for insertion into the C−C bond. We should note that in both the $\eta^3$ $C_s$ and $\eta^2$ $C_2$ structures, *sd* hybridization appears to be smaller than in $Co(CH_4)^+$ and the two $Co(C_2H_6)^+$ structures in which the $Co^+$ is coordinated to only one carbon. The distances are such that Pauli repulsion to the $d_\sigma$ orbital is less on coordination to two carbons rather than one.

The $\eta^2$ coordination of two C−H bonds on the *same* carbon center in $C_s$ symmetry is only 0.3 kcal/mol higher in energy than the lowest energy $\eta^3$ $C_s$ state and only 0.2 kcal/mol higher in energy than the $\eta^2$ $C_2$ state. There is a strong similarity to the $C_{2v}$ $^3B_2$ state of $Co(CH_4)^+$ both electronically and geometrically. This can be seen in the extent of *sd* hybridization (both clusters have $3d$ populations of 7.88 electrons) and the results of the geometry relaxation. It appears that $\eta^2$ coordination to C−H bonds is favorable for $Co^+$ regardless of whether the bonds are on the same center or different centers.

The $\eta^3$ coordination to a single carbon of $C_2H_6$ in $C_{3v}$ symmetry is worth $D_e$=23.6 kcal/mol. This is higher in energy than the ground state $\eta^3$ $C_s$ structure by 1.4 kcal/mol and the nature of the bond is entirely analogous to that of

$C_{3v}$ $Co(CH_4)^+$. It should be noted that this geometry is consistent with coordination to the negative quadrupole moment of $C_2H_6$, but this effect is small.

The increased bond strength of $Co(C_2H_6)^+$ as compared to that of $Co(CH_4)^+$ is principally due to an increase in the polarizability of the ligand [$\alpha(CH_4)$=2.59 Å$^3$, $\alpha(C_2H_6)$=4.47 Å$^3$]. The relationship is clearly not linear, however, reflecting the fact that the increasing size of the ligand reduces the effective value of the metal-ligand distance. We calculate the contribution from ion-induced polarization in $Co(C_2H_6)^+$ to range from 21.3 kcal/mol (for the $\eta^2$ $C_s$ structure) to 25.5 kcal/mol (for the $\eta^3$ $C_s$ structure). In addition, a decrease in the ionization potential of the ligand [IP($CH_4$)=12.70 eV, IP($C_2H_6$)=11.52 eV] may facilitate increased charge transfer [the charge on the metal is in fact smaller for $Co(C_2H_6)^+$ than for $Co(CH_4)^+$]. Evidence for the importance of polarizability and charge transfer on the bond strength is also seen in the large increase in the dipole moment in going from $Co(CH_4)^+$ to $Co(C_2H_6)^+$.

In Figure 16, we illustrate the four most likely structures for $Co(C_2H_6)_2^+$. The structures are predicted based on the results of these $Co(C_2H_6)^+$ calculations in addition to the results for $Co(CH_4)_2^+$. Bowers[4] finds the second bond to be weaker than the first by 1.2 kcal/mol ($D_0^\circ$=26.8±1.0 vs. $D_0^\circ$=28.0±1.6 kcal/mol). Based on the $Co(CH_4)^+$ results, we might expect the second ethane molecule to actually form a stronger bond than the first. However, sterics is more of a problem with ethane (particularly in structures 17*a* and 17*b*) and *sd* hybridization [the cause of the increase in the second bond strength of $Co(CH_4)^+$] is slightly smaller in the two lowest energy states of $Co(C_2H_6)^+$. These effects will tend to lead to either a decrease (sterics) or only a small increase (*sd* hybridization) in the second bond strength.

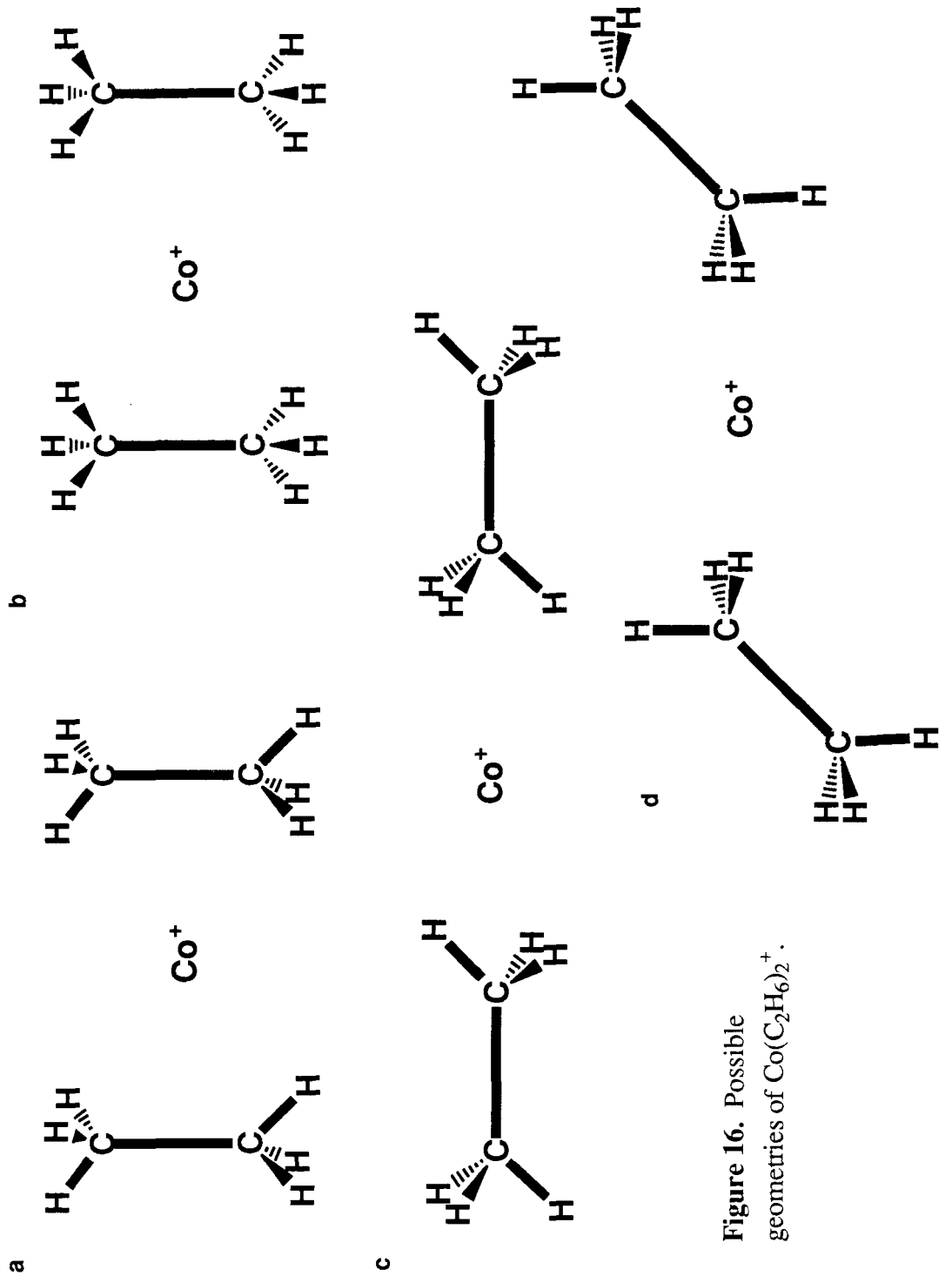


**Figure 16.** Possible geometries of $Co(C_2H_6)_2^+$.

### 5.5.2 $Rh(C_2H_6)^+$ and $Ir(C_2H_6)^+$

Following the discussion on the differences between $Co(CH_4)^+$ and $Rh(CH_4)^+$, the most interesting comparison to make for various possible configurations of $Rh(C_2H_6)^+$ might be between the $^3A_2$-like and $^3B_2$-like states of the $\eta^2$ $C_2$ structure. Since *sd* hybridization is more difficult to achieve in $Rh^+$, Pauli repulsion is best reduced by singly occupying the most repulsive orbital. In the case of $Rh(CH_4)^+$ this is the $d_{z^2}$ orbital. (The $d_{xy}$ orbital is also singly occupied as explained previously to obtain a $^3A_2$ ground state.) In the case of $Co(CH_4)^+$, the repulsion of the $d_{z^2}$ orbital can be reduced by *sd* hybridization such that the second most repulsive orbital ($d_{yz}$) is singly occupied. (The $d_{x^2}$ orbital is also singly occupied as explained to obtain a $^3B_2$ ground state.) For $Co(C_2H_6)^+$, the analogous state was found to be the lowest lying in $C_2$ symmetry, with a $d_\pi$ orbital (in the H−Co−H plane) singly occupied instead of the $d_{z^2}$ orbital. However, it was noticed that *sd* hybridization is less extensive in $Co(C_2H_6)^+$ when the $Co^+$ is coordinated to two carbons rather than one, suggesting that the $d_{z^2}$ orbital is less repulsive to the ligand with this coordination. Thus, if *sd* hybridization is of minimal importance in the $\eta^2$ $C_2$ geometry, does the lowest lying state of $\eta^2$ $C_2$ $Rh(C_2H_6)^+$ have the $d_{z^2}$ or $d_\pi$ orbital singly occupied?

The results of this comparison of states are given in Table XI and Figure 17. The $^3B$ state [the lowest lying $C_2$ state for $Co(C_2H_6)^+$ and the analogue to the $^3B_2$ state of $\eta^2$ $Rh(CH_4)^+$] is 7.0 kcal/mol more favorable than the $^3A$ state [the analogue to the $^3A_2$ state of $\eta^2$ $Rh(CH_4)^+$]. The $^3A$ bond length (2.76 Å to the center of the C−C bond) is also significantly longer than the $^3B$ bond length (2.47 Å). These two properties strongly indicate that the dominant interaction of the metal with the ligand is with the C−H bonds and not the C−C bond,

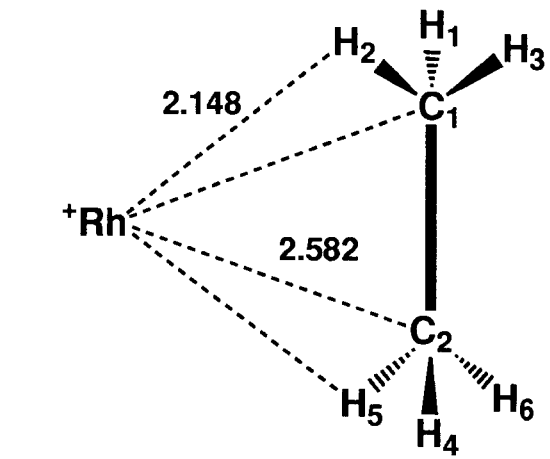


$\eta^2 C_2\ ^3B$

| | | | |
|---|---|---|---|
| Rh | 0.0000 | 0.0000 | -2.4560 |
| $C_1$ | 0.0000 | 0.7683 | 0.0000 |
| $C_2$ | 0.0000 | -0.7683 | 0.0000 |
| $H_1$ | 1.0014 | 1.1786 | 0.0260 |
| $H_2$ | -0.5642 | 1.2555 | -0.8161 |
| $H_3$ | -0.5256 | 1.1231 | 0.8765 |
| $H_4$ | -1.0014 | -1.1786 | 0.0260 |
| $H_5$ | 0.5642 | -1.2555 | -0.8161 |
| $H_6$ | 0.5256 | -1.1231 | 0.8765 |

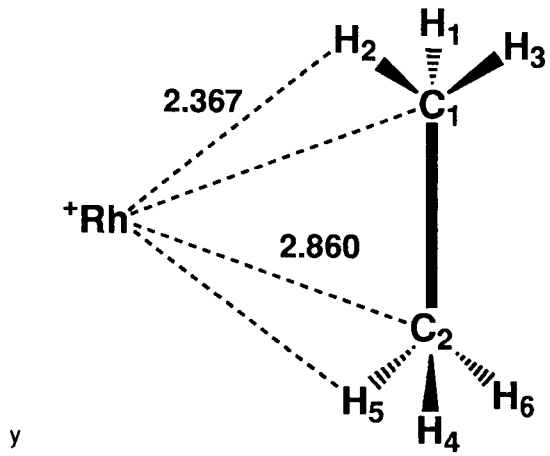


$\eta^2 C_2\ ^3A$

| | | | |
|---|---|---|---|
| Rh | 0.0000 | 0.0000 | -2.7550 |
| $C_1$ | 0.0000 | 0.7678 | 0.0000 |
| $C_2$ | 0.0000 | -0.7678 | 0.0000 |
| $H_1$ | 1.0039 | 1.1744 | -0.0148 |
| $H_2$ | -0.5815 | 1.2211 | -0.8119 |
| $H_3$ | -0.4804 | 1.1337 | 0.8986 |
| $H_4$ | -1.0039 | -1.1744 | -0.0148 |
| $H_5$ | 0.5815 | -1.2211 | -0.8119 |
| $H_6$ | 0.4804 | -1.1337 | 0.8986 |

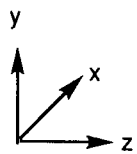


**Figure 17.** Geometries for two states of $Rh(C_2H_6)^+$. Cartesian coordinates are in Å.

**Table XI.** Properties of $Rh(C_2H_6)^+$.

| | $\eta^2$ $C_2$ $^3$B | $\eta^2$ $C_2$ $^3$A |
|---|---|---|
| $D_e$ (kcal/mol) | 19.1 | 12.1 |
| $D_e$ (unrelaxed) | 17.6 | 11.5 |
| $\omega_e$ (Rh–C, $cm^{-1}$) | 216 | 151 |
| $r_e$ (Rh–C, Å) | 2.58 | 2.86 |
| $r_e$ (Rh–H) | 2.15 | 2.37 |
| $E_\alpha$ | 16.4 | 11.4 |
| $r_\alpha$ | 2.59 | 2.84 |
| $4d$ population | 7.92 | 7.91 |
| $\mu$ (D) | +3.085 | +2.489 |
| charge on Rh | +0.78 | +0.90 |

with the implication that the $d_{z^2}$ orbital is no longer the most repulsive orbital to the ligand and that *sd* hybridization is not as important as in the methane clusters. Thus, the ground state is the same as in $Co(C_2H_6)^+$.

A similar comparison can be made for $Ir(C_2H_6)^+$. However, in this case, because *sd* hybridization is more effective with $Ir^+$ than with the other metals, a comparison between the two $\eta^2$ structures of $Ir(C_2H_6)^+$ (involving coordination to two C–H bonds on either the same or different carbons) is more interesting (see Figure 18). Since in $Co(C_2H_6)^+$ there is less *sd* hybridization in the $\eta^2$ $C_2$ structure than in the $\eta^2$ $C_s$ structure, one might expect then that the structure which benefits more from *sd* hybridization would be favored in $Ir(C_2H_6)^+$. From Table XII, it can be seen that this is indeed the case. The ground state has a geometry in which the $Ir^+$ is coordinated to two C–H bonds on the same metal. The adiabatic bond strength for this structure is $D_e$=26.0 kcal/mol compared to the $C_2$ geometry, with coordination of the metal to two C–H bonds on different centers, which is 2.1 kcal/mol weaker. It should be kept in mind that

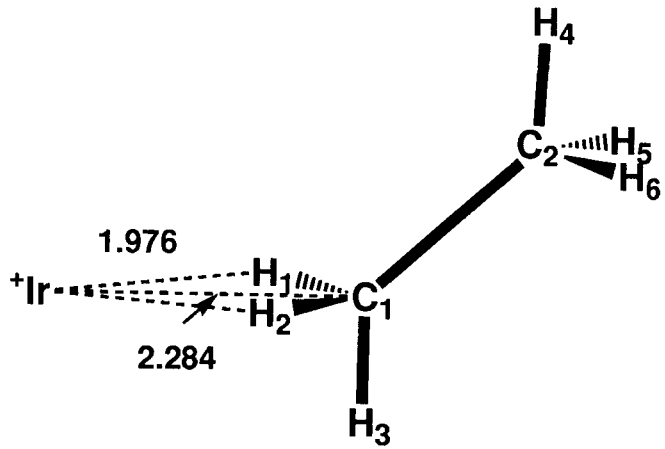


$\eta^2$ $C_s$ $^3A''$

| | | | |
|---|---|---|---|
| Ir | 0.0000 | 0.0000 | -2.2840 |
| $C_1$ | 0.0000 | 0.0000 | 0.0000 |
| $C_2$ | 0.0000 | 1.2136 | 0.9324 |
| $H_1$ | 0.9746 | 0.0000 | -0.5647 |
| $H_2$ | -0.9746 | 0.0000 | -0.5647 |
| $H_3$ | 0.0000 | -0.9426 | 0.5276 |
| $H_4$ | 0.0000 | 2.1433 | 0.3759 |
| $H_5$ | 0.8790 | 1.1904 | 1.5628 |
| $H_6$ | -0.8790 | 1.1904 | 1.5628 |

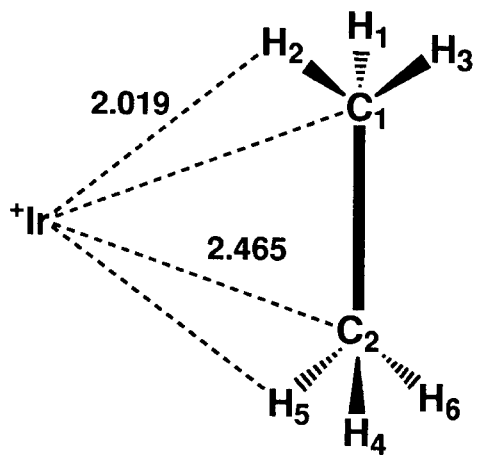


$\eta^2$ $C_2$ $^3B$

| | | | |
|---|---|---|---|
| Ir | 0.0000 | 0.0000 | -2.3420 |
| $C_1$ | 0.0000 | 0.7698 | 0.0000 |
| $C_2$ | 0.0000 | -0.7698 | 0.0000 |
| $H_1$ | 0.9944 | 1.1826 | 0.1074 |
| $H_2$ | -0.4982 | 1.2828 | -0.8647 |
| $H_3$ | -0.6088 | 1.1325 | 0.8184 |
| $H_4$ | -0.9944 | -1.1826 | 0.1074 |
| $H_5$ | 0.4982 | -1.2828 | -0.8647 |
| $H_6$ | 0.6088 | -1.1325 | 0.8184 |

**Figure 18.** Geometries for two states of $Ir(C_2H_6)^+$. Cartesian coordinates are in Å.

**Table XII.** Properties of $Ir(C_2H_6)^+$.

| | $\eta^2$ $C_s$ $^3A''$ | $\eta^2$ $C_2$ $^3B$ |
|---|---|---|
| $D_e$ (kcal/mol) | 26.0 | 23.9 |
| $D_e$ (unrelaxed) | 22.1 | 20.0 |
| $\omega_e$ (Ir–C, $cm^{-1}$) | 289 | 261 |
| $r_e$ (Ir–$C_1$, Å) | 2.28 | 2.47 |
| $r_e$ (Ir–$C_2$, Å) | 3.44 | 2.47 |
| $r_e$ (Ir–H) | 1.98 | 2.02 |
| $E_\alpha$ | 18.8 | 20.2 |
| $r_\alpha$ | 2.51 | 2.46 |
| $5d$ population | 7.74 | 7.87 |
| $\mu$ (D) | +3.886 | +3.806 |
| charge on Ir | +0.56 | +0.59 |

these two structures are nearly degenerate for $Co(C_2H_6)^+$.

The difference is clearly in the *sd* hybridization. The $5d$ population in the $C_s$ geometry is 7.74 electrons whereas in the $C_2$ geometry it is 7.87 electrons. This indicates that significantly more *sd* hybridization is present in the $C_s$ geometry, as expected.

## 5.6 $M(C_3H_8)^+$

### 5.6.1 $Co(C_3H_8)^+$

Due to the size of the $Co(C_3H_8)^+$ calculations, we considered only two high symmetry coordinations in detail. A third coordination (with a lower symmetry) was also considered by making a guess at the geometry and calculating only a single energy. The high symmetry geometries are the $\eta^2$ coordination to the secondary carbon (see Figure 19*a*) and the $\eta^4$ coordination to the two primary carbons (19*b*). Both of these structures have $C_{2v}$ symmetry. Other possible sites, including the $\eta^2$ and $\eta^3$ coordinations to a primary carbon or $\eta^2$ and $\eta^3$ coordination to a primary and secondary carbon, have $C_s$ or $C_1$ symmetry and have not been looked at. The $C_s$ structure involving coordination of the metal to all three carbons (19*c*) was considered due to the likelihood of this being the optimal geometry.

Results of these calculations are detailed in Table XIII. Of the two $C_{2v}$ structures, we find the $\eta^4$ coordination to be lower in energy than the $\eta^2$ coordination by 0.8 kcal/mol out of 27.6 kcal/mol. This is somewhat shy of the experimental value of $D_0^\circ$=30.9±1.4 kcal/mol.[5] While the $\eta^2$ structure shows the same characteristics as $Co(CH_4)^+$ and $Co(C_2H_6)^+$, the $\eta^4$ structure is somewhat different, but it still appears to be more appropriately described as coordination to four C−H bonds rather than coordination to the carbons. The ground state has a $Co^+$ configuration of

$$(a_1 d_{y^2-z^2})^2 (a_2 d_{xy})^2 (b_1 d_{xz})^2 (a_1 d_{x^2})^1 (b_2 d_{yz})^1$$

The Co and the C-C-C backbone are in the $yz$ plane and $z$ is the principal axis. The singly occupied $d_{yz}$ orbital minimizes repulsion to the ligand. However, the

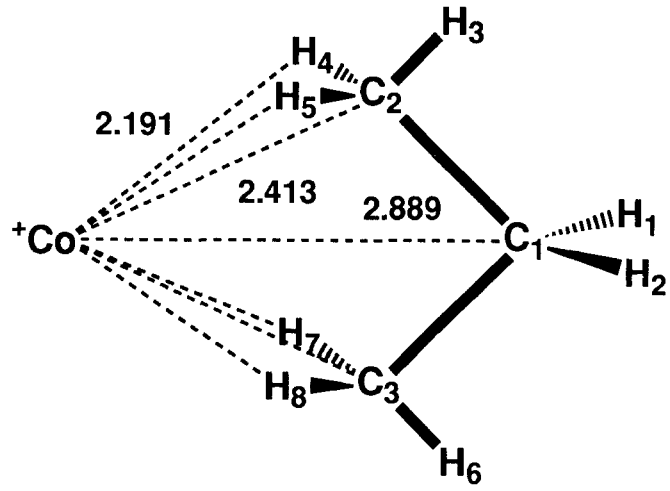


## $\eta^4\ C_{2v}\ ^3B_2$

| | | | |
|---|---|---|---|
| Co | 0.0000 | 0.0000 | 0.0000 |
| $C_1$ | 0.0000 | 0.0000 | 2.8890 |
| $C_2$ | 0.0000 | 1.2930 | 2.0371 |
| $C_3$ | 0.0000 | -1.2930 | 2.0371 |
| $H_1$ | 0.8686 | 0.0000 | 3.5290 |
| $H_2$ | -0.8686 | 0.0000 | 3.5290 |
| $H_3$ | 0.0000 | 2.1790 | 2.6523 |
| $H_4$ | 0.9075 | 1.3867 | 1.4334 |
| $H_5$ | -0.9075 | 1.3867 | 1.4334 |
| $H_6$ | 0.0000 | -2.1790 | 2.6523 |
| $H_7$ | 0.9075 | -1.3867 | 1.4334 |
| $H_8$ | -0.9075 | -1.3867 | 1.4334 |

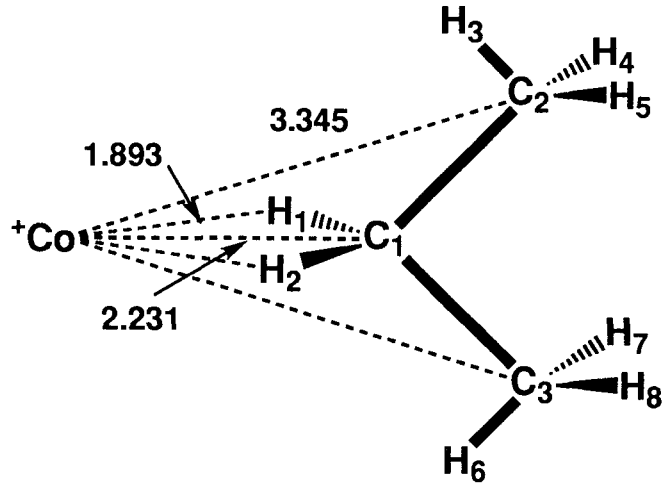


## $\eta^2\ C_{2v}\ ^3B_1$

| | | | |
|---|---|---|---|
| Co | 0.0000 | 0.0000 | 0.0000 |
| $C_1$ | 0.0000 | 0.0000 | 2.2310 |
| $C_2$ | 0.0000 | 1.2860 | 3.0877 |
| $C_3$ | 0.0000 | -1.2860 | 3.0877 |
| $H_1$ | 0.9362 | 0.0000 | 1.6457 |
| $H_2$ | -0.9362 | 0.0000 | 1.6457 |
| $H_3$ | 0.0000 | 2.1807 | 2.4805 |
| $H_4$ | 0.8775 | 1.3044 | 3.7173 |
| $H_5$ | -0.8775 | 1.3044 | 3.7173 |
| $H_6$ | 0.0000 | -2.1807 | 2.4805 |
| $H_7$ | 0.8775 | -1.3044 | 3.7173 |
| $H_8$ | -0.8775 | -1.3044 | 3.7173 |

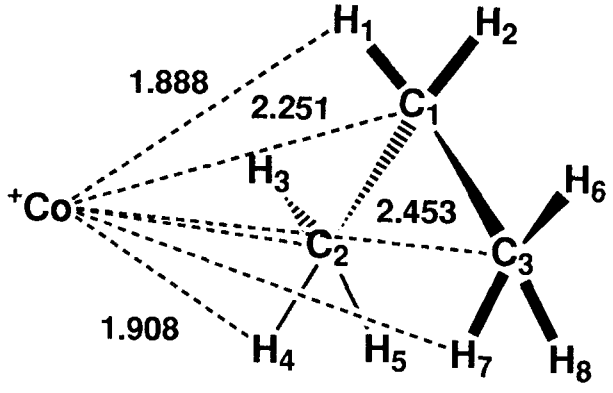


$\eta^3$ $C_s$ $^3A''$

| | | | |
|---|---|---|---|
| Co | 0.0000 | 0.0000 | 0.0000 |
| $C_1$ | 0.0000 | 0.8100 | 2.1000 |
| $C_2$ | 1.2681 | -0.0389 | 2.1000 |
| $C_3$ | -1.2681 | -0.0389 | 2.1000 |
| $H_1$ | 0.0000 | 1.4677 | 1.2233 |
| $H_2$ | 0.0000 | 1.4677 | 2.9767 |
| $H_3$ | 2.1666 | 0.5763 | 2.1000 |
| $H_4$ | 1.2986 | -0.6852 | 1.2178 |
| $H_5$ | 1.2986 | -0.6852 | 2.9822 |
| $H_6$ | -2.1666 | 0.5763 | 2.1000 |
| $H_7$ | -1.2986 | -0.6852 | 1.2178 |
| $H_8$ | -1.2986 | -0.6852 | 2.9822 |

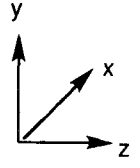


**Figure 19.** Geometries of three states of $Co(C_3H_8)^+$. The geometry of $\eta^3$ $C_s$ $^3A''$ was not optimized. Cartesian coordinates are in Å.

Co−H distance is 2.19 Å compared to 1.89 Å for the $\eta^2$ strucure and less charge is transferred to the metal. The finding that the $\eta^4$ conformation is more stable is probably a result of better charge-induced polarization which we calculate to be 25.9 kcal/mol vs. 23.3 kcal/mol for the $\eta^2$ structure.

On the basis of the results of the $Co(CH_4)^+$ and $Co(C_2H_6)^+$ calculations, we were able to attempt a guess at a geometry for coordination of the metal to all three carbons above the plane of the molecule. The position of the $Co^+$ is such that it is 1.91 Å from each of the three hydrogens to which it is coordinated. The metal is then 2.25 Å from the secondary carbon and 2.45 Å from each of the primary carbons. Only a single point was calculated and the propane geometry was not allowed to relax. The motivation for doing such a calculation came from the large estimate for the charge-induced polarization for this geometry−34.9 kcal/mol. The magnitude of this number strongly suggested that this conformation is the ground state. Our calculations give a bond energy of $D_e$=27.7 kcal/mol, 1.4 kcal/mol better than the unrelaxed $D_e$ of the $\eta^4$ $C_{2v}$ structure. Based on similar calculations on $Fe(C_3H_8)^+$, including a geometry optimization, we estimate that this calculated dissociation energy is low by 2.5 kcal/mol. We therefore find the bond strength to be worth $D_e$=30.2 kcal/mol, in good agreement with experiment.

### 5.6.2 $Fe(C_3H_8)^+$

The clustering of $Fe^+$ with propane is of particular interest. Like $Co^+$, the smallest alkane which leads to elimination of $H_2$ (and $CH_4$) upon reaction with ground state $Fe^+$ is propane. However, unlike $Co^+$, there is a question of where on the potential energy surface the spin changes from sextet to quartet. It is clear that there must indeed be a change of spin, since an insertion product such as $Fe(H)(C_3H_7)^+$ with a sextet spin state would lie high in energy above the $Fe^+$ ($^6D$) + $C_3H_8$ asymptote and would not be an intermediate in the dehydrogenation or demethanation reactions. On the other hand, there is a strong probability that the quartet state of this insertion product is bound with respect to the $Fe^+$ ($^6D$) + $C_3H_8$ asymptote and that this is the intermediate which leads to the fragmentation channels.

Van Koppen, Kemper, and Bowers[25a] have suggested, based on gas phase chromotography studies, that the change of spin occurs with the formation of the $Fe(C_3H_8)^+$ cluster and not with the subsequent insertion into a C−H bond. This is illustrated in Figure 20. We find this to be the case, with the quartet adiabatic bond dissociation energy calculated to be $D_e$=19.8 kcal/mol while the sextet is only $D_e$=15.5 kcal/mol. The ground state dissociation energy is also in agreement with the experimentally determined value of $D_0^\circ$=19±2 kcal/mol.[7] Once again, these calculations are consistent with the measurement of adiabatic bond dissociation energies in these TCA and CID experiments.

Based on the results for $Co(C_3H_8)^+$, the quartet and sextet ground state geometries were assumed to involve coordination of the metal to all three carbons in $C_s$ symmetry. Again, a guess was taken for the geometry based on the results for $Fe(CH_4)^+$. The geometry for the quartet state was the same as that for

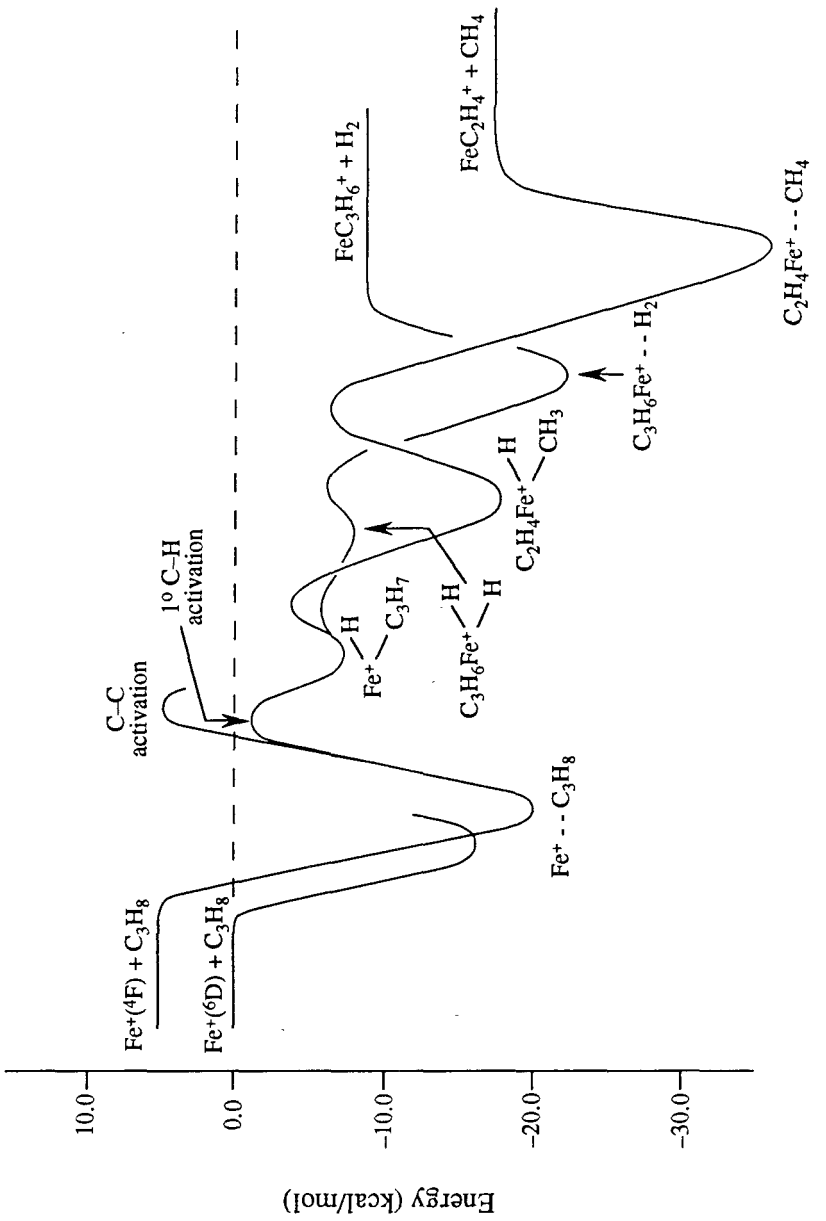


**Figure 20.** Best estimate from experiment to the potential energy surface for dehydrogenation and demethanation of propane by $Fe^+$. The crossing of the sextet and quartet surfaces upon formation of the ion-molecule complex is consistent with our results. From van Koppen, P.A.M.; Bowers, M.T.; Fisher, E.R.; Armentrout, P.B. *J. Am. Chem. Soc.*, submitted.

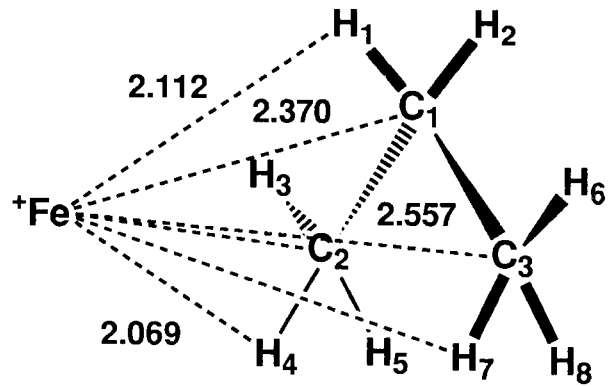


$\eta^3$ $C_s$ $^4A''$

| | | | |
|---|---|---|---|
| Fe | 0.0000 | 0.0000 | 0.0000 |
| $C_1$ | 0.0000 | 0.8300 | 2.2200 |
| $C_2$ | 1.2681 | -0.0189 | 2.2200 |
| $C_3$ | -1.2681 | -0.0189 | 2.2200 |
| $H_1$ | 0.0000 | 1.5764 | 1.4052 |
| $H_2$ | 0.0000 | 1.4602 | 3.1034 |
| $H_3$ | 2.1658 | 0.5921 | 2.2370 |
| $H_4$ | 1.3847 | -0.7104 | 1.3636 |
| $H_5$ | 1.2866 | -0.6738 | 3.0864 |
| $H_6$ | -2.1658 | 0.5921 | 2.2370 |
| $H_7$ | -1.3847 | -0.7104 | 1.3636 |
| $H_8$ | -1.2866 | -0.6738 | 3.0864 |

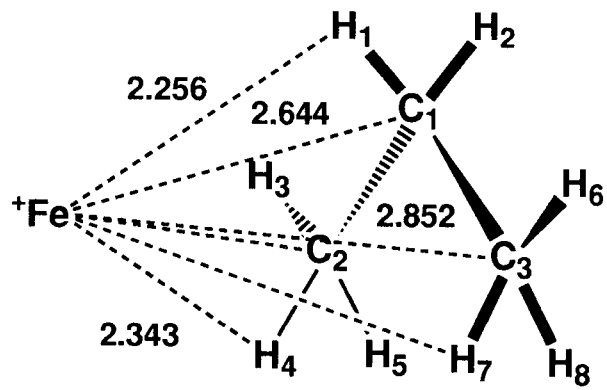


$\eta^3$ $C_s$ $^6A''$

| | | | |
|---|---|---|---|
| Fe | 0.0000 | 0.0000 | 0.0000 |
| $C_1$ | 0.0000 | 0.7000 | 2.5500 |
| $C_2$ | 1.2681 | -0.1489 | 2.5500 |
| $C_3$ | -1.2681 | -0.1489 | 2.5500 |
| $H_1$ | 0.0000 | 1.4467 | 1.7312 |
| $H_2$ | 0.0000 | 1.3418 | 3.4262 |
| $H_3$ | 2.1700 | 0.4576 | 2.5301 |
| $H_4$ | 1.3418 | 0.8662 | 1.7150 |
| $H_5$ | 1.2988 | 0.7714 | 3.4399 |
| $H_6$ | -2.1700 | 0.4576 | 2.5301 |
| $H_7$ | -1.3418 | 0.8662 | 1.7150 |
| $H_8$ | -1.2988 | 0.7714 | 3.4399 |

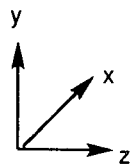


**Figure 21.** Geometries of two states of $Fe(C_3H_8)^+$. Cartesian coordinates are in Å.

$Co(C_3H_8)^+$ (Fe–C=2.25 and 2.45 Å, Fe–H=1.91 Å). The geometry for the sextet state placed the metal 0.4 Å further out of the C–C–C plane relative to the quartet state (Fe–C=2.63 and 2.80 Å, Fe–H=2.19 Å). The energies calculated at these geometries were $D_e$=17.3 kcal/mol for the quartet state and $D_e$=13.6 kcal/mol for the sextet state, making the appropriate empirical corrections to the quartet energy based on the 3*d* populations (6.89 electrons). An estimate to the relaxation energy was obtained by performing the complete geometry optimization as outlined in the appendix using a smaller basis set. The resulting geometries (shown in Figure 21) improved the quartet bond energy by 2.5 kcal/mol (from 9.7 to 12.2 kcal/mol) and the sextet bond energy by 1.8 kcal/mol (from 7.4 to 9.2 kcal/mol). These relaxation energies were then added to the energies obtained with the guessed geometries in the larger basis set.

## 5.7 Conclusions

We have looked at the complexation of small alkanes ($CH_4$, $C_2H_6$, and $C_3H_8$) to various transition metal ions ($Co^+$, $Rh^+$, $Ir^+$, and $Fe^+$). The calculated bond dissociation energies are summarized in Table XIV and compare well to experimental data, where available. As expected, we find the bonding to be dominated by the charge-induced dipole interaction. Consequently, the bond energy increases with the increasing polarizability of the ligand [*i.e.*, $D_e(M^+-CH_4) < D_e(M^+-C_2H_6) < D_e(M^+-C_3H_8)$]. Of secondary importance are charge transfer from ligand to metal, the ion-dipole interaction, and the ion-quadrupole interaction. Yet for each cluster, there exist many coordinations of the metal to the neutral molecule which are strongly bound. We have demonstrated that a few simple rules can aid in determining the most favorable geometries and electronic states for these clusters.

Of primary importance is the reduction in Pauli repulsion of the metal valence electrons to the ligand. This is generally accomplished by having the most repulsive orbitals of the metal empty or only partially occupied. As a result, a metal with an empty valence $s$ orbital will bond more strongly to a ligand than one with an occupied valence $s$ orbital. This is clearly seen in the results for $Fe(CH_4)^+$, $Fe(C_3H_8)^+$, and $Ir(CH_4)^+$ where a comparison of the high spin ($s^1d^{n-1}$) states and the low spin ($d^n$) states showed that in each case the ground state of the complex is low spin despite the fact that the ground state of the metal ion is high spin. The $d$ orbitals are also affected by this same principal of minimizing the occupations of the most repulsive orbitals. However, $sd$ hybridization is often just as effective in reducing Pauli repulsion in doubly occupied $d$ orbitals as having these orbitals singly occupied. Moreover, since the

**Table XIV. Summary of calculated dissociation energies, best estimates of dissociation energies, and experimental dissociation energies (in kcal/mol).**

| | theory | | experiment | |
|---|---|---|---|---|
| | $D_e$ | $D_0^\circ$ [a] | Armentrout | Bowers |
| $Co^+-CH_4$ | 21.4 | 21.7±2 | 21.4±1.2 | 22.9±0.7 |
| $(CH_4)Co^+-CH_4$ | 23.1 | 23.4±2 | 23.3±1.2 | 24.8±0.8 |
| $Co^+-C_2H_6$ | 25.0 | 25.4±2 | 24.0±0.7 | 28.0±1.6 |
| $Co^+-C_3H_8$ | 30.2 | 30.7±2 | 30.9±1.4 | |
| $Fe^+-CH_4$ | 12.9 | 13.1±2 | 13.7±0.8 | |
| $(CH_4)Fe^+-CH_4$ | 22.7 | 22.9±2 | 23.3±1.0 | |
| $Fe^+-C_3H_8$ | 19.8 | 20.3±2 | 19±2 | |
| $Rh^+-CH_4$ | 14.4 | 15.0±2 | | |
| $(CH_4)Rh^+-CH_4$ | 15.4 | 16.1±2 | | |
| $Rh^+-C_2H_6$ | 19.1 | 19.8±2 | | |
| $Ir^+-CH_4$ | 20.6 | 21.1±2 | | |
| $Ir^+-C_2H_6$ | 26.0 | 26.6±2 | | |

[a] The theoretical $D_0^\circ$ includes an estimate for the zero-point correction plus an empirical correction of 1 kcal/mol to account for deficiencies in the basis set and method of correlation.

ion-molecule interaction represents only a weak purturbation to the metal, the preservation of atomic coupling is a top priority. Thus, in these metal ions with >5 valence electrons, it is either the case that

(1) the most repulsive *d* orbital is singly occupied and the other *d* orbitals are singly occupied or doubly occupied to maintain the lowest energy atomic coupling, or

(2) the most repulsive *d* orbital is doubly occupied and hybridizes with the *s* orbital, the second most repulsive *d* orbital is singly occupied, and the other *d* orbitals are singly or doubly occupied to maintain the lowest energy atomic coupling.

Similar rules may be developed for metal ions with <5 valence electrons. The ordering of electronic states and the favorability of various geometries are then largely determined by the effectiveness of *sd* hybridization (dependent on the relative sizes and energies of the *s* and *d* orbitals) and the nature of the atomic couplings (dependent on the number of *d* electrons). These properties, in addition to variations in the sizes of the metal ions, lead to a unique chemistry for each of these transition metals.

A knowledge of these small clusters can improve the understanding of solvation. The observed variations in successive ligand bond energies in these clusters can be traced to spin changes, changes in hybridization and ligand-ligand interactions. For instance, it is often the case that the ground state of a given cluster may not be suitable for bonding an additional ligand but an excitated state may be more appropriate. This could be the case for $Co(CH_4)_2^+$ bonding a third methane, for instance. The ground state of the $Co(CH_4)_2^+$ cluster, while appropriate for bonding two ligands, does not appear to be appropriate for bonding a third. Thus, an excitation to a state more suitable to bonding this additional ligand may be important and this will weaken the third bond with respect to the second.

As detailed in the introduction, these ion-alkane complexes also have implications in the chemistry of alkane dehydrogenation and demethanation. The results suggest that, while there does indeed appear to be a correlation between the efficiency of various alkanes reacting with a particular metal and the ion-alkane well depth, a comparison between various metals reacting with a particular alkane does not appear to be related. In all cases studied, the ion-alkane well depth increases with the size of the ligand. This is as expected, as the polarizability of the alkane also increases with the size of the molecule. This

trend is also consistent with the experimental observations that the reactivity of alkanes toward a given metal ion generally increases with the size of the alkane. However, a comparison of the reactivity of a given alkane with various metals appears to be unconnected to the ion-alkane well depth. For instance, $Co^+$ is more strongly bound to ethane than is $Rh^+$ by nearly 6 kcal/mol. Yet, $Rh^+$ is capable of dehydrogenation of ethane while $Co^+$ is unreactive. In addition, the $Co^+$ bond to propane is 10 kcal/mol stronger than the $Fe^+$ bond, but both metals react with low efficiency. Clearly, the ion-alkane attraction is just the initial interaction on a complicated potential energy surface. There are many other factors which ultimately lead to the large variation in the chemistry of these metal ions toward alkanes and Chapters III–V have lain the groundwork to understand them. The impact of these various factors on the chemistry of $Co^+$, $Rh^+$, and $Ir^+$ will be explored in the next three chapters.

## Appendix

Geometry optimizations were performed at both the MCPF and HF levels. Since it was expected that the alkane geometries would not change dramatically upon complexation to the metal, a geometry optimization at the MCPF level was possible by holding the geometry of the alkane fixed and just optimizing the metal-alkane distance [in the case of $C_s$ $\eta^3$ $M(C_2H_6)^+$, this involved optimization of two degrees of freedom]. A full gradient geometry optimization at the HF level, while accounting for subtle changes in the alkane geometry, leads to a metal-alkane distance which is too long, and hence an MCPF done at this geometry would underestimate the bond strength by a few kcal/mol. However, we found that relaxation of the alkane geometry also adds a few kcal/mol to the bond energy, so a compromise was worked out. We first carried out the MCPF minimization with fixed *alkane* coordinates and followed this with an HF gradient geometry optimization in which the *metal* − *alkane* distance was fixed to the MCPF optimum. The MCPF energy was then recomputed at this new geometry.

The vibrational frequency of the metal-alkane stretch was computed by fitting a cubic polynomial to four points about the minimum (at increments of 0.1 Å) and treating the system as a diatomic. This was based on data from the MCPF optimization and did not include the relaxation of the alkane. As a result, we expect these frequencies to be underestimated by ~10%. In the case of $C_s$ $\eta^3$ $M(C_2H_6)^+$ and $C_s$ $M(C_3H_8)^+$, no frequencies were computed. From these data, it was possible to calculate approximate zero-point corrections for the bond energy. To roughly account for contributions from other modes (such as hindered rotations), we scaled the metal-alkane stretching frequency by a

factor of 1.5 (empirically derived).

We also made estimates of the contribution to the bond energy from the charge-induced polarization. This quantity was determined from

$$E_\alpha = -\frac{1}{2}\alpha q^2 r_\alpha^{-4}$$

where the average polarizability, $\alpha$, was taken from the literature, the charge on the ion, $q$, was taken as +1.0 esu, and the value of $r_\alpha$ was determined as

$$r_\alpha = \left( \left( \frac{1}{n} \right) \sum_{i=1}^{n} r_A^{-4} \right)^{-\frac{1}{4}}$$

where $r_A$ is the distance from the ion to one of $n$ atoms in the ligand. Determining $r_\alpha$ in such a manner takes into account the fact that the gradient of the electric field is quite large across the neutral molecule.

Basis set superposition error calculations indicated that we overestimate the metal-alkane bond strengths by ~2 kcal/mol. This is due primarily to a deficiency in the ligand basis set. However, our experience suggests that this BSSE is more than compensated by basis set incompleteness. Improvements to the ligand basis set would lead to a better description of the polarizability and thus a stronger bond. Factoring in other sources of error such as the limitations in the method of correlation and the geometry optimization, we estimate that we *underestimate* bond strengths by 1±1 kcal/mol.

The basis sets and effective potentials are as described in Chapter II. Only a single polarization function was used on the hydrogen atoms ($\alpha_p$=1.00). Using the standard two sets of polarization functions on the hydrogen atoms appeared to affect the bond energies by only a small fraction of a kcal/mol, so the smaller basis set was deemed sufficient. For $Fe^+$, a basis set for the Christiansen and Ermler relativistic effective potentials[26] was developed to be comparable to that for $Co^+$. It is given in Table XV.

**Table XV.** Basis set for $Fe^+$ for use with the relativistic effective core potential of Christiansen and Ermler.[26]

| | Exponent | Coef. | Coef. | Coef. | Coef. |
|---|---|---|---|---|---|
| *s* | 53.50 | -0.015466 | 0.000000 | 0.000000 | 0.000000 |
| | 17.72 | 0.072855 | 0.000000 | 0.000000 | 0.000000 |
| | 7.377 | -0.432016 | 0.000000 | 0.000000 | 0.000000 |
| | 2.018 | 0.437058 | 0.060968 | 0.000000 | 0.000000 |
| | 0.7799 | 0.000000 | 0.158266 | 0.000000 | 0.000000 |
| | 0.1142 | 0.000000 | 0.000000 | 1.000000 | 0.000000 |
| | 0.04189 | 0.000000 | 0.000000 | 0.000000 | 1.000000 |
| *p* | 49.12 | -0.009613 | 0.000000 | 0.000000 | 0.000000 |
| | 20.50 | -0.005904 | 0.000000 | 0.000000 | 0.000000 |
| | 8.987 | -0.069615 | 0.000000 | 0.000000 | 0.000000 |
| | 3.682 | 0.302486 | 0.000000 | 0.000000 | 0.000000 |
| | 1.522 | 0.588118 | 0.000000 | 0.000000 | 0.000000 |
| | 0.5927 | 0.000000 | 1.000000 | 0.000000 | 0.000000 |
| | 0.1976 | 0.000000 | 0.000000 | 1.000000 | 0.000000 |
| | 0.0659 | 0.000000 | 0.000000 | 0.000000 | 1.000000 |
| *d* | 47.10 | 0.018983 | 0.000000 | 0.000000 | |
| | 13.12 | 0.107205 | 0.000000 | 0.000000 | |
| | 4.478 | 0.294747 | 0.000000 | 0.000000 | |
| | 1.581 | 0.422007 | 0.000000 | 0.000000 | |
| | 0.5498 | 0.000000 | 1.000000 | 0.000000 | |
| | 0.1854 | 0.000000 | 0.000000 | 1.000000 | |
| *f* | 1.78 | 1.000000 | 0.000000 | | |
| | 0.45 | 0.000000 | 1.0000000 | | |

**References**

(1) Tonkyn, R.; Ronan, M.; Weisshaar, J.C. *J. Phys. Chem.* **1988**, *92*, 92.

(2) (a) Armentrout, P.B.; Beauchamp, J.L. *J. Am. Chem. Soc.* **1981**, *103*, 784. (b) Georgiadis, R.; Gisher, E.R.; Armentrout, P.B. *J. Am. Chem. Soc.* **1989**, *111*, 4251. (c) Jacobson, D.B.; Freiser, B.S. *J. Am. Chem. Soc.* **1983**, *105*, 5197.

(3) (a) van Koppen, P.A.M.; Brodbelt-Lustig, J.; Bowers, M.T.; Dearden, D.V.; Beauchamp, J.L.; Fisher, E.R.; Armentrout, P.B. *J. Am. Chem. Soc.* **1990**, *112*, 5663. (b) van Koppen, P.A.M.; Brodbelt-Lustig, J.; Bowers, M.T.; Dearden, D.V.; Beauchamp, J.L.; Fisher, E.R.; Armentrout, P.B. *J. Am. Chem. Soc.* **1991**, *113*, 2359.

(4) Kemper, P.R.; Bushnell, J.; van Koppen, P.; Bowers, M.T. *J. Phys. Chem.* **1993**, *97*, 52.

(5) Haynes, C.L.; Armentrout, P.B. Personal communication.

(6) Schultz, R.H.; Armentrout, P.B. *J. Phys. Chem.* **1993**, *97*, 596.

(7) Schultz, R.H.; Armentrout, P.B. *J. Phys. Chem.* **1992**, *96*, 1662.

(8) Schultz, R.H.; Armentrout, P.B. *J. Am. Chem. Soc.* **1991**, *113*, 729.

(9) Rosi, M.; Bauschlicher, C.W.; Langhoff, S.R.; Partridge, H. *J. Phys. Chem.* **1990**, *94*, 8656.

(10) Berthier, G.; Cimaraglia, R.; Caoudi, A.; Mestdagh, J.; Rolando, C.; Suard, M. *THEOCHEM* **1992**, *254*, 43.

(11) Hill, Y.D.; Freiser, B.S.; Bauschlicher, C.W. *J. Am. Chem. Soc.* **1991**, *113*, 1507.

(12) Maitre, P.; Bauschlicher, C.W., to be published.

(13) Perry, J.K.; Ohanessian, G.; Goddard, W.A., III *J. Phys. Chem.* **1993**, *97*, 5238.

(14) *Handbook of Chemistry and Physics*, 68th ed.; Weast, R.C., Ed.; Chemical Rubber Co.: Boca Raton, FL, 1987.

(15) Moore, C.E. *Atomic Energy Levels*; Natl. Bur. Stand., U.S. G.P.O.: Washington, DC, 1949.

(16) Nicholson, A.J.C. *J. Chem. Phys.* **1965**, *43*, 1171.

(17) Blomberg, M.R.A.; Siegbahn, P.E.M.; Svensson, M. *J. Phys. Chem.* **1991**, *95*, 4313.

(18) Low, J.J; Goddard, W.A., III *Organometallics* **1986**, *5*, 609.

(19) Periana, R.A.; Bergman, R.G. *J. Am. Chem. Soc.* **1986**, *108*, 7332.

(20) Koga, N.; Morokuma, K. *J. Am. Chem. Soc.* **1990**, *94*, 5454.

(21) Rappé, A.K., Ph.D. thesis, California Institute of Technology, 1980.

(22) Armentrout, P.B. Personal communication.

(23) Bauschlicher, C.W.; Partridge, H.; Langhoff, S.R. *J. Phys. Chem.* **1992**, *96*, 2475.

(24) Sugar, J.; Corliss, C.H. *J. Phys. Chem. Ref. Data, Suppl.* **1985**, *14*, no. 2.

(25) (a) Van Koppen, P.A.M.; Kemper, P.R.; Bowers, M.T. *J. Am. Chem. Soc.* **1992**, *114*, 10941. (b) Van Koppen, P.A.M.; Bowers, M.T.; Fisher, E.R.; Armentrout, P.B., to be submitted.

(26) Hurley, M.M; Pacios, L.F.; Christiansen, P.A.; Ross, R.B.; Ermler, W.C. *J. Chem. Phys.* **1986**, *84*, 6840.

Chapter VI

# Inequivalence of Equivalent Bonds: Symmetry Breaking in $Co(CH_3)_2^+$

# Chapter VI

## Inequivalence of Equivalent Bonds: Symmetry Breaking in $Co(CH_3)_2^+$

### 6.1 Introduction

When two ligands such as H or $CH_3$ are covalently bonding to $Co^+$, a curious phenomenon is observed. Wavefunctions including intermediate levels of electron correlation lead to two metal-ligand bonds which are decidedly different in character. One bond is derived dominantly from the $4s$ orbital and the other is derived dominantly from a $3d$ orbital. This occurs even when the two ligands are strictly equivalent [such as $C_{2v}$ $Co(H)_2^+$ or $C_{2v}$ $Co(CH_3)_2^+$]. In these instances, the wavefunctions break the molecular symmetry to form inequivalent bonds. Sufficiently accurate wavefunctions restore the appropriate symmetry by introducing resonance, but some unusual character is retained in the Co–R bonds. This behavior stands in contrast to that of similar $Rh^+$ and $Ir^+$ complexes where symmetry breaking is not observed. In these complexes, bonding is achieved by the expected $sd$ hybridization. This chapter discusses the qualitative aspects of the bonding in $MR_2^+$ complexes (M = Co, Rh, Ir; R=H, $CH_3$) with an emphasis on the causes of symmetry breaking. The text is taken largely verbatim from reference 1.

Symmetry breaking is often ignored but is by no means exceptional in the quantum chemistry literature.[2–10] It generally occurs whenever there is a competition between resonance among various valence bond (VB) bond couplings on the one hand and the energy gain by better describing just one of these bond couplings on the other. One classical example is the description of core-hole

states in homonuclear diatomics, *e.g.*, in $O_2^+$ and $N_2^+$.[4-8] Here the localized hole in the $1s$ orbital polarizes the other orbitals much more efficiently than if the hole is delocalized in a symmetry orbital ($\sigma_g$ or $\sigma_u$). The final wavefunction is a superposition of the two localized structures:

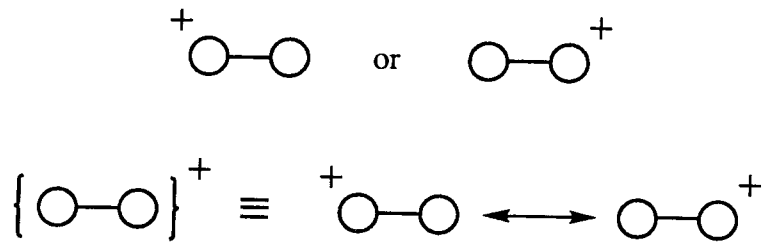


Another case concerns three-electron three-center radicals such as allyl[9] and formoxyl,[10] where the competition is between a state having the radical delocalized over all three centers and a single valence bond structure:

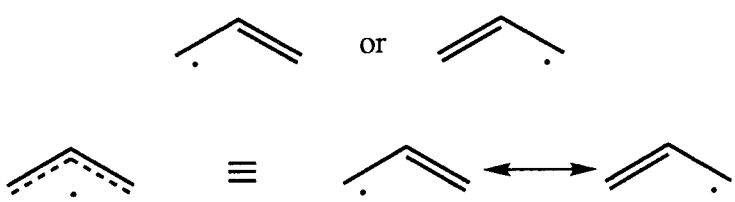


Symmetry breaking in these systems is observed at the HF level and can be corrected by correlation.

Recent work by Buijse and Baerends has shown symmetry breaking to occur in the HF description of certain transition metal complexes.[11,12] They studied $MnO_4^-$ and $MnO^+$ and found the bonds to be strongly polarized with the orbitals localized on either the metal or the oxide centers. With the introduction of correlation, the bonds become covalent, each having character on both the metal and the ligands. They attributed this unphysical behavior to the weak interaction of the metal $3d$ orbitals with the O $2p$ orbitals coupled with the incorrect description of the dissociation limit at the HF level. They argued that HF over-estimates the extent of ionic contributions to the bonds such that a multiply bonded system can reduce Coulombic repulsion by localizing the bonds on different centers. We find that in some cases involving $CoR_2^+$ complexes, this type of symmetry breaking also occurs [$Co(H)(CH_3)^+$ and $Co(H)(C_2H_5)^+$, for instance]. However, the situation is novel for $CoR_2^+$ in that symmetry breaking is observed at the correlated level for cases in which there does not appear to be a problem at the HF level. In this regard, the symmetry breaking phenomenon described here is closely related to that of benzene.[13] Benzene is adequately described at the HF level, but with intermediate levels of correlation, it is possible to optimize a symmetry broken wavefunction which corresponds to one of the two Kekulé structures

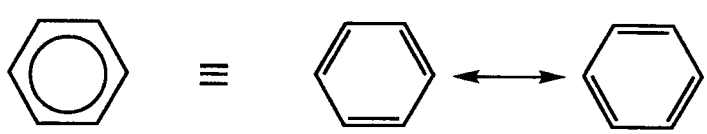

Only the introduction of resonance between these two VB configurations leads to a proper description of the molecule.

The discussion of symmetry breaking in $CoR_2^+$ complexes is illustrated by calculations on $Co(CH_3)_2^+$. Comparison is made to similar calculations on $Rh(CH_3)_2^+$ and $Ir(CH_3)_2^+$. We note that a study of $Co(H)_2^+$ would be computationally simpler; however, as detailed in Chapter IV, no *stable* dihydride exists. Early calculations[14] on $Co(CH_3)_2^+$ indicated a barrier exists between the production of C−C bond cleavage and the precursor $Co(C_2H_6)^+$ molecular complex making the dimethyl complex a metastable structure. This property is advantageous for symmetry breaking studies since a geometry can be fully optimized and vibrational frequencies computed. Thus, the bulk of the discussion that follows concerns symmetry breaking in $Co(CH_3)_2^+$ but is applicable to a variety of systems.

## 6.2 Description of the bonding

As was shown in Chapter III, the bonding of $CoH^+$ and $CoCH_3^+$ arises from the $s^1d^7\ ^5F$ state of the metal ion despite the fact that the $d^8\ ^3F$ state is 9.9 kcal/mol lower in energy. It is argued that a stronger bond would result from a $4s$ orbital than a $3d$ orbital due to the compact nature of the $3d$ orbital and thus the promotion energy was a trivial concern. However, in forming a second covalent bond a $3d$ orbital must be used since promotion to the $s^2d^6$ state, where both ligands could bond to $4s$ electrons, is prohibitive (116 kcal/mol). (Note that neutral $Co(CH_3)_2$ is derived from the $s^2d^7$ ground state.[15]) Thus the two Co−C bonds in $Co(CH_3)_2^+$ are formed by the $4s$ orbital and a $3d$ orbital.

The geometry of $Co(CH_3)_2^+$ used in these calculations (see Figure 1) has $C_{2v}$ symmetry with the two methyl groups eclipsed and geometrically equivalent and the four out-of-plane hydrogens nearer each other than the two in-plane hydrogens (a conformation similar to dimethyl ether). The staggered ($C_s$) conformation is nearly degenerate so the higher symmetry structure does not represent an unrealistic geometry. With the C−Co−C backbone in the $yz$ plane and $z$ the $C_2$ axis of rotation, the two methyl groups form bonds to the $4s$ and $3d_{yz}$ orbitals of the metal. There are two common approaches using these orbitals to describe the metal-ligand bonds in such a system. The first involves delocalized orbitals possessing the full symmetry of the molecule [molecular orbital (MO) theory]. In this case, the $4s$ orbital forms a bond with the symmetric combination of the carbon $sp^3$ hybrid orbitals and the $3d_{yz}$ orbital forms a bond with the antisymmetric combination of these hybrids:

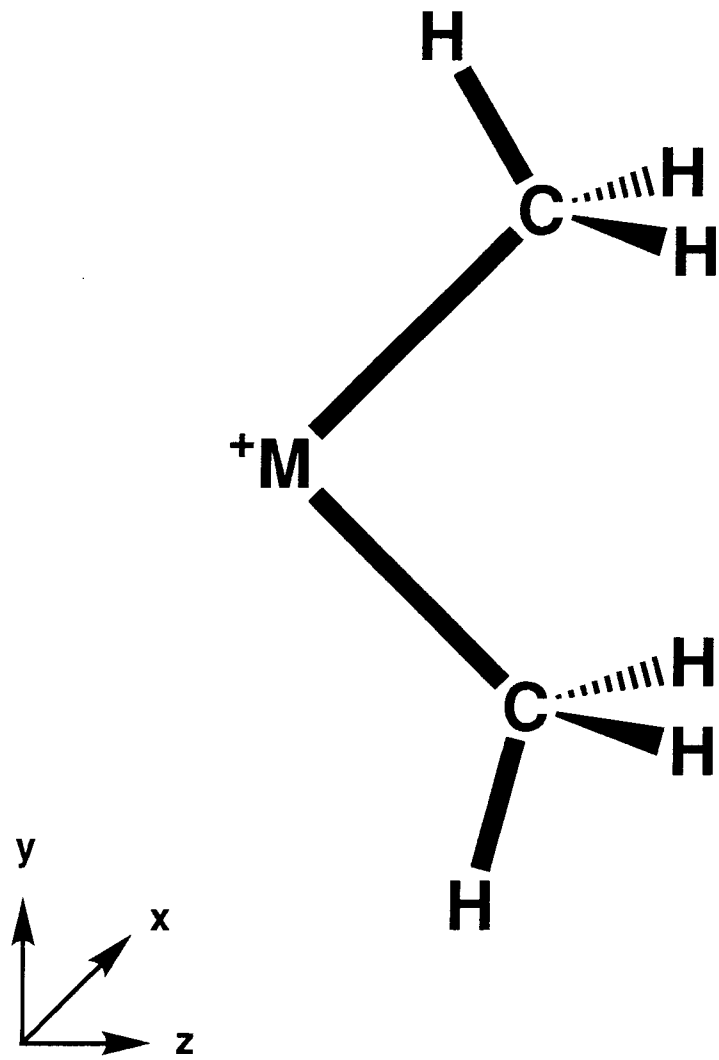


**Figure 1:** Basic bent geometry with eclipsed methyl groups used in these calculations.

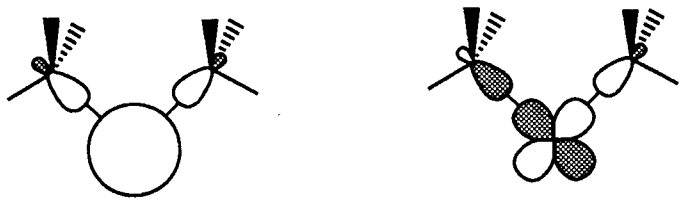

The second way of looking at the bonding in such a system involves localized *sd* hybrid orbitals (VB theory). Thus, $s + d_{yz}$ gives a bond in the direction of one of the two ligands while $s - d_{yz}$ gives a bond in the direction of the other:

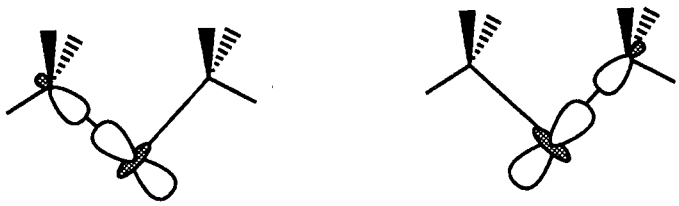

It is often considered that these two descriptions are identical since the two equivalent localized orbitals can be obtained by plus and minus combinations of the delocalized orbitals. GVB calculations suggest a third way of looking at these types of systems. It involves localized but *inequivalent* bonds which resonate to obtain the proper symmetry of the molecule. In the case of $Co(CH_3)_2^+$, one carbon forms a bond to an orbital which is dominantly $4s$ on the metal and the other forms a bond which is dominantly $3d$:

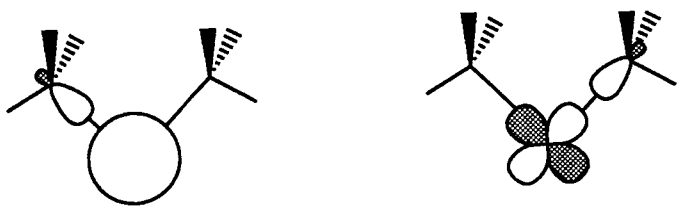

Since there are two ways of localizing the orbitals (equivalent by a mirror reflec-

tion or $C_2$ rotation), a resonance exists between these two configurations which leads to a molecule with symmetric bonds:

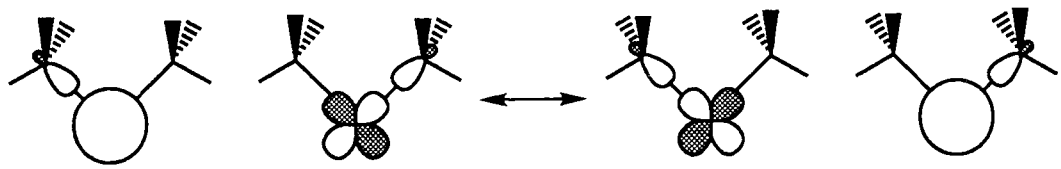

Wavefunctions which include resonance, such as resonating-GVB ($R$-GVB)[16] or CASSCF, properly describe the bonding in $Co(CH_3)_2^+$ and related systems.

## 6.3 Results

### 6.3.1 HF and GVB-PP Calculations

At the HF level of calculation, the bonding orbitals are delocalized and belong the the $a_1$ and $b_2$ irreducible representations of the $C_{2v}$ point group. The bond in $a_1$ symmetry is chiefly composed of the Co $4s$ orbital and the symmetric combination of the two C $sp^3$ hybrids. The bond in $b_2$ symmetry is composed of the $3d_{yz}$ orbital and the antisymmetric combination of the C hybrids. The six remaining nonbonding $3d$ electrons can be arranged in a number of ways, with the ground state being $^3B_1$ [the occupations of the nonbonding $3d$ orbitals are $(z^2)^2(xy)^2(xz)^1(x^2-y^2)^1$]. This ground state is consistent with arguments made on the states of $CoH_2^+$ in Chapter IV. The sterics between the two methyl groups forces the bond angle to be greater than 90° which favors the $^3B_1$ state over the $^3A_2$ state.

When the symmetry constraint on the orbitals of the HF wavefunction is intentionally lowered to $C_s$, optimization of the wavefunction does not lead to symmetry breaking. The orbitals maintain their $C_{2v}$ character. Although these HF calculations provide a decent qualitative picture of the bonding in this system, the energetic results are quite poor, with $Co(CH_3)_2^+$ unbound by 14 kcal/mol with respect to its diabatic limit of $Co^+$ ($^5F$) and two $CH_3$ radicals! However, because of the improper dissociation of the HF wavefunction, the inserted complex is a local minimum on the potential energy surface. This unphysical result can be remedied by the inclusion of electron correlation in the wavefunction.

As described in Chapter II, one of the simplest means of improving upon HF is with a GVB-PP(6/6) wavefunction in which the four electrons of the

two bonds are correlated. The type of correlation described by GVB leads to localized bond pairs, a starting guess for which can be obtained from the HF orbitals by taking plus and minus linear combinations of the $a_1$ and $b_2$ bonding orbitals and a similar linear combination of appropriate virtuals. This leads to two sets of first and second natural orbitals describing equivalent bonds formed from *sd* hybrids. Optimization of the GVB-PP(6/6) wavefunction stablized the insertion product by 50 kcal/mol with respect to the HF results, as expected; however, inspection of the orbitals (Figure 2a) reveals that the two localized bonds are *inequivalent*. One methyl group bonds to an orbital which is clearly 4*s*-like on the metal and the other bonds to an orbital which is just as clearly 3*d*-like.

Optimizing the geometry for this wavefunction leads to a structure with $C_s$ symmetry, where the 3*d* bond is 2.086 Å and the 4*s* bond is 2.022 Å, a difference of 0.064 Å. Strangely, the 4*s* orbital is significantly larger than the 3d orbital but the Co−C 4*s* bond is the shorter of the two. As we would expect the 3*d* bond to be intrinsically shorter than the 4*s* bond, the likely explanation is that Pauli repulsion to the stronger 4*s* bond increases the 3*d* bond length.

Analysis of the Mulliken populations (Table I) demonstrates that the 4*s* bond is essentially covalent with 45% metal character and 52% methyl character (the remainder being on the second methyl group). On the other hand, the 3*d* bond shows a fair amount of charge transfer; the metal character is 61% and the methyl character is only 38%. While there is still a negative charge on the carbon center (as is the case of isolated $CH_3$ and for the 4*s*-bonded methyl group), the charge transfer leads to a net *positive* charge on the 3*d* bonded methyl group.

We view the main reason for the bonds having different character as being due to the disparity in the sizes of the 4*s* and 3*d* orbitals, a ratio computed

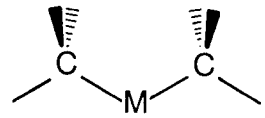
C
M
C

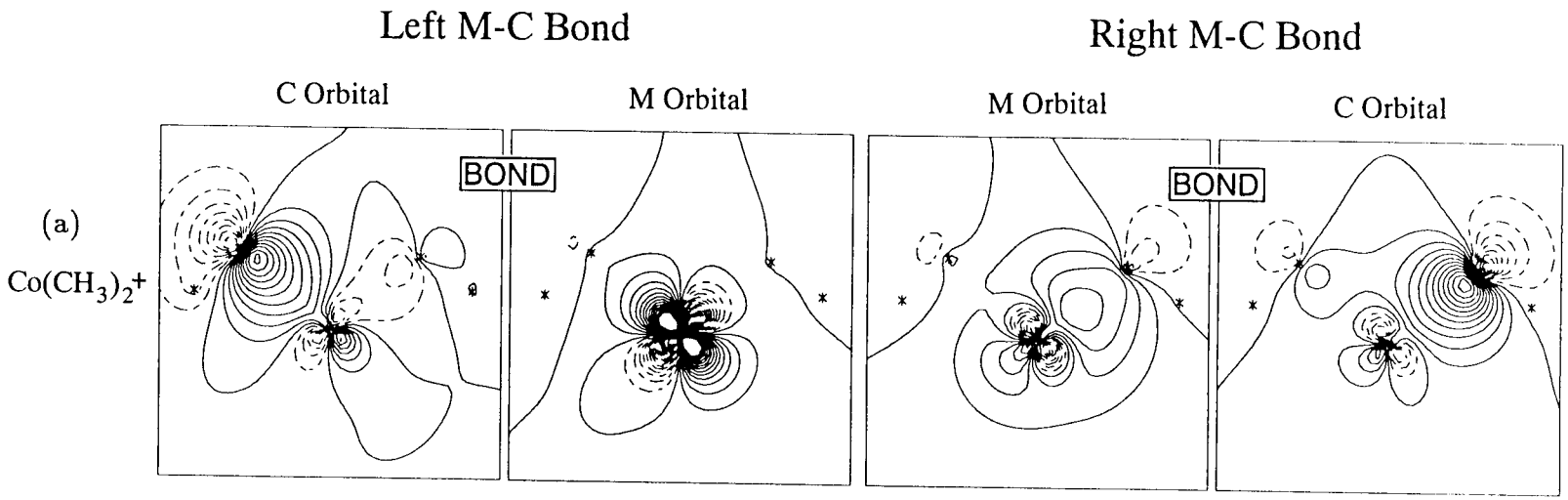
Left M-C Bond
Right M-C Bond
C Orbital
M Orbital
M Orbital
C Orbital
BOND
BOND
(a)
Co(CH3)2+

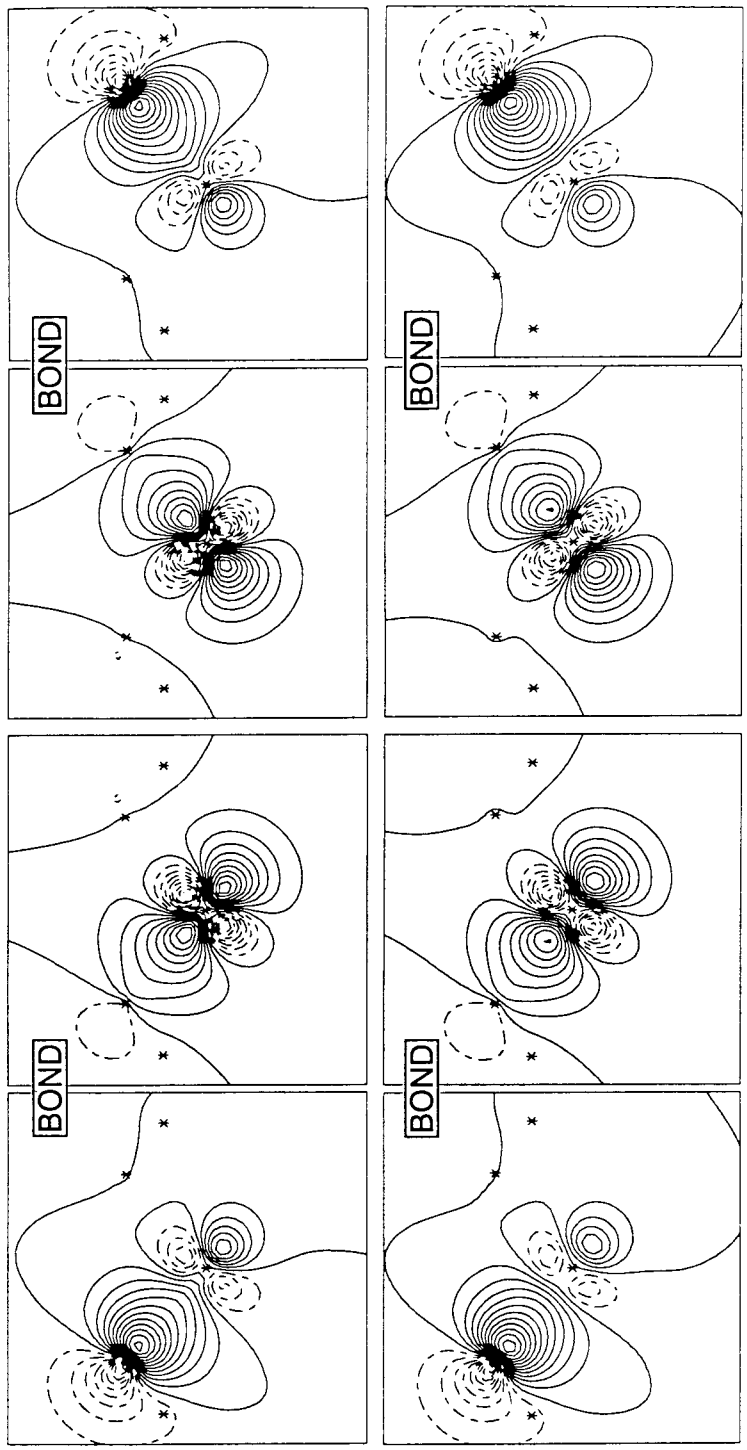


**Figure 2.** (a) GVB bonding orbitals for $Co(CH_3)_2^+$ from GVB-PP(6/6) calculations. (Left, M–C Bond Pair) Here the metal orbital has primarily *d* character. (Right, M–C Bond Pair) Here the metal orbital has primarily *sp* character. (b) Same as (a) for $Rh(CH_3)_2^+$. Here both metal bonding orbitals have the same *sd* hybrid character. (c) Same as (b) for $Ir(CH_3)_2^+$.

**Table I.** Mulliken population analysis for the GVB-PP(6/6) wavefunction of $Co(CH_3)_2^+$. Only valence electrons considered.

| | Bond 1 | Bond 2 | Total Populations | Total Charges |
|---|---|---|---|---|
| Co total | 0.902 | 1.212 | 8.172 | +0.828 |
| $4s$ | 0.671 | 0.062 | 0.734 | |
| $4p$ | 0.077 | 0.063 | 0.190 | |
| $3d$ | 0.155 | 1.088 | 7.248 | |
| C(1) | 1.054 | 0.029 | 4.793 | −0.793 |
| Me(1) total | 1.022 | 0.032 | 7.032 | −0.032 |
| C(2) | 0.073 | 0.718 | 4.615 | −0.615 |
| Me(2) total | 0.076 | 0.758 | 6.796 | +0.204 |
| Total | 2.000 | 2.000 | | |

to be 2.58:1 for $Co^+$.[17] This large discrepancy reduces the effectiveness of *sd* hybridization to increase the overlap of the metal bonding orbitals with the ligands and to decrease the Pauli repulsion between the bonds. The ratio decreases to 1.97:1 and 1.65:1 for $Rh^+$ and $Ir^+$, respectively, suggesting that Rh and Ir may not demonstrate the same type of behavior as Co in an $M(CH_3)_2^+$ complex. Indeed, GVB-PP(6/6) calculations on $Rh(CH_3)_2^+$ and $Ir(CH_3)_2^+$ show that the metal-methyl bonds are equivalent and formed from *sd* hybrids, each directed toward one carbon (see Figures 2b and 2c and Tables II and III). Thus, symmetry breaking does not occur in these systems and optimizing the geometry leads to a $C_{2v}$ minimum structure.

As further evidence of the problem in the $^3B_1$ state of $Co(CH_3)_2^+$ being a result of poor *sd* hybridization, GVB-PP(4/4) calculations on the $^1A_1$ state of

$Co(CH_3)_2^+$ do not lead to symmetry breaking. This state does not involve $sd$ hybridization but $dd$ hybridization as it is derived principally from the $d^8\ ^3F$ configuration of $Co^+$. These results support the argument that the problem at hand is the inefficiency of the hybridization of the $4s$ and $3d$ orbitals.

**Table II.** Mulliken population analysis for the GVB-PP(6/6) wavefunction of $Rh(CH_3)_2^+$. Populations for only one bond are given as the second is equivalent by symmetry.

| | Bond | Total Populations | Total Charges |
|---|---|---|---|
| Metal total | 1.120 | 8.188 | +0.812 |
| 5*s* | 0.263 | 0.652 | |
| 5*p* | 0.033 | 0.092 | |
| 4*d* | 0.824 | 7.444 | |
| C | 0.847 | 4.681 | −0.681 |
| Me total | 0.850 | 6.906 | +0.094 |
| Total | 2.000 | | |

**Table III.** Mulliken population analysis for the GVB-PP(6/6) wavefunction of $Ir(CH_3)_2^+$. Populations for only one bond are given as the second is equivalent by symmetry.

| | Bond | Total Populations | Total Charges |
|---|---|---|---|
| Metal total | 1.123 | 8.165 | +0.835 |
| 6*s* | 0.302 | 0.799 | |
| 6*p* | 0.039 | 0.084 | |
| 5*d* | 0.782 | 7.282 | |
| C | 0.862 | 4.693 | −0.693 |
| Me total | 0.868 | 6.918 | +0.082 |
| Total | 2.000 | | |

### 6.3.2 R-GVB Calculations

An important element missing from the GVB-PP calculations on $Co(CH_3)_2^+$ is resonance. Since it is intuitive that the GVB-PP wavefunction has two possible ways of localizing the bonds ($d$ bond to one methyl and $s$ bond to the other and the reverse situation), the question remains as to whether inclusion of resonance between the two leads to equivalent bonds. Thus, we consider the two equivalent wavefunctions $\Psi_{sd}$ and $\Psi_{ds}$ where

$$\Psi_{sd} = c_1(\phi_{s-Me_1})^2(\phi_{d-Me_2})^2 + c_2(\phi_{s-Me_1})^2(\phi^*_{d-Me_2})^2 + c_3(\phi^*_{s-Me_1})^2(\phi_{d-Me_2})^2 + c_4(\phi^*_{s-Me_1})^2(\phi^*_{d-Me_2})^2$$

and

$$\Psi_{ds} = c_1(\phi_{d-Me_1})^2(\phi_{s-Me_2})^2 + c_2(\phi_{d-Me_1})^2(\phi^*_{s-Me_2})^2 + c_3(\phi^*_{d-Me_1})^2(\phi_{s-Me_2})^2 + c_4(\phi^*_{d-Me_1})^2(\phi^*_{s-Me_2})^2$$

and calculate the energy of

$$E_+ = \frac{\langle \Psi_{sd} + \Psi_{ds} | H | \Psi_{sd} + \Psi_{ds} \rangle}{\langle \Psi_{sd} + \Psi_{ds} | \Psi_{sd} + \Psi_{ds} \rangle}$$

and

$$E_- = \frac{\langle \Psi_{sd} - \Psi_{ds} | H | \Psi_{sd} - \Psi_{ds} \rangle}{\langle \Psi_{sd} - \Psi_{ds} | \Psi_{sd} - \Psi_{ds} \rangle}.$$

This requires calculation of $\langle \Psi_{sd} | \Psi_{ds} \rangle$ and $\langle \Psi_{sd} | H | \Psi_{ds} \rangle$ between the two GVB-PP wavefunctions and solving the $2 \times 2$ nonorthogonal CI for $C_{sd}\Psi_{sd} + C_{ds}\Psi_{ds}$. This resonating GVB ($R$-GVB) wavefunction has the proper symmetry at $C_{2v}$

geometries, so the question then arises whether it also restores structural $C_{2v}$ symmetry for the molecule. Reoptimization of the geometry in a point-by-point manner for the $R$-GVB wavefunction leads to an optimal geometry possessing $C_{2v}$ symmetry with a Co−C bond length of 2.07 Å and a C−Co−C angle of 104.6°. We find that resonance contributes a total of 12.5 kcal/mol worth of stabilization to the bond energy. Asymmetric distortions that shorten one bond and lengthen the other lower the energy of one of the perfect pairing resonance configurations but raise the energy of the other. However, the energy gained by one configuration upon distortion of the geometry is not enough to balance the loss in resonance energy and, thus, the stabilization is at a maximum when the two bonds have equal lengths.

### 6.3.3 CASSCF and CI Calculations

Ideally, since the resonance is such a strong effect, we would like to optimize the orbitals self-consistently in a wavefunction which possesses both the correlation of the bonds and the resonance between them. Optimization of the $R$-GVB wavefunction in such a manner (a GRVB or generalized resonating valence bond calculation)[18] is difficult and the resulting wavefunction does not lend itself to dynamical correlation at the CI level. Instead we have considered a CASSCF(6/6) wavefunction constructed using a full CI of the six nonclosed shell orbitals of the GVB(6/6) wavefunction (two from each of the bond pairs and the open shell or triplet orbitals). Symmetry breaking is not observed for this level of wavefunction and the natural orbitals of the CASSCF are delocalized, belonging to the irreducible representations of the $C_{2v}$ point group. Asymmetric distortions of the geometry are unfavorable (as in the $R$-GVB calculations) leading to a minimum with geometrically equivalent methyl groups. Similar calculations were done for the $Rh^+$ and $Ir^+$ complexes with little qualitative change from the GVB results.

Table IV gives a breakdown of the most important configurations in the CASSCF wavefunctions of $Co(CH_3)_2^+$, $Rh(CH_3)_2^+$, and $Ir(CH_3)_2^+$. The most striking feature of the CI expansion of $Co(CH_3)_2^+$ is the strong correlation of the $3d_{yz}$ $b_2$ bond pair to both methyl groups: the single and double excitations to the antibonding orbital have unusually large weights. The rather prominent importance of the single excitation (missing from the perfect pairing wavefunction) is to allow the proper description of spin polarization in the $3d$ bond, a strong effect due to the sizeable exchange interaction among the high spin $3d$ electrons ($\sim$20 kcal/mol per pair). The importance of this configuration is greatly diminished

**Table IV.** Configuration weights in the CASSCF(6/6) wavefunctions of $Co(CH_3)_2^+$, $Rh(CH_3)_2^+$, and $Ir(CH_3)_2^+$. The configurations used as references in the MRCI/3 calculations are given in bold. Only the orbitals of the two metal-methyl bonds are shown.

| Occupations | | | | $Co(CH_3)_2^+$ | $Rh(CH_3)_2^+$ | $Ir(CH_3)_2^+$ |
|---|---|---|---|---|---|---|
| $a_1$ | $a_1^*$ | $b_2$ | $b_2^*$ | Weight | Weight | Weight |
| 2 | 0 | 2 | 0 | **0.7547** | **0.8889** | **0.9178** |
| 2 | 0 | 1 | 1 | **0.0865** | 0.0079 | 0.0080 |
| 1 | 1 | 2 | 0 | 0.0098 | 0.0026 | 0.0042 |
| 2 | 0 | 0 | 2 | **0.0932** | **0.0237** | **0.0190** |
| 0 | 0 | 2 | 2 | 0.0072 | **0.0190** | **0.0107** |
| 0 | 2 | 2 | 0 | 0.0052 | 0.0031 | 0.0049 |
| 2 | 2 | 0 | 0 | 0.0003 | 0.0009 | 0.0021 |
| 1 | 1 | 1 | 1 | 0.0336 | 0.0235 | 0.0260 |
| all others | | | | 0.0095 | 0.0304 | 0.0073 |

in a CASSCF(4/4) calculation on the $^1A_1$ state of the Co complex since no such coupling can occur. The large coefficient of the double excitation reflects the fact that the $3d$ orbital is small and does not overlap well with the two methyl radicals. This excitation takes care of the left-right correlation which grows in importance with decreasing overlap in covalent bonds. In contrast, comparable excitations out of the $4s$ $a_1$ bond are an order of magnitude smaller in weight. The significance of this will become apparent in the next section.

Due to concern that the GVB and CASSCF(6/6) calculations may not properly account for one electron bonding to the $d^8$ state in the $Co^+$ systems (see Chapter III), we have also considered a CASSCF(10/10) calculation and a multireference singles plus doubles CI (MRCI). The CASSCF(10/10) calculation includes the in-out correlation of the two doubly-occupied nonbonding $d$

orbitals on the metal while the MRCI includes the effect of dynamical correlation of all valence electrons. In the CI calculation, the three configurations in the CASSCF(6/6) with the largest weights—the dominant configuration and the single and double excitations for the $b_2$ bond to the $b_2$ antibond are used as references. The (111111) configuration (the product of two singles from the $a_1$ and $b_2$ bonds to the $a_1$ and $b_2$ antibonds) also has a large weight; however, due to the large number of spin couplings associated with this configuration (nine), including it in the reference space leads to an expensive CI with 2,150,000 configuration state functions (CSF). As it is, the three-reference CI (further referred to as MRCI/3) has 790,000 CSF in $C_{2v}$ symmetry and 1,570,000 CSF in $C_s$ symmetry. The geometry was optimized at this level in $C_{2v}$ symmetry ($R_{Co-C} = 1.977$Å and $\theta_{CCo-C} = 98.3°$) and distortions were made in $C_s$ symmetry. No symmetry breaking was observed. A single point calculation was then done at this optimized geometry at the CASSCF(10/10) and the four-reference CI (MRCI/4) levels with no qualitative changes in the wavefunction observed in comparison to the CASSCF(6/6). Tables V and VI give properties of the CASSCF(6/6) and MRCI/4 wavefunctions, respectively. Results of CASSCF(6/6) calculations on the $Rh^+$ and $Ir^+$ complexes are given in Tables VII and VIII, respectively.

**Table V.** Mulliken population analysis for the CASSCF(6/6) wavefunction of $Co(CH_3)_2^+$. Only valence electrons are considered.

| | $a_1$ Bond | $b_1$ Bond | Total Populations | Total Charges |
|---|---|---|---|---|
| Co total | 0.827 | 1.087 | | +0.794 |
| $4s$ | 0.708 | 0.000 | 0.770 | |
| $4p$ | 0.040 | 0.043 | 0.174 | |
| $3d$ | 0.079 | 1.044 | 7.261 | |
| Me(1) + Me(2) | 1.094 | 0.591 | | +0.205 |
| Total | 1.921 | 1.678 | | |

**Table VI.** Mulliken population analysis for the MRCI/4 wavefunction of $Co(CH_3)_2^+$. Only valence electrons are considered.

| | $a_1$ Bond | $b_2$ Bond | Total Populations | Total Charges |
|---|---|---|---|---|
| Co total | 0.783 | 1.157 | | +0.733 |
| $4s$ | 0.659 | 0.000 | | |
| $4p$ | 0.037 | 0.041 | 0.185 | |
| $3d$ | 0.086 | 1.116 | 7.307 | |
| Me(1) + Me(2) | 1.153 | 0.586 | | +0.227 |
| Total | 1.935 | 1.743 | | |

**Table VII.** Mulliken population analysis for the CASSCF(6/6) wavefunction of $Rh(CH_3)_2^+$. Only valence electrons are considered.

| | $a_1$ Bond | $b_2$ Bond | Total Populations | Total Charges |
|---|---|---|---|---|
| Rh Total | 0.894 | 1.295 | | +0.818 |
| $5s$ | 0.282 | 0.000 | 0.523 | |
| $5p$ | 0.026 | 0.026 | 0.093 | |
| $4d$ | 0.586 | 1.269 | 7.566 | |
| Me(1) + Me(2) | 1.002 | 0.599 | | +0.182 |
| Total | 1.896 | 1.894 | | |

**Table VIII.** Mulliken population analysis for the CASSCF(6/6) wavefunction of $Ir(CH_3)_2^+$. Only valence electrons are considered.

| | $a_1$ Bond | $b_2$ Bond | Total Populations | Total Charges |
|---|---|---|---|---|
| Ir total | 0.925 | 1.214 | | +0.842 |
| $6s$ | 0.492 | 0.000 | 0.752 | |
| $6p$ | 0.026 | 0.037 | 0.083 | |
| $5d$ | 0.408 | 1.177 | 7.323 | |
| Me(1) + Me(2) | 1.004 | 0.702 | | +0.158 |
| Total | 1.930 | 1.916 | | |

## 6.4 Discussion

### 6.4.1 The search for resonance in the CASSCF description of $Co(CH_3)_2^+$

We have proposed that the underlying cause of the symmetry breaking in $Co(CH_3)_2^+$ is the dramatic difference in the sizes of the $4s$ and $3d$ orbitals of $Co^+$ and the inefficiency of $sd$ hybridization. Indeed, the overlap of the two GVB-PP orbitals in the $3d$-methyl bond (0.41) is significantly smaller than that of the $4s$-methyl bond (0.78) [the corresponding overlaps for both pairs are 0.69 in $Rh(CH_3)_2^+$ and 0.70 in $Ir(CH_3)_2^+$]. This difference can be seen in the CASSCF and MRCI wavefunctions where the delocalized $3d$ bond requires more correlation than the $4s$ bond, resulting in bonding natural orbitals with significantly different occupation numbers [1.921 for the $a_1$ and 1.678 for the $b_2$ CASSCF(6/6) first natural orbitals]. This is at variance with CASSCF(6/6) results (Tables VII and VIII) for $RH(CH_3)_2^+$ (1.896 and 1.894, respectively) and $Ir(CH_3)_2^+$ (1.930 and 1.916, respectively). Indeed, a requirement for strict hybridization of orbitals to occur is that their occupation numbers be identical. For instance, in methane, widely recognized to involve bonding from four equivalent $sp^3$ C hybrid orbitals, the CASSCF(8/8) occupation of the symmetry adapted $s$ bonding orbital (1.984) is essentially identical to that of the three $p$ bonds (1.978) even though the orbitals are distinctly different energetically ($-0.941$ vs $-0.546$ hartree). This point can be better understood by considering a GVB-PP wavefunction which involves the correlation of two equivalent bonds. Thus, we define the GVB wavefunction as

$$\Psi_{GVB} = c_1|(\psi_{1a})^2(\psi_{2a})^2| + c_2|(\psi_{1b})^2(\psi_{2a})^2| + c_2|(\psi_{1a})^2(\psi_{2b})^2| + c_3|(\psi_{1b})^2(\psi_{2b})^2| \quad (1)$$

These localized bonds can be formed from delocalized symmetry orbitals by making the appropriate linear combinations:

$$\psi_{1a} = \frac{1}{\sqrt{2}}(a_1 + b_2)$$
$$\psi_{2a} = \frac{1}{\sqrt{2}}(a_1 - b_2)$$
$$\psi_{1b} = \frac{1}{\sqrt{2}}(a_1^* + b_2^*)$$
$$\psi_{2b} = \frac{1}{\sqrt{2}}(a_1^* - b_2^*)$$

When expanded the GVB-PP wavefunction in terms of delocalized orbitals becomes

$$\Psi_{GVB} = c_1|(a_1)^2(b_2)^2| - c_2|1/2[(a_1)^1(b_2)^1 + (b_2)^1(a_1)^1][(a_1^*)^1(b_2^*)^1 + (b_2^*)^1(a_1^*)^1]| + \frac{1}{2}c_2[|(a_1)^2(a_1^*)^2| + |(a_1)^2(b_2^*)^2| + |(a_1^*)^2(b_2)^2| + |(b_2^*)^2(b_2)^2|] + c_3|(a_1^*)^2(b_2^*)^2|, \quad (2)$$

where the spin term is $(\alpha\beta - \beta\alpha) \times (\alpha\beta - \beta\alpha)$. From this seemingly more complicated wavefunction it can be proved from inspection that the occupations of the $a_1$ and $b_2$ orbitals are necessarily identical (as is also the case for the $a_1^*$ and $b_2^*$ orbitals). Thus, a system which is well described by bonding of equivalent hybrid orbitals (such as $CH_4$) will exhibit this property. From an analysis of the CASSCF(6/6) wavefunction (Table IV), we find some deviations from the simple picture in the bonding of $Rh(CH_3)_2^+$ and $Ir(CH_3)_2^+$. While excitations

from both the first natural orbitals of the two bonds are of the same magnitude, the occupations of the second natural orbitals are not equal. We associate this discrepancy with the inclusion of ionic terms and one electron bonding terms in the GVB wavefunction, such as

$$(a_1 + b_2)^2(a_1^* + b_2^*)^1(a_1^* - b_2^*)^1$$

and

$$(a_1 - b_2)^2(a_1^* + b_2^*)^1(a_1^* - b_2^*)^1.$$

These deviations in the wavefunctions of the $Rh(CH_3)_2^+$ and $Ir(CH_3)_2^+$ systems from the simple GVB picture are relatively minor in comparison to the qualitative change that clearly exists in the wavefunction of $Co(CH_3)_2^+$. Here the weights of the single and double excitations from the $b_2$ bond to the $b_2$ antibond are nearly three times larger than that of the (111111) configuration, which should be the most important excitation according to Eq. (2). These excitations are also an order of magnitude larger than the weights of all other excitations. It is difficult to credit this discrepancy to the effect of ionic terms alone. We maintain that these differences evidence the presence of resonance in the wavefunction.

Determining if the CASSCF and MRCI wavefunctions are describing a system involving hybridization or resonating bonds is rather difficult. To that end we find that when the (111111) configuration is removed from the wavefunction the orbitals tend to localize. This is apparent from the two expressions for the GVB-PP wavefunction in Eqs. (1) and (2). Using localized orbitals,

**Table IX.** Comparison of the energies of the CAS - (111111) calculations for various localizations of the CASSCF natural orbitals. Energies are expressed relative to the full CASSCF energy in kcal/mol.

| | $Co(CH_3)_2^+$ (6/6) | $Co(CH_3)_2^+$ (10/10) | $Rh(CH_3)_2^+$ (6/6) | $Ir(CH_3)_2^+$ (6/6) |
|---|---|---|---|---|
| $E_{ll}^a$ | 6.91 | 3.38 | 0.39 | 0.45 |
| $E_{ld}$ | 1.02 | 0.66 | 0.18 | 0.04 |
| $E_{dl}$ | 0.76 | 0.44 | 0.16 | 0.03 |
| $E_{dd}$ | 15.52 | 12.78 | 13.55 | 16.38 |

[a] The first subscript indicates the localization of the bonding pair of natural orbitals and the second, the localization of the antibonding pair of natural orbitals.

the (111111) configuration is not included in the CI, but using delocalized orbitals, it is the most prominant excitation, implying that the importance of this configuration can be minimized by localizing the orbitals. We have done a number of CI calculations which amount to a GVBCI (or CAS) with the (111111) configuration removed. We used the CASSCF natural orbitals and made linear combinations of the $a_1$ and $b_2$ bonds (and their antibonds) to localize equivalent orbitals. The results are given in Table IX. As expected, it is costly to remove this configuration from the CI when the orbitals are delocalized ($E_{dd}$ is greater than 12 kcal/mol for all three metal complexes). When the orbitals are localized, the cost in energy ($E_{ll}$) is quite small for the Rh and Ir complexes (0.39 and 0.45 kcal/mol, respectively) but large in the case of $Co(CH_3)_2^+$ [6.91 kcal/mol for the (6/6) and 3.38 kcal/mol for the (10/10)]. However, when one set of natural orbitals (either the first or second) is localized but the other is delocalized, the cost of energy to $Co(CH_3)_2^+$ ($E_{dl}$ or $E_{ld}$) is small and negligible in the case of $Rh(CH_3)_2^+$ and $Ir(CH_3)_2^+$. We thus suggest that the role of the

(111111) configuration in the wavefunction of $Co(CH_3)_2^+$ is markedly different from that of the Rh and Ir complexes.

As the question of resonance is mainly an issue of spin pairing (the $4s$ orbital can spin pair with either methyl group as can the $3d_{yz}$ orbital), when the CASSCF orbitals are localized to equivalent bonds, this is largely accomplished through the (111111) configuration with non-perfect pairing spin couplings. A careful analysis of the nine spin couplings associated with this configuration in the CASSCF(6/6) wavefunction (six open-shell electrons coupled triplet, shown schematically in Figure 3) indicates that one CSF is dominant. This is the G2 state,[19,20] in which the two electrons of the first bond are coupled triplet as are the two electrons of the second bond. These four electrons are coupled antiferromagnetically into a singlet and the remaining two open-shell $3d$ electrons lead to a total spin of triplet. This CSF, in which the perfect pairing of the bonds is broken, has a weight of 0.0185 compared to the G1 state (singlet coupling of the two bond pairs) which has a weight of 0.0016 and the GF state (quintet coupling of the four bonding electrons) which has a weight of 0.0003. No other spin couplings have significant weights as they break the triplet coupling of the two open shell $3d$ orbitals.

We make the assumption that when one set of natural orbitals is delocalized, resonance is accounted for without the (111111) configuration, perhaps because the partial delocalization allows bonds to be formed to both methyl groups by either the $4s$ or $3d_{yz}$ orbital. If it is indeed the case that the (111111) configuration accounts for most of the resonance when the orbitals are localized, then the difference in energy between $E_{ll}$ and $E_{dl}$ (or $E_{ld}$) should be a measure of the stability of the resonating bonds vs. the hybridized bonds. Our calculations indicate that the resonating wavefunction is stable by about 6 kcal/mol with

respect to hybridization at the CASSCF(6/6) level, while it is stable by only about 3 kcal/mol at the CASSCF(10/10) level. Following our discussion in Chapter III, it is evident that the complex is stabilized by one electron bonding which becomes apparant only with extensive correlation. This explains the decrease in the energy gap at the higher level.

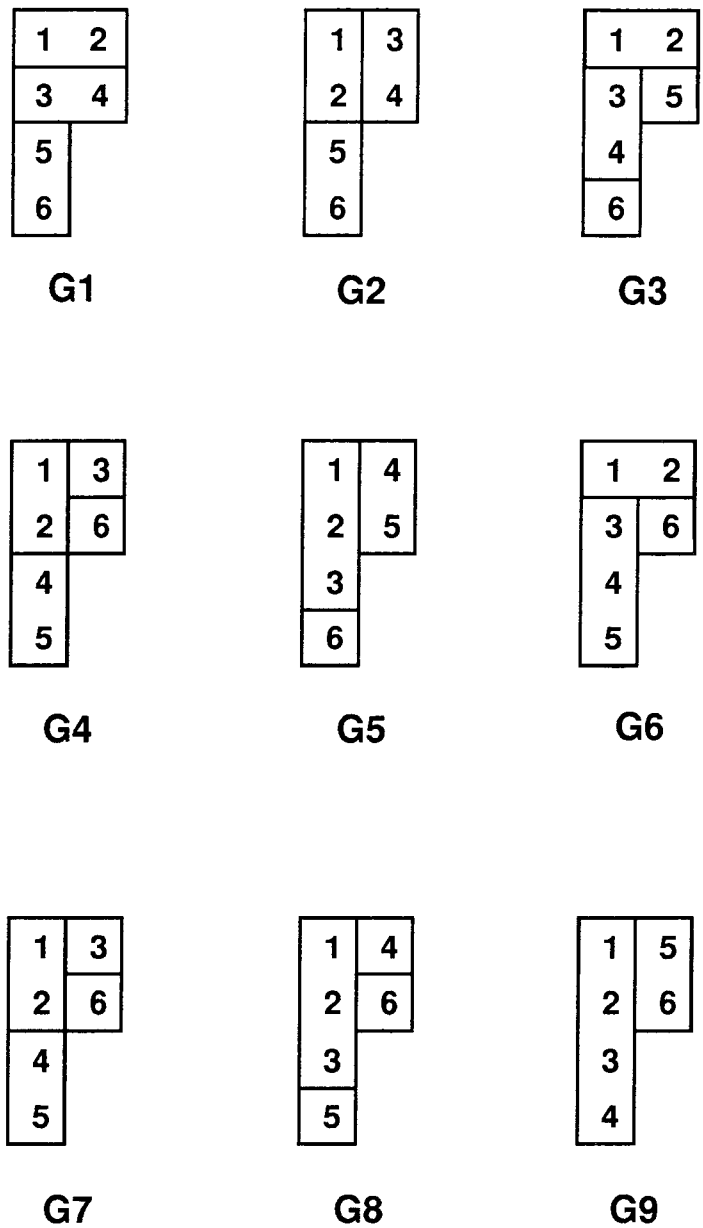


**Figure 3.** Spin couplings of 6 electrons into an overall triplet. Horizontal pairing indicates a low-spin coupling and vertical pairing indicates a high-spin coupling. Note that only the G1, G2, and G9 states preserve the high-spin coupling of electrons 5 and 6. The G9 state is also called the GF state.

### 6.4.2 The search for the cause of inequivalent bonds

Following the discussion in Chapter III (see Figure 6 of that chapter), much of the cause of symmetry breaking in the $Co^+$ complexes can be traced to two factors dependent on the large size difference between the $4s$ and $3d$ orbitals: the intrisic strengths of $s$, $d$, and $sd$ hybrid bonds, and the repulsion between $s$ and $d$ bonds and between $sd$ hybrid bonds. It is known that the $4s$ bond is intrinsically stronger than the $3d$ bond but it is not clear that two $sd$ hybrid bonds are intrinsically stronger than one $s$ bond and one $d$ bond. Perhaps even more significantly, the repulsion of the $d$ bond to the $s$ bond should be small but the repulsion of the $s$ bond to the $d$ bond should be large. However, it is not clear that the total repulsion will be reduced with $sd$ hybrid bonds. These are strong qualitative reasons why inequivalent bonding might be seen for $Co^+$, but no definate conclusions can be made. For $Rh^+$ and $Ir^+$, the situation is more straightforward: $sd$ hybrid bonds are instrinsically stronger than either $s$ bonds or $d$ bonds, and two $sd$ hybrid bonds have less repulsion between one another than one $s$ bond and one $d$ bond. Thus, it is the case that $Rh^+$ and $Ir^+$ should lead to $sd$ hybridization.

An important difference between $Co(CH_3)_2^+$ and the complexes of the other two metals is that both Rh and Ir have significantly more $d$ character in their bonds to the two methyl groups [Co: 37.0% $s$, 4.3% $p$, 58.7% $d$; Rh: 12.9% $s$, 2.4% $p$, 84.8% $d$; Ir: 23.9% $s$, 3.2% $p$, 72.9% $d$ at the CASSCF(6/6) level]. This is not a reflection of the total $s$ and $d$ populations on the metal as the numbers for $Co^+$ are intermediate to those of $Rh^+$ and $Ir^+$. The chief difference is that, in the Co complex, virtually all of the $s$ character goes into forming bonds to the two methyl groups leaving the singly occupied $a_1$ orbital with almost pure

$3d$ character (only 8.1% $s$). For Rh and Ir, this nonbonding orbital includes a sizeable portion of $s$ character (46.1% and 31.3%, respectively). It has been argued that the optimum mixture of $s$ and $d$ character in the bonds leading to the greatest overlap with the ligands, the principle advantage of hybridization, often includes more $d$ character than $s$.[21] This is especially true for the second and third row metals and the early metals of the first row.

Further examinations of the CI expansion for $\Psi_{GVB}$ [Eq. (2)] yields more insight into the nature of $sd$ hybridization. Assuming pure $sd$ hybridization, the dominant bonding configuration is $s^1d^7$. However, the correlation of the bonds introduces some $s^2d^6$ and some $d^8$ character through double excitations of the type

$$1b_2^2 \rightarrow 2a_1^2$$

and

$$1a_1^2 \rightarrow 2b_2^2,$$

respectively. This is especially acute in the GVB-PP wavefunction where the coefficient of each of these configurations is $\frac{1}{2}c_2$. While an accurate description of the atomic state splittings would tend to favor an increase in the $d^8$ contribution to the bonding for $Rh^+$ especially, the $s^2d^6$ state is virtually inaccessible in all three metals. The CASSCF calculations can reduce the degree of $s^2d^6$ character by easing the constraints on the coefficients of these excitations. Thus, the coefficient of the $1a_1^2 \rightarrow 2b_2^2$ excitation increases (increasing $d^8$ character) and the coefficient of the $1b_2^2 \rightarrow 2a_1^2$ excitation decreases (decreasing $s^2d^6$ character).

Alternatively, by mixing more $d$ character into the bonds, the contribution of the $s^2d^6$ metal configuration is also reduced.

Eliminating this problem is more difficult in the case of $Co(CH_3)_2^+$ as mixing more $d$ character into the bonds reduces the intrinsic bond strengths. However, if the bonds are inequivalent, as in the GVB-PP(6/6) calculations, only the $s^1d^7$ configuration is involved. Since the principal advantage in $sd$ hybridization is to increase the overlap with the ligands and decrease the repulsion between the ligands, and since the effectiveness of this is small for Co due to the disparity in the sizes of the $4s$ and $3d$ orbitals, the costs for hybridization outweigh the gains. As a result, inequivalent bonding is seen.

### 6.4.3 Vibrational Frequencies

In an attempt to determine if any physical differences arise as a result of the different qualities of the wavefunctions, we have also examined the vibrational frequencies of the modes associated with motions of the M−C bonds of $Co(CH_3)_2^+$, $Rh(CH_3)_2^+$, and $Ir(CH_3)_2^+$. Table X lists the force constants and vibrational frequencies associated with the symmetric and asymmetric stretches and the bending mode. Both the stretching modes increase in strength as Co < Rh < Ir, while the bending mode decreases in strength as Co > Rh > Ir. The asymmetric stretch is the mode which should be of most interest to the question of symmetry breaking in the $Co(CH_3)_2^+$ system; however, no unusual behavior associated with this mode is observed. It is lower in energy than the asymmetric stretches of the Rh and Ir complexes, but this reflects the fact that the symmetric stretch is weaker as well. Ironically, the most unusual aspect of these calculations is the behavior of the CASSCF(6/6) wavefunction for $Rh(CH_3)_2^+$ and $Ir(CH_3)_2^+$ in response to an asymmetric distortion of the geometry. We find that as the geometry is increasingly distorted, the first natural orbitals of the M−C bonds change from delocalized *s* and *d* bonds to localized *sd* hybrids (the second natural orbitals remain delocalized). This qualitative change in the natural orbitals leads to problems in obtaining a consistent description of the system at the MRCI level. With only three reference configurations, the MRCI based on localized orbitals is lower in energy than that based on delocalized orbitals. Thus, the MRCI leads to an unphysical description of the asymmetric stretch. Instead, we use the GVB-PP orbitals as a basis for CI calculations. These orbitals consistently localize as *sd* hybrids (both first and second natural orbitals) and a three-reference CI (including the dominant and double excita-

**Table X.** Approximate force constants and vibrational frequencies for the symmetric stretch, asymmetric stretch, and bend of the two $M-CH_3$ bonds in $Co(CH_3)_2^+$, $Rh(CH_3)_2^+$, and $Ir(CH_3)_2^+$, calculated at the MRCI/3+Q level. The force constants are expressed in kcal/Å$^2$ and the frequencies in $cm^{-1}$.

| | $Co(CH_3)_2^+$ | | $Rh(CH_3)_2^+$ | | $Ir(CH_3)_2^+$ | |
|---|---|---|---|---|---|---|
| | Force Const. | Freq. | Force Const. | Freq. | Force Const. | Freq. |
| Sym. | 238 | 477 | 281 | 496 | 355 | 542 |
| Asym.[a] | 226 | 479 | 269 | 499 | 329 | 532 |
| Bend | 19.1 | 197 | 17.3 | 179 | 15.0 | 161 |

[a] The asymmetric stretches for $Rh(CH_3)_2^+$ and $Ir(CH_3)_2^+$ were determined at the GVBSD/3+Q level as discussed in the text.

tions for bond 1 to its antibond and bond 2 to its antibond) leads to a wavefunction comparable to the MRCI based on the CASSCF orbitals. In fact, the GVBSD/3 level gives a lower energy than the MRCI/3 level. This is due to the fact, as already illustrated, that the GVB-PP wavefunction includes the most important effects of correlation in just three configurations while the CASSCF (or any wavefunction based on delocalized orbitals) has a more complicated CI expansion. On the other hand, using the GVB-PP orbitals as a basis for MRCI calculations on $Co(CH_3)_2^+$ would be most inappropriate due to the symmetry breaking. This it is necessary to use the CASSCF orbitals as a basis.

### 6.4.4 Related Systems

Chapter III demonstrated the strong similarity between the hydride and methyl ligands. As a result we expect that $CoH_2^+$ (see Chapter IV) would be the species most similar to $Co(CH_3)_2^+$. In fact, at a geometry typical of an inserted complex ($R_{Co-H} = 1.55$Å and $\theta = 90°$), the GVB-PP(6/6) wavefunction shows the same type of symmetry breaking seen in the dimethyl system. However, as was shown in Chapter IV, the most stable form of $CoH_2^+$ is a dihydrogen molecular complex. In contrast to $Co(CH_3)_2^+$, $CoH_2^+$ has no barrier between the insertion complex and the lower energy molecular complex. The lack of a barrier is due to the absence of directionality in the H 1*s* orbital while the highly directional $sp^3$ hybrid orbital of the $CH_3$ ligand leads to a destablized transition state and a high barrier to reductive elimination of ethane from $Co(CH_3)_2^+$. This distinction between the behavior of H and $CH_3$ as ligands was previously noted by Low and Goddard in their study of the oxidative addition of $H_2$, $CH_4$, and $C_2H_6$ to complexes of Pd and Pt.[23] Blomberg, Siegbahn, and co-workers made similar conclusions about these two ligands.[24] Thus, although, theoretically $CoH_2^+$ is simpler to treat than $Co(CH_3)_2^+$, additional insight into the nature of symmetry breaking in the inserted complex is obscured by the facile dissociation to the molecular complex.

A second consideration of the $CoH_2^+$ results prompted us to look at the case of $Co(H)(CH_3)^+$. The motivation for looking at such a complex is that the $M-H^+$ and $M-CH_3^+$ bonds are similar and that both the dihydride (though unstable) and the dimethyl complexes show inequivalent bonding. The mixed ligand complex then separates a system in which the same effects found in $Co(CH_3)_2^+$ and $CoH_2^+$ should be present but strict symmetry breaking cannot

be observed.

The nature of the symmetry breaking in $Co(CH_3)_2^+$ suggests that replacing one methyl by a hydrogen atom, a small perturbation by itself, might lead to a large change in the wavefunction, with one resonance configuration being dominant in $Co(H)(CH_3)^+$. Consider the following:

(i) The $4s$ bond in $Co(CH_3)_2^+$ is found to be covalent but the $3d$ bond is found to involve charge transfer from the ligand to the metal (see Table I).

(ii) The ionization potential of hydrogen is 13.6 eV and that of the methyl radical is 9.8 eV.

(iii) A positive charge on the hydrogen ligand would be repulsive to the positively charged metal center.

From these considerations, we expected that the hydrogen ligand would bond to the $4s$ orbital (without charge transfer) and the methyl ligand would bond to the $3d$ orbital (with charge transfer). From Figure 4a and Table XI, this is observed at the GVB-PP(6/6) level. The other resonance configuration ($3d$-H and $4s$-$CH_3$ bonds) could not be converged. Moreover, higher level calculations (CASSCF and MRCI), while leading to some delocalization of the bonds, do not alter this picture of inequivalent bonds. On the other hand, $Rh(H)(CH_3)^+$ and $Ir(H)(CH_3)^+$ each have M−H and M−$CH_3$ bonds which are essentially the same. [GVB-PP(6/6) results for these systems are given in Figures 4b and 4c and Tables XII and XIII, respectively.] While the same charge-transfer character can be observed in these complexes (the H is neutral and the methyl group is positively charged), bonding still occurs to metal $sd$ hybrids. The significance of this result is that it shows that the metals of the second and third row have a propensity to bond with $sd$ hybrid orbitals while in the first row bonds are formed with uncoupled $s$ and $d$ orbitals.

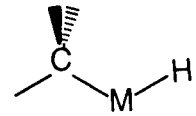
C
M
H

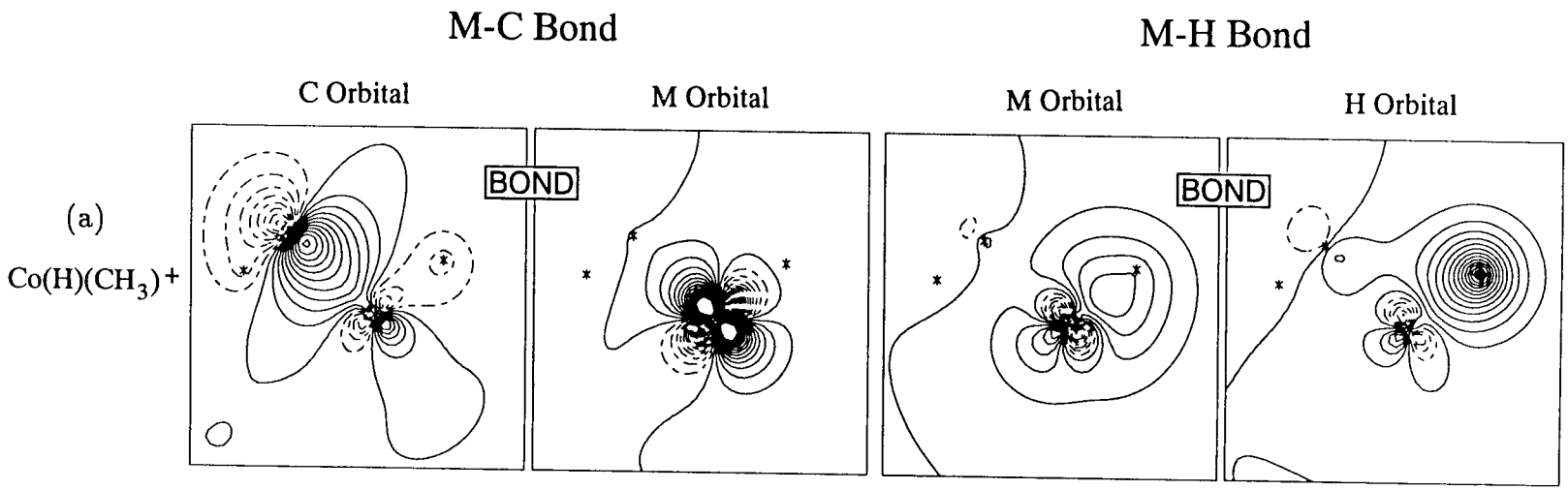
M-C Bond
M-H Bond
C Orbital
M Orbital
M Orbital
H Orbital
BOND
BOND
(a)
Co(H)(CH3)+

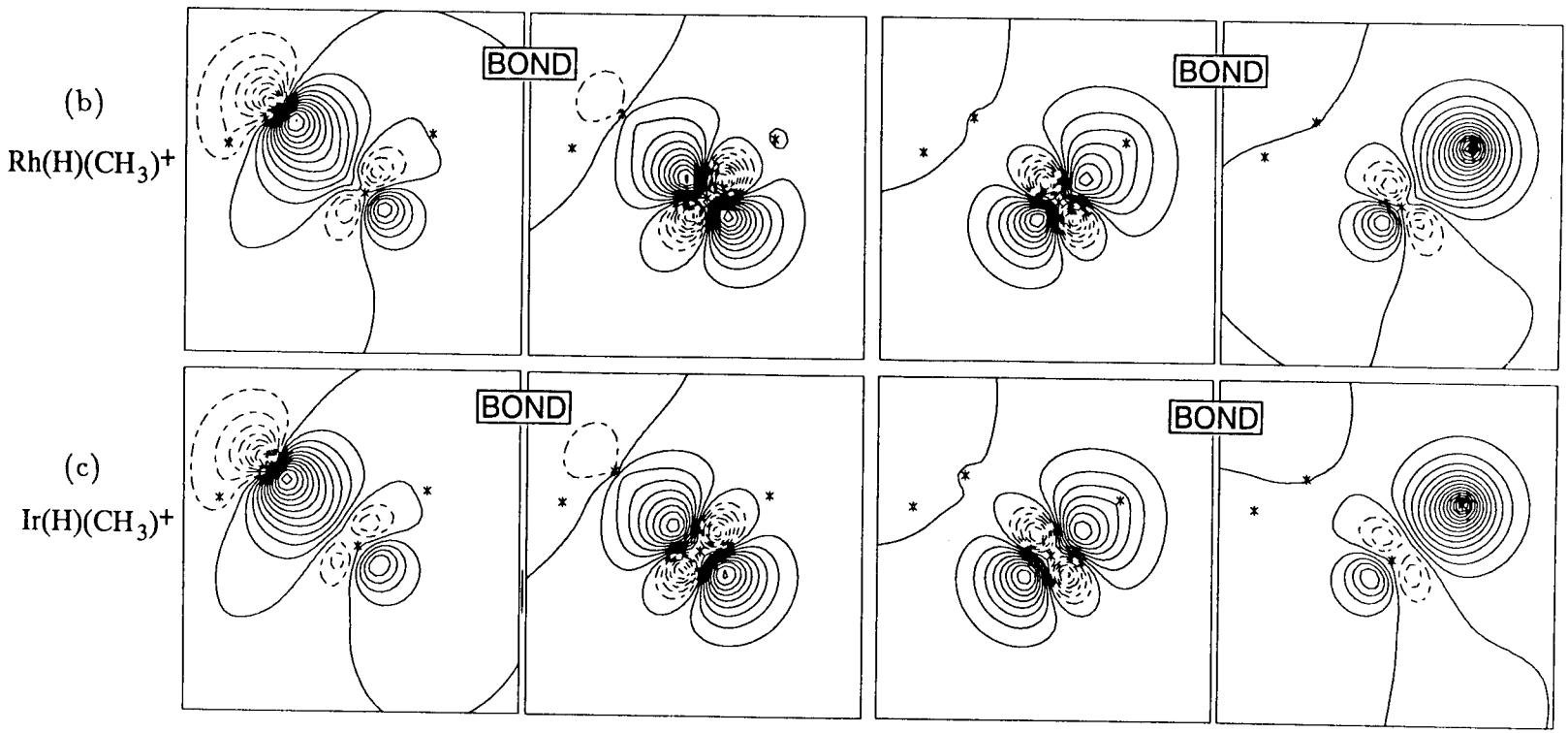


**Figure 4.** (a) GVB bonding orbitals for $Co(H)(CH_3)^+$ from GVB-PP(6/6) calculations. (Left, M−C Bond Pair) Here the metal orbital has primarily *d* character. (Right, M−H Bond Pair) Here the metal orbital has primarily *sp* character. (b) Same as (a) for $Rh(H)(CH_3)^+$. Here both metal bonding orbitals have similar *sd* hybrid character. (c) Same as (b) for $Ir(H)(CH_3)^+$.

**Table XI.** Mulliken population analysis for the GVB-PP(6/6) wavefunction of $Co(H)(CH_3)^+$. Only valence electrons are considered.

| | H Bond | $CH_3$ Bond | Total Populations | Total Charges |
|---|---|---|---|---|
| Co total | 0.935 | 1.231 | 8.209 | +0.791 |
| $4s$ | 0.650 | 0.069 | 0.740 | |
| $4p$ | 0.127 | 0.067 | 0.222 | |
| $3d$ | 0.158 | 1.095 | 7.247 | |
| H total | 1.012 | 0.018 | 1.037 | −0.037 |
| C total | 0.052 | 0.715 | 4.591 | −0.591 |
| Me total | 0.053 | 0.750 | 6.754 | +0.246 |
| Total | 2.000 | 2.000 | | |

As a final word on the subject, the problem of inequivalent bonds manifests itself at the HF level in $Co(H)(C_2H_5)^+$. While we expect the bonds to be inequivalent as discussed above, the $3d$-ethyl bond is so poorly described at this level that no bond is actually formed. Instead, the triplet complex is best described as a radical ethyl group loosely bound to doublet $CoH^+$. A geometry optimization of this complex then leads to a $Co-C_2H_5$ bond which is 0.3 Å too long. In this case, the GVB-PP wavefunction leads to a more accurate description of the bonding in the complex.

**Table XII.** Mulliken population analysis for the GVB-PP(6/6) wavefunction of $Rh(H)(CH_3)^+$. Only valence electrons are considered.

| | H Bond | $CH_3$ Bond | Total Populations | Total Charges |
|---|---|---|---|---|
| Rh total | 1.047 | 1.182 | 8.175 | +0.825 |
| 5*s* | 0.303 | 0.215 | 0.652 | |
| 5*p* | 0.052 | 0.035 | 0.099 | |
| 4*d* | 0.693 | 0.933 | 7.424 | |
| H total | 0.927 | 0.023 | 0.990 | +0.010 |
| C total | 0.026 | 0.779 | 4.640 | −0.640 |
| Me total | 0.026 | 0.795 | 6.835 | +0.165 |
| Total | 2.000 | 2.000 | | |

**Table XIII.** Mulliken population analysis for the GVB-PP(6/6) wavefunction of $Ir(H)(CH_3)^+$. Only valence electrons are considered.

| | H Bond | $CH_3$ Bond | Total Populations | Total Charges |
|---|---|---|---|---|
| Ir total | 1.079 | 1.153 | 8.162 | +0.838 |
| 6*s* | 0.316 | 0.279 | 0.800 | |
| 6*p* | 0.050 | 0.037 | 0.084 | |
| 5*d* | 0.712 | 0.836 | 7.279 | |
| H total | 0.914 | 0.014 | 0.964 | +0.036 |
| C total | 0.007 | 0.832 | 4.672 | −0.672 |
| Me total | 0.007 | 0.834 | 6.875 | +0.125 |
| Total | 2.000 | 2.000 | | |

## 6.5 Conclusions

GVB calculations on the insertion products $M(CH_3)_2^+$, with M = Co, Rh, and Ir, show that M = RH and Ir leads to *sd* hybridization but M = Co does not. For $Co^+$, the large difference in the sizes of the 4*s* and 3*d* orbitals results in inefficient hybridization. Instead, uniquely different bonds are formed—one methyl bonds to the 4*s* orbital and the other bonds to a 3*d* orbital. Thus, the GVB-PP(6/6) wavefunction, with only one VB coupling, leads to symmetry breaking. The *R*-GVB wavefunction, with two resonating VB couplings, restores symmetry. Higher order wavefunctions (CASSCF and MRCI) do not exhibit symmetry breaking and, although not transparent, we find that these wavefunctions lead to the same description as *R*-GVB (resonance of decoupled *s* and *d* bonds). These results are contrasted with those for the $Rh(CH_3)_2^+$ and $Ir(CH_3)_2^+$ complexes in which both bonds are *sd* hybrids at the GVB level and in higher level calculations. Additional systems showing the new type of bonding include $CoH_2^+$. For $Co(H)(CH_3)^+$, this preference for one bond to be *d* and the other *s* results in the hydrogen bonding to the 4*s* orbital and the methyl group bonding to a 3*d*. Again this is contrasted with the behavior of M = Rh and Ir, where $M(H)(CH_3)^+$ leads to similar *sd* hybrids for both M—H and $M—CH_3$ bonds.

## Appendix

As this study was not meant to be a quantitative determination of the energetics of insertion into the C−C bond of ethane but instead a qualitative determination of the nature of the wavefunction, a smaller basis set was employed. The standard valence triple-$\zeta$ basis was used for the metals but without polarization functions. For carbon the Dunning/Huzinaga[25] (9s5p/3s2p) valence double-$\zeta$ basis set with a single set of $d$ polarization functions ($\alpha = 0.75$) was used. For hydrogens bound to carbon atoms, the Dunning/Huzinaga (4s/2s) double-$\zeta$ basis set, scaled by a factor of 1.2 was used. For hydrogens bound to a metal, the Dunning/Huzinaga (6s/3s) triple-$\zeta$ basis set (unscaled) was used with one set of $p$ polarization functions ($\alpha = 0.6$).

Gradient geometry optimizations were performed for the GVB-PP wavefunctions for $Co(CH_3)_2^+$, $Rh(CH_3)_2^+$, $Ir(CH_3)_2^+$, $Co(H)(CH_3)^+$, $Rh(H)(CH_3)^+$, and $Ir(H)(CH_3)^+$. These geometries are given in Figures 5 and 6. Geometries of the dimethyl complexes of $Co^+$, $Rh^+$, and $Ir^+$ were also optimized at the MRCI/3 level in a point by point manner. Only the M−C bond length and the C−M−C angle were optimized. All other coordinates were fixed after Rosi *et al.*[15] The C−H bond distance was fixed to 1.095Å and the H−C−Co angle was fixed to 105.2°. The geometries were also restricted to local $C_{3v}$ symmetry of the methyl groups about each Co−C bond. These geometries are also summarized in Figure 7. A similar geometry optimization was performed for the $R$-GVB wavefunction of $Co(CH_3)_2^+$, the results of which were mentioned in the text.

Finally, Tables XIV-XVI give a comparison of the energetics of various levels of calculation for the $Co(CH_3)_2^+$, $Rh(CH_3)_2^+$, nd $Ir(CH_3)_2^+$. Dissociation energies are computed with respect to the $s^1d^7\ ^5F$ state of the metal atom + $2CH_3$. For

$Co^+$ and $Rh^+$, an empirical correction is made to obtain the $D_e$ with respect to the $d^8\ ^3F$ ground state. More quantitative results are presented in Chapter XIII.

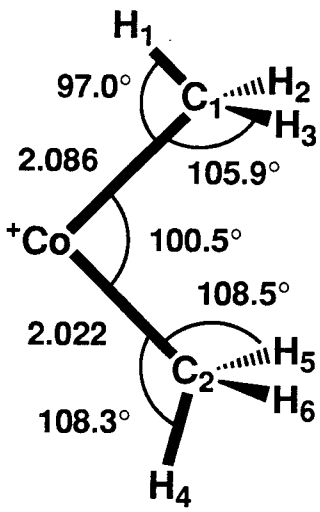


## $^3B_1$ $Co(CH_3)_2^+$

| | | | |
|---|---|---|---|
| Co | 0.0000 | 0.0000 | 0.0000 |
| $C_1$ | 0.0000 | 1.5729 | 1.3700 |
| $C_2$ | 0.0000 | -1.5827 | 1.2579 |
| $H_1$ | 0.0000 | 2.3809 | 0.6432 |
| $H_2$ | 0.9101 | 1.4684 | 1.9391 |
| $H_3$ | -0.9101 | 1.4684 | 1.9391 |
| $H_4$ | 0.0000 | 2.4906 | 0.6639 |
| $H_5$ | 0.8907 | 1.5343 | 1.8724 |
| $H_6$ | -0.8907 | 1.5343 | 1.8724 |

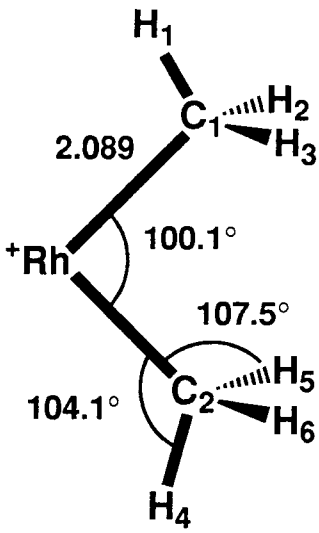


$^3B_1$ $Rh(CH_3)_2^+$

| | | | |
|---|---|---|---|
| Rh | 0.0000 | 0.0000 | 0.0000 |
| $C_1$ | 0.0000 | 1.6013 | 1.3412 |
| $C_2$ | 0.0000 | -1.6013 | 1.3412 |
| $H_1$ | 0.0000 | 2.4790 | 0.7043 |
| $H_2$ | 0.8992 | 1.5275 | 1.9366 |
| $H_3$ | -0.8992 | 1.5275 | 1.9366 |
| $H_4$ | 0.0000 | -2.4790 | 0.7043 |
| $H_5$ | 0.8992 | -1.5275 | 1.9366 |
| $H_6$ | -0.8992 | -1.5275 | 1.9366 |

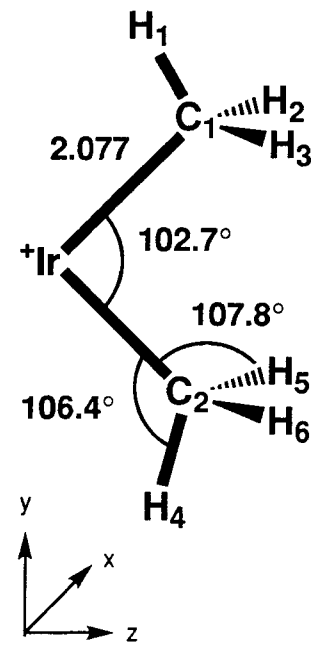


$^3B_1$ $Ir(CH_3)_2^+$

| | | | |
|---|---|---|---|
| Ir | 0.0000 | 0.0000 | 0.0000 |
| $C_1$ | 0.0000 | 1.6225 | 1.2970 |
| $C_2$ | 0.0000 | -1.6225 | 1.2970 |
| $H_1$ | 0.0000 | 2.5126 | 0.6758 |
| $H_2$ | 0.8964 | 1.5628 | 1.9011 |
| $H_3$ | -0.8964 | 1.5628 | 1.9011 |
| $H_4$ | 0.0000 | -2.5126 | 0.6758 |
| $H_5$ | 0.8964 | -1.5628 | 1.9011 |
| $H_6$ | -0.8964 | -1.5628 | 1.9011 |

**Figure 5.** GVB-PP(6/6) optimized geometries for the $^3B_1$ states of $M(CH_3)_2^+$, M = Co, Rh, and Ir. $Co(CH_3)_2^+$ is asymmetric while $Rh(CH_3)_2^+$ and $Ir(CH_3)_2^+$ are symmetric. Cartesian coordinates are in Å.

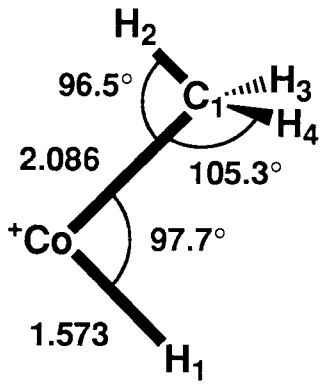


$^3$A" Co(H)(CH$_3$)$^+$

| | | | |
|---|---|---|---|
| Co | 0.0000 | 0.0000 | 0.0000 |
| C | 0.0000 | 1.5053 | 1.4443 |
| $H_1$ | 0.0000 | -1.2310 | 0.9796 |
| $H_2$ | 0.0000 | 2.3418 | 0.7499 |
| $H_3$ | 0.9112 | 1.3627 | 2.0037 |
| $H_4$ | -0.9112 | 1.3627 | 2.0037 |

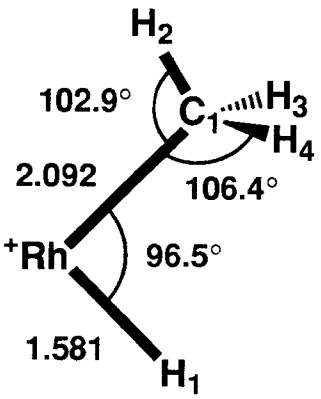


$^3$A" Rh(H)(CH$_3$)$^+$

| | | | |
|---|---|---|---|
| Rh | 0.0000 | 0.0000 | 0.0000 |
| C | 0.0000 | 1.5249 | 1.4314 |
| $H_1$ | 0.0000 | -1.2053 | 1.0237 |
| $H_2$ | 0.0000 | 2.4247 | 0.8261 |
| $H_3$ | 0.9018 | 1.3970 | 2.0128 |
| $H_4$ | -0.9018 | 1.3970 | 2.0128 |

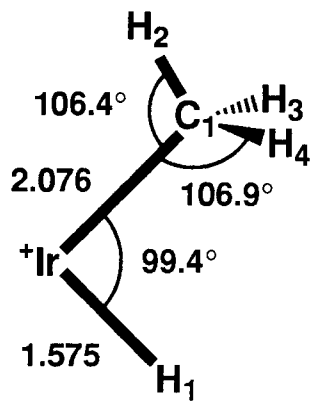


$^3$A" Ir(H)(CH$_3$)$^+$

| | | | |
|---|---|---|---|
| Ir | 0.0000 | 0.0000 | 0.0000 |
| C | 0.0000 | 1.5409 | 1.3915 |
| $H_1$ | 0.0000 | -1.2322 | 0.9809 |
| $H_2$ | 0.0000 | 2.4660 | 0.8244 |
| $H_3$ | 0.8974 | 1.4266 | 1.9868 |
| $H_4$ | -0.8974 | 1.4266 | 1.9868 |

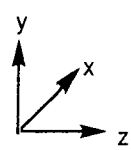


**Figure 6.** GVB-PP(6/6) optimized geometries for the $^3$A" states of M(H)(CH$_3$)$^+$, M = Co, Rh, and Ir. Cartesian coordinates are in Å.

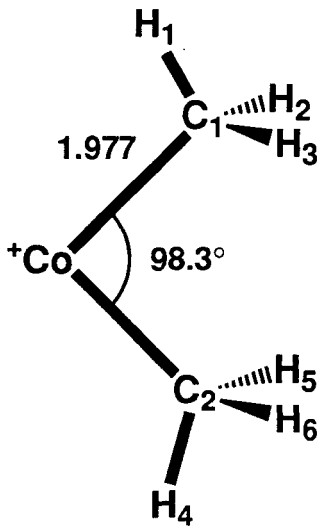


## $^3B_1$ $Co(CH_3)_2^+$

| | | | |
|---|---|---|---|
| Co | 0.0000 | 0.0000 | 0.0000 |
| $C_1$ | 0.0000 | 1.4955 | 1.2931 |
| $C_2$ | 0.0000 | -1.4955 | 1.2931 |
| $H_1$ | 0.0000 | 2.4041 | 0.6814 |
| $H_2$ | 0.9151 | 1.3670 | 1.8808 |
| $H_3$ | -0.9151 | 1.3670 | 1.8808 |
| $H_4$ | 0.0000 | -2.4041 | 0.6814 |
| $H_5$ | 0.9151 | -1.3670 | 1.8808 |
| $H_6$ | -0.9151 | -1.3670 | 1.8808 |

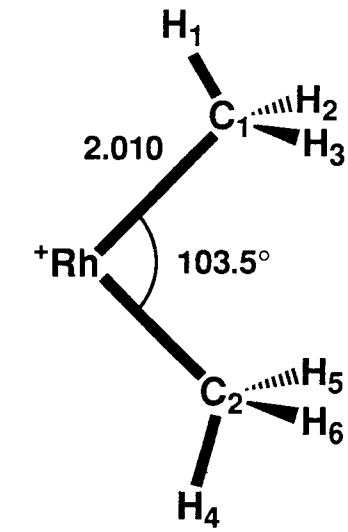


$^3B_1$ $Rh(CH_3)_2^+$

| | | | |
|---|---|---|---|
| Rh | 0.0000 | 0.0000 | 0.0000 |
| $C_1$ | 0.0000 | 1.5785 | 1.2444 |
| $C_2$ | 0.0000 | -1.5785 | 1.2444 |
| $H_1$ | 0.0000 | 2.4581 | 0.5923 |
| $H_2$ | 0.9151 | 1.4769 | 1.8370 |
| $H_3$ | -0.9151 | 1.4769 | 1.8370 |
| $H_4$ | 0.0000 | -2.4581 | 0.5923 |
| $H_5$ | 0.9151 | -1.4769 | 1.8370 |
| $H_6$ | -0.9151 | -1.4768 | 1.8370 |

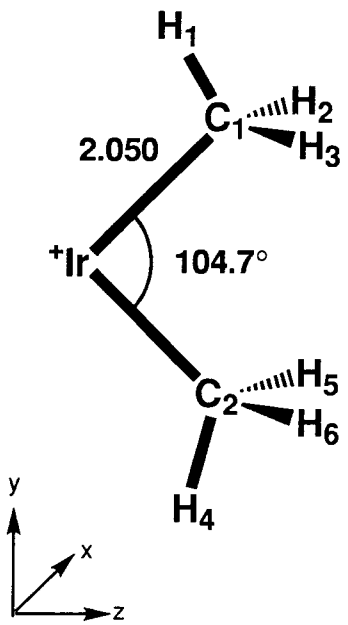


$^3B_1$ $Ir(CH_3)_2^+$

| | | | |
|---|---|---|---|
| Ir | 0.0000 | 0.0000 | 0.0000 |
| $C_1$ | 0.0000 | 1.6231 | 1.2522 |
| $C_2$ | 0.0000 | -1.6231 | 1.2522 |
| $H_1$ | 0.0000 | 2.4959 | 0.5909 |
| $H_2$ | 0.9151 | 1.5277 | 1.8459 |
| $H_3$ | -0.9151 | 1.5277 | 1.8459 |
| $H_4$ | 0.0000 | -2.4959 | 0.5909 |
| $H_5$ | 0.9151 | -1.5277 | 1.8459 |
| $H_6$ | -0.9151 | -1.5277 | 1.8459 |

**Figure 7.** CI optimized geometries for the $^3B_1$ states of $M(CH_3)_2^+$, M = Co, Rh, and Ir. All three complexes are symmetric. The H-C-M angles were constrained to 105.2° and the C-H bond lengths were constrained to 1.095 Å. Cartesian coordinates are in Å.

**Table XIV.** Comparison of energetics for $Co(CH_3)_2^+$ at various levels of calculation.

| | Energy | $D_e$ |
|---|---|---|
| HF | −223.19569 | −23.8 |
| GVB-PP(6/6) | −223.27141 | 23.7 |
| *R*-GVB | −223.28967 | 35.2 |
| CASSCF(6/6) | −223.31001 | 47.9 |
| CASSCF(10/10) | −223.36445 | 63.1 |
| MRCI/3 | −223.66461 | 69.8 |
| MRCI/3+Q | −223.71679 | 82.1 |
| MRCI/4 | −223.67215 | 74.5 |
| MRCI/4+Q | −223.72004 | 84.1 |

**Table XV.** Comparison of energetics for $Rh(CH_3)_2^+$ at various levels of calculation.

| | Energy | $D_e$ |
|---|---|---|
| HF | −188.21631 | −3.7 |
| GVB-PP(6/6) | −188.26440 | 26.5 |
| CASSCF(6/6) | −188.28855 | 41.7 |
| MRCI/3 | −188.60099 | 58.9 |
| MRCI/3+Q | −188.64648 | 69.7 |
| GVBSD/3 | −188.60487 | 61.3 |
| GVBSD/3+Q | −188.64705 | 70.0 |

**Table XVI.** Comparison of energetics for $Ir(CH_3)_2^+$ at various levels of calculation.

| | Energy | $D_e$ |
|---|---|---|
| HF | −182.91894 | 59.7 |
| GVB-PP(6/6) | −182.96804 | 90.5 |
| CASSCF(6/6) | −182.97868 | 97.2 |
| MRCI/3 | −183.28817 | 114.9 |
| MRCI/3+Q | −183.33180 | 124.4 |
| GVBSD/3 | −183.29572 | 119.7 |
| GVBSD/3+Q | −183.33459 | 126.1 |

**References**

(1) Perry, J. K.; Goddard, W. A., III: Ohanessian, G. *J. Chem. Phys.* **1992**, *97*, 7560.

(2) (a) Thouless, D. J., *The Quantum Mechanics of Many-Body Systems*; Academic: New York, 1967. (b) Cizek, J.; Paldus, J. *J. Chem. Phys.* **1967**, *47*, 3976. (c) Davidson, E. R.; Borden, W. T. *J. Phys. Chem.* **1983**, *87*, 4783.

(3) Allen, W. D.; Horner, D. A.; Dekock, R. L.; Remington, R. B.; Schaefer, H. F., III *Chem. Phys.* **1989**, *133*, 11.

(4) (a) Denis, A.; Langlet, J.; Malrieu, J. P. *Theor. Chim. Acta*, **1975**, *33*, 49. (b) Cederbaum, L. S.; Domcke, W. J. *J. Chem. Phys.* **1977**, *66*, 5084.

(5) Bacskay, G. B.; Bryant, G.; Hush, N. S. *Int. J. Quantum Chem.* **1987**, *31*, 471.

(6) Agren, H.; Bagus, P. S.; Roos, B. O. *Chem. Phys.* **1981**, *82*, 505.

(7) Lozes, R. L.; Goscinski, O.; Wahlgren, U. *Chem. Phys. Lett.* **1979**, *63*, 77.

(8) Murphy, R.; Schaefer, H. F., III; Nobes, R H.; Radom, L.; Pitzer, R. M. *Int. Rev. Phys. Chem.* **1986**, *5*, 229.

(9) (a) Paldus, J.; Veillard, A. *Mol. Phys.* **1978**, *35*, 445. (b) Cook, D. B. *J. Chem. Soc. Faraday Trans. II* **1986**, *82*, 187.

(10) McLean, A. D.; Lengsfield, B. H.; Pacansky, J.; Ellinger, Y. *J. Chem. Phys.* **1985**, *83*, 3567.

(11) Buijse, M. A.; Baerends, E. J. *J. Chem. Phys.* **1990**, *93*, 4129.

(12) Buijse, M. A.; Baerends, E. J. *Theor. Chem. Acta* **1991**, *79*, 389.

(13) Voter, A. F., Ph.D. thesis, California Institute of Technology, 1983.

(14) Ohanessian, G.; Goddard, W. A., III, unpublished.

(15) Rosi, M.; Bauschlicher, C. W.; Langhoff, S. R.; Partridge, H. *J. Phys. Chem.* **1990**, *94*, 8656.

(16) (a) Voter, A. F.; Goddard, W. A., III *Chem. Phys.* **1981**, *57*, 253. (b) See also Jackels, C. F.; Davidson, E. R. *J. Chem. Phys.* **1976**, *64*, 2908.

(17) This ratio is computed with $\langle\phi|r^2|\phi\rangle^{\frac{1}{2}}$ using the singly occupied $(n+1)s$ and $nd$ HF orbitals of the $^5F$ states of the metal cations.

(18) (a) Voter, A. F.; Goddard, W. A., III *J. Chem. Phys.* **1981**, *75*, 3638. (b) Voter, A. F.; Goddard, W. A., III *J. Am. Chem. Soc.* **1986**, *108*, 2830.

(19) (a) Goddard, W. A., III *Phys. Rev.* **1967**, *157*, 73. (b) Goddard, W. A., III *Phys. Rev.* **1967**, *157*, 81. (c) Goddard, W. A., III *J. Chem. Phys.* **1968**, *48*, 450.

(20) Bobrowicz, F. W., Ph.D. thesis, California Institute of Technology, 1974.

(21) Steigerwald, M., Ph.D. thesis, California Institute of Technology, 1983.

(22) Ohanessian, G.; Goddard, W. A., III *Acc. Chem. Res.* **1990**, *23*, 386.

(23) (a) Low, J. J.; Goddard, W A., III *J. Am. Chem. Soc.* **1984**, *106*, 6928. (b) Low, J. J.; Goddard, W A., III *J. Am. Chem. Soc.* **1984**, *106*, 8321. (c) Low, J. J.; Goddard, W A., III *J. Am. Chem. Soc.* **1986**, *108*, 6115. (d) Low, J. J.; Goddard, W A., III *Organometallics* **1986**, *5*, 609.

(24) (a) Blomberg, M.; Brandemark, U.; Pettersson, L.; Siegbahn, P. *Int. J. Quantum Chem.* **1983**, *23*, 855. (b) Blomberg, M. R. A.; Siegbahn, P. E. M. *J. Chem. Phys.* **1983**, *78*, 986. (c) Blomberg, M. R. A.; Siegbahn, P. E. M. *J. Chem. Phys.* **1983**, *78*, 5682. (d) Blomberg, M. R. A.; Brandemark, U.; Siegbahn, P. E. M. *J. Phys. Chem.* **1984**, *88*, 4617. (e) Blomberg, M. R. A.; Schüle, J.; Siegbahn, P. E. M. *J. Am. Chem. Soc.* **1989**, *111*, 6156. (f) Blomberg, M. R. A.; Siegbahn, P. E. M.; Nagashima, U.; Wennerberg, J. *J. Am. Chem. Soc.* **1991**, *113*, 424.

(25) (a) Dunning, T. H. *J. Chem. Phys.* **1972**, *53*, 1293. (b) Huzinaga, S. *J. Chem. Phys.* **1965**, *42*, 1293.

Chapter VII

# Transition Metal Ion Mediated Dehydrogenation of Methane

# Chapter VII

## Transition Metal Ion Mediated Dehydrogenation of Methane

### 7.1. Introduction

Under the low pressure conditions of an FTICR spectrometer, Irikura and Beauchamp[1] showed that the third row transition metal cations are generally much more reactive towards $CH_4$ in the gas phase than their first and second row counterparts. In particular, they found that $Ir^+$ is 70% efficient in the dehydrogenation of $CH_4$, whereas the next best ions are $Pt^+$ (39%), $Ta^+$ (34%), $Os^+$ (34%), and $W^+$ (12%). While the majority of transition metals have been observed to react spontaneously with larger alkanes (for instance $Rh^+$ can dehydrogenate $C_2H_6$ and larger alkanes[2] and $Co^+$ can dehydrogenate *and* demethanate $C_3H_8$ and larger alkanes[3]), only one non-third row transition metal ($Zr^+$) has been observed to react with $CH_4$ under ICR conditions.[4] However, the efficiency of this reaction is quite small (1%) and it is suspected that the reactivity is largely due to contamination with excited states of the ion.

It has been argued that the high reactivity of the third row metals is due to a dramatic increase in the intrinsic $M^+-H$, $M^+-CH_3$, and $M^+=CH_2$ bond strengths.[5] This increase has already been partly verified (Chapter III) and represents a reasonable explanation for the observed higher reactivity of the third row metals as compared to the first and second row metals. Yet the trend in reactivity across the third row metals is not well defined. Is the efficiency determined by the exothermicity of the reaction or a rate limiting transition state? To garner better insight into these reactions, we have carried out theoretical

studies of the various steps involved in the most efficient reaction:

$$Ir^+ + CH_4 \longrightarrow H_2 + IrCH_2^+ \qquad (1)$$

An understanding of the nature of the potential energy surface makes it clear why $Ir^+$ is better than any other transtion metal cation at dehydrogenation of $CH_4$. By means of contrast, we include data related to the chemistry of $Co^+$ and $Rh^+$ with $CH_4$. As will be shown, the only exothermic process for these two metals is the formation of the cluster $M(CH_4)^+$. Portions of this work have previously been published.[6]

We should mention that much of the motivation for the study of methane activation comes from the petroleum industry. Because of the enormous world-wide reserves of methane and the difficulty associated with its transportation, there is a great deal of interest in finding catalysts to convert this most abundant natural gas to easily transportable liquid fuels such a methanol. Current techniques for methane conversion generally involve the heterogeneous production of syngas (a mixture of CO and $H_2$) by reaction of $CH_4$ and $H_2O$ at high temperatures (>800°C) over a variety of metal based catalysts.[7] Further reaction of this syngas over various additional metal catalysts leads to the desired products of either methanol or higher hydrocarbons. Despite significant advances, this process is not yet economical and a more direct synthesis route is desired.

Progress on alkane activation and functionalization has also been made by organometallic chemists.[8] Development of solution phase catalysts capable of breaking C−H bonds has proceeded on a number of fronts. The mechanisms of these catalysts generally fall into the catagories of $\sigma$-bond metathesis, electrophilic displacement, or oxidative addition. Of these, electrophilic displacement reactions involving electron deficient complexes of Pt(II), for example,

are particularly notable in their ability to convert $CH_4$ to methanol.[8a] Unfortunately, these reactions generally lead to low yields and difficulties in making the process catalytic. The recent report of an $Hg(II)/H_2SO_4$ catalyst, however, appears to represent a significant advance in this field.[9] The younger field of oxidative addition based catalysis involving coordinatively unsaturated Ir(I) complexes (among others) shows promise in the functionalization of alkanes, yet success has so far been limited.[10]

The gas phase ion-methane reactions represent the ideal. Knowledge of the nature of these reactions should be used as a guide to research done in the condensed phase.

## 7.2 Comparison between $Co^+$, $Rh^+$, and $Ir^+$

### 7.2.1 $CoCH_2^+$, $RhCH_2^+$, and $IrCH_2^+$

The primary restriction in these ICR studies of methane dehydrogenation is that only reactions which are exothermic and have no barriers in excess of the reactant energy will be observed. This being the case, the logical starting point in a study of these reactions is then the product $MCH_2^+$ species.

In order for an exothermic reaction to occur, the $M^+{=}CH_2$ bond energy must be >111 kcal/mol, the endothermicity of reaction 2.[11]

$$CH_4 \longrightarrow CH_2 + H_2 \qquad (2)$$

Considering the trends in transition metal hydride and metal-alkyl bond strengths in which metals of the third row bond more strongly than metals of the first two rows, one is naturally led to believe that the metals with the highest probability of having $MCH_2^+$ bond strenths in excess of 111 kcal/mol would belong to the third row. The experimental results for $CH_4$ dehydrogenation suggest that there are at least five metals with $MCH_2^+$ bond strengths in excess of 111 kcal/mol.[1]

The bonding in a metal methylidene can be classified as one of two types.[12] The first type is a Schrock carbene,[12b] in which $^3B_1$ $CH_2$ bonds to the metal to form covalent $\sigma$- and $\pi$-bonds. For a metal in the $s^1d^7$ configuration, this leads to a triplet state with an M−C $\sigma$-bond formed from the $s$ orbital and an M−C $\pi$-bond formed from the $d_{xz}$ orbital.

For a metal in the $d^8$ configuration, this leads to a singlet state with an M−C $\sigma$-bond formed from the $d_{z^2}$ orbital and an M−C $\pi$ bond formed from the $d_{xz}$ orbital.

The second type is a Fischer carbene,[12c] in which $^1A_1$ $CH_2$ bonds to the metal as a $\sigma$-donor and $\pi$-acceptor. As with the molecular complexes (Chapter V), bonding to a $d^8$ state is preferable to bonding to an $s^1d^7$ state as the interaction is largely electrostatic. Thus, for a metal in the $d^8$ configuration, this leads to a triplet state with donation from the $CH_2$ to the empty $s$ orbital and backdonation from the doubly occupied $d_{xz}$ orbital to the $CH_2$.

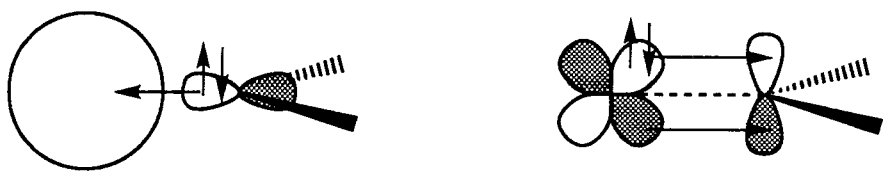

These descriptions represent two extremes of a continuum. Since a triplet state of $MCH_2^+$ (M = Co, Rh, or Ir) could be either a Schrock or Fischer carbene, a mixture is expected. For a singlet state, the Schrock picture is expected to

dominate.

Since the $MCH_2^+$ bond is formally a double bond and the strength of a typical $Co^+-C$ or a $Rh^+-C$ $\sigma$-bond is less than half of 111 kcal/mol, it is not expected that either of these metals would be able to form a metal-methylidene bond that would lead to an exothermic reaction for methane dehydrogenation. A Schrock $\pi$-bond is surely weaker than a $\sigma$-bond and it is difficult to envision a Fischer carbene with a bond strength of 111 kcal/mol. On the other hand, a typical $Ir^+-C$ $\sigma$-bond is worth about 70 kcal/mol. With a $\pi$-bond worth >41 kcal/mol, dehydrogenation of methane by $Ir^+$ to form $IrCH_2^+$ will be exothermic.

Our results are presented in Table I and Figures 1 and 2. Indeed, it is the case that the $CoCH_2^+$ and $RhCH_2^+$ bonds are significantly weaker than the $IrCH_2^+$ bond ($D_0$=76±3, 79±3, and 119±4 kcal/mol, respectively). More importantly, the $IrCH_2^+$ bond is strong enough for dehydrogenation of methane to be an exothermic reaction. We estimate that this reaction is exothermic by 8 kcal/mol for $Ir^+$ but endothermic by 35 kcal/mol for $Co^+$ and 32 kcal/mol for $Rh^+$. As discussed, the experimentally observed reactivity of the metals of the third row with methane indicate that at least five of the product $MCH_2^+$ complexes must have bond strengths in excess of 111 kcal/mol. One of these metals is $Ir^+$, as we have confirmed.

These results are also consistent with other studies. Experimental data on the first row transition metal $MCH_2^+$ complexes indicate that none of these species have bond strengths in excess of 100 kcal/mol ($D_0$=76.0±2.3 kcal/mol for $CoCH_2^+$).[13] Furthermore, a theoretical study by Bauschlicher *et al.*[14] of the transition metal methylidenes of the first and second rows indicates that the strongest bond is to $Zr^+$, with $D_0$=101±3 kcal/mol, 11 kcal/mol stronger than the next strongest bond (to $Y^+$). These calculations led to esti-

**Table I.** Properties of $MCH_2^+$ for M = Co, Rh, and Ir. The values of $r_e$, $\omega_e$, $\mu$, the $d$ population, and the charge on M were determined at the MCPF level.

| | $CoCH_2^+$ $^3A_2$ | $RhCH_2^+$ $^1A_1$ | $IrCH_2^+$ $^3A_2$ |
|---|---|---|---|
| $D_0$ (kcal/mol)[a] | 76±3[b] | 79±3 | 119±4 |
| $D_e$ (MRCI+Q) | 74.8 | 77.5 | 116.5 |
| $D_e$ (MCPF) | 67.3 | 74.7 | 112.2 |
| $r_e$ (M−C, Å) | 1.80 | 1.79 | 1.84 |
| $\omega_e$ (M−C, $cm^{-1}$) | 655 | 835 | 822 |
| $d$ population | 7.55 | 8.04 | 7.37 |
| $\mu$ (D)[c] | +0.831 | +1.951 | +2.078 |
| charge on M | +0.58 | +0.64 | +0.58 |

[a] Our best estimate for $D_0^\circ$ was obtained by adding 3±3 kcal/mol to the MRCI+Q bond strength for $CoCH_2^+$ and $RhCH_2^+$ and 4±4 kcal/mol for $IrCH_2^+$. The zero-point correction was determined from the M−C stretching frequency scaled by 1.5. It is 1.4 kcal/mol for $CoCH_2^+$ and 1.8 kcal/mol for $RhCH_2^+$ and $IrCH_2^+$.

[b] The $CoCH_2^+$ bond energies have been empirically corrected to account for the error in the $^3F$-$^5F$ state splittings. This correction was based on the MCPF 3$d$ populations. This was not done for either $RhCH_2^+$ or $IrCH_2^+$. The experimental value for the $CoCH_2^+$ bond energy is $D_0$=76.0±2.3 kcal/mol.[13] It has been adjusted to 0 K.[14]

[c] The metal was at the origin and the positive charge indicates polarization of electron density toward the metal.

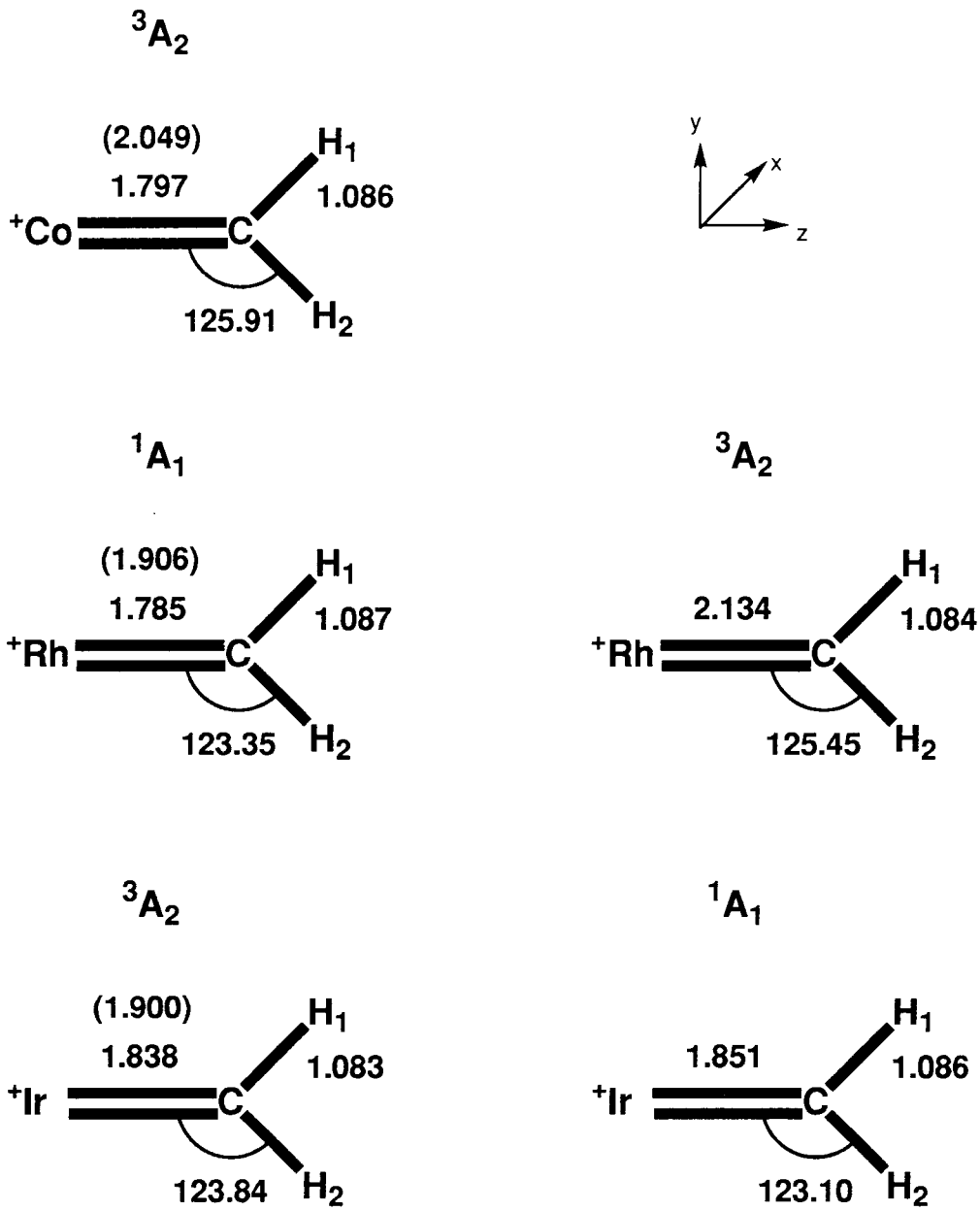


**Figure 1.** Optimized geometries for the $MCH_2^+$ species, M=Co, Rh, and Ir. The ground states of each complex were optimized at the HF/MCPF/HF level and results for the HF optimized M-C bond distance are given in parenthesis. The triplet excited state of $RhCH_2^+$ and the singlet excited state of $IrCH_2^+$ were optimized at the HF level. Distances are in Å and angles in degrees.

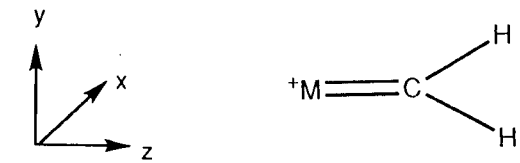
y
x
z
+M
C
H
H

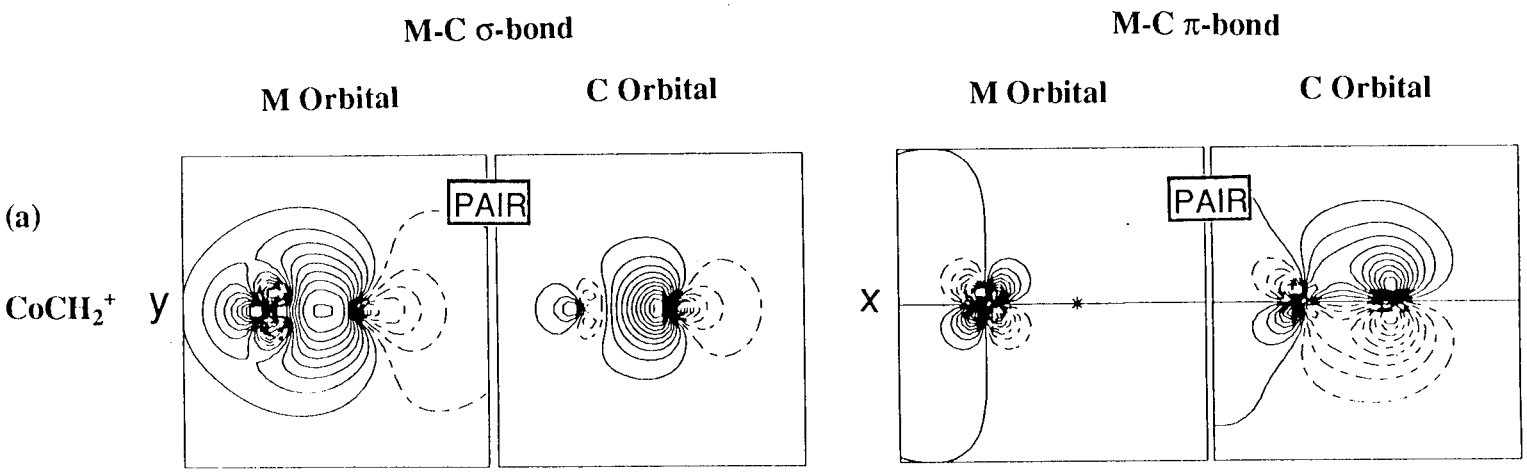
M-C σ-bond
M Orbital
C Orbital
PAIR
(a)
CoCH2+
y
M-C π-bond
M Orbital
C Orbital
PAIR
x

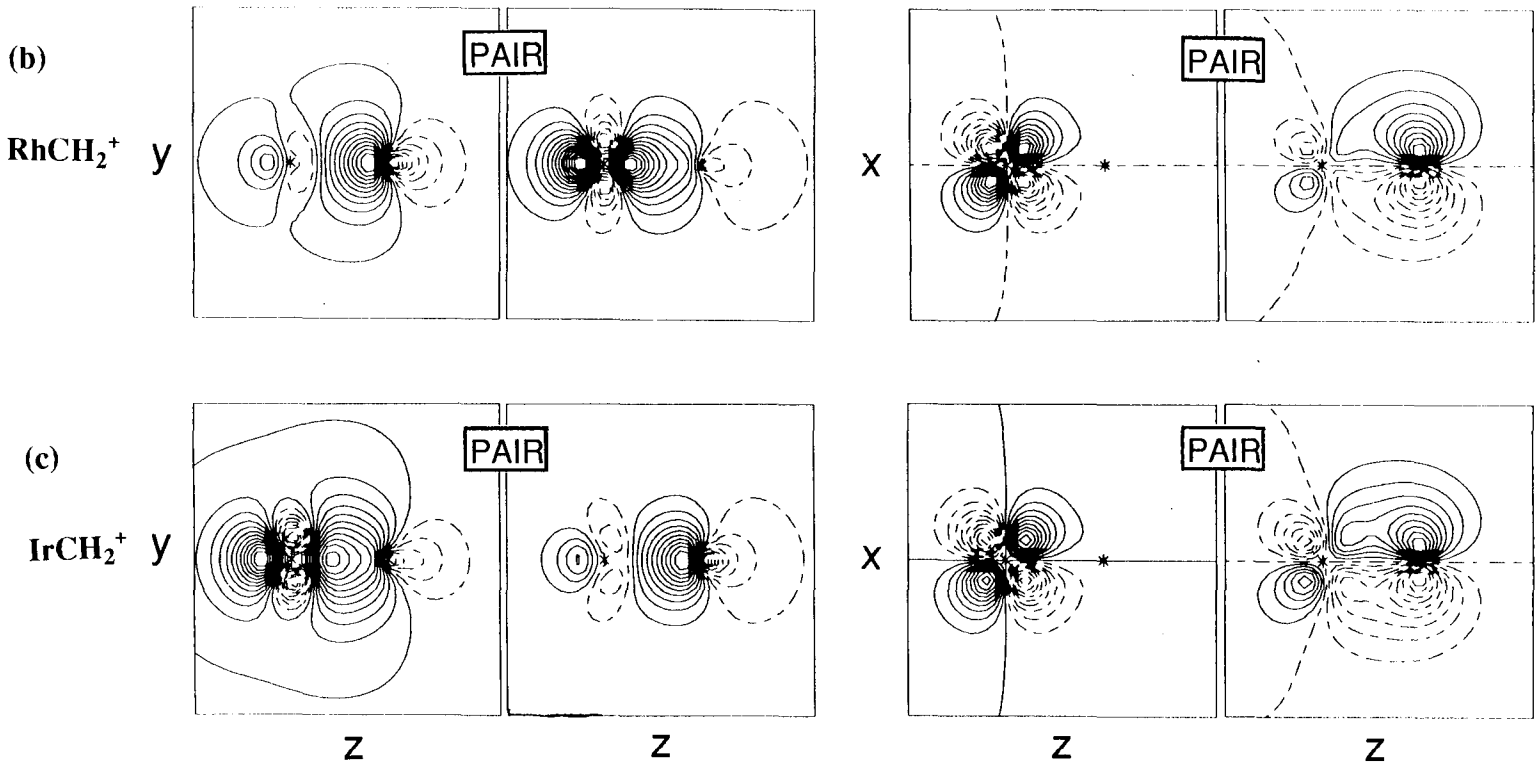


**Figure 2.** GVB-PP bonding orbitals for the ground states of (a) $CoCH_2^+$, (b) $RhCH_2^+$, and (c) $IrCH_2^+$.

mates of the $Co^+$ and $Rh^+$ $M^+=CH_2$ bond strengths of $D_0=79\pm4$ and $D_0=84\pm4$ kcal/mol, respectively, in good agreement with our results.

For $CoCH_2^+$, $RhCH_2^+$, and $IrCH_2^+$, each has a ground state which is best described as a Schrock carbene. The principal differences between the three metal-methylidenes are:

(1) $CH_2$ bonds to the $s^1d^7$ configuration of $Co^+$ and $Ir^+$ but to the $d^8$ configuration of $Rh^+$, similar to the metal-alkyls (Chapter III); and

(2) the $\sigma$-bond is composed mostly of $s$ character for $CoCH_2^+$, $d$ character for $RhCH_2^+$, and $sd$ hybrid character for $IrCH_2^+$.

The ground state for both $CoCH_2^+$ and $IrCH_2^+$ is $^3A_2$, with singly occupied $a_1$ and $a_2$ orbitals. For both metals, the singly occupied $a_2$ orbital is the $d_{xy}$. However, for $IrCH_2^+$, the singly occupied $a_1$ orbital is an $sd$ hybrid (58% $sp$ character and 42% $d$ character at the MCPF level) while, for $CoCH_2^+$, this orbital is dominantly the $d_{z^2}$ (21% $sp$ character and 79% $d$ character). Conversely, $IrCH_2^+$ shows more $d$ character in the $\sigma$ bonding orbital (29% $sp$ character and 71% $d$ character) as compared to $CoCH_2^+$ (61% $sp$ character and 39% $d$ character). Note that in the lower level wave functions [HF, GVB(6/6), and CASSCF(6/6)], even less $sd$ hybridization is observed in $CoCH_2^+$ [84% $sp$ character and 16% $d$ character for the pair of $\sigma$ bonding orbitals of the GVB(6/6) wavefunction]. This is in line with previous arguments that $sd$ hybridization is more effective in the third row metal than the first row metal. As has been discussed in great detail (Chapter VI), the discrepancy in the hybridization of the two metals is the result of the difference in the valence $s$ and $d$ orbital sizes.

The large difference in size between the $Co^+$ $4s$ and $3d$ orbitals also produces problems with the $Co^+=CH_2$ bond length. Since the optimal $\sigma$-bond distance is longer than the optimal $\pi$-bond distance, due to the fact that the $\sigma$-bond has $4s$

character while the $\pi$-bond has $3d$ character, the resulting double bond distance represents a compromise which is not optimal for either, weakening the bond. For $IrCH_2^+$, where the difference in orbital sizes is not so dramatic, the optimal $\sigma$ and $\pi$ bond lengths are more similar and a stronger bond results.

The ground state of $RhCH_2^+$ is $^1A_1$. The $\sigma$-bond is formed from the $d_{z^2}$ orbital (9% $sp$ character and 91% $d$ character) and the $\pi$-bond is formed from the $d_{xz}$ orbital. This configuration of the atom, $d^8$ with $\sigma$ and $\pi$ holes, is derived from 40% $^3F$ and 60% $^3P$. An excitation energy of 16.3 kcal/mol is required to obtain the bonding configuration. This excitation energy is small, however, compared to the excitation energy of 49.0 kcal/mol necessary to obtain the $s^1d^7$ configuration. The $^3A_2$ state, which is bound by $D_e$=57.5 kcal/mol at the MCPF level, 17.2 kcal/mol higher in energy than the $^1A_1$ ground state, is in fact not derived from the $^5F$ ($s^1d^7$) state of the metal, but instead diabatically dissociates to $^3F$ ($d^8$) $Rh^+ + {}^1A_1$ $CH_2$. Thus, this triplet excited state is actually a Fischer carbene, with donor-acceptor character. The difference can be seen in the population of the C $p_x$ orbital. While less than 1 electron in the ground states of all three $MCH_2^+$ complexes (0.47, 0.67, and 0.57 electron for M = Co, Rh, and Ir, respectively), the occupation of the C $p_x$ orbital is significantly smaller in the $^3A_2$ excited state of $RhCH_2^+$ (0.29 electron).

Thus, once again, the stronger bond in $IrCH_2^+$ is consistent with arguments made about the issue of orbital size and $sd$ hybridization when compared to $CoCH_2^+$ and the issue of accessibility of suitable bonding states when compared to $RhCH_2^+$.

### 7.2.2 Insertion of $Co^+$, $Rh^+$, and $Ir^+$ into a C–H bond $CH_4$

Perhaps the step in the proposed reaction sequence for alkane dehydrogenation and demethanation which has gained the most attention is the initial C–H insertion. It has been identified as the rate determining step in the reactions of propane with $Co^+$, creating a barrier which lies only 2.5±0.7 kcal/mol below the asymptotic energy of the reactants.[15] Therefore, it is of interest to determine the stability of the hydrido methyl insertion product. Even though we have already shown that methane does not react with either $Co^+$ or $Rh^+$ because the product species ($MCH_2^+ + H_2$) lead to endothermicities of over 30 kcal/mol, it would be informative to know how far along the potential energy surface the reaction actually can proceed before reaching an insurmountable barrier. In the case of $Ir^+$, where the dehydrogenation reaction is exothermic, it is then of interest to determine the energetics of C–H insertion as it relates to the reaction efficiency. It would clearly be useful to know whether C–H insertion is the rate determining step for $Ir^+$ as it is proposed to be for $Co^+$.

The $M(H)(CH_3)^+$ complex was described in qualitative terms in Chapter VI. There, it was shown that $Co(H)(CH_3)^+$ is very different from $Rh(H)(CH_3)^+$ and $Ir(H)(CH_3)^+$. The Co–H bond is dominantly composed of metal *s* character while the Co–C bond is dominantly composed of metal *d* character. In contrast, the M–H and M–C bonds of the $Rh^+$ and $Ir^+$ complexes are each derived from *sd* hybrids. In this section, we emphasize the energetics of C–H insertion.

Our results are presented in Figure 3. We have optimized geometries for $Co(H)(CH_3)^+$ and $Rh(H)(CH_3)^+$ using GVB wavefunctions and for $Ir(H)(CH_3)^+$ using a HF wavefunction (see Appendix). These geometries are slightly different from those used in Chapter VI and are given in Figure 4. Clearly,

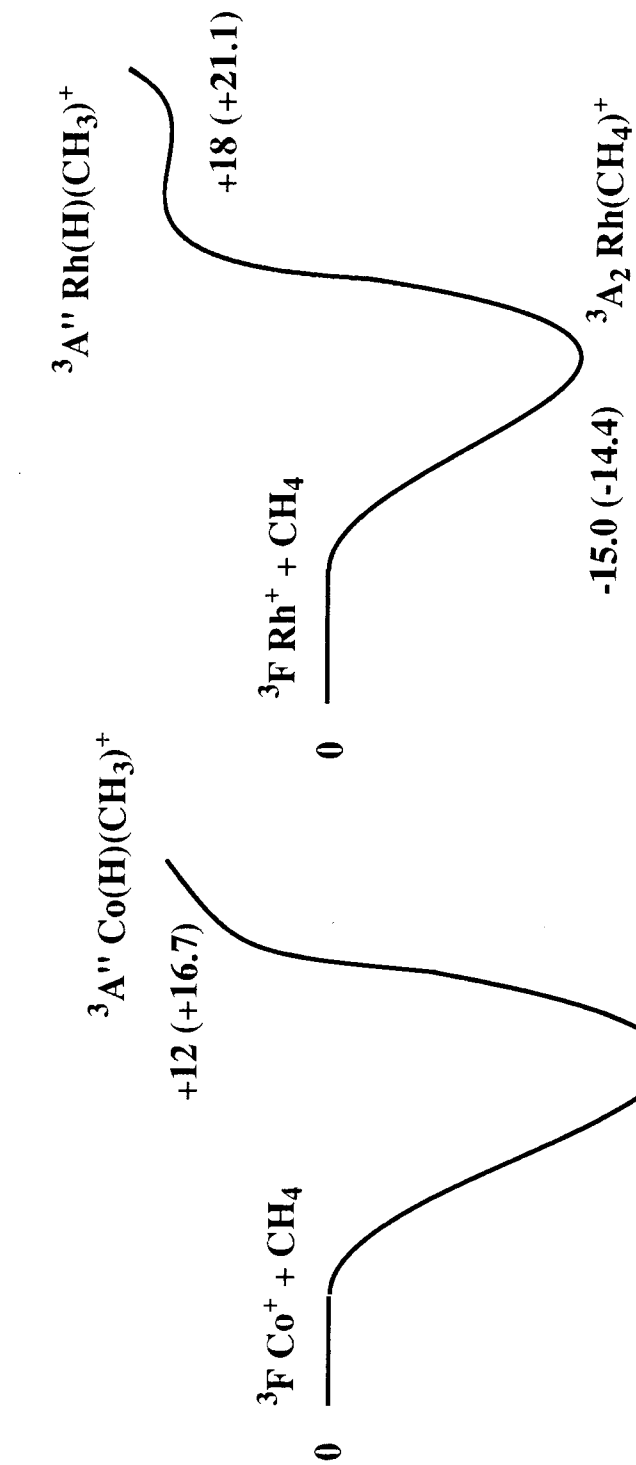
$^3A''$ Rh(H)$(CH_3)^+$
+18 (+21.1)
$^3F$ Rh$^+$ + $CH_4$
0
-15.0 (-14.4)
$^3A_2$ Rh$(CH_4)^+$
$^3A''$ Co(H)$(CH_3)^+$
+12 (+16.7)
$^3F$ Co$^+$ + $CH_4$
0
-21.7 (-21.4)
$^3B_2$ Co$(CH_4)^+$

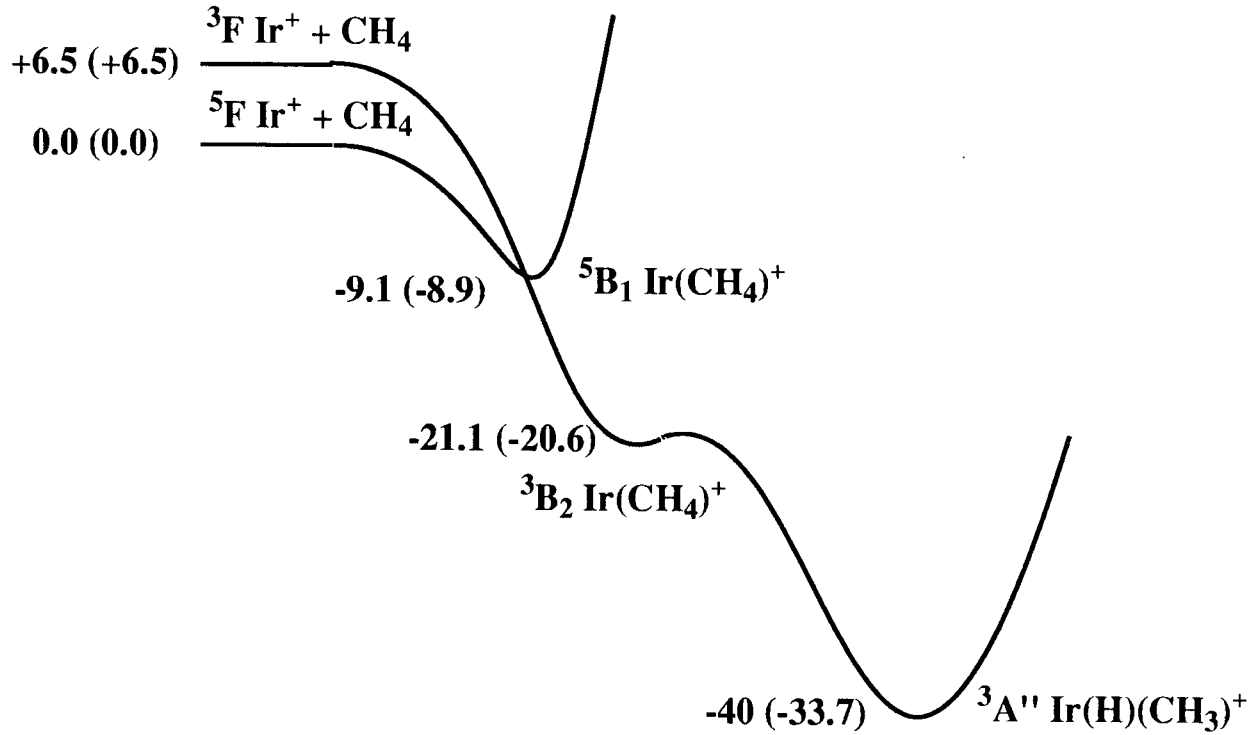


**Figure 3.** Potential energy surfaces for the initial complexation and C-H insertion in the reactions $M^+ + CH_4 \longrightarrow MCH_2^+ + H_2$, M=Co, Rh, and Ir. Energies are in kcal/mol and represent our best estimates to the true values of $D_0$. MCPF results for $D_e$ are in parenthesis.

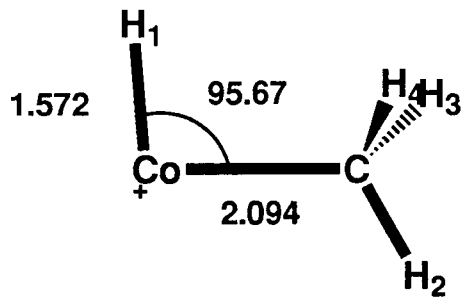


## $^3$A" staggered

| | | | |
|---|---|---|---|
| Co | 0.0000 | 0.0000 | 0.0000 |
| C | 0.0000 | 0.0000 | 2.0936 |
| $H_1$ | 0.0000 | 1.5644 | -0.1554 |
| $H_2$ | 0.0000 | -1.0778 | 2.2345 |
| $H_3$ | 0.9104 | 0.5089 | 2.3637 |
| $H_4$ | -0.9104 | 0.5089 | 2.3637 |

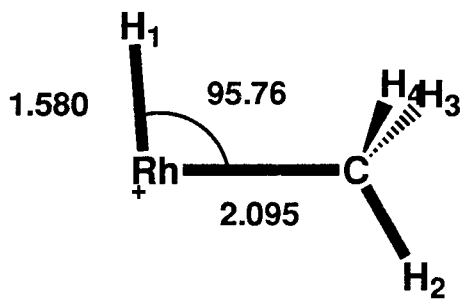


## $^3$A" staggered

| | | | |
|---|---|---|---|
| Rh | 0.0000 | 0.0000 | 0.0000 |
| C | 0.0000 | 0.0000 | 2.0949 |
| $H_1$ | 0.0000 | 1.5722 | -0.1585 |
| $H_2$ | 0.0000 | -1.0578 | 2.3318 |
| $H_3$ | 0.9016 | 0.5135 | 2.3914 |
| $H_4$ | -0.9016 | 0.5135 | 2.3914 |

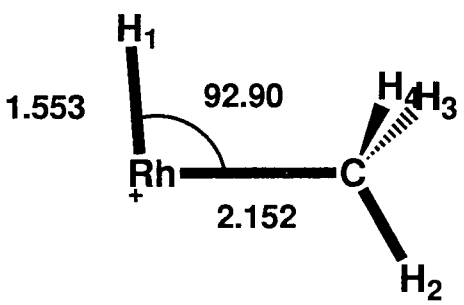


## $^1$A' staggered

| | | | |
|---|---|---|---|
| Rh | 0.0000 | 0.0000 | 0.0000 |
| C | 0.0000 | 0.0000 | 2.1519 |
| $H_1$ | 0.0000 | 1.5506 | -0.0786 |
| $H_2$ | 0.0000 | -1.0519 | 2.4049 |
| $H_3$ | 0.9099 | 0.5243 | 2.3982 |
| $H_4$ | -0.9099 | 0.5243 | 2.3982 |

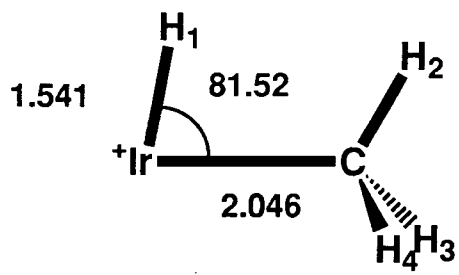


**$^3$A" eclipsed**

| | | | |
|---|---|---|---|
| Ir | 0.0000 | 0.0000 | 0.0000 |
| C | 0.0000 | 0.0000 | 2.0458 |
| $H_1$ | 0.0000 | 1.5241 | 0.2271 |
| $H_2$ | 0.0000 | 0.9829 | 2.4822 |
| $H_3$ | 0.8966 | -0.5549 | 2.3085 |
| $H_4$ | -0.8966 | -0.5549 | 2.3085 |

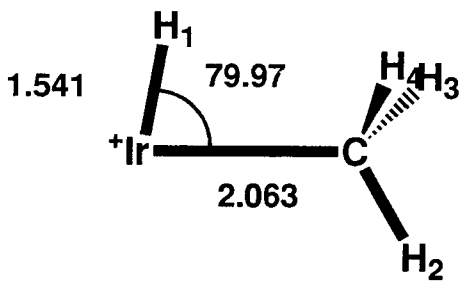


**$^3$A" staggered**

| | | | |
|---|---|---|---|
| Ir | 0.0000 | 0.0000 | 0.0000 |
| C | 0.0000 | 0.0000 | 2.0632 |
| $H_1$ | 0.0000 | 1.5174 | 0.2685 |
| $H_2$ | 0.0000 | -1.0517 | 2.3325 |
| $H_3$ | 0.8885 | 0.5018 | 2.4123 |
| $H_4$ | -0.8885 | 0.5018 | 2.4123 |

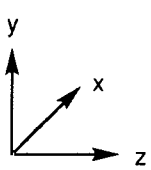


**Figure 4.** Geometries for the $M(H)(CH_3)^+$ species, M=Co, Rh, and Ir. The $Co(H)(CH_3)^+$ and $Rh(H)(CH_3)^+$ geometries were optimized at the GVB-PP level and the $Ir(H)(CH_3)^+$ geometries were optimized at the HF level. Cartesian coordinates are in Å.

$Ir^+$ is quite unique from $Co^+$ and $Rh^+$. Insertion into the C−H bond of methane by $Ir^+$ is exothermic by $D_e$=33.7 kcal/mol (at the MCPF level) with respect to the $^5F$ ($s^1d^7$) $Ir^+$ + $CH_4$ asymptote. With respect to the initial molecular complex (bound by 20.5 kcal/mol using the $C_{2v}$ $^3B_2$ geometry of Chapter V but a TZDP basis set consistent with the calculations presented here) insertion is exothermic by $D_e$=13.2 kcal/mol. This is surely an underestimate. Since the accuracy of MCPF calculations is better for electrostatic bonds than covalent bonds, the exothermicity, with respect to the molecular complex, could be more like 19±4 kcal/mol, or with respect to the separated fragments, 40±4 kcal/mol.

Insertion into the C−H bond is endothermic for the other two metals. Perhaps surprisingly, this process is slightly more difficult for $Rh^+$ than $Co^+$. Since (1) the C−H activation has been identified[15] as the rate determining step in at least one of the alkane dehydrogenation reactions with $Co^+$ and (2) $Rh^+$ is capable of ethane dehydrogenation[2] while $Co^+$ is not,[3] we might have expected insertion to be easier for $Rh^+$ than $Co^+$. Instead, we calculate that insertion is endothermic by $D_e$=−16.7 kcal/mol for $Co^+$ and $D_e$=−21.1 kcal/mol for $Rh^+$ with respect to their $^3F$ ($d^8$) $M^+$ + $CH_4$ asymptotes (both numbers have taken into account the error in the $^3F$-$^5F$ state splittings and the uncorrected numbers are $D_e$=−14.4 kcal/mol for $Co^+$ and $D_e$=−19.4 kcal/mol for $Rh^+$). However, with respect to their molecular complexes (bound by 21.4 and 14.4 kcal/mol for $Co^+$ and $Rh^+$, respectively, using the numbers of Chapter V), insertion is in fact slightly easier for $Rh^+$, being endothermic by 35.5 kcal/mol as compared to 38.1 kcal/mol for $Co^+$. Similar to $Ir^+$, these numbers probably overestimate the endothermicity and the actual values are best estimated (with respect to the $M^+$ + $CH_4$ asymptote) as endothermic by 12±4 kcal/mol for $Co^+$ and 18±4 kcal/mol for $Rh^+$.

For each metal, the $M(H)(CH_3)^+$ complex has a $^3A''$ ground state. This state is analogous to the $^3B_1$ state of $MH_2^+$ (Chapter IV). For $Ir^+$, both the staggered and eclipsed conformations of the methyl group with respect to the hydride were optimized at the HF level. Using these geometries, the eclipsed conformation was 2.0 kcal/mol lower in energy than the staggered conformation at the MCPF level ($D_e$=33.7 vs. $D_e$=31.7 kcal/mol). For $Co^+$ and $Rh^+$, only the staggered conformation was studied and these geometries were optimized at the GVB(6/6) level. This was done in part because the $M(H)(CH_3)^+$ geometry collapses to the $M(CH_4)^+$ geometry at the HF level (an accurate reflection of the lack of a barrier for this process, to be discussed below) and in part because it was wished to make a comparison to $M(H)(C_2H_5)^+$ (detailed in Chapter VIII) and this structure for M = Co is not accurately described at the HF level but is at the GVB level. As will be shown, the use of either HF optimized geometries or GVB optimized geometries will have a neglible effect on the final MCPF energetics provided a comparison is made between geometries with similar H−M−C angles. In fact, this angle appears to be the only coordinate which is sensitive to both the level of wavefunction and the state of the complex. Small variations in other coordinates have little effect on the MCPF energies and these coordinates appear to be similar for different states.

Since $Rh^+$ has a greater tendancy to bond with the $d^8$ configuration than the other two metals, we have also investigated the $^1A_1$ state of $Rh(H)(CH_3)^+$. Using the same methods [a GVB(4/4) geometry optimization followed by an MCPF calculation] the energy of this state was only slightly higher than that of the triplet state ($D_e$=−22.4 kcal/mol vs. $D_e$=−21.1 kcal/mol). This indicates that the greater strength of two *sd* hybrid bonds as compared to two pure *d* bonds is enough to overcome the 49.0 kcal/mol excitation energy to the $s^1d^7$

state.

Surprisingly, the optimized geometries of the triplet states for all three metal complexes and the singlet state of $Rh(H)(CH_3)^+$ are nearly the same. The M−C bond length ranges from 2.05 Å to 2.15 Å, the M−H bond length ranges from 1.54 Å to 1.58 Å, and the H−M−C bond angle ranges from 80.0° to 95.8°. While we maintain that the similarity in the bond lengths is largely coincidental, the triplet bond angles are all ~90° due to *sd* hybridization. Even in the case of the inequivalent bonds of $Co(H)(CH_3)^+$, a small amount of hybridization or resonance will lead to the 90° bond angle. For the singlet state of $Rh(H)(CH_3)^+$, on the other hand, it would normally be the case that the optimal angle between two pure *d* bonds be 54.74° (or 125.26°). At this angle, two $d_\sigma$ orbitals can be formed to bond to the ligands. However, this ignores the atomic coupling and a $d^8$ configuration such as this is composed of 60% $^3$F character and 40% $^3$P character with an excitation energy of 10.9 kcal/mol. At the GVB(4/4) level of the geometry optimization, it is actually better to form one bond to a $d_\sigma$ orbital (the Rh−H bond) and the second to a $d_\delta$ orbital (the Rh−C bond) to retain the $^3$F coupling of the metal. This leads to a bond angle of ~90°.

Of primary importance to the issue of C−H insertion is whether the $M(H)(CH_3)^+$ complex is stable (or metastable) and whether a barrier exists to its formation. For $Ir^+$, in which insertion is exothermic, in addition to the molecular complex and the insertion complex, we optimized a series of structures at the HF level with a constrained C−H bond length [$r$(C−H)=1.3, 1.5, and 1.7 Å]. With these geometries, we were able to determine the barrier to insertion at the MCPF level. We found this barrier to occur at a C−H bond length of 1.5 Å. It is only 2.2 kcal/mol above the energy of the molecular complex but it should be noted that, with a geometry optimized at the HF level, the molecular

complex is only bound by 17.4 kcal/mol, as compared to 20.5 kcal/mol with the more rigorous optimization. This is due to an $Ir^+-CH_4$ bond length which is too long. We suspect that with a shorter (more optimal) bond length, insertion will be easier and the barrier will disappear. The molecular complex is unstable for $Ir^+$ and C−H insertion is a facile (non-rate determining) process.

A similar study was done for $Co(H)(CH_3)^+$ and $Rh(H)(CH_3)^+$ by constraining the H−M−C angle to 10° intervals from 50° to 110° for M = Co and from 40° to 120° for M = Rh and optimizing all other coordinates. A number of states were considered at the MCPF level, but to reduce the expense of these calculations, geometries were optimized for only one state. This was the $^3A'$ state for $Co(H)(CH_3)^+$ and the $^1A'$ state for $Rh(H)(CH_3)^+$. Test calculations using geometries optimized for other states did not change the MCPF energetics by more than ±1 kcal/mol, and so we felt this approximation was justified.

Results are shown in Figures 5 and 6. Similar to insertion of $M^+$ into the H−H bond (Chapter IV), there are three triplet states which are important to the chemistry of C−H insertion. These are:

( 1) the $^3A'$ state, analogous to the $^3A_1$ state of $MH_2^+$ and the lowest lying state at H−M−C angles less than ~75°,

( 2) the $^3A''$ state, analogous to the $^3A_2$ state of $MH_2^+$ and the lowest lying state at angles between ~75° and ~90°, and

( 3) the $^3A''$ state, analogous to the $^3B_1$ state of $MH_2^+$ and the lowest lying state at angles greater than ~90°.

If one considers each of these states diabatically, there is a barrier to reductive elimination of $CH_4$ from $M(H)(CH_3)^+$ only for the $^3A''$ state which is analogous to the $^3B_1$ state of $MH_2^+$. This barrier is about 1 kcal/mol for M = Co and about 14 kcal/mol for M = Rh. However, the two $^3A''$ states should have an

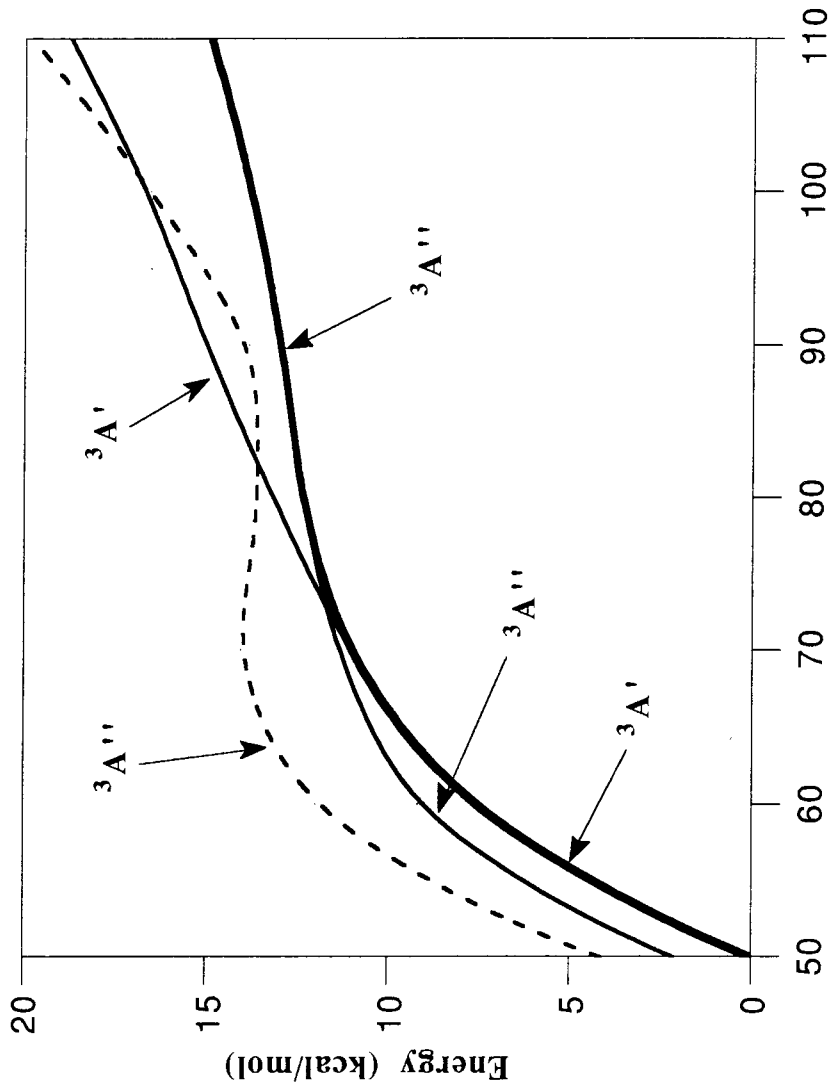


**Figure 5.** Potential energy curves for insertion of $Co^+$ into a C-H bond of $CH_4$. Note the higher energy $^3A''$ potential is not explicitly orthogonal to the lower energy $^3A''$ potential.

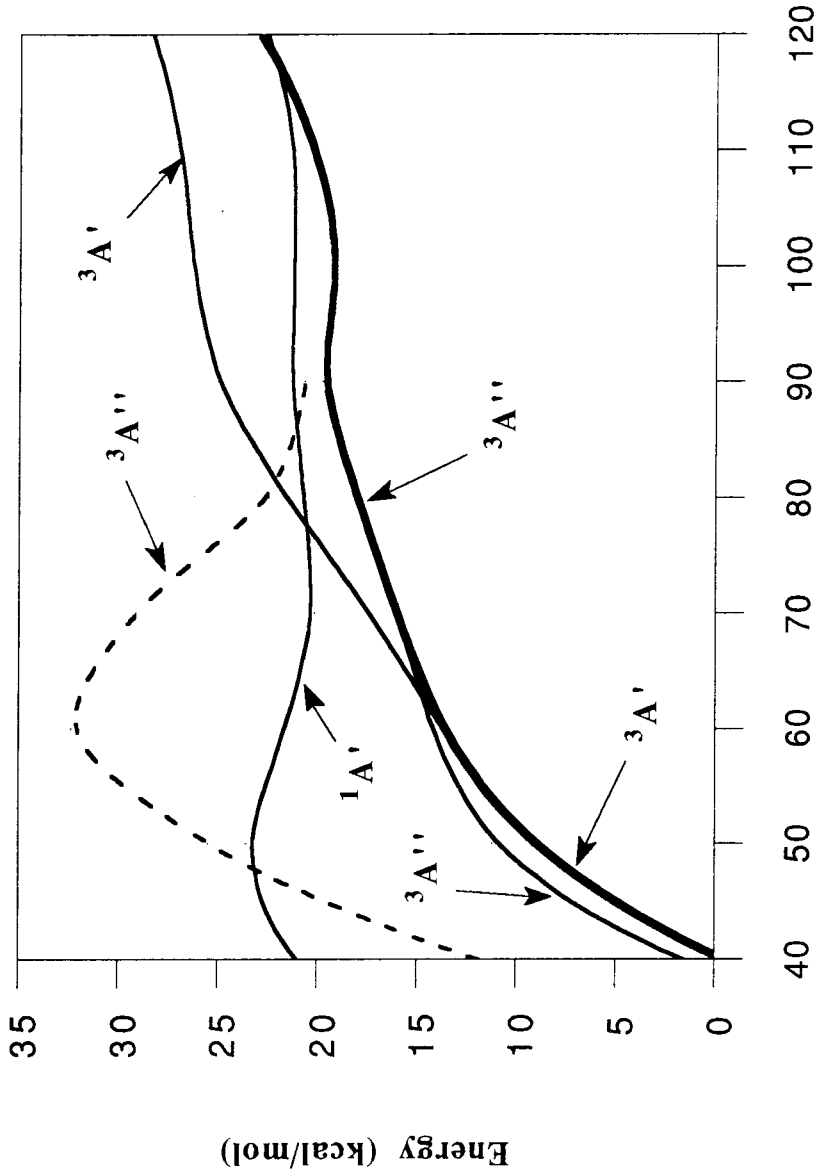


**Figure 6.** Potential energy curves for insertion of $Rh^+$ into a C-H bond of $CH_4$. Note the higher energy $^3$A" potential is not explicitly orthogonal to the lower energy $^3$A" potential and could not be calculated for angles >90°.

avoided crossing in the vicinity of $\theta$(H−M−C)=90° and this will eliminate the barrier on the lowest energy $^3A''$ surface for $Co^+$ and reduce the barrier to about 1 kcal/mol for $Rh^+$. The triplet $Rh(H)(CH_3)^+$ complex is thus barely metastable. We calculate an optimal H−Rh−C angle of 99.0° compared to the GVB optimal angle of 95.8°. The energy of this geometry is also comparable to that at the GVB geometry ($D_e$=−19.1 kcal/mol for the HF/MCPF geometry vs. $D_e$=−19.4 kcal/mol for the GVB geometry, with uncorrected numbers).

The singlet potential energy surface for $Rh(H)(CH_3)^+$, while just as energetically unfavorable as the triplet surface, is interesting in that it possesses a double minimum. This surface is very flat between the H−Rh−*C* angles of 60° and 110° but minima occur at angles of 72.4° and 104.6°. The miminum at the more acute angle is unbound by $D_e$=−20.1 kcal/mol and the minimum at the more obtuse angle is unbound by $D_e$=−21.2 kcal/mol with respect to the triplet asymptote of the reactants. There is a 1.2 kcal/mol barrier with respect to the acute angle structure seperating the two minima. This barrier is only 0.1 kcal/mol with respect to the obtuse angle structure. Still, the double minimum, and indeed the flatness of the singlet surface, arises from the possibility of bonding to two $d_\sigma$ orbitals at angles of 54.74° and 125.26°. As discussed, this ignores the atomic coupling which favors bonding to a $d_\sigma$ orbital and a $d_\delta$ orbital at an angle of 90°. At the GVB level, the Rh−C bonds are weak and the atomic coupling then determines the bonding. As the bonds are stronger at the MCPF level, the $d_\sigma/d_\sigma$ bonding scheme becomes more favorable, and as a result two minima are formed at angles which represent a compromise between 54.74° and 90° and between 125.26° and 90°.

As a final note, estimating for the errors in the calculations, we find that the H−Co−C angle should reach 50° to 60° before insertion crosses the threshold

energy. The H−Rh−C angle should reach only 40° to 50° before insertion crosses the threshold energy. It is clear that insertion is an unfavorable process for both metals and only clustering should be observed at room temperature if the species are thermalized. In contrast, $Ir^+ + CH_4$ appears to be quite different and it is the complete potential energy surface for dehydrogenation which concerns the remainder of this chapter.

## 7.3 Complete Potential Energy Surface for Dehydrogenation of $CH_4$ by $Ir^+$

### 7.3.1 Summary

The reaction steps for the dehydrogenation of $CH_4$ are (see Figure 7):

*i.* Initial formation of an $\eta^2$-molecular complex, $Ir(CH_4)^+$ (Figure 7*b*).

*ii.* Oxidative addition to a single C−H bond to form the hydrido methyl iridium complex, $Ir(H)(CH_3)^+$ (Figure 7*d*).

*iii.* Insertion into a second C−H bond to form the pyramidal bis-hydrido iridium methylidene complex, $Ir(H)_2(CH_2)^+$ (Figure 7*f*).

*iv.* Coupling of the H−H bond to form the planar dihydrogen iridium methylidene complex, $Ir(H_2)(CH_2)^+$ (Figure 7*h*).

*v.* Elimination of $H_2$ (Figure 7*i*).

The overall exothermicity (*v*) of the reaction is estimated to be 8±4 kcal/mol as already discussed. Since the initial complexation (*i*) and C−H insertion (*ii*) steps have also already been discussed, most of the discussion in this section will concern steps *iii* and *iv*.

It should be mentioned at this point that there are two striking features of this potential energy surface. The first is the change of spin from $S$=2 to $S$=1 to $S$=0 and back to $S$=1, reflecting the changing number of covalent bonds to $Ir^+$. This should be facilitated by the strong spin-orbit coupling of the heavy metal and should not pose a hindrance to reaction. The second is the deepness of the well for the global minimum, estimated to be 61±8 kcal/mol with respect to the reactants. The global minimum is the $Ir(H)_2(CH_2)^+$ structure, resulting from step *iii* above. As will be discussed, the stability of this structure is significant in distinguishing the chemistry of $Ir^+$ from other metals of the third row.

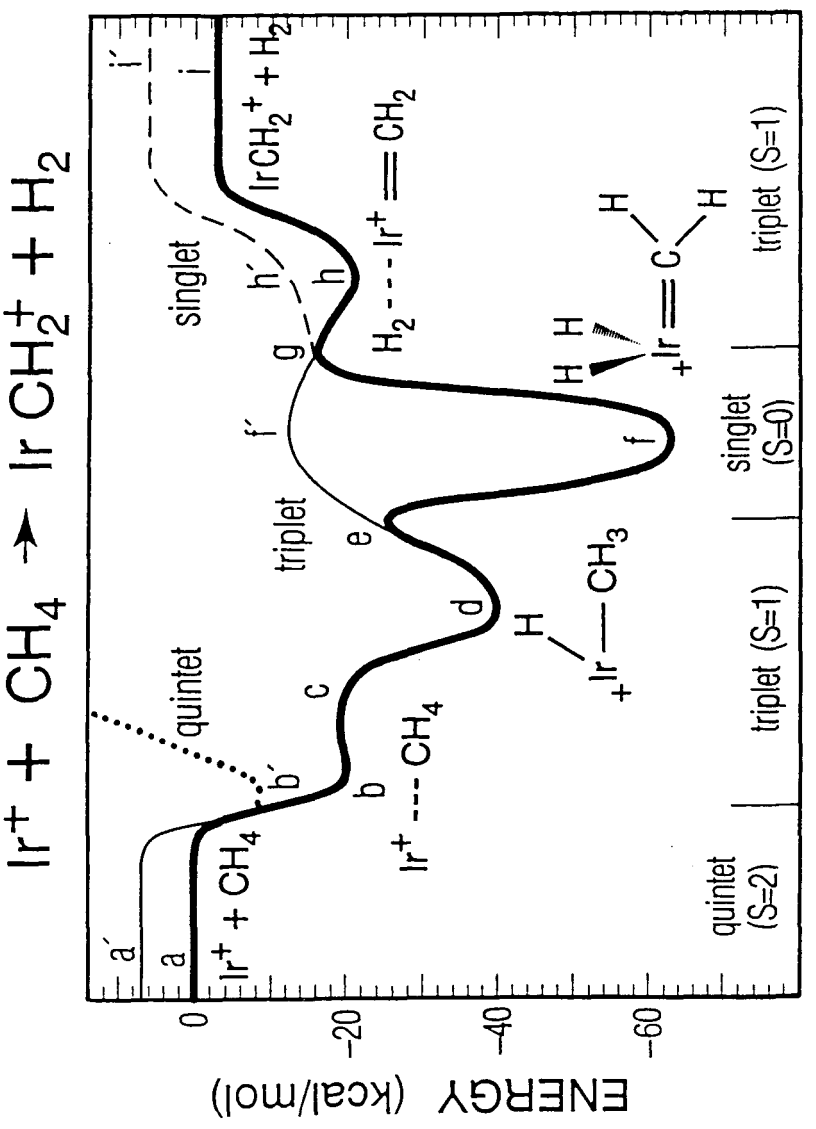


**Figure 7.** Best estimate to the potential energy surface for $CH_4$ dehydrogenation by $Ir^+$.

### 7.3.2 $Ir(H)_2(CH_2)^+$

The global minimum on the $Ir^+ + CH_4$ potential energy surface is the dihydride methylidene structure, $Ir(H)_2(CH_2)^+$ (Figure 7*f*). It is bound by an estimated 61±8 kcal/mol with respect to the reactants. While this well depth is very large for a complex of this type (similar complexes for $Co^+$ and $Rh^+$ are expected to be unbound), given the strengths of the $Ir^+-H$ and $Ir^+=CH_2$ bonds (77 and 119 kcal/mol, respectively), it is not too surprising.

The spin of the complex is singlet which is consistent with the formation of four covalent bonds to the $s^1d^7$ state of the metal [Ir(V)]. The geometry, however, is somewhat unusual; it is pyramidal. There are two low lying pyramidal conformations: the first with the methylidene hydrogens in the plane bisecting the two Ir−H bonds (*i.e.*, staggered) and the second with a 90° rotation of the methylidene group about the Ir−C axis (*i.e.*, eclipsed). The staggered conformer is calculated to be 0.9 kcal/mol more stable than the eclipsed conformer ($D_e$=50.7 and 49.8 kcal/mol, respectively, at the MCPF level). In contrast, a planar conformation was found to be bound by only 19±8 kcal/mol ($D_e$=11.1 kcal/mol at the MCPF level), 42 kcal/mol higher in energy than the pyramidal structure. The optimized geometries for all three of these structures are shown in Figure 8 and the GVB-PP(8/8) orbitals for the lowest energy structure are shown in Figure 9.

We find that there are two primary reasons for the strong preference of the pyramidal geometries over the planar geometry. The first involves occupation of the metal orbitals and the atomic couplings, and the second concerns the effectiveness of *sd* hybridization.

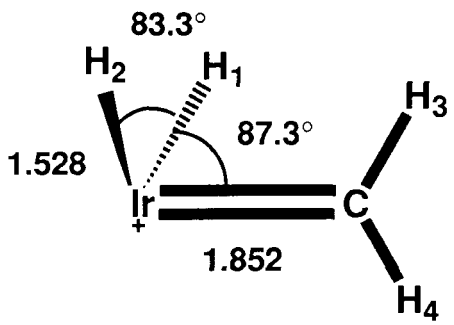


**pyramidal staggered $C_s$ $^1A'$**

| | | | |
|---|---|---|---|
| Ir | 0.0000 | 0.0000 | 0.0000 |
| C | 0.0000 | 0.0000 | 1.8519 |
| $H_1$ | 1.0154 | 1.1389 | 0.0726 |
| $H_2$ | -1.0154 | 1.1389 | 0.0726 |
| $H_3$ | 0.0000 | 0.9040 | 2.4425 |
| $H_4$ | 0.0000 | -0.9146 | 2.4392 |

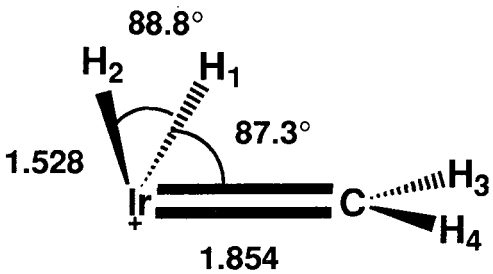


**pyramidal eclipsed $C_s$ $^1A'$**

| | | | |
|---|---|---|---|
| Ir | 0.0000 | 0.0000 | 0.0000 |
| C | 0.0000 | 0.0000 | 1.8543 |
| $H_1$ | 1.0690 | 1.0894 | 0.0707 |
| $H_2$ | -1.0690 | 1.0894 | 0.0707 |
| $H_3$ | 0.9093 | 0.0163 | 2.4400 |
| $H_4$ | -0.9093 | 0.0163 | 2.4400 |

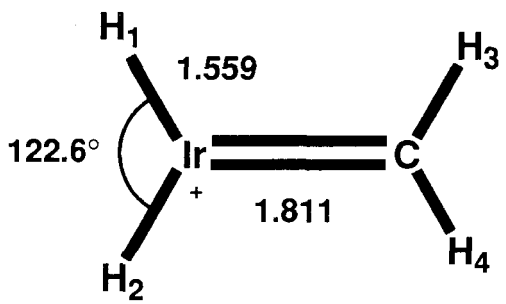


**planar $C_{2v}$ $^1A_1$**

| | | | |
|---|---|---|---|
| Ir | 0.0000 | 0.0000 | 0.0000 |
| C | 0.0000 | 0.0000 | 1.8113 |
| $H_1$ | 0.0000 | 1.3670 | -0.7485 |
| $H_2$ | 0.0000 | -1.3670 | -0.7485 |
| $H_3$ | 0.0000 | 0.9275 | 2.3746 |
| $H_4$ | 0.0000 | -0.9275 | 2.3746 |

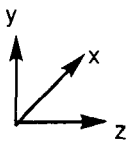


**Figure 8.** Geometries for three states of $Ir(H)_2(CH_2)^+$. Cartesian coordinates in Å.

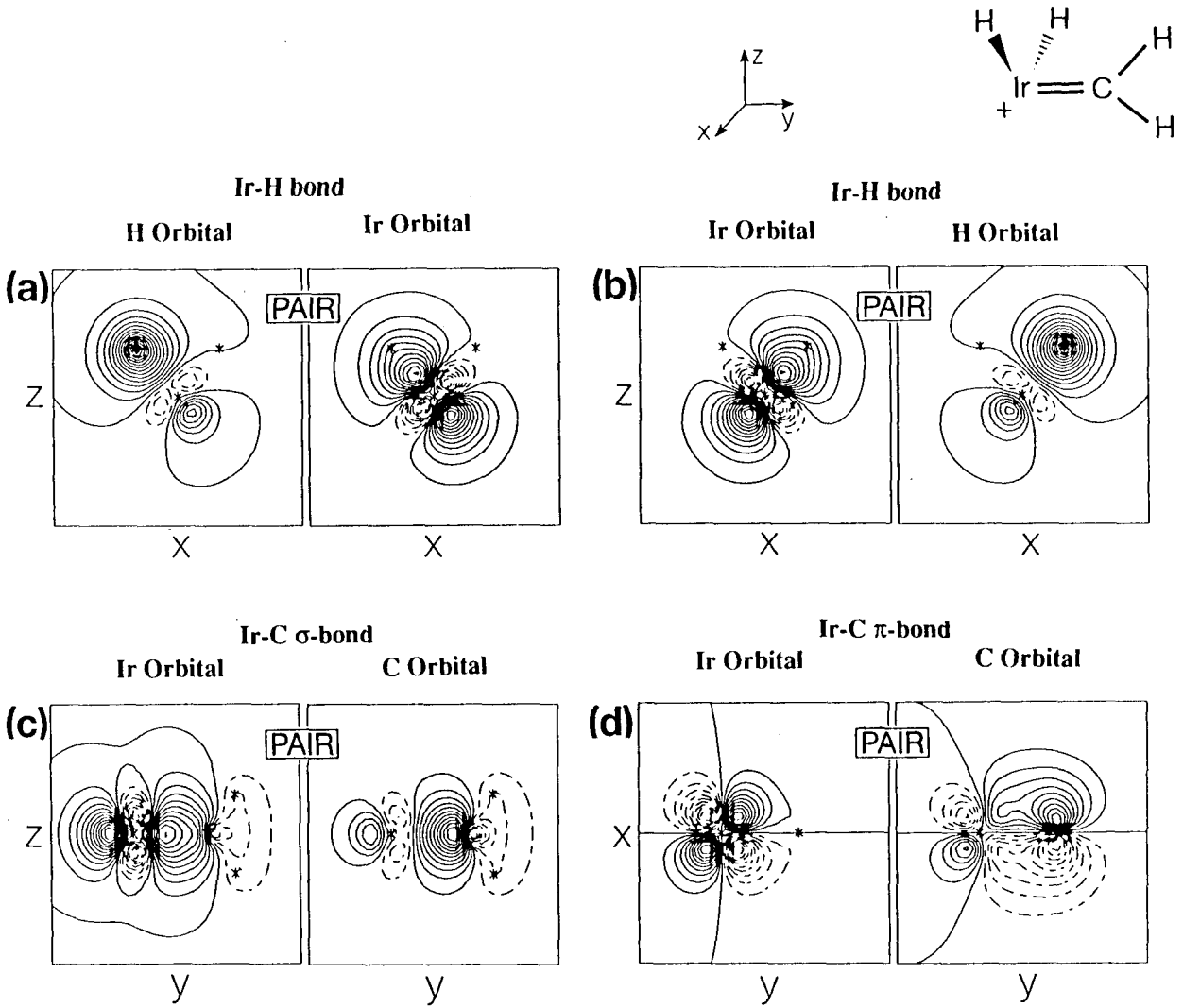


**Figure 9.** GVB-PP bonding orbitals for $Ir(H)_2(CH_2)^+$. (a) and (b) Ir−H bonds. (c) and (d) Ir−C bonds.

For the staggered pyramidal geometry, the dominant bonding configuration is

$$(d_{x^2-y^2})^2(d_{yz})^2(d_{z^2})^1(d_{xz})^1(d_{xy})^1(s)^1$$

where an $s + d_{z^2}$ hybrid is used in forming the Ir−C $\sigma$-bond, the $d_{xz}$ orbital is used in forming the Ir−C $\pi$-bond, and the $d_{xy}$ orbital and an $s - d_{z^2}$ hybrid are used in forming the Ir−H bonds. This state, with the configuration $\sigma^1\pi^3\delta^3s^1$, is 80% $^5$F and 20% $^5$P.

For the eclipsed pyramidal geometry, the dominant bonding configuration is

$$(d_{x^2-y^2})^2(d_{xz})^2(d_{z^2})^1(d_{yz})^1(d_{xy})^1(s)^1$$

where an $s + d_{z^2}$ hybrid is used in forming the Ir−C $\sigma$-bond, the $d_{yz}$ orbital is used in forming the Ir−C $\pi$-bond, and the $d_{xy}$ orbital and an $s - d_{z^2}$ hybrid are used in forming the Ir−H bonds. This state, with the configuration $\sigma^1\pi^3\delta^3s^1$, is also 80% $^5$F and 20% $^5$P.

For the planar geometry, the dominant bonding configuration is

$$(d_{x^2})^2(d_{xy})^2(d_{y^2-z^2})^1(d_{xz})^1(d_{yz})^1(s)^1$$

where an $s - d_{y^2-z^2}$ hybrid is used in forming the Ir−C $\sigma$-bond, the $d_{xz}$ orbital is used in forming the Ir−C $\pi$-bond, and the $d_{yz}$ orbital and an $s + d_{y^2-z^2}$ orbital are used in forming the Ir−H bonds. This state, with the configuration $\sigma^2\pi^3\delta^2s^1$, is 40% $^5$F + 60% $^5$P.

From this analysis it can be seen that the planar geometry employs greater $^5$P character in the wavefunction and we estimate this effect to account for 12 kcal/mol of the energy difference between the pyramidal and planar structures.

In valence bond terms, the Ir−C $\sigma$-bond is formed from a metal orbital which is 50% $s$ and 50% $d$ while the Ir−H $\sigma$-bonds are formed from metal orbitals

which are 25% $s$ and 75% $d$. An important result of the above analysis, however, is that it appears that hybridization of the $s$ orbital with a $d_\sigma$ orbital is more effective than hybridization of the $s$ orbital with a $d_\delta$ orbital in the formation of three covalent bonds. This point is subtle, but can be concluded based on the following observation. Both the pyramidal structures show hybridization of the $s$ orbital with the $d_{z^2}$ orbital in order to form $\sigma$-bonds to the $CH_2$ and the two hydrides. The $s + d_{z^2}$ hybrid should clearly be effective in the formation of the Ir−C bond since the density of the $d_\sigma$ orbital is then increased along the $z$ axis. Similarly, the $s - d_{z^2}$ hybrid has increased density in the $xy$ plane and hybridization with the $d_{xy}$ orbital will direct the hybrid toward either of the two hydrides. However, hybridization with the $d_{y^2-z^2}$ or the $d_{x^2-z^2}$ orbitals could also be envisioned. An $s+d_{y^2-z^2}$ hybrid would have increased density along the $y$ axis and hybridization with the $d_{xy}$ orbital would tend to lead to a more acute H−Ir−H angle. An $s + d_{x^2-z^2}$ hybrid would have increased density along the $x$ axis and hybridization with the $d_{xy}$ orbital would tend to lead to a more obtuse H−Ir−H angle. We note this in particular because the bonding configurations

$$(d_{x^2})^2(d_{yz})^2(d_{y^2-z^2})^1(d_{xz})^1(d_{xy})^1(s)^1$$

for the staggered geometry and

$$(d_{y^2})^2(d_{xz})^2(d_{x^2-z^2})^1(d_{yz})^1(d_{xy})^1(s)^1$$

for the eclipsed geometry represent pure $^5$F states. These configurations mix into the wavefuctions to a very small degree which is why the eclipsed structure has a slightly larger H−Ir−H angle than the staggered structure (88.8° vs. 83.3°). However, since hybridization with the $d_{z^2}$ dominates in both cases, we can conclude that this is more favorable than hybridization with a $d_\delta$ orbital by

*at least* 6 kcal/mol (the excitation energy required to obtain the bonding state, 80% $^5$F + 20% $^5$P).

For the planar structure, the only feasible option is to form hybrids with the $s$, $d_{y^2-z^2}$, and $d_{yz}$ orbitals. Since the $s + d_{y^2-z^2}$ hybrid is polarized along the $y$ axis, the H−Ir−H angle is obtuse and found to be 122.6°. Following the above dicussion, the bonds in this structure are then weaker as compared to those in the pyramidal structure.

An additional consideration may be that polarization of the metal orbitals by hybridization with the valence $p$ orbitals is more effective in the pyramidal geometries than in the planar geometry. The reasoning behind this is that in the pyramidal geometries, all three $p$ orbitals can be used to polarize the three $\sigma$-bonds in the direction of the ligands. In the planar geometry, only the $p_y$ and $p_z$ orbitals are available to polarize these bonds. The added degree of freedom for hybridization in the pyramidal structures should also favor these geometries over the planar structure.

For the triplet potential energy surface, a maximum of only two covalent bonds can be formed (as two of the four singly occupied orbitals must be high spin). Consequently, the triplet state of $Ir(H)_2(CH_2)^+$ is unstable and this structure (Figure 7*f'*) represents a transition state for the conversion of the $Ir(H)(CH_3)^+$ complex (Figure 7*d*) to the $Ir(H_2)(CH_2)^+$ complex (Figure 7*h*). A geometry was optimzed at the HF/MCPF level by constraining the length of the newly breaking C−H bond to 1.3, 1.5, 1.7, 1.9, and 2.3 Å. All other coordinates were optimized at the HF level for each of these C−H bond lengths and an MCPF calculation was done on the resulting geometry. A maximum was found at a C−H bond length of 1.7 Å and that geometry is shown in Figure 10. The energy of this structure was calculated to be 2.3 kcal/mol below the energy of

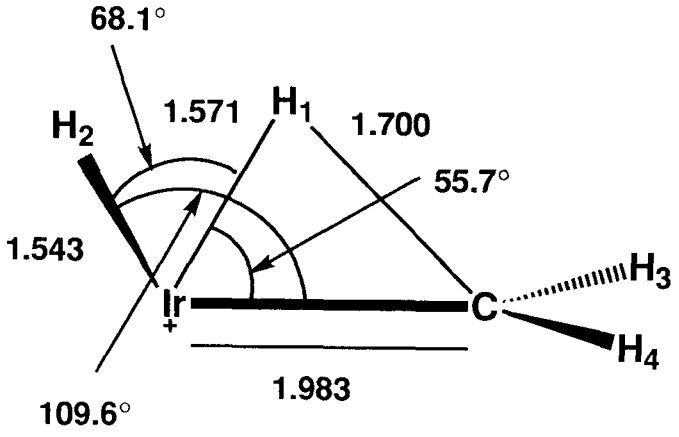


**transition state $C_1$ $^3A$**

| | | | |
|---|---|---|---|
| Ir | 0.0000 | 0.0000 | 0.0000 |
| C | 0.0000 | 0.0000 | 1.9825 |
| $H_1$ | 0.0000 | 1.2982 | 0.8849 |
| $H_2$ | -1.0074 | 1.0480 | -0.5166 |
| $H_3$ | 0.8866 | 0.2507 | 2.5385 |
| $H_4$ | -0.9454 | -0.0129 | 2.4966 |

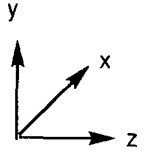


**Figure 10.** Geometry for the $Ir(H)(CH_3)^+ \longrightarrow Ir(H_2)(CH_2)^+$ transition state on the triplet potential energy surface. Cartesian coordinates are in Å.

the reactants and estimated to be bound by 9±6 kcal/mol. With respect to the $Ir(H)(CH_3)^+$ complex, this represents a barrier of 31 kcal/mol for conversion to the $Ir(H_2)(CH_2)^+$ complex.

The fact that such a structure is bound is somewhat surprising in that two covalent bonds have been broken in comparison to the singlet state of this complex. The triplet state is only 52 kcal/mol higher in energy than the singlet state even though a typical $Ir^+-R$ $\sigma$-bond is worth 70-80 kcal/mol. However, when one views the bonding in the triplet state as two covalent bonds to the hydrides and a donor-acceptor (or Fischer type) bond to the methylidene, the relative stability of the structure becomes apparant. Since the reaction $CH_4 \rightarrow CH_2 + H_2$ is endothermic by 111 kcal/mol and the reaction $H_2 + Ir^+ \rightarrow IrH_2^+$ is estimated to be exothermic by 40±4 kcal/mol, the methylidene must be bound to $IrH_2^+$ by 80 kcal/mol (111 - 40 + 9). This quantity is consistent with the strengths of similar bonds to $Ir^+$. As will be shown (Chapter VIII), the $Ir^+-C_2H_4$ bond, which is an electrostatic donor-acceptor bond, is calculated to be bound by $D_e$=74.3 kcal/mol.

The significance of this finding (a triplet transition state which is below the energy of the reactants by 9 kcal/mol) is that it is a confirmation of the facile nature of this reaction. That is, the dehydrogenation reaction has been found to be exothermic and there are no barriers which prevent the reaction from proceeding. However, since the singlet state of the dihydride methylidene conformer is the lowest energy state for this system, it is expected that a triplet to singlet crossing occurs which further reduces the size of the barriers along the reaction pathway and thereby increases the efficiency of the reaction. To determine where the singlet-triplet crossing occurs, we optimized a series of geometries for the singlet state just as we did for the triplet state (*i.e.*, constraining the second

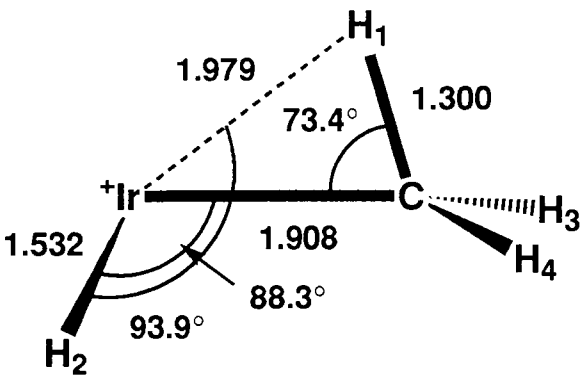


**singlet-triplet crossing $C_1$**

| | | | |
|---|---|---|---|
| Ir | 0.0000 | 0.0000 | 0.0000 |
| C | 0.0000 | 0.0000 | 1.9075 |
| $H_1$ | 0.0000 | 1.2461 | 1.5370 |
| $H_2$ | -1.5151 | -0.2192 | 0.0447 |
| $H_3$ | 0.9342 | -0.1956 | 2.4176 |
| $H_4$ | -0.8754 | -0.1432 | 2.5178 |

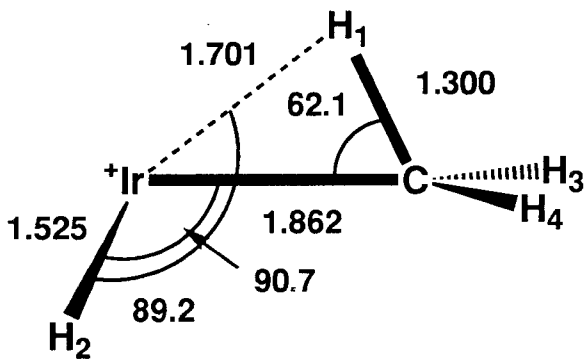


**singlet geometry $C_1$**

| | | | |
|---|---|---|---|
| Ir | 0.0000 | 0.0000 | 0.0000 |
| C | 0.0000 | 0.0000 | 1.8612 |
| $H_1$ | 0.0000 | 1.1491 | 1.2539 |
| $H_2$ | -1.5244 | 0.0531 | -0.0185 |
| $H_3$ | 0.9306 | -0.0725 | 2.4082 |
| $H_4$ | -0.8845 | -0.0087 | 2.4774 |

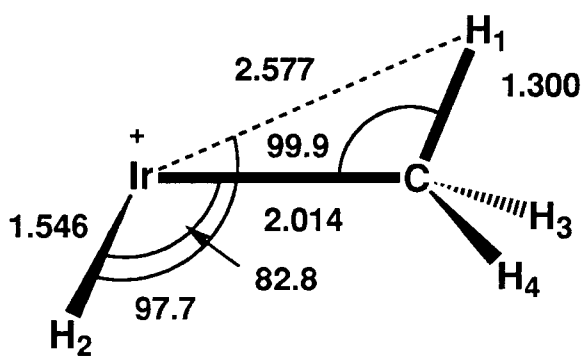


**triplet geometry $C_1$**

| | | | |
|---|---|---|---|
| Ir | 0.0000 | 0.0000 | 0.0000 |
| C | 0.0000 | 0.0000 | 2.0142 |
| $H_1$ | 0.0000 | 1.2808 | 2.2365 |
| $H_2$ | -1.3339 | -0.7563 | 0.1933 |
| $H_3$ | 0.9411 | -0.4261 | 2.3416 |
| $H_4$ | -0.8531 | -0.4369 | 2.4994 |

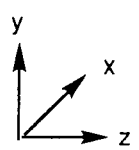


**Figure 11.** Geometry for the singlet-triplet crossing (Figure 7*e*). The geometry is a weighted average of optimized singlet (0.70) and triplet (0.30) geometries. Cartesian coordinates are in Å.

**Table II.** Coordinates used in obtaining a weighted average of the singlet and triplet geometries. The weight is 70% singlet and 30% triplet. Distances are in Å and angles in degrees.

| Coordinate | Singlet | Triplet | Average |
|---|---|---|---|
| $r(\mathrm{Ir-C})$ | 1.8618 | 2.0142 | 1.9075 |
| $r(\mathrm{C-H_1})$ | 1.3000 | 1.3000 | 1.3000 |
| $r(\mathrm{Ir-H_2})$ | 1.5255 | 1.5456 | 1.5315 |
| $r(\mathrm{C-H_3})$ | 1.0777 | 1.0743 | 1.0767 |
| $r(\mathrm{C-H_4})$ | 1.0816 | 1.0837 | 1.0822 |
| $\theta(\mathrm{H_1-C-Ir})$ | 62.124 | 99.847 | 73.441 |
| $\theta(\mathrm{H_2-Ir-C})$ | 90.693 | 82.814 | 88.329 |
| $\theta(\mathrm{H_3-C-H_1})$ | 105.915 | 108.873 | 106.802 |
| $\theta(\mathrm{H_4-C-H_1})$ | 107.184 | 109.616 | 107.914 |
| $\theta(\mathrm{H_2-Ir-C-H_3})$ | 2.558 | -2.432 | 1.061 |
| $\theta(\mathrm{H_3-C-H_1-Ir})$ | -121.409 | -122.940 | -121.868 |
| $\theta(\mathrm{H_4-C-H_1-Ir})$ | 115.766 | 112.796 | 114.875 |

C−H bond length to 1.3, 1.5, and 1.7 Å). Using both sets of geometries, we calculated the energy of the singlet and triplet states at the MCPF level. From these results, we were able to determine that the crossing occured at a C−H bond length of approximately 1.3 Å. However, since the optimal singlet and triplet geometries are different, to obtain the lowest energy crossing, we took a weighted average of the two geometries. The coordinates which were averaged are listed in Table II and the optimal weighting was found to be 70% singlet and 30% triplet. The geometry at the crossing, as well as the optimal singlet and triplet geometries for a C−H bond length of 1.3 Å, are shown in Figure 11.

The crossing was found to occur at an energy 27±4 kcal/mol below the energy of the reactants ($D_e$=18.2 kcal/mol for the singlet state and $D_e$=18.9 kcal/mol for the triplet state at the MCPF level). This produces a barrier of

13 kcal/mol with respect to the $Ir(H)(CH_3)^+$ complex. This barrier is less than half the size of the barrier produced by the triplet state and therefore represents a more viable pathway along the reaction surface. Thus, a change of spin from $S = 1$ to $S = 0$ is expected in this reaction as dehydrogenation proceeds through the $Ir(H)_2(CH_2)^+$ intermediate.

### 7.3.3 $Ir(H_2)(CH_2)^+$

Following the oxidative addition of a C−H bond to form the $Ir(H)(CH_3)^+$ complex and the hydrogen shift (coupled with a change of spin from $S = 1$ to $S = 0$) to form the $Ir(H)_2(CH_2)^+$ complex, the last major step in the reaction profile for methane dehydrogenation is reductive elimination of dihydrogen. The lowest energy dihydrogen Ir(III) methylidene complex [$Ir(H_2)(CH_2)^+$] is a triplet with a linear and planar geometry (see Figure 12). The ground state is $^3A_2$ (in $C_{2v}$ symmetry), consistent with the bonding in both $IrH_2^+$ and $IrCH_2^+$, and the complex lies 21±6 kcal/mol ($D_e$=11.9 kcal/mol at the MCPF level) below the energy of the reactants (Figure 7*h*). Rotation of the methylidene group by 90° about the Ir−C axis leads to a staggered geometry which is 4.6 kcal/mol higher in energy than the planar conformer. This can be understood based on the arguments presented in Chapters IV and V, where dihydrogen preferentially associates to a doubly occupied $d_\pi$ orbital over a singly occupied orbital in order to increase backbonding. Since the $d_\pi$ orbital out of the plane of the $CH_2$ group is singly occupied and used to form the Ir−C $\pi$-bond and the $d_\pi$ orbital in the plane of the $CH_2$ group is doubly occupied and non-bonding, the planar eclipsed conformer is energetically favored.

The barrier to formation of the $Ir(H_2)(CH_2)^+$ complex directly from the $Ir(H)(CH_3)^+$ complex on the triplet surface has already been discussed. For the singlet state, no stable $Ir(H_2)(CH_2)^+$ complex exists. The reverse reaction, oxidatative addition of $H_2$ to singlet $IrCH_2^+$, occurs without barrier. A detailed look at this process was undertaken by optimizing a series of geometries with a constrained H−Ir−H angle. The lowest energy process for elimination of $H_2$ occurs in $C_s$ symmetry from the eclipsed pyramidal structure for $Ir(H)_2(CH_2)^+$.

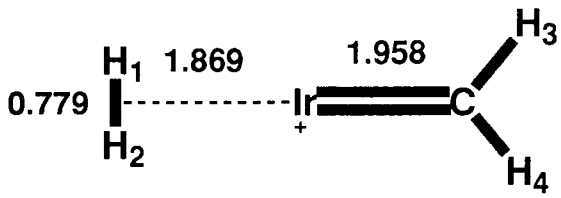


**eclipsed $C_{2v}$ $^3A_2$ $Ir(H_2)(CH_2)^+$**

| | | | |
|---|---|---|---|
| Ir | 0.0000 | 0.0000 | 0.0000 |
| C | 0.0000 | 0.0000 | 1.9583 |
| $H_1$ | 0.0000 | 0.3897 | -1.8691 |
| $H_2$ | 0.0000 | -0.3897 | -1.8691 |
| $H_3$ | 0.0000 | 0.8927 | 2.5718 |
| $H_4$ | 0.0000 | -0.8927 | 2.5718 |

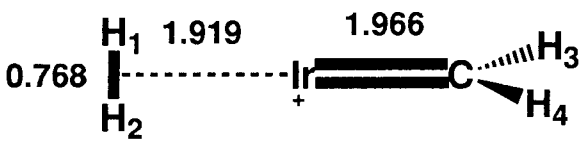


**staggered $C_{2v}$ $^3A_1$ $Ir(H_2)(CH_2)^+$**

| | | | |
|---|---|---|---|
| Ir | 0.0000 | 0.0000 | 0.0000 |
| C | 0.0000 | 0.0000 | 1.9659 |
| $H_1$ | 0.0000 | 0.3839 | -1.9189 |
| $H_2$ | 0.0000 | -0.3839 | -1.9189 |
| $H_3$ | 0.8947 | 0.0000 | 2.5774 |
| $H_4$ | -0.8947 | 0.0000 | 2.5774 |

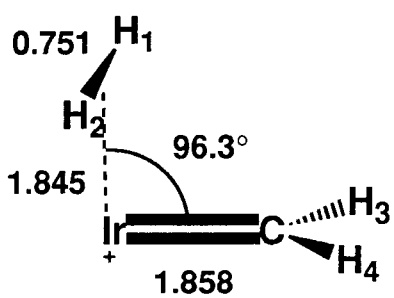


**singlet-triplet crossing $C_s$**

| | | | |
|---|---|---|---|
| Ir | 0.0000 | 0.0000 | 0.0000 |
| C | 0.0000 | 0.0000 | 1.8578 |
| $H_1$ | 0.3754 | 1.8340 | -0.2016 |
| $H_2$ | -0.3754 | 1.8340 | -0.2016 |
| $H_3$ | 0.9107 | 0.0000 | 2.4467 |
| $H_4$ | -0.9107 | 0.0000 | 2.4467 |

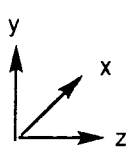


**Figure 12.** Geometries for three states of $Ir(H_2)(CH_2)^+$. The bottom geometry represents the point on the optimal singlet surface for $H_2$ elimination where the triplet crosses. Cartesian coordinates are in Å.

At a geometry consistent with an $Ir(H_2)(CH_2)^+$ structure [$r$(H−H)=0.75 Å, $\theta$(H−Ir−H)=23°], the geometry is still pyramidal (or bent) with an H−Ir−C angle of 96.3°. This structure is bound by 17±6 kcal/mol ($D_e$=8.1 kcal/mol at the MCPF level), 3.8 kcal/mol higher in energy than the optimum triplet state. The $^3A'$ state at this geometry is bound by 16 kcal/mol ($D_e$=6.9 kcal/mol at the MCPF level), so we estimate the singlet-triplet crossing to occur at approximately this point (Figure 7*g*). (Note, unlike how we determined the geometry, for the first singlet-triplet crossing, the optimal singlet and triplet geometries were not averaged. This is because it was found that the singlet energy was quite sensitive to changes in geometry but the triplet surface was rather flat in this region. Thus, the crossing was determined using only the pure singlet geometries.) This crossing creates a barrier of ~4.4 kcal/mol for the back-reaction.

There is some experimental evidence to suggest that the change of spin from $S = 0$ to $S = 1$ does not occur, and elimination of $H_2$ proceeds along the singlet surface. Our calculations suggest that production of singlet $IrCH_2^+$ is a slightly endothermic reaction (by 4±4 kcal/mol), but this is within the realm of possibilities. This point will be discussed further in the next section.

## 7.4 Discussion

### 7.4.1 Gas phase methane dehydrogenation

The aim of this work has largely been to understand why $Ir^+$ has the distinction of being the most efficient element at dehydrogenating $CH_4$. Based on the potential energy surface that we have calculated, we find that this is due to the ability of $Ir^+$:

(1) to form four covalent bonds (with a formal oxidation state of V),

(2) to optimally hybridize valence 6s and 5d orbitals, thereby forming strong bonds to C and H (50-60% stronger than $Co^+$ and $Rh^+$), and

(3) to change spin easily.

The combination of these effects leads to $Ir(H)_2(CH_2)^+$ (Figure 7*f*) as the global minimum.

Much of the reason for the activity of $Ir^+$ is due to the strong bonds it can form. A comparison of the $M^+-H$ and $M^+-$alkyl bond strengths (Chapter III) shows that the bonds to $Ir^+$ are significantly stronger than the bonds to its first and second row counterparts. In addition, a theoretical study of the $MH^+$ species for the entire transition series found $IrH^+$ to be the strongest bond ($La^+$, $Hf^+$, and $Pt^+$ form $MH^+$ bonds which are less than 6 kcal/mol weaker than the $IrH^+$ bond).[16] For methane dehydrogenation, the reaction efficiency appears to rest largely on the reaction exothermicity (or $MCH_2^+$ bond strength). These have been calculated for the first and second row metals by Bauschlicher *et al.*,[14] with no $MCH_2^+$ species having a bond strong enough for dehydrogenation to occur. Irikura and Goddard[17] have calculated these bond strengths for the third

**Table III.** Calculated $MCH_2^+$ bond strengths for the third row transition metals (from Irikura and Goddard).[17] Also included are estimated bond energies and intrinsic bond energies which account for promotion energy and exchange energy loss (in kcal/mol) and the experimentally observed reaction efficiencies.

| Metal | Calculated $D_e$ | Estimated[a] $D_0$ | Intrinsic[a] $D_0$ | Efficiency |
|---|---|---|---|---|
| $La^+$ | 90 | 102 | 110 | – |
| $Hf^+$ | 98 | 110 | 139 | – |
| $Ta^+$ | 103 | 115 | 146 | 0.34 |
| $W^+$ | 99 | 111 | 155 | 0.12 |
| $Re^+$ | 83 | 95 | 153 | – |
| $Os^+$ | 100 | 112 | 154 | 0.34 |
| $Ir^+$ | 110 | 122 | 153 | 0.70 |
| $Pt^+$ | 111 | 123 | 155 | 0.39 |

[a] The error bars on these estimated numbers are ±6 kcal/mol.

row metals and the results are presented in Table III. In order for these results to be consistent with experiment, we estimate that the bond strengths are low by 12±6 kcal/mol. This estimate is based on the observation that the dehydrogenation of methane by $W^+$ is a thermoneutral reaction (and assuming a transition state is not rate determining).[1]

The trends in these calculated $MCH_2^+$ bond strengths are enough to explain the observed trends in the reactivities of the metals $La^+$–$Ir^+$. For instance, the $ReCH_2^+$ bond is 27 kcal/mol weaker than the $IrCH_2^+$ bond. This is due to the large loss of exchange energy on the metal in forming the double bond (2.5 $K_{sd}$ + 2 $K_{dd}$ for $Re^+$ vs. 1.5 $K_{sd}$ + 1 $K_{dd}$ for $Ir^+$, where $K_{sd}$ ~12 kcal/mol and $K_{dd}$ ~14 kcal/mol).[18] $Re^+$ has not been observed to react with $CH_4$.[1] To underscore the importance of this effect, it has been observed that $ReCH_2^+$ *does* lead to dehydrogenation of $CH_4$ (efficiency=16%). The loss of exchange

energy is significantly reduced by the presence of the $CH_2$ ligand, thus, a second methylidene bond is stronger than the first by an estimated 23 kcal/mol. $ReCH^+$ is even more reactive with $CH_4$ (41%) as the exchange energy loss is further reduced by 14 kcal/mol. When promotion energy and exchange energy loss are properly taken into account, in fact, the intrinsic $M^+{=}CH_2$ bond strengths are nearly constant for M = W, Re, Os, Ir, and Pt. For M = La, Hf, and Ta, the bonds appear to be intrinsically weaker, perhaps due to a greater discrepancy in the sizes of the $6s$ and $5d$ orbitals (see Table III).

While the trends in the $MCH_2^+$ bond strengths can be readily explained, a significant deviation from the correlation between these bond strengths and the observed reaction efficiencies can be seen with $Pt^+$. The $PtCH_2^+$ bond is 1 kcal/mol *stronger* than the $IrCH_2^+$ bond but $Pt^+$ is observed to react *less* efficiently with $CH_4$ than $Ir^+$ (39% vs. 70%, respectively). The various electronic structure considerations outlined here (promotion energy, $6s$ and $5d$ orbital sizes, and exchange energy loss) suggest that $Ir^+$ and $Pt^+$ should indeed form the strongest bonds to $CH_2$. This indicates that another factor is responsible for the discrepancy in the reaction efficiencies.

Consideration of the complete potential energy surface for $Ir^+ + CH_4$ shows that the difference between the two metals should center around the stability of the $M(H)_2(CH_2)^+$ intermediate. With a valence configuration of $s^1d^8$ (excitation energy = 17.5 kcal/mol from the $d^9$ configuration), $Pt^+$ is capable of forming only three covalent bonds (oxidation state IV). Thus, the doublet $Pt(H)_2(CH_2)^+$ conformer should be unstable, being analogous to the triplet state of $Ir(H)_2(CH_2)^+$ (Figure $7f'$) rather than the stable singlet state (Figure $7f$). While dehydrogenation should be a thermodynamically and kinetically allowed process for $Pt^+$, the efficiency of the reaction should thus be reduced

compared to $Ir^+$. As a result, $Ir^+$ is the most reactive ion for dehydrogenation of $CH_4$.

In summary, not only are the bond strengths important to this chemistry, but the ability of the metal to form four covalent bonds using oxidation state V and the ability of the metal to change spin states must be considered.

### 7.4.2 Additional gas phase reactions

While $CH_4$ dehydrogenation is an important process in catalysis, it should be understood that the ion product, $IrCH_2^+$, is itself an intermediate. We thus consider the chemistry of subsequent reactions of $CH_4$ with $IrCH_2^+$ using the information we have on the potential energy surface for $Ir^+ + CH_4$ and the experimentally observed kinetics for these additional reactions. To understand this chemistry it is also necessary to know the bond strength of the ethylene $\pi$-complex $[Ir(C_2H_4)^+]$, a possible product of reaction of $IrCH_2^+$ with a second molecule of $CH_4$. This complex is considered in more detail in Chapter VIII. In this chapter, a comparison is made to the stability of the $Ir(CH_2)_2^+$ complex (another possible product) which is shown in Figure 13.

The kinetics of the dehydrogenation reaction suggest that $IrCH_2^+$ is actually formed in an excited state.[1] Our results indicate that this could be the $^1A_1$ state which would be the spin allowed product of reductive elimination of $H_2$ from $Ir(H)_2(CH_2)^+$ (Figure 7*f*). We estimate production of the singlet state of $IrCH_2^+$ to be slightly endothermic (by 4 kcal/mol), but considering that our estimates are conservative, it may indeed be a viable option. The evidence for the production of this excited state is that collision with a second $CH_4$ molecule appears to quench the $IrCH_2^+$ to its ground state rather than react. Only a second collision with a $CH_4$ molecule leads to a dehydrogenation reaction and production of $IrC_2H_4^+$ with an efficiency of 25%.

The structure of the product ion is unknown and could be either the ethylene $\pi$-complex $[Ir(C_2H_4)^+]$ or the bis-methylidene complex $[Ir(CH_2)_2^+]$. We calculate that the $Ir(C_2H_4)^+$ bond strength is $D_e$=74.3 kcal/mol, which is very strong for a bond which is electrostatic. (Note, this is not a metalocycle. The C−C bond

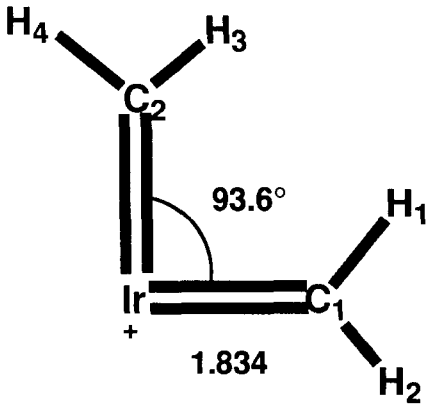


$C_{2v}$ $^1A_1$ $Ir(CH_2)_2^+$

| | | | |
|---|---|---|---|
| Ir | 0.0000 | 0.0000 | 0.0000 |
| $C_1$ | 0.0000 | -0.0581 | 1.8330 |
| $C_2$ | 0.0000 | 1.8330 | -0.0581 |
| $H_1$ | 0.0000 | 0.7992 | 2.4900 |
| $H_2$ | 0.0000 | -1.0033 | 2.3683 |
| $H_3$ | 0.0000 | 2.4900 | 0.7992 |
| $H_4$ | 0.0000 | 2.3683 | -1.0033 |

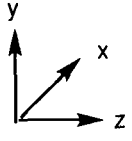


**Figure 13.** Geometry for $Ir(CH_2)_2^+$. Cartesian coordinates are in Å.

length is 1.382 Å compared to 1.339 Å for free $C_2H_4$ and 1.529 Å for free $C_2H_6$.) We expect that the error in this bond energy is small and estimate the exact number to be $D_0$=76±3 kcal/mol. For the $Ir(CH_2)_2^+$ structure, we calculate this to be bound by $D_e$=71.7 kcal/mol with respect to $Ir^+ + C_2H_4$. However, we expect that the error is large and estimate the exact number to be $D_0$=80±8 kcal/mol. The energy difference between the two structures is too small to make a definative statement as to the ground state, however, there is the strong possibility that it is the bis-methylidene structure.

The energy of the bis-methylidene structure can also be estimated based on the strength of the first $Ir^+$=$CH_2$ bond. Using our best estimate for this bond strength of $D_0$=119±4 kcal/mol and accounting for exchange energy loss, we expect a second methylidene to be bound by $D_0$=144 kcal/mol [119 (first bond strength) + 32 (1.5 $K_{sd}$+ 1 $K_{dd}$) − 7 (0.5 $K_{dd}$) = 144 (second bond strength)]. Siegbahn[19] recently noted that bond energies can be significantly weakened as a result of rehybridization when numerous ligands are covalently bound to the metal. This might have an effect on the Ir−C $\sigma$-bonds, but we expect the changes in hybridization in forming the second bond to be relatively minor. Using the experimental heats of formation of $C_2H_4$ and $CH_2$ (12.5 and 93 kcal/mol, respectively)[11] and the predicted $Ir^+$ bond energies indicates that the bis-methylidene structure is more stable than the ethylene $\pi$-complex by 14 kcal/mol, compared to the 4 kcal/mol difference estimated from our calculated numbers above.

We should note that the structure that we have optimized for $Ir(CH_2)_2^+$ is planar and bent. This allows the bonds to be formed from a pure $^5F$ state of the metal:

$$(x^2)^2(yz)^2(y^2-z^2)^1(xz)^1(xy)^1(s)^1$$

**Scheme I**

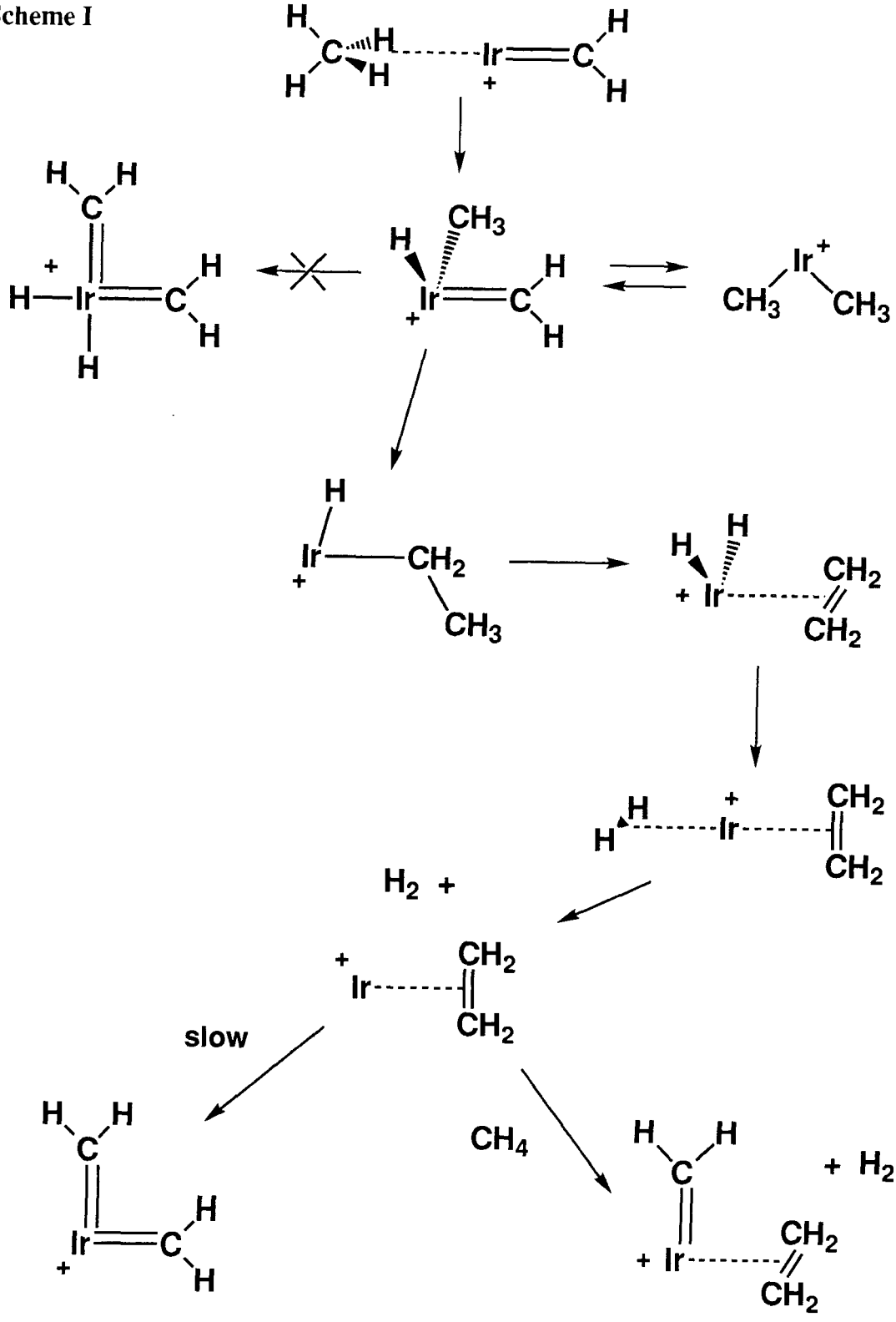

where the two Ir−C $\sigma$-bonds are formed from $s + d_{y^2-z^2}$ and $s - d_{y^2-z^2}$ hybrids and the two Ir−C $\pi$-bonds are formed from the $d_{xz}$ and $d_{xy}$ orbitals. Other orientations either introduce $^5$P character into the wavefunction or compromise the formation of the $\pi$-bonds and were not investigated.

While formation of $Ir(CH_2)_2^+$ may be favored thermodynamically, we expect that formation of $Ir(C_2H_4)^+$ is favored kinetically. Based on the potential energy surface for $Ir^+ + CH_4$, dehydrogenation of a second $CH_4$ to form $Ir(CH_2)_2^+$ would require a bound intermediate complex (whether a minimum or a transition state) with the structure $Ir(H)_2(CH_2)_2^+$. As this complex has a formal oxidation state of VII for Ir, it is clearly unstable and probably inaccessible ($Re^+$ would be the only third row metal for which this intermediate is likely to be stable). Thus, we predict that the product of a second $CH_4$ dehydrogenation reaction is the higher energy ethylene $\pi$-complex, leading to an exothermicity of 20±5 kcal/mol.

This conclusion is consistent with the observed kinetics which indicate that $IrC_2H_4^+$ is initially reactive towards a third $CH_4$ but slowly converts to an unreactive form. We expect that the triplet ethylene $\pi$-complex would be reactive towards $CH_4$, but the closed-shell bis-methylidene complex would be inert. The proposed reaction sequence is outlined in Scheme I. It is likely that this chemistry is unique to $Ir^+$ due to the strengths of the first and second methylidene bonds. For the other third row metals (with the possible exception of $Re^+$), formation of the ethylene $\pi$-complex should be both kinetically *and* thermodynamically favored.

### 7.4.3 Solution phase chemistry

In many ways the chemistry of organometallic complexes in solution is far removed from that in the gas phase. The thermalizing conditions of the solvent is a notable example and has the consequence that reaction efficiencies are related to how high barriers are *above* local minima on the potential energy surface in contrast to the situation in the gas phase where the efficiency is related to how far barriers are *below* the threshold energy. In addition, there is the factor of steric hindrance of bulky ligands which puts geometric constraints on the reaction. However, the electronic structure aspects of methane activation revealed in these gas phase ion-molecule reactions should be intrinsic to the chemistry in the condensed phase. Thus, an understanding of how the energetics are modified by the presence on the metal of stabilizing ligands should be quite valuable in developing an analogous solution phase catalyst.

Unfortunately, the situation does not look promising. The reaction of $Ir^+$ with $CH_4$ is almost the ideal situation and small changes to the electronic structure could easily produce insurmountable barriers in the condensed phase. The $IrCH_2^+$ bond is as strong as it is in large part because *sd* hybridization is so effective. If this is restricted in any way, as would be the case if the metal has substituent ligands, the bond will surely be weakened. Moreover, one of the most important electronic structure aspects of the gas phase reaction between $Ir^+$ and $CH_4$ which distinguishes the chemistry of this metal from others of the third row is the ability of the metal to change formal oxidation states from I to III to V concomitant with formation of the appropriate bonds. For bare metal ions, the energetics of these changes in oxidation state depend on promotion energy and exchange energy loss. $Ir^+$ is the most efficient gas phase ion for the methane

dehydrogenation reaction in part because these energy costs are minimal and each oxidation state is easily accessible. These same factors of promotion and exchange energies also determine the accessibility of various oxidation states for ligated complexes. However, ligation alters the energetics such that a solution phase Ir complex may have easily accesible oxidation states of I and III, but the oxidation state of V may be difficult to achieve. In general, the effect of multiple $X^-$ ligands (such as $Cp^-$ or $Cl^-$) and L ligands (such a $PPh_3$ or CO) on a metal is to destabilize the valence *s* orbital and to favor lower spin states. As a result, for the coordinatively unsaturated 14 electron Ir complex, $(Cl)Ir(PPh_3)_2$, oxidation state III (from a $d^8$ configuration) should be intrinsically favorable and oxidation state V (from an $s^1d^7$ configuration) should be less easily obtained.[20]

The chemistry observed in the gas phase has been seen to a limited extent in solution. Coordinatively unsaturated 16 electron Ir(I) complexes, such as $(Cp^*)Ir(L)$ (L=$PMe_3$ or CO), have been successful in inserting into unactivated C−H bonds, changing the oxidation state of the metal from I to III.[10] However, as the resulting alkyl hydride complex satisfies the 18 electron rule, further reaction is not expected. The chemistry can be extended by substitution of the $Cp^*$ with an indenyl ($C_9H_7$) since this ligand is capable of easily converting from $\eta^5$ to $\eta^3$ to $\eta^1$ coordination and Foo and Bergman[10e,f] took advantage of this property to faciliate the migratory insertion of an associated CO ligand into the metal alkyl bond of the alkane adduct. This chemistry is promising for alkane functionalization, but still elusive are goals such as the oxidative addition of two methane C−H bonds to form a bis-hydrido methylidene or the oxidative addition of a C−H bond from a second molecule of methane to form a bis-hydrido bis-methyl species. While such chemistry has been achieved (or is easily envisioned) in the gas phase, it will be extremely difficult to duplicate in solution. Reactions

such as these would require a 14 electron active complex with a metal capable of accessing the I, III, and V oxidation states. This places an incredible demand on the catalyst, and we find it unlikely that such a catalyst could be developed.

We should conclude by stating that while an Ir(I) catalyst in solution is likely less active than $Ir^+$ in the gas phase, many metal complexes may be more reactive in solution than their gas phase atomic ions. For instance, consideration of the effects of ligands on the electronic states of $Re^+$ (an unreactive ion in the gas phase) suggests that a complex based on this metal may come closest to being able to mimic the gas phase behavior of unligated $Ir^+$. Higher oxidation states are common for Re, and there are numerous examples of Re complexes with multiple hydride[21] and alkyl[22] bonds. A 14 electron species such as ($\eta^3$-Ind)Re($PMe_3$)$_2$ is probably a quintet state formed from the $d^6$ configuration of the metal ion, and this state would then be capable of forming the four covalent bonds required for the bis-hydrido methylidene. Whether these bonds are strong enough and whether the barriers are low enough for reaction to occur is unclear, but the situation is more promising than it is for Ir(I). In fact, the first step in the reaction–the oxidative addition of a C–H bond–has already been demonstrated for 16 electron complexes of Re which are analogous to those of Ir.[23] These complexes tend to be more selective than the Ir complexes, for example activating methane in preference to cyclohexane, and they also tend to lead to more intramolecular attack. Yet we suggest that ultimately the chemistry of Re complexes may prove to be richer than that of Ir complexes in the field of methane activation and functionalization.

## 7.5 Conclusions

In this chapter, we have shown that $Ir^+$ has a unique capability of activating $CH_4$. The origins of this uniqueness involve the intrinsic strengths of the Ir−C and Ir−H bonds and the ability of the metals to change spin easily (due to strong spin-orbit coupling). Both of these traits are generally common to all of the third row metals. $Ir^+$ is distinguished from $La^+$, $Hf^+$, and $Pt^+$, however, in its ability to form the stable intermediate $M(H)_2(CH_2)^+$ (requiring a formal oxidation state of V on the metal). This intermediate provides a lower energy pathway for dehydrogenation, thereby increasing the reaction efficiency. The other metals of the third row capable of forming such an intermediate ($Ta^+$ through $Os^+$) experience greater loss of exchange energy in forming covalent bonds ($W^+$ through $Os^+$) or have slightly weaker intrinsic $MCH_2^+$ bond strengths ($Ta^+$), both effects leading to less stable intermediate and product species and reduced efficiencies for dehydrogenation. The reactivities of these metals may be improved, however, by appropriate ligands.

For $Co^+$ and $Rh^+$, only clustering of the metal with $CH_4$ is observed. While the overall dehydrogenation reaction is found to be endothermic by over 30 kcal/mol for both of these metals, even the first step in the reaction profile–insertion into a C−H bond–is an unfavorable process and only partial activation of the bond occurs.

## References

(1) Irikura, K.K.; Beauchamp, J.L. *J. Phys. Chem.* **1991**, *95*, 8344.

(2) (a) Byrd, G.D.; Freiser, B.S. *J. Am. Chem. Soc.* **1982**, *104*, 5944. (b) Tolbert, M.A.; Mandich, M.L.; Halle, L.F.; Beauchamp, J.L. *J. Am. Chem. Soc.* **1986**, *108*, 5675.

(3) (a) Armentrout, P.B.; Beauchamp, J.L. *J. Am. Chem. Soc.* **1981**, *103*, 784. (b) van Koppen, P.A.M.; Bodbelt-Lustig, J.; Bowers, M.T.; Dearden, D.V.; Beauchamp, J.L.; Fisher, E.R.; Armentrout, P.B. *J. Am. Chem. Soc.* **1991**, *113*, 2359, and references therein.

(4) Ranasinghe, Y.A.; MacMahon, T.J.; Freiser, B.S. *J. Phys. Chem.* **1991**, *95*, 7721.

(5) Ohanessian, G.; Goddard, W.A., III, unpublished.

(6) Perry, J.K.; Ohanessian, G.; Goddard, W.A., III *Organometallics*, in press.

(7) Satterfield, C.N. *Heterogeneous Catalysis in Industrial Practice, Ed. 2*; McGraw-Hill: New York, 1991.

(8) (a) Shilov, A.E. *Activation of Saturated Hydrocarbons by Transition Metal Complexes*; Reidel: Netherlands, 1984. (b) Crabtree, R.H. *Chem. Rev.* **1985** *85*, 245, and references therein.

(9) Periana, R.A.; Taube, D.J.; Evitt, E.R.; Löffler, D.G.; Wentrcek, P.R.; Voss, G.; Masuda, T. *Science* **1993**, *259*, 340.

(10) (a) Janowicz, A.H.; Bergman, R.G. *J. Am. Chem. Soc.* **1982**, *104*, 352. (b) Hoyano, J.K.; Graham, W.A.G. *J. Am. Chem. Soc.* **1982**, *104*, 3723. (c) Hoyano, J.K.; McMaster, A.D.; Graham, W.A.G. *J. Am. Chem. Soc.* **1986**, *108*, 1537. (e) Foo, T.; Bergman, R.G. *Organometallics* **1992**, *11*, 1801. (f) *Ibid.*, 1811.

(11) Lias, S.G.; Bartmess, J.E.; Liebman, J.F.; Holmes, J.L.; Levin, R.D.; Mallard, W.G. *J. Phys. Chem. Ref. Data, Suppl.* **1988**, *17*, no. 1.

(12) (a) Crabtree, R.H. *The Organometallic Chemistry of the Transition Metals*; Wiley: New York, 1988, Chap. 11. (b) Schrock, R.R. *J. Am. Chem. Soc.* **1974**, *96*, 6796. (c) Fischer, E.O.; Maasbol, A. *Angew. Chem. Int. Ed.* **1964**, *3*, 580.

(13) Armentrout, P.B.; Sunderlin, L.S.; Fisher, E.R. *Inorg. Chem.* **1989**, *28*, 4436.

(14) Bauschlicher, C.W., Jr.; Partridge, H.; Sheehy, J.A.; Langhoff, S.R.; Rosi, M. *J. Phys. Chem.* **1992**, *96*, 6969.

(15) van Koppen, P.A.M.; Brodbelt-Lustig, J.; Bowers, M.T.; Dearden, D.V.; Beauchamp, J.L.; Fisher, E.R.; Armentrout, P.B. *J. Am. Chem. Soc.* **1991**, *113*, 2359.

(16) Ohanessian, G.; Goddard, W.A., III *Acc. Chem. Res.* **1990**, *23*, 386.

(17) Irikura, K.K.; Goddard, W.A., III, to be published.

(18) Carter, E.A.; Goddard, W.A. *J. Phys. Chem.* **1988**, *92*, 5679.

(19) Siegbahn, P.E.M.; Blomberg, M.R.A.; Svensson, M. *J. Am. Chem. Soc.* **1993**, *115*, 4191.

(20) A notable example of an Ir(V) complex is $H_5Ir(P\textit{i}\text{-}Pr_3)_2$. Crabtree, R.H.; Lavin, M.; Bonneviot, L. *J. Am. Chem. Soc.* **1986**, *108*, 4032.

(21) Abrahams, S.C.; Ginsberg, A.P.; Knox, K. *Inorg. Chem.* **1964**, *3*, 558.

(22) Floë, M.; Hedtweck, E.; Wagner, W.; Kulpe, J.; Harter, P.; Herrmann, W.A. *Angew. Chem. Int. Ed. Engl.* **1987**, *26*, 787.

(23) (a) Wenzel, T.T.; Bergman, R.G. *J. Am. Chem. Soc.* **1986**, *108*, 4856. (b) Bergman, R.G.; Seidler, P.F.; Wenzel, T.T. *J. Am. Chem. Soc.* **1985**, *107*, 4358.

Chapter VIII

# Transition Metal Ion Mediated Dehydrogenation of Ethane

# Chapter VIII

## Transition Metal Ion Mediated Dehydrogenation of Ethane

### 8.1. Introduction

The chemistry of ethane with transition metal ions is a great deal richer than the chemistry of methane.[1] More metals are reactive toward ethane than methane ($Sc^+$ and $Rh^+$, for instance, lead to dehydrogenation of ethane but not methane)[2-4] and the possibility of C−C activation in addition to C−H activation opens up a number of new reaction channels. Furthermore, some of the products can have multiple isomers (such as $M(C_2H_4)^+$ vs. $M(CH_2)_2^+$) and these are not well characterized by experiment.

The most likely reactions that could be observed are:

$$M^+ + C_2H_6 \longrightarrow MC_2H_4^+ + H_2 \quad (1)$$

$$\longrightarrow MC_2H_2^+ + 2H_2 \quad (2)$$

$$\longrightarrow MCH_2^+ + CH_4 \quad (3)$$

$$\longrightarrow MH_2^+ + C_2H_4 \quad (4)$$

$$\longrightarrow MC_2H_5^+ + H \quad (5)$$

$$\longrightarrow MCH_3^+ + CH_3 \quad (6)$$

$$\longrightarrow MH^+ + C_2H_5 \quad (7)$$

$$\longrightarrow MC_2H_6^+ \quad (8)$$

Most of these products have already been discussed. However, the bonding of ethylene to a metal ion, which is the product of 1,2-dehydrogenation in reaction

1, was only alluded to in Chapter VII. It will be discussed in detail in the next section.

To date, experimental data on the interaction of ethane with transition metal ions exists for all of the first row,[2,5] most of the second row,[3,4,6-7] but only $La^+$ and $Os^+$ in the third row.[7,8] While the second and third row metals are reactive toward ethane at room temperature, only $Sc^+$ and $Ti^+$ in the first row lead to products.[2] Despite the multitude of reaction channels available, generally only the 1,2-dehydrogenation (1) is observed to occur under these conditions. For a few metals, the double dehydrogenation reaction (2) is also observed.[6-8] The other reactions have only been observed using ion beam techniques.[9]

The bulk of the chemistry that will be discussed in this chapter will concern the single 1,2-dehydrogenation of ethane (1) by the metals $Co^+$, $Rh^+$, and $Ir^+$. The working mechanism for this process is analogous to that found for $Ir^+ + CH_4$ (Chapter VII). It involves:

(i) Initial formation of a molecular complex, $M(C_2H_6)^+$.

(ii) Oxidative addition of a C–H bond to form the hydrido ethyl complex, $M(H)(C_2H_5)^+$.

(iii) A $\beta$-hydrogen shift to form the bis-hydrido ethylene complex, $M(H)_2(C_2H_4)^+$.

(iv) Reductive coupling of the H–H bond to form the dihydrogen ethylene molecular complex, $M(H_2)(C_2H_4)^+$.

(v) Elimination of $H_2$ to produce $M(C_2H_4)^+$.

Based on the mechanism for dehydrogenation of $CH_4$ by $Ir^+$, we assume that the key steps are (*ii*), the oxidative addition to a C–H bond, and (*iii*), the $\beta$-hydrogen shift. Most of the work in this chapter will concentrate on these two steps.

In the case of $Co^+$, the single dehydrogenation reaction has been determined by experiment to be exothermic, yet the reaction has not been observed.[10] This is presumably due to a barrier on the potential energy surface. Based on mechanistic studies of propane dehydrogenation and demethanation by this metal,[11] it is assumed that the barrier arises from the initial C−H insertion step. For the propane reaction, this barrier was determined from phase space theory to lie 2.5±0.7 kcal/mol *below* the threshold energy.[11] Based on this number and the calculated difference between the $Sc^+-C_2H_5$ and $Sc^+-C_3H_7$ bond strengths,[12] we might reasonably estimate that the barrier for initial insertion of $Co^+$ into a C−H bond of ethane is about 2−3 kcal/mol *above* the threshold energy, thus barring reaction from occurring.

We find, however, that the potential energy surfaces for each of these metals is dramatically different. This leads to the proposal of three unique mechanisms for the reaction, only one of which (for $Ir^+$) resembles the mechanism outlined above. While many of the ideas detailed in the previous five chapters lead to an understanding of the potential energy surfaces outlined here, it is experiment which provides the greatest support for the theory. In the exposition of the nature of these reaction mechanisms, the reader should keep in mind that: (1) $Co^+$ is unreactive toward ethane, but 1,2-dehydrogenation and demethanation are observed to occur with propane;[2,9] (2) 1,2-dehydrogenation of propane is observed for $Rh^+$, but not demethanation;[3,4] and (3) 1,4-dehydrogenation of *n*-butane is seen for $Co^+$ but 1,2-dehydrogenation (single and double) is seen for $Rh^+$.[4]

## 8.2 $Co(C_2H_4)^+$, $Rh(C_2H_4)^+$, and $Ir(C_2H_4)^+$

The bonding of ethylene to the metals $Co^+$, $Rh^+$, and $Ir^+$ is dominantly electrostatic in origin and the mechanism of bond formation is entirely analogous to that of the $MH_2^+$ species detailed in Chapter IV. This leads to $\pi$-complexes following the Dewar-Chatt model.[13] Insertion into the C−C $\pi$-bond to form the metalacyclopropane appears to be minimal for $Co^+$ and $Rh^+$ and moderately extensive for $Ir^+$.

Calculations done for the $M(C_2H_4)^+$ complexes were similar to the ones done for the alkane molecular complexes in Chapter V. Results are detailed in Figure 1 and Table I. In each case, the metal ion in its $^3F$ $d^n$ state coordinates to the ethylene $\pi$-bond. On purely electrostatic grounds, this is consistent with coordination of the ion to the large positive quadrupole moment of the molecule (calculated to be 1.00 Å$^2$ at the MCPF level). In fact, the $Co(C_2H_4)^+$ and $Rh(C_2H_4)^+$ bond strengths are dominated by the charge-induced dipole and charge-quadrupole interactions to give estimated bond energies of 41.6 and 32.7 kcal/mol, respectively, compared to the calculated bond energies of $D_e$=44.9 and $D_e$=41.1 kcal/mol, respectively. On the other hand, the estimated bond strength from these quantities for $Ir(C_2H_4)^+$ is 42.1 kcal/mol, which is well short of the calculated $D_e$=74.7 kcal/mol.

There is, however, the additional element of charge transfer, which is shown schematically in Figure 2. This involves donation of charge from the ethylene $\pi$-bond to the empty metal valence $a_1$ $s$ orbital and backdonation of charge from the doubly occupied metal $b_2$ $d_{yz}$ orbital to the empty $\pi^*$ orbital on the ethylene. Based on the populations of the $d_{yz}$ orbitals (1.82, 1.84, and 1.65, for M = Co, Rh, and Ir, respectively), this charge transfer is most effective in the

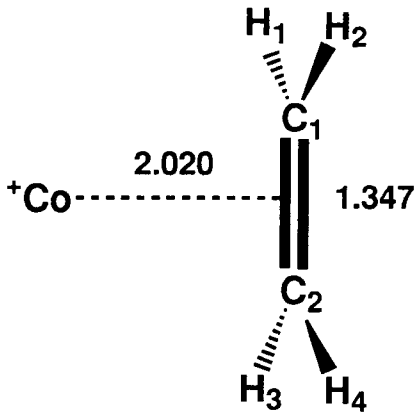


$C_{2v}$ $^3A_2$ $Co(C_2H_4)^+$

| | | | |
|---|---|---|---|
| Co | 0.0000 | 0.0000 | -2.0200 |
| $C_1$ | 0.0000 | 0.6737 | 0.0000 |
| $C_2$ | 0.0000 | -0.6737 | 0.0000 |
| $H_1$ | 0.9190 | 1.2338 | 0.0934 |
| $H_2$ | -0.9190 | 1.2338 | 0.0934 |
| $H_3$ | 0.9190 | -1.2338 | 0.0934 |
| $H_4$ | -0.9190 | -1.2338 | 0.0934 |

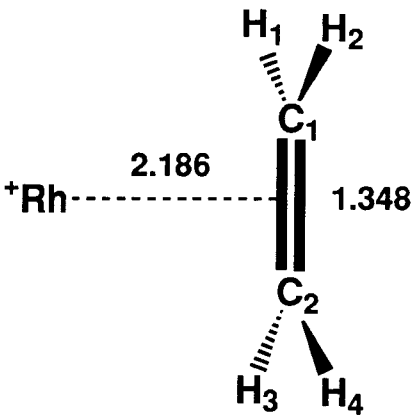


$C_{2v}$ $^3A_2$ $Rh(C_2H_4)^+$

| | | | |
|---|---|---|---|
| Rh | 0.0000 | 0.0000 | -2.1860 |
| $C_1$ | 0.0000 | 0.6741 | 0.0000 |
| $C_2$ | 0.0000 | -0.6741 | 0.0000 |
| $H_1$ | 0.9179 | 1.2329 | 0.0981 |
| $H_2$ | -0.9179 | 1.2329 | 0.0981 |
| $H_3$ | 0.9179 | -1.2329 | 0.0981 |
| $H_4$ | -0.9179 | -1.2329 | 0.0981 |

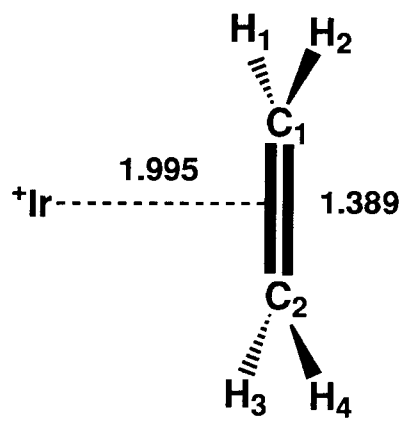


$C_{2v}$ $^3A_2$ $Ir(C_2H_4)^+$

| | | | |
|---|---|---|---|
| Ir | 0.0000 | 0.0000 | -1.9950 |
| $C_1$ | 0.0000 | 0.6944 | 0.0000 |
| $C_2$ | 0.0000 | -0.6944 | 0.0000 |
| $H_1$ | 0.9144 | 1.2399 | 0.1744 |
| $H_2$ | -0.9144 | 1.2399 | 0.1744 |
| $H_3$ | 0.9144 | -1.2399 | 0.1744 |
| $H_4$ | -0.9144 | -1.2399 | 0.1744 |

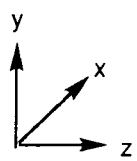


**Figure 1.** Geometries of ethylene π-complexes, $M(C_2H_4)^+$, for M = Co, Rh, and Ir. Cartesian coordiates are in Å.

a

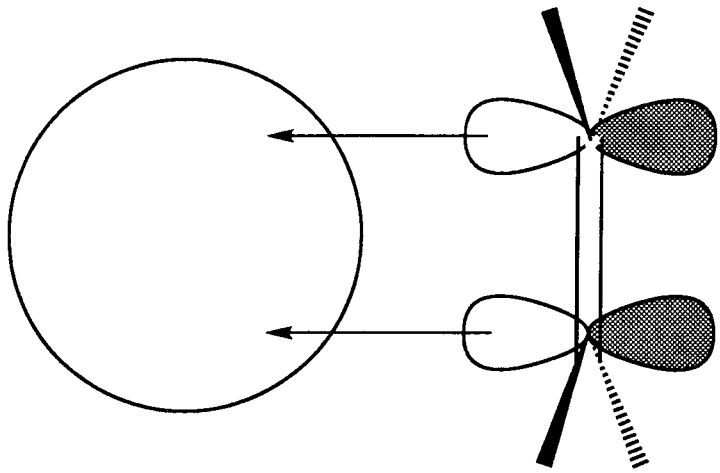

b

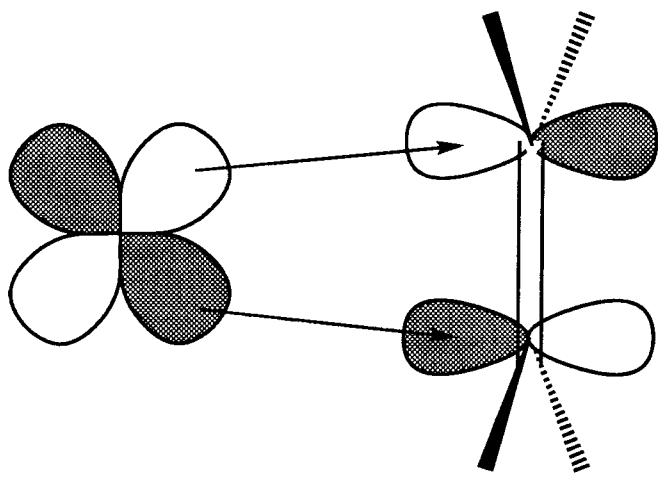

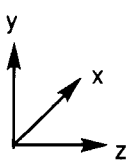


**Figure 2.** Dewar-Chatt model of ethylene bonding to a transtion metal. (a) Donation of charge in $a_1$ symmetry from the doubly occupied $\pi$ bond to the empty $s$ orbital of the metal. (b) Backdonation of charge in $b_2$ symmetry from the doubly occupied $d_{yz}$ orbital to the empty $\pi^*$ antibond.

**Table I.** Properties of $M(C_2H_4)^+$, for M = Co, Rh, and Ir. For each case the ground state is $C_{2v}$ $^3A_2$.

| | $Co(C_2H_4)^+$ | $Rh(C_2H_4)^+$ | $Ir(C_2H_4)^+$ [a] |
|---|---|---|---|
| $D_e$ (kcal/mol) | 45.0[b] | 41.1 | 74.7 |
| $D_e$ (unrelaxed) | 42.3 | 40.0 | 66.3 |
| $\omega_e$ (M−$C_2H_4$, $cm^{-1}$) | 327 | 283 | 433 |
| $r_e$ (M−$C_2H_4$, Å) | 2.020 | 2.186 | 2.051 |
| $E_\alpha$ | 21.5 | 16.8 | 21.2 |
| $r_\alpha$ | 2.39 | 2.55 | 2.40 |
| $E_\theta$ | 20.1 | 15.9 | 20.9 |
| $3d$ population | 7.80 | 7.83 | 7.58 |
| $\mu$ (D) | +1.826 | +2.617 | +2.737 |
| charge on M | +0.65 | +0.75 | +0.56 |

[a] Except for $D_e$(unrelaxed), properies are for the second iteration of geometry optimization for $Ir(C_2H_4)^+$. See text.
[b] The experimentally determined dissociation energy for $Co(C_2H_4)^+$ is $D_0$=46±8 kcal/mol.[10a] Sodupe *et al.*[14] obtain a theoretical value of $D_e$=36.4 kcal/mol using the MCPF method with HF geometries.

case of $Ir(C_2H_4)^+$. In the extreme, this donation and backdonation leads to the formation of covalent bonds and a metalacyclopropane.

The polarization of the metal orbitals should also be considered as it relates to the bond strength. The ground state of each of these $M(C_2H_4)^+$ complexes is $^3A_2$, with the metal configuration

$$(a_1 d_{x^2-y^2})^2 (b_1 d_{xz})^2 (b_2 d_{yz})^2 (a_1 d_{z^2})^1 (a_2 d_{xy})^1$$

consistent with the description of $MH_2^+$ given in Chapter IV. The singly occupied $a_1$ orbital on the metal is dominantly the $d_{z^2}$ orbital for $Co^+$ and $Rh^+$ (94% $d$ and 6% $sp$ for $Co^+$ and 88% $d$ and 12% $sp$ for $Rh^+$), but for $Ir^+$ there is significantly more $sd$ hybridization, resulting in an orbital which is 70% $d$ and

30% *sp*. As seen before (Chapter V), this hybridization polarizes the occupied orbital (usually doubly occupied) in the $xy$ plane, reducing its repulsion to the ligand along the $z$ axis and increasing the effective charge of the metal by exposing more of the core. In turn, the empty $s$ orbital is then polarized along the $z$ axis, increasing its ability to accept charge from the $\pi$-bond. Consequently, the bond of $Ir^+$ to ethylene is significantly stronger than that of either $Co^+$ or $Rh^+$.

We should emphasize that $Co(C_2H_4)^+$ and $Rh(C_2H_4)^+$ are best described as $\pi$-complexes, but $Ir(C_2H_4)^+$ is intermediate to the $\pi$-complex and the metalacyclopropane. The C−C bond length only increases slightly for each metal: from 1.318 Å for free ethylene, to 1.347 Å for $Co(C_2H_4)^+$, to 1.348 Å for $Rh(C_2H_4)^+$, and to 1.389 Å for $Ir(C_2H_4)^+$. This should be compared to the C−C single bond length for $C_2H_6$ of 1.529 Å. The relaxation of the ethylene geometry upon complexation to $Ir^+$ did, however, increase the bond energy by a great deal so two iterations of MCPF/HF geometry optimization were done for this complex. After the first iteration of MCPF geometry optimization (with $C_2H_4$ in its experimental geometry and $r_e(Ir-C_2H_4$=2.051 Å), the bond energy was 66.3 kcal/mol. Upon relaxation of the ethylene geometry at the HF level, it was 73.7 kcal/mol. With a second iteration, the bond length shortened to 1.995 Å and the bond energy increased to 74.3 kcal/mol before relaxation and 74.7 kcal/mol after relaxation. This was considered converged. Most of the relaxation in the ethylene geometry was in the dihedral angle describing the planarity of the C−H bonds. This is an indicator of metalacycle formation and appears to suggest at least partial insertion for $Ir^+$. For all three metals, these bonds bend back away from the metal and out of the plane formed by free ethylene: by 9.5° for $Co(C_2H_4)^+$, by 10.0° for $Rh(C_2H_4)^+$, and by 17.7° for $Ir(C_2H_4)^+$.

### 8.3 C-H Insertion

The C−H insertion process has been described in detail for methane (Chapter VII) and is very similar for ethane. Results are presented in Figures 3 and 4. In the case of ethane, C−H insertion is still an endothermic process for $Co^+$ and $Rh^+$, but a very exothermic process for $Ir^+$. While these results are not unexpected, based on the methane results, the endothermicity of the $Rh^+$ C−H insertion appears to be inconsistent with the experimentally observed chemistry of this metal.[3,4] In order to achieve dehydrogenation, it is generally assumed that oxidative addition to a C−H bond must be the first step. Our calculations, however, indicate that this process is solidly uphill.

On the triplet surface of $Rh^+ + C_2H_6$, C−H insertion is calculated to be endothermic by $E$=+13.0 kcal/mol (an empirical correction to the MCPF result was used to account for the error in the state splittings). Our best estimate for this number is an endothermicity of 9±4 kcal/mol. We considered the singlet state as well by optimizing the geometry at the HF level for a fixed H−Rh−C angle of 90°. At this bond angle, we find the singlet state to be only marginally lower in energy than the triplet state, with an endothermicity calculated to be $E$=+12.0 kcal/mol. Given the probable flatness of this surface (and, thus, an insensitivity to the fixed angle of 90°), we estimate that the singlet state minimum (or minima) is still endothermic by 7±5 kcal/mol.

Based on the $Rh^+ + CH_4$ results, insertion should occur with only a small barrier in excess of the endothermicity. Moreover, we expect that the triplet crosses the threshold energy at an H−Rh−C angle of 50-60° and the singlet and triplet curves cross at an H−Rh−C angle of 80-90°. Thus, we conclude that oxidative addition to a C−H bond of ethane is not favorable and dehydrogenation

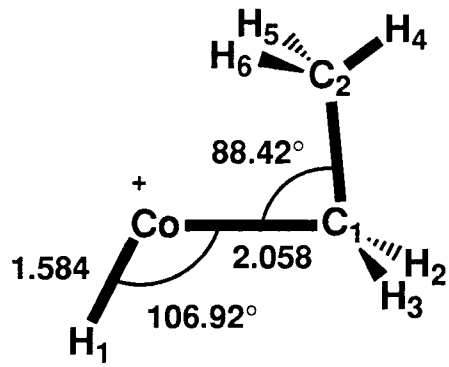


$C_s$ $^3A''$ $Co(H)(C_2H_5)^+$

| | | | |
|---|---|---|---|
| Co | 0.0000 | 0.0000 | 0.0000 |
| $C_1$ | 0.0000 | 0.0000 | 2.0579 |
| $C_2$ | 0.0000 | 1.5159 | 2.0161 |
| $H_1$ | 0.0000 | -1.5159 | -0.4610 |
| $H_2$ | 0.9066 | -0.4950 | -0.4610 |
| $H_3$ | -0.9066 | -0.4950 | 2.3768 |
| $H_4$ | 0.0000 | 1.8758 | 3.0452 |
| $H_5$ | 0.8967 | 1.9384 | 1.5602 |
| $H_6$ | -0.8967 | 1.9384 | 1.5602 |

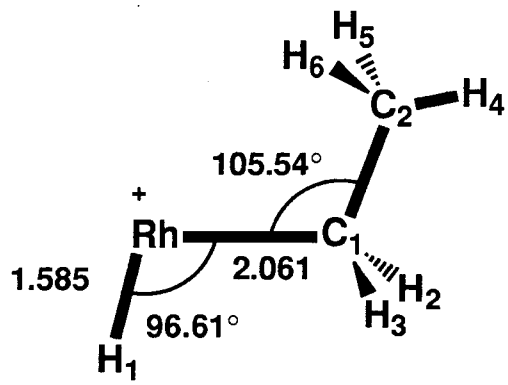


$C_s$ $^3A''$ $Rh(H)(C_2H_5)^+$

| | | | |
|---|---|---|---|
| Rh | 0.0000 | 0.0000 | 0.0000 |
| $C_1$ | 0.0000 | 0.0000 | 2.0608 |
| $C_2$ | 0.0000 | 1.4859 | 2.4741 |
| $H_1$ | 0.0000 | -1.5746 | -0.1824 |
| $H_2$ | 0.8958 | -0.5464 | 2.3336 |
| $H_3$ | -0.8958 | -0.5464 | 2.3336 |
| $H_4$ | 0.0000 | 1.5244 | 3.5630 |
| $H_5$ | 0.8897 | 2.0088 | 2.1325 |
| $H_6$ | -0.8897 | 2.0088 | 2.1325 |

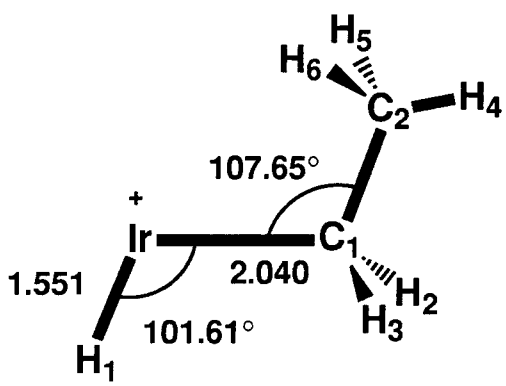


$C_s$ $^3A''$ $Ir(H)(C_2H_5)^+$

| | | | |
|---|---|---|---|
| Ir | 0.0000 | 0.0000 | 0.0000 |
| $C_1$ | 0.0000 | 0.0000 | 2.0395 |
| $C_2$ | 0.0000 | 1.4519 | 2.5016 |
| $H_1$ | 0.0000 | -1.5196 | -0.3122 |
| $H_2$ | 0.8884 | -0.5555 | 2.3274 |
| $H_3$ | -0.8884 | -0.5555 | 2.3274 |
| $H_4$ | 0.0000 | 1.4575 | 3.5912 |
| $H_5$ | 0.8890 | 1.9800 | 2.1829 |
| $H_6$ | -0.8890 | 1.9800 | 2.1829 |

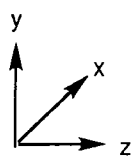


**Figure 3.** Geometries of C-H insertion products, $M(H)(C_2H_5)^+$, for M = Co, Rh, and Ir. Cartesian coordiates are in Å.

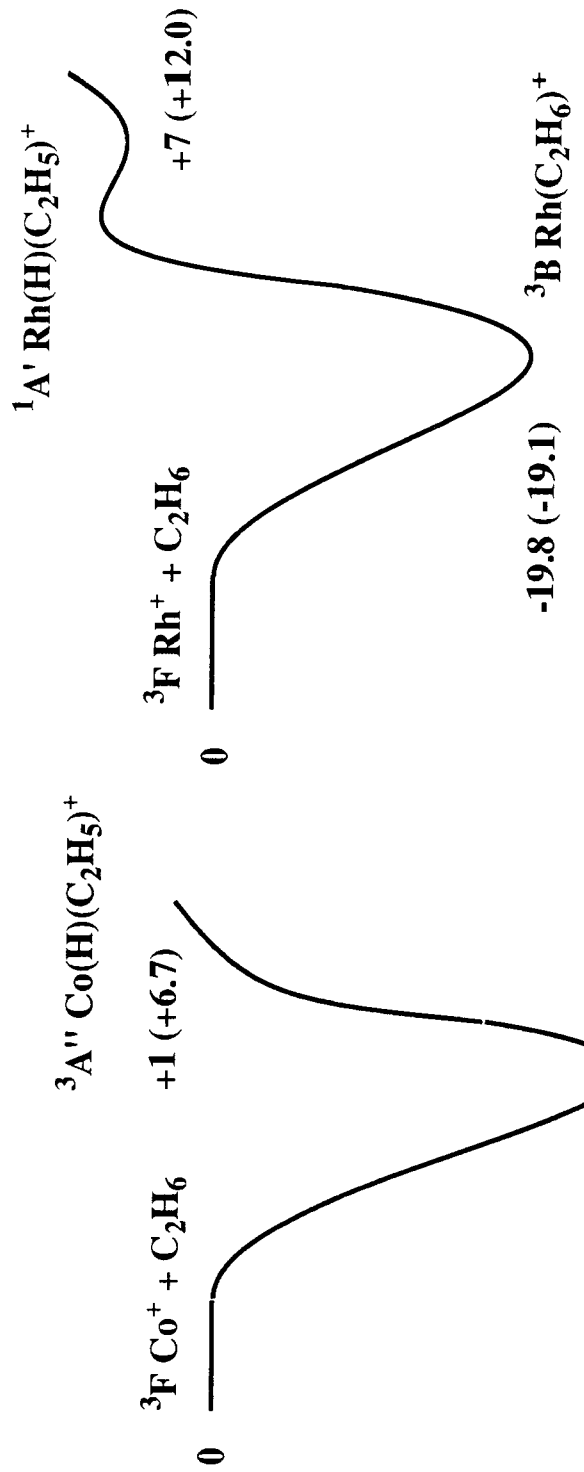
$^1$A' Rh(H)(C$_2$H$_5$)$^+$
+7 (+12.0)
$^3$F Rh$^+$ + C$_2$H$_6$
0
-19.8 (-19.1)
$^3$B Rh(C$_2$H$_6$)$^+$
$^3$A'' Co(H)(C$_2$H$_5$)$^+$
+1 (+6.7)
$^3$F Co$^+$ + C$_2$H$_6$
0
-25.4 (-25.0)
$^3$A'' Co(C$_2$H$_6$)$^+$

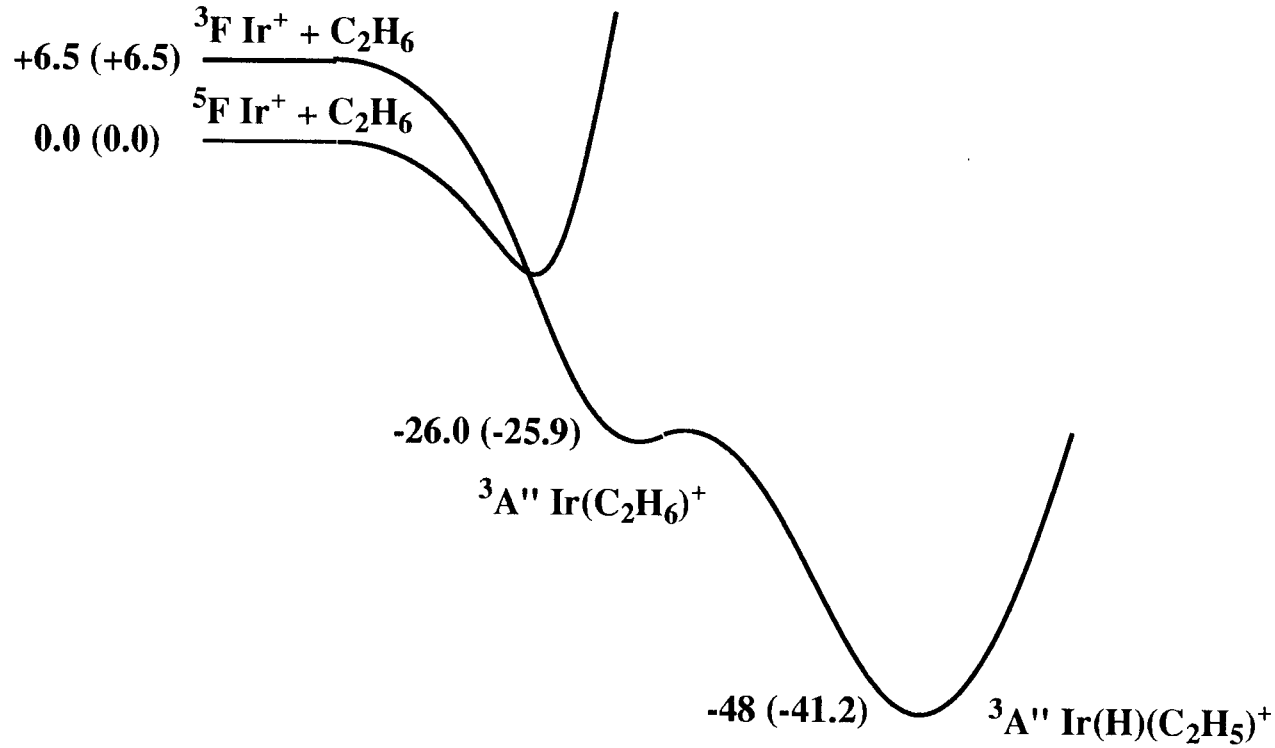


**Figure 4.** Potential energy surfaces for the initial complexation and C-H insertion in the reactions $M^+ + C_2H_6 \longrightarrow MC_2H_4^+ + H_2$, M=Co, Rh, and Ir. Energies are in kcal/mol and represent our best estimates to the true values of $D_0$. MCPF results for $D_e$ are in parenthesis.

must occur via another pathway.

Perhaps to confound the matter, insertion of $Co^+$ into the ethane C−H bond is more facile than for $Rh^+$. It is nearly a thermoneutral process. Insertion into the C−H bond to an angle of 106.9° is estimated to be endothermic by only 1±4 kcal/mol ($E$=+6.7 kcal/mol at the MCPF level). This is certainly a reasonable value for this number, given the experimental determination for propane that the rate determining C−H insertion step is 2.5 kcal/mol below the $^3F$ $Co^+$ + $C_3H_8$ asymptote.[11]

In contrast, insertion for $Ir^+$ is exothermic by an estimated 48 kcal/mol ($E$=−41.2 kcal/mol, calculated). As for $Ir^+$ + $CH_4$, we expect little to no barrier for oxidative addition to a C−H bond of $C_2H_6$.

For all three metals, $Co^+$, $Rh^+$, and $Ir^+$, insertion into an ethane C−H bond is easier than insertion into a methane C−H bond, in part reflecting the weaker C−H bond strength of ethane ($D_0$=101.0 vs. $D_0$=104.7 kcal/mol). However, our calculations indicate that insertion is easier for ethane than methane by 10.0 kcal/mol for $Co^+$, 8.1 kcal/mol for $Rh^+$, and 7.5 kcal/mol for $Ir^+$. Accounting for the difference in our calculated C−H bond strengths, this means that the $HM^+$−$C_2H_5$ bond is stronger than the $HM^+$−$CH_3$ bond by 6.7, 4.8, and 4.2 kcal/mol, for $Co^+$, $Rh^+$, and $Ir^+$, repsectively. [A full comparison between the $M^+$−R and (H)$M^+$−R (R = H, $CH_3$, and $C_2H_5$) bond strengths is given in Table II.] This does not follow from the data for the $M^+$−$CH_3$ and $M^+$−$C_2H_5$ bond strengths (Chapter III) where only for $Rh^+$ is the ethyl bond stronger than the methyl bond (by 7.3 kcal/mol). For $Co^+$, the reverse is true ($CoC_2H_5^+$ is weaker than $CoCH_3^+$ by 1.7 kcal/mol) and for $Ir^+$, the bond strengths are comparable [$D_e(IrC_2H_5^+)$=70.2 vs. $D_e(IrCH_3^+)$=70.3 kcal/mol].

However, as was argued in Chapter III, the $M^+$−$C_2H_5$ bond is strength-

**Table II.** Comparison of $M^+-R$ and $(H)M^+-R$ bond strengths (M = Co, Rh, and Ir; R = H, $CH_3$, and $C_2H_5$). The M−C−C bond angle for R = $C_2H_5$ is also shown. Energies in kcal/mol and angles in degrees.[a]

| R | $Co^+-R$ | $(H)Co^+-R$ | $Rh^+-R$ | $(H)Rh^+-R$ | $Ir^+-R$ | $(H)Ir^+-R$ |
|---|---|---|---|---|---|---|
| H | 48.7 | 43.3 | 43.9 | 46.3 | 74.9 | 73.6 |
| $CH_3$ | 47.5 | 43.2 | 38.9 | 43.6 | 70.3 | 67.4 |
| $C_2H_5$ | 45.8 | 49.9 | 46.2 | 48.4 | 70.2 | 71.6 |
| angle | 114.9 | 88.4 | 106.2 | 105.5 | 113.9 | 107.7 |

[a] Note that there is a discrepancy in the methods used to calculate these bond energies. For $M^+-H$, the ACPF method was used; for $(H)M^+-H$, the MRCI+Q method was used; and for all others, the MCPF method was used. The $(H)M^+-R$ bond energies were determined by calculating the total M−H and M−C bond energies and subtracting the ACPF calculated $MH^+$ bond energy.

ened by the ion-induced dipole interaction between the metal and the $\alpha$-methyl group. This interaction is strongest when the M−C−C bond angle is small, as in $Rh(C_2H_5)^+$. As can be seen in Table II, this angle has decreased for all three metals in the $M(H)(C_2H_5)^+$ complex as compared to the $M(C_2H_5)^+$ complex. In particular, this angle is 88.4° for $Co(H)(C_2H_5)^+$ compared to 114.9° for $Co(C_2H_5)^+$. The more acute bond angles result from inequivalencies in the M−C and M−H bonds. As was detailed in Chapter VI, this is most extreme for $Co^+$, where the H forms a covalent bond to the $4s$ orbital and the $C_2H_5$ forms a largely ionic bond (with charge transfer from ligand to metal) to the $3d$ bond. The weak overlap of the metal $3d$ orbital with the carbon $sp^3$ hybrid and the ionic character of the bond reduce the strain energy associated with an acute bond angle as compared to that of a strong covalent bond. The advantage of an ion-induced dipole attraction to the $\alpha$-methyl group with this coordination then

outweighs any costs associated with bending the bond. Such inequivalencies arise in the $Rh^+$ and $Ir^+$ complexes as well (*i.e.*, the M−H bond tends to be more covalent and the M−C bond tends to be more ionic), but the strength and directionality of the *sd* hybrid bond prevents the M−C−C angle from becoming more acute than 105.5° [for $Rh(H)(C_2H_5)^+$] or 107.7° [for $Ir(H)(C_2H_5)^+$].

From a computational standpoint, we should note another result of the weakness of the Co−C bond in $Co(H)(C_2H_5)^+$ is that the HF wavefunction is qualitatively incorrect. Similar to the symmetry breaking problems discussed in Chapter VI, we found that at the HF level, the wavefuction is best described as a *one electron* bond of the ethyl to the *doublet state* of $CoH^+$. A geometry optimization with this wavefunction led to a Co−C bond which was 0.3 Å too long. On the other hand, the GVB(6/6) level leads to a qualitatively correct wavefunction and this was used instead to obtain an optimum geometry. [The geometry of $Rh(H)(C_2H_5)^+$ was also optimized at the GVB(6/6) level but $Ir(H)(C_2H_5)^+$ was optimized at the HF level.] Moreover, since the HF level is incorrect, it is inappropriate to use the orbitals as a basis for MCPF calculations. Instead we used the orbitals of a CASSCF(6/6) wavefunction. (Unlike coupled-cluster, this is an acceptable procedure.[15]) We tested this first for $Co(H)(CH_3)^+$ and found only a negligible (1.2 kcal/mol) difference between the MCPF calculation done with the HF orbitals and that done with the CASSCF orbitals, validating the alternative method.

## 8.4 C-C Insertion

While not directly relevant to the issue of dehydrogenation, a discussion of the energetics associated with oxidative addition to the C−C bond of ethane is appropriate as it pertains to competing reaction channels. Using the geometries optimized in Chapter VI (the CI geometry for $Co(CH_3)_2^+$, Figure 6 of Chapter VI; and the GVB geometries for $Rh(CH_3)_2^+$ and $Ir(CH_3)_2^+$, Figure 4 of Chapter VI), we calculated the energetics for the bis-methyl insertion product at the MCPF level using the standard TZDP basis sets. As can be seen in Figure 5, the bis-methyl insertion product, $M(CH_3)_2^+$, is more stable than the hydrido ethyl insertion product, $M(H)(C_2H_5)^+$, by 9.2 kcal/mol for M = Co, 5.4 kcal/mol for M = Rh, and 4.8 kcal/mol for M = Ir. This does not reflect the fact that the sum of the two $M^+-CH_3$ bond energies is greater than the sum of the $M^+-H$ and $M^+-C_2H_5$ bond energies. In fact, the opposite is true. The greater stability of the bis-methyl complex is due to the weaker C−C bond as compared to the C−H bond (89.7 kcal/mol vs. 101.0 kcal/mol, a difference of 11.3 kcal/mol).

This is not to say that insertion into the C−C bond is easier than insertion into a C−H bond. While we have not determined the barrier to formation of the $M(CH_3)_2^+$ complex, we can point to the work of Low and Goddard[16] on Pd and Pt complexes that showed that the barriers to oxidative addition and reductive elimination increase as H−H < C−H < C−C. This trend was argued to be the result of the directionality of the carbon $sp^3$ hybrid orbital vs. the nondirectionality of the hydrogen $s$ orbital. Such considerations lead to a stabilization of the transition state for hydrogen, where the nondirectional orbital can form two good "half"-bonds to both the metal and the other ligand. This is not the case for carbon, where the directionality of the $sp^3$ hybrid destabilizes the transtion

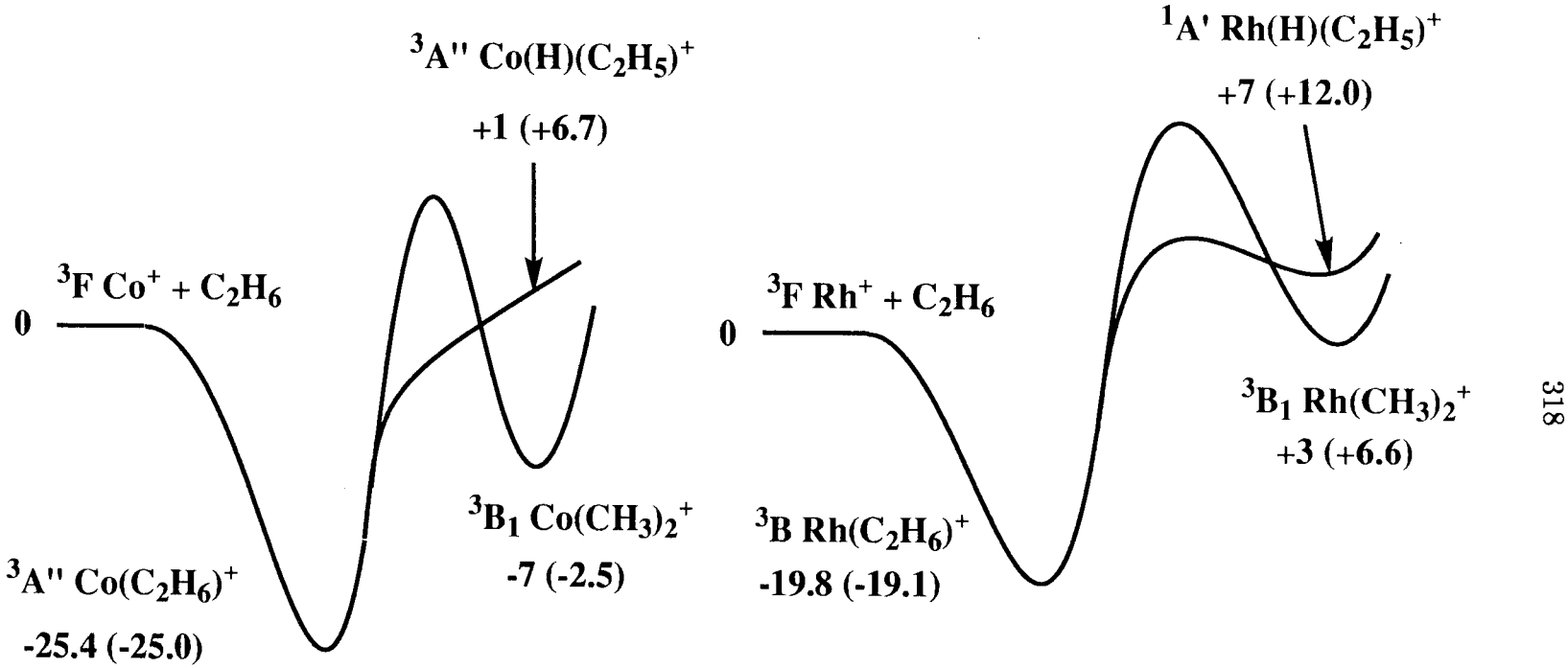
$^3$A'' Co(H)(C$_2$H$_5$)$^+$
+1 (+6.7)
$^3$F Co$^+$ + C$_2$H$_6$
0
$^3$B$_1$ Co(CH$_3$)$_2^+$
-7 (-2.5)
$^3$A'' Co(C$_2$H$_6$)$^+$
-25.4 (-25.0)
$^1$A' Rh(H)(C$_2$H$_5$)$^+$
+7 (+12.0)
$^3$F Rh$^+$ + C$_2$H$_6$
0
$^3$B$_1$ Rh(CH$_3$)$_2^+$
+3 (+6.6)
$^3$B Rh(C$_2$H$_6$)$^+$
-19.8 (-19.1)

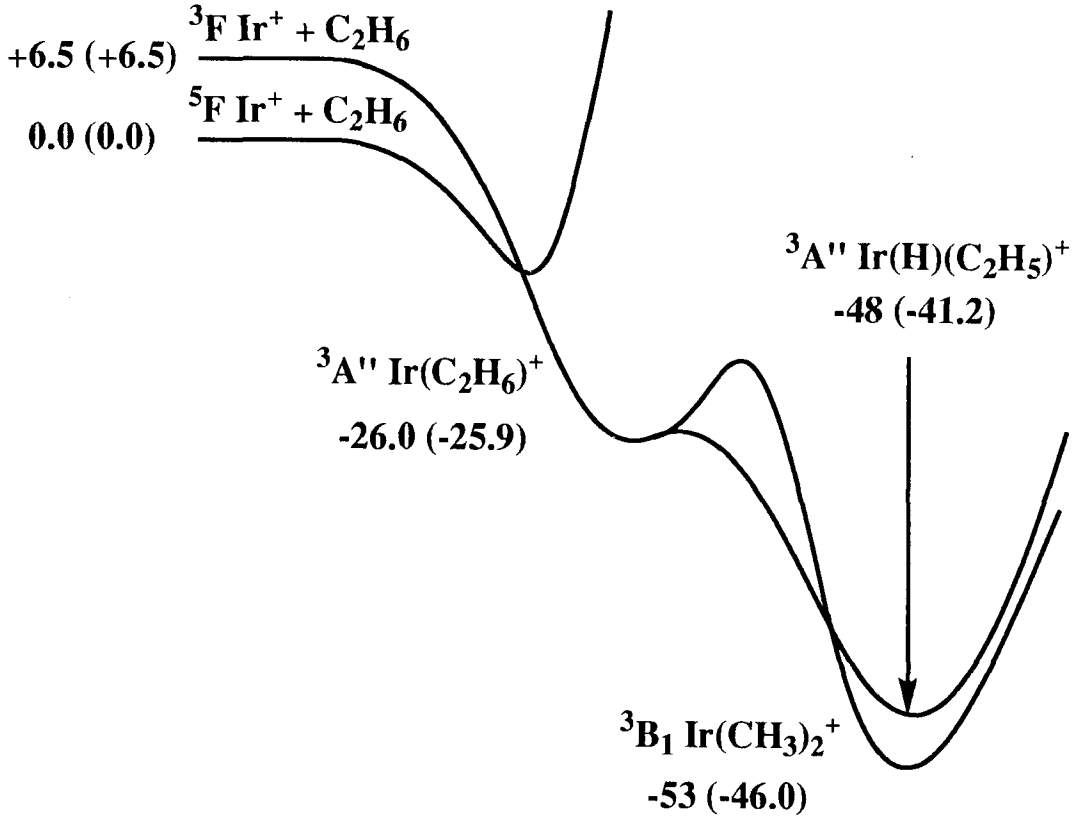


**Figure 5.** Potential energy surfaces for the initial complexation and C-C insertion in the reactions $M^+ + C_2H_6$, M=Co, Rh, and Ir. A comparison is made to the energetics of C-H insertion. Energies are in kcal/mol and represent our best estimates to the true values of $D_0$. MCPF results for $D_e$ are in parenthesis.

state. Thus, insertion into a C−H bond should be more facile than insertion into a C−C bond.

We also argue that the barriers for oxidative addition to the C−C bond of ethane should increase as $Ir^+ < Co^+ < Rh^+$. This in part reflects the relative energetics of the insertion products. Since $Ir^+$ is the only metal of these three for which insertion into the C−C bond is exothermic with respect to the $M(C_2H_6)^+$ molecular complex, the barrier with respect to this complex should be smallest. In a comparison of $Co^+$ and $Rh^+$, on the other hand, there is the element of the *metal* bond directionality. For $Co^+$, the inequivalent bonds leads to less directionality in the *d* bond than in the *sd* hybrid bonds of $Rh^+$. As was seen in the tilt of the ethyl ligand in $Co(H)(C_2H_5)^+$, the directionality of the carbon $sp^3$ hybrid is not particularly important when bonding to this *d* orbital. This may facilitate a lowering of the barrier for oxidative addition and reductive elimination.

For $Fe^+$, Schultz and Armentrout[17] have determined that an additional reaction channel for propane demethanation opens up at an energy ~8 kcal/mol above the barrier assigned to C−H activation. This is assumed to correspond to initial C−C activation. While we believe that it is an accurate assessment of the data that this barrier lies on the reaction pathway corresponding to initial C−C insertion, we warn that this does not infer that the initial C−C insertion is rate limiting. Thus we take the 8 kcal/mol barrier (over and above the height of the barrier to C−H insertion) to be an upper bound on the barrier to C−C insertion.

As a final word, the bis-methyl intermediate is largely a dead end for $Co^+$ and $Rh^+$, leading only to endothermic products. For $Ir^+$, such an intermediate can also lead to demethanation to form the exothermic product $IrCH_2^+$.

## 8.5 $\beta$-H Shift

The next step in the standard proposed reaction sequence after the oxidative addition to a C−H bond is the $\beta$-H shift to form the $M(H)_2(C_2H_4)^+$ complex. Based on the nature of the analogous $Ir(H)_2(CH_2)^+$ complex discussed in Chapter VII, we expected the lowest energy states to be singlet spin with a pyramidal structure. As with the $Ir(H)_2(CH_2)^+$ complex, there are two candidates for the ground state. They are the eclipsed structure (a),

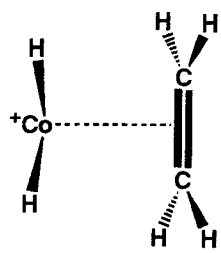


(a)

[electronically similar to the staggered conformation of $Ir(H)_2(CH_2)^+$], and the staggered structure (b),

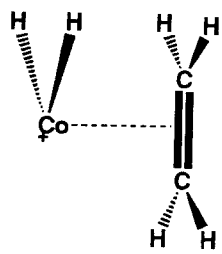


(b)

[electronically similar to the eclipsed conformation of $Ir(H)_2(CH_2)^+$]. Since the analogous $Ir(H)_2(CH_2)^+$ structures were so close in energy (separated by 0.9 kcal/mol), we saw no reason why one of these conformers should be more favorable than the other and we opted to do calculations only on the eclipsed

conformer (due to the equivalence of the two carbons, these calculations were computationally simpler). We find that both $Rh^+$ and $Ir^+$ form stable bis-hydrido ethylene complexes, but $Co^+$ does not.

The optimum HF geometries for $Rh^+$ and $Ir^+$ are given in Figure 6. These geometries are indeed very similar to those optimized for $Ir(H)_2(CH_2)^+$ in Chapter VII. The $Rh^+$ complex is calculated to be bound with respect to $Rh^+ + C_2H_6$ by $E$=−9.1 kcal/mol, and we estimate that this complex is bound by $\Delta H$=−20 kcal/mol. (Note: the zero-point energy is estimated to add 7 kcal/mol to the bond energy for this complex, accounting for the large correction to the energetics.) The $Ir^+$ complex is calculated to be bound by $E$=−67.8 kcal/mol and estimated to be bound by $\Delta H$=−82 kcal/mol. This is not a surprising number, but it should be pointed out that the complex is so strongly bound that it is possible that loss of a single hydrogen atom [with an $Ir^+$−H bond strength of $D_0$=71.5 kcal/mol (Chapter III)] to form the $Ir(H)(C_2H_4)^+$ complex could represent an exothermic reaction for $Ir^+ + C_2H_6$!

In contrast, the $Co(H)_2(C_2H_4)^+$ complex does not appear to be bound and does not appear to be stable. We have considered both the singlet and triplet states of this complex with a number of orientations of the H's, without success. In order to be sure that this was not a problem with the HF geometry optimization, we conducted geometry optimizations at the MCPF level using a smaller basis set (see Appendix). We optimized the M−$C_2H_4$ distance, the M−H distance, the H−M−H angle, and the H−M−$C_2H_4$ angle. For both the singlet and triplet states, optimization of the H−M−H angle led to a dihydrogen molecular complex. Concluding that there was no barrier to reductive elimination of $H_2$ from the $Co(H)_2(C_2H_4)^+$ complex, we attempted to assess the stability of the complex by constraining the H−M−H angle to 90°. Optimizing the other three

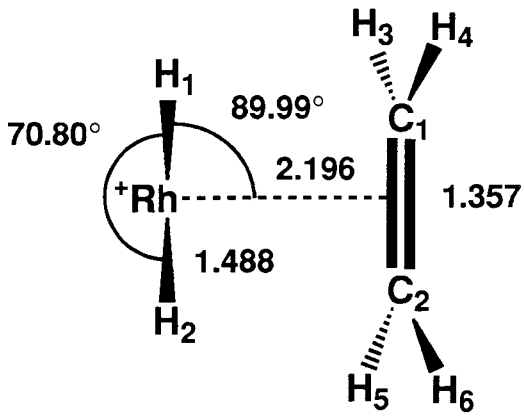


$C_s$ $^1A'$ $Rh(H)_2(C_2H_4)^+$

| | | | |
|---|---|---|---|
| Rh | 0.0000 | 0.0000 | 0.0000 |
| $C_1$ | 0.0000 | 0.6783 | 2.1964 |
| $C_2$ | 0.0000 | -0.6783 | 2.1964 |
| $H_1$ | -1.2131 | 0.8620 | 0.0002 |
| $H_2$ | -1.2131 | -0.8620 | 0.0002 |
| $H_3$ | 0.9247 | 1.2347 | 2.2353 |
| $H_4$ | -0.9063 | 1.2362 | 2.3525 |
| $H_5$ | 0.9247 | -1.2347 | 2.2353 |
| $H_6$ | -0.9063 | -1.2362 | 2.3525 |

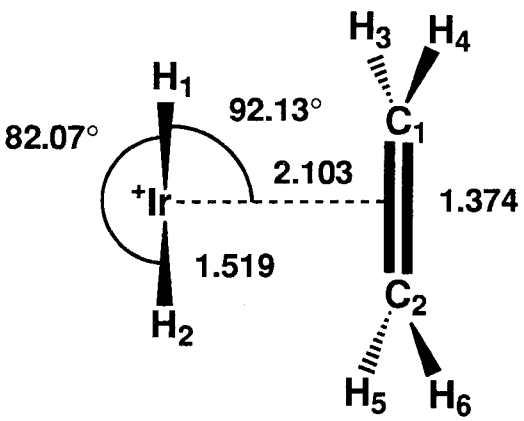


$C_s$ $^1A'$ $Ir(H)_2(C_2H_4)^+$

| | | | |
|---|---|---|---|
| Ir | 0.0000 | 0.0000 | 0.0000 |
| $C_1$ | 0.0000 | 0.6872 | 2.1032 |
| $C_2$ | 0.0000 | -0.6872 | 2.1032 |
| $H_1$ | -1.1443 | 0.9971 | -0.0564 |
| $H_2$ | -1.1443 | -0.9971 | -0.0564 |
| $H_3$ | 0.9269 | 1.2370 | 2.1853 |
| $H_4$ | -0.9013 | 1.2413 | 2.2930 |
| $H_5$ | 0.9269 | -1.2370 | 2.1853 |
| $H_6$ | -0.9013 | -1.2413 | 2.2930 |

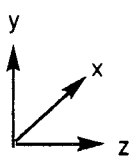


**Figure 6.** Geometries of the intermediate complexes, $M(H)_2(C_2H_4)^+$, for M = Rh and Ir. Cartesian coordinates are in Å.

**Table III.** Comparison of the energetics for $H_2$ oxidative addition to $M^+$ and $M(C_2H_4)^+$ (M = Co, Rh, and Ir). Insertion angles are given in parenthesis. Numbers are based on calculated well depths (in kcal/mol).[a]

| $M$ | $M^+ + H_2 \rightarrow MH_2^+$ | $M(C_2H_4)^+ + H_2 \rightarrow M(H)_2(C_2H_4)^+$ |
|---|---|---|
| Co | 15.2 (90°) | 31.6 (90°) |
| Rh | 7.7 (70°) | −8.2 (70.8°) |
| Ir | −41.3 (71.4°) | −33.3 (82.1°) |

[a] Numbers for $M^+ + H_2$ were calculated at the MRCI+Q level from Chapter IV. Numbers for $M(C_2H_4)^+ + H_2$ were calculated at the MCPF level.

coordinates at the MCPF level and the remaining coordinates at the HF level, geometries for the singlet state as well as two triplet states were obtained. These are given in Figure 7.

The singlet state, very similar to the optimized complexes of $Rh^+$ and $Ir^+$, is unbound by an estimated 23 kcal/mol ($E$=+33.9 kcal/mol). The eclipsed triplet state, in which the dihedral angle between the H−M−H and C−M−C planes is 150°, is estimated to be unbound by 16 kcal/mol ($E$=+26.9 kcal/mol). The staggered $C_{2v}$ triplet state was found to be unbound by an estimated 17 kcal/mol ($E$=+27.8 kcal/mol).

A better understanding of the nature of the stability (or lack thereof) of this intermediate complex can be had by considering the energetics of $H_2$ oxidative addition to $M(C_2H_4)^+$, the reverse of the final step in the reaction sequence. Comparison can be made to the energetics for oxidative addition of $H_2$ to $M^+$ to understand what changes have occurred in the wavefunction. These energetics are summarized in Table III.

For $Co^+$, it is about 16 kcal/mol more difficult to insert into the H−H bond when the metal is bound to $C_2H_4$. The singlet state of the $Co(H)_2(C_2H_4)^+$

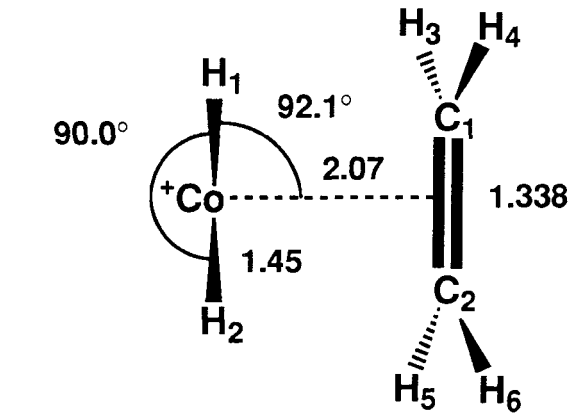


**$C_s$ $^1A'$ $Co(H)_2(C_2H_4)^+$**

| | | | |
|---|---|---|---|
| Co | 0.0000 | 0.0000 | 0.0000 |
| $C_1$ | 0.0000 | 0.6691 | 2.0700 |
| $C_2$ | 0.0000 | -0.6691 | 2.0700 |
| $H_1$ | -1.0239 | 1.0253 | -0.0534 |
| $H_2$ | -1.0239 | -1.0253 | -0.0534 |
| $H_3$ | 0.9262 | 1.2304 | 2.0648 |
| $H_4$ | -0.9053 | 1.2345 | 2.1994 |
| $H_5$ | 0.9262 | -1.2304 | 2.0648 |
| $H_6$ | -0.9053 | -1.2345 | 2.1994 |

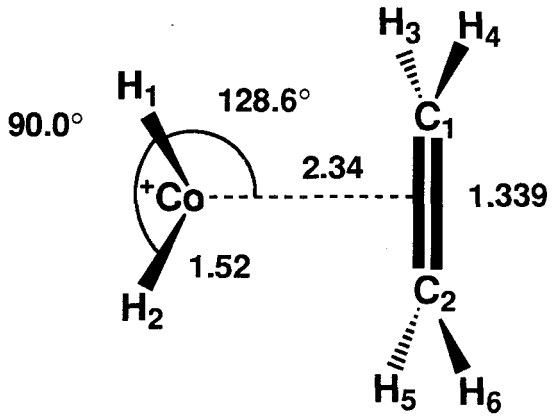


**$C_s$ $^3A'$ $Co(H)_2(C_2H_4)^+$**

| | | | |
|---|---|---|---|
| Co | 0.0000 | 0.0000 | 0.0000 |
| $C_1$ | 0.0000 | 0.6697 | 2.3400 |
| $C_2$ | 0.0000 | -0.6697 | 2.3400 |
| $H_1$ | -0.5046 | 1.0748 | -0.9490 |
| $H_2$ | -0.5046 | -1.0748 | -0.9490 |
| $H_3$ | 0.9214 | 1.2331 | 2.3882 |
| $H_4$ | -0.9208 | 1.2332 | 2.3875 |
| $H_5$ | 0.9214 | -1.2331 | 2.3882 |
| $H_6$ | -0.9208 | -1.2332 | 2.3875 |

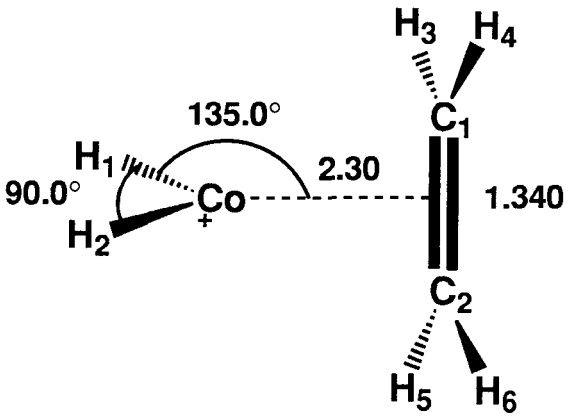


**$C_{2v}$ $^3A_2$ $Co(H)_2(C_2H_4)^+$**

| | | | |
|---|---|---|---|
| Co | 0.0000 | 0.0000 | 0.0000 |
| $C_1$ | 0.0000 | 0.6702 | 2.3000 |
| $C_2$ | 0.0000 | -0.6702 | 2.3000 |
| $H_1$ | 1.0819 | 0.0000 | -1.0819 |
| $H_2$ | -1.0819 | 0.0000 | -1.0819 |
| $H_3$ | 0.9213 | 1.2337 | 2.3476 |
| $H_4$ | -0.9213 | 1.2337 | 2.3476 |
| $H_5$ | 0.9213 | -1.2337 | 2.3476 |
| $H_6$ | -0.9213 | -1.2337 | 2.3476 |

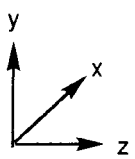


**Figure 7.** Geometries for three states of the intermediate complex, $Co(H)_2(C_2H_4)^+$. Cartesian coordinates are in Å.

complex is derived from the $d^8$ state of the metal and thus indroduces more $d$ character into the bonds, weakening them and destabilizing insertion. (Note: there is a great deal of ligand to metal charge transfer such that the Co is nearly in its neutral $s^1d^8$ configuration.) The triplet state of the complex has reasonably strong Co−H bonds derived from the $s^1d^7$ configuration, but the large occupied $4s$ orbital is repulsive to the $C_2H_4$ ligand, weakening that bond and destabilizing the complex. This is a direct result of the inefficiency of $sd$ hybridization in $Co^+$. Thus, it is more difficult for $Co^+$ to insert into the H−H bond when bound to a $C_2H_4$ ligand, and the purported intermediate in the dehydrogenation of $C_2H_6$ by $Co^+$, $Co(H)_2(C_2H_4)^+$, is unstable.

The opposite appears to be true for $Rh^+$, and it is more favorable by about 16 kcal/mol to insert into the H−H bond when the metal is bound to $C_2H_4$. As noted by Blomberg *et al*[18] for oxidative addition to $Rh^+$, RhCl, $RhCO^+$, and $RhPH_3^+$, $sd$ hybridization creates a potential well along the axis perpendicular to the plane of reaction which strengthens the bonds of donor ligands on that axis. This effect follows from the $sd$ hybridization scheme oulined for the bonding of $Ir(H)_2(CH_2)^+$ in Chapter VII. Hybridization of the $d_{z^2}$ orbital and the $s$ orbital leads to one hybrid polarized along the $z$ axis ($s + d_{z^2}$) and one hybrid polarized in the $xy$ plane ($s - d_{z^2}$). This hybridization biases the bonding in $Ir(H)_2(CH_2)^+$ toward a pyramidal geometry and does the same for $Rh(H)_2(C_2H_4)^+$. For this complex, the $s + d_{z^2}$ hybrid is empty and accepts charge from the $C_2H_4$ ligand more readily than a pure $s$ orbital, and the $s - d_{z^2}$ hybrid combines with the $d_{xy}$ orbital to form two strong Rh−H bonds. While $sd$ hyrbidization is efficient for $Rh^+$ in the sense that intrinsically strong bonds result, it is achieved at the large cost of promotion to the $s^1d^7$ configuration. With additional ligands bound to the metal which benefit from increased $sd$ hybridization, this cost is diffused

over more bonds and the result is a stable $Rh(H)_2(C_2H_4)^+$ complex.

For $Ir^+$, it appears that insertion into the H−H bond is more difficult by about 8 kcal/mol when the metal is bound to $C_2H_4$. However, in this comparison, it should be noted that the $Rh(H)_2(C_2H_4)^+$ and $Ir(H)_2(C_2H_4)^+$ geometries were optimized at the HF level and are not as good as the CI geometries optimized for the other structures. Thus, this 8 kcal/mol difference is actually an overestimate. We expect only a slight decrease in the effectiveness of oxidative addition with the $C_2H_4$ ligand present. Since *sd* hybridization is already efficient in $IrH_2^+$ and $Ir(C_2H_4)^+$, it should only deteriorate with more ligands. The cost of rehybridization is small however (Chapter III), and the energetics are only marginally weaker.

For completeness, we have also calculated the stabilities of the $M(H_2)(C_2H_4)^+$ complexes. The geometries for these were based on the $M(H_2)^+$ and $M(C_2H_4)^+$ geometries with the two ligands staggered with respect to each other. (For $Ir^+$, the H−H distance was taken as 0.80 Å and the Ir−$H_2$ distance was taken as 1.70 Å.) The ground states were assumed to be $^3A_2$. We did not explicitly determine the energetics associated with transition states, but, in a number of instances, such as the initial C−H insertion step, little or no barrier is expected. In cases where there is a change of spin, such as the evolution of singlet $Rh(H)_2(C_2H_4)^+$ to triplet $Rh(H_2)(C_2H_4)^+$, a larger barrier may occur. All results are summarized in the potential energy surfaces of Figures 8-10. In order for our calculations to comply with experiment, modifications of the proposed mechanism is required for both $Co^+$ and $Rh^+$. These modifications will be discussed in the next section.

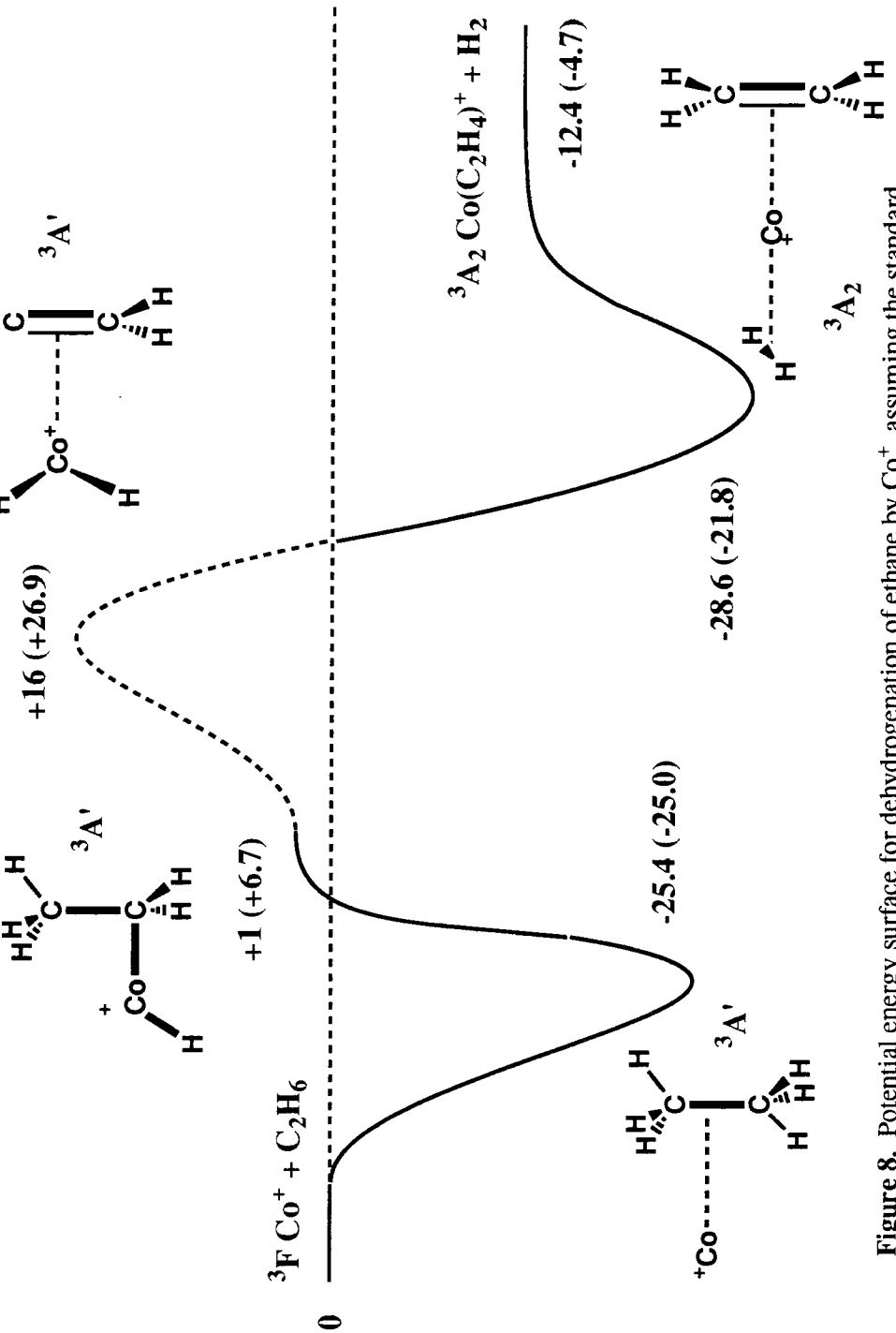


**Figure 8.** Potential energy surface for dehydrogenation of ethane by $Co^+$, assuming the standard oxidative addition/β-H shift/reductive elimination mechanism. Energies represent our best estimates. Energies in parenthesis are our calculated well depths. In kcal/mol.

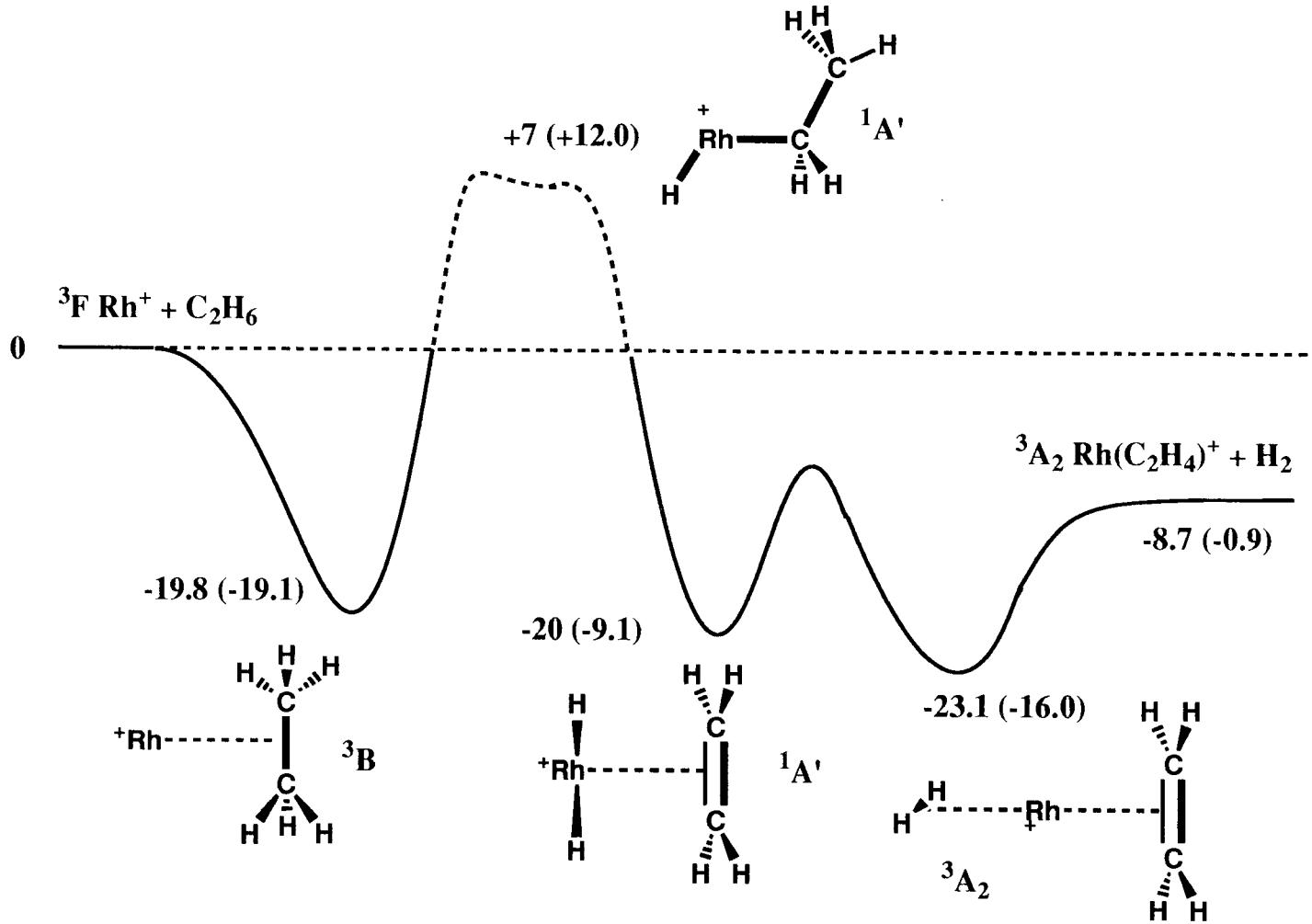


**Figure 9.** Potential energy surface for dehydrogenation of ethane by $Rh^+$, assuming the standard oxidative addition/β-H shift/reductive elimination mechanism. Energies represent our best estimate. Energies in parenthesis are our calculated well depths. In kcal/mol

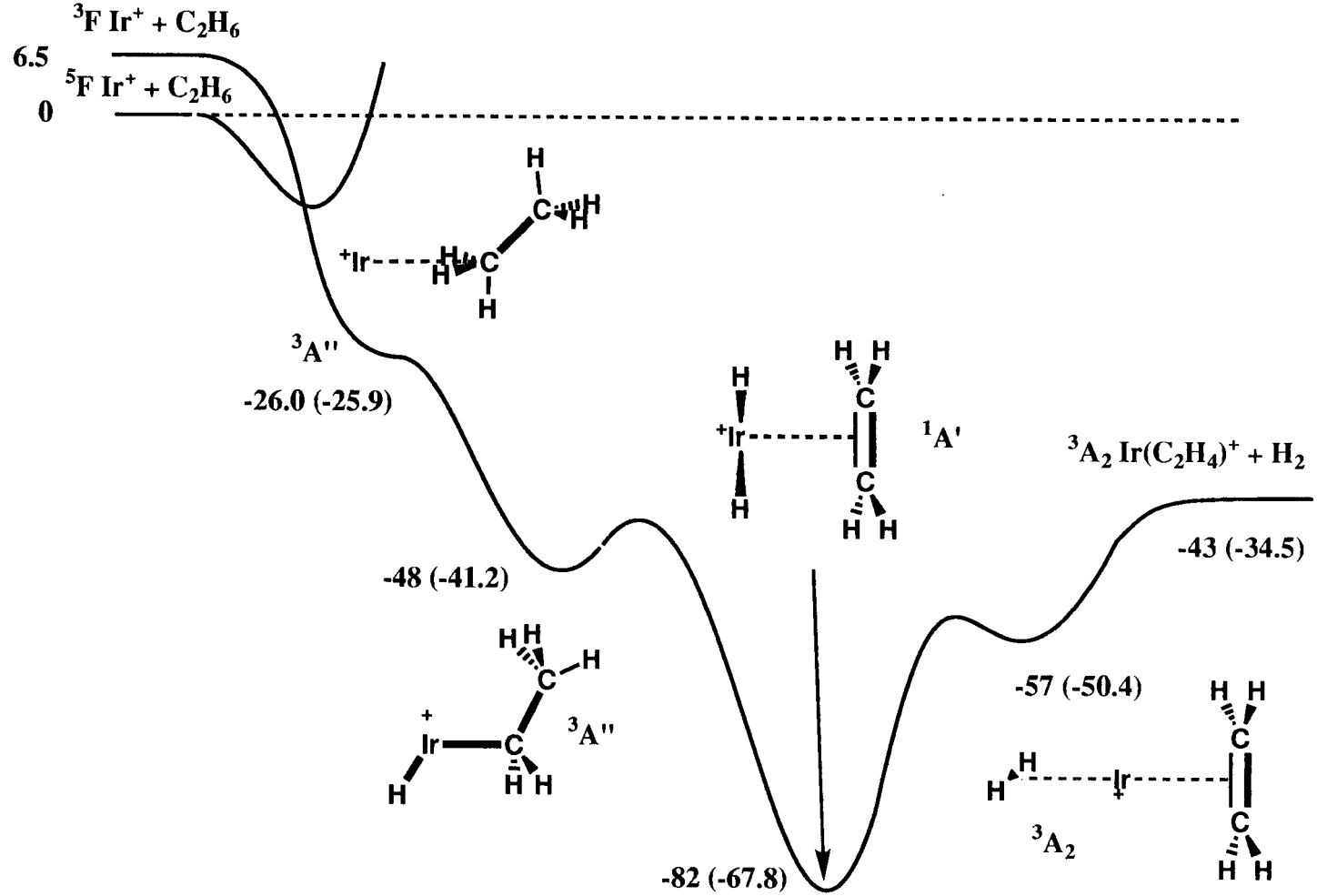


**Figure 10.** Potential energy surface for dehydrogenation of ethane by $Ir^+$, assuming the standard oxidative addition/β-H shift/reductive elimination mechanism. Energies represent our best estimates. Energies in parenthesis are our calculated well depths. In kcal/mol.

## 8.6 Reaction Mechanisms

### 8.6.1 1,2-Dehydrogenation of Alkanes by $Co^+$

On the face of things, our results for dehydrogenation of $C_2H_6$ by $Co^+$ are in agreement with experiment. We find the reaction to be exothermic by $\Delta H$=−12.4±2 kcal/mol compared to the experimental exothermicity of $\Delta H$=−13±8 kcal/mol.[10a] We also find a prohibitively high barrier for reaction, as does experiment.[9,10b] However, we do not see any clear reason why the mechanism for 1,2-dehydrogenation of propane should be any different from that for ethane, yet our calculated barrier for ethane dehydrogenation appears to be too high to be consistent with the observed chemistry for propane dehydrogenation. Since the energetics for the reaction with propane are expected to be only modestly more favorable than for the reaction with ethane, our calculations suggest that propane dehydrogenation should have a prohibitively high barrier for reaction as well.

To understand this discrepancy, it must be stressed that the $Co(H)_2(C_2H_4)^+$ structure is not stable. Our calculations on this structure were done at an H−Co−H angle of 90°, but this does not imply that such a structure is a necessary intermediate for the dehydrogenation reaction to occur. Therefore, instead of the more traditional stepwise mechanism, we propose a mechanism for 1,2-dehydrogenation of alkanes by $Co^+$ which involves a concerted $\beta$-H shift and $H_2$ reductive elimination as follows (see Figure 11):

i. Initial formation of a molecular complex.

ii. Oxidative addition to a single C−H bond to form the hydrido alkyl complex in the *anti* conformation.

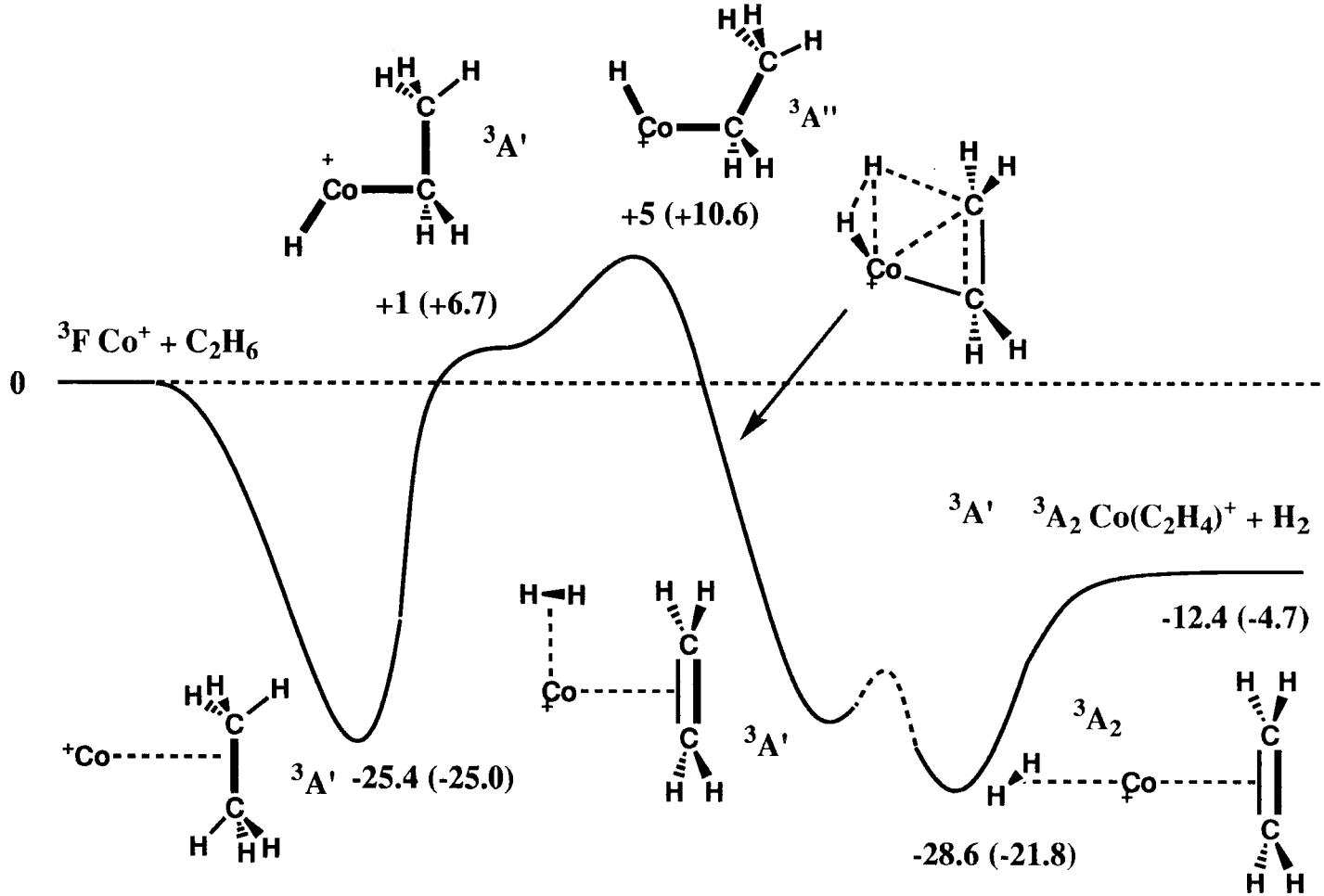


**Figure 11.** Proposed potential energy surface for dehydrogenation of ethane by $Co^+$. The presence of the barrier in the exit channel is uncertain and may depend on geometric constraints. Energies represent our best estimate. Energies in parenthesis are our calculated well depths. In kcal/mol.

iii. Rotation of the Co−H bond about the Co−C bond to form the hydrido alkyl complex in either the *gauche* or *eclipsed* conformations.

iv. Direct formation of the dihydrogen alkene molecular complex through a multi-center transition state.

v. Elimination of $H_2$.

This entire reaction occurs on the triplet surface.

Much of the reasoning behind this mechanism has been to reconcile the results of our calculations with experimental studies by van Koppen *et al.*[11] Their principal conclusion was that the rate determining step for propane dehydrogenation by $Co^+$ (and $Fe^+$ and $Ni^+$ as well[19]) is the initial C−H oxidative addition. Their evidence is largely irrefutable and comes from deuterium labeling of the primary and secondary C−H bonds and the effect this has on *both* dehydrogenation *and* demethanation. The total cross section for $Co^+$ reacting with $C_3D_8$ is a factor of 2.8 smaller than it is for $C_3H_8$.[11] However, the branching ratio for loss of $CH_4$ (or $CD_4$) vs. $H_2$ (or $D_2$) is unchanged by the isotopic labeling. This can only make sense if C−H insertion is the initial and rate determining step for both reactions. In connection with our calculations, this can only make sense if the dihydride structure is not an intermediate in the reaction profile.

The dihydride structure is unbound with respect to the reactants by an estimated 16 kcal/mol at an H−Co−H angle of 90°. However, it should be emphasized that this is just a reference energy to indicate how unstable the dihydride structure is. With more complete calculations on $CoH_2^+$ (Chapter IV), it was shown that at a bond angle of 90°, the complex is unbound by $E$=+15.9 kcal/mol. At an angle of 70°, it is unbound by $E$=+7.5 kcal/mol, and at an angle

of 50°, it is bound by $E$=−2.3 kcal/mol. This correlates with the decreasing $s^1d^7$ and increasing $d^8$ character of the metal. A similar dependency on the H−Co−H bond angle may be expected for $Co(H)_2(C_2H_4)^+$, such that if this angle remains acute (*i.e.*, $< \sim 50°$) throughout the concerted transition state, the reaction could conceivably be completely downhill from the $Co(H)(C_2H_5)^+$ intermediate. If this is the case, then the initial C−H insertion is rate determining.

We have estimated that the initial C−H insertion is endothermic by $\Delta H$=+1 kcal/mol ($E$=+6.7 kcal/mol). Again, as with the dihydride ethylene complex, this is just a reference energy because the complex should be unstable with respect to reductive elimination of $C_2H_6$. However, in order for dehydrogenation to occur, as outlined above, it is necessary to form an acute H−Co−H angle. This is not so for the *anti* conformer of $Co(H)(C_2H_5)^+$ (c).

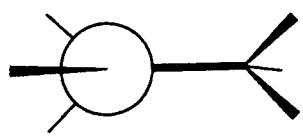

(c)

In fact, this angle is at a maximum in the *anti* conformer. Thus, a rotation of the Co−H bond about the Co−C bond is required to bring the hydrogen bound to the metal in closer proximity to the hydrogens bound to the $\beta$-carbon. We have considered the *eclipsed* conformer (d),

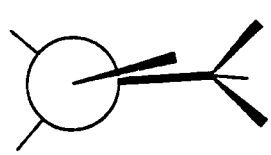

(d)

with the optimized geometry given in Figure 12, in order to determine how facile such a rotation would be. We find that it is unbound by an estimated $\Delta H$=+5 kcal/mol ($E$=+10.6 kcal/mol), only 4 kcal/mol higher in energy than the *anti* conformer. We should note, however, that the $\beta$-H shift/$H_2$ reductive elimination probably originates from the *gauche* conformer (e),

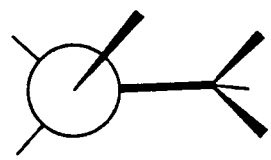

(e)

and this structure may have an energy intermediate to the *anti* and *eclipsed* conformers. We, thus, conclude that the nature of the barrier created by C−H oxidative addition is such that insertion must occur to a large enough angle that rotation about the Co−C bond can be achieved.

Although we have done no calculations on the proposed reaction pathway for the evolution of $Co(H)(C_2H_5)^+$ to $Co(H_2)(C_2H_4)^+$, we envision the reaction to take place as follows. Based on the nature of the triplet transition state for dehydrogenation of $CH_4$ by $Ir^+$ (Chapter VII), we expect that as one of the $\beta$-C−H bonds begins to lengthen, the $\beta$-methyl group then rotates by 60° to become eclipsed with the $\alpha$-carbon (f).

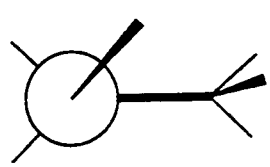

(f)

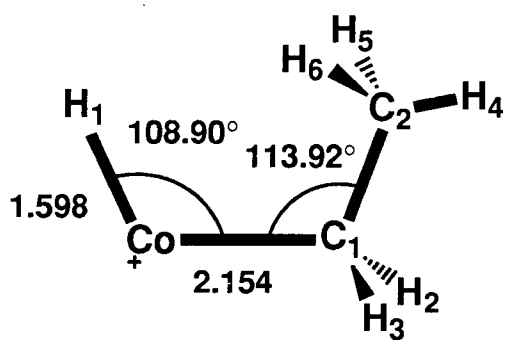


$C_s$ $^3A''$ $Co(H)(C_2H_5)^+$

| | | | |
|---|---|---|---|
| Co | 0.0000 | 0.0000 | 0.0000 |
| $C_1$ | 0.0000 | 0.0000 | 2.1542 |
| $C_2$ | 0.0000 | 1.3768 | 2.7649 |
| $H_1$ | 0.0000 | 1.5115 | -0.5174 |
| $H_2$ | 0.9136 | -0.5855 | 2.2569 |
| $H_3$ | -0.9136 | -0.5855 | 2.2569 |
| $H_4$ | 0.0000 | 1.2595 | 3.8494 |
| $H_5$ | 0.8863 | 1.9391 | 2.4889 |
| $H_6$ | -0.8863 | 1.9391 | 2.4889 |

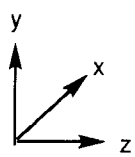


**Figure 12.** Geometry of the eclipsed C-H insertion product, $Co(H)(C_2H_5)^+$. Cartesian coordiates are in Å.

In so doing, the activated $\beta$-C−H bond is in the Co−C−C plane and the Co−H bond is out of the plane. This facilitates the transformation of the carbon $sp^3$ hybrid orbitals (used in bonding to the Co and the $\beta$-H) into the $p_z$ orbitals of the C−C $\pi$ bond. As the reaction evolves, the geometry progresses toward the dihydride ethylene complex (having an acute H−Co−H angle) with a structure which is intermediate to the eclipsed (a) and staggered (b) geometries. As the reaction progresses further, the H−H bond should form and the geometry should settle into either an eclipsed or staggered conformation [analogous to structures (a) and (b), respectively]. It is unclear which may be preferable. Such a mechanism may be termed a hydrogen abstraction, but this implicitly understates the role of the metal in the transition state, and therefore, we refer to the mechanism as a concerted $\beta$-hydride shift $H_2$ reductive elimination.

We argue that the transition state for this concerted reaction pathway should be stabilized by (a) the exothermicity of the reaction (calculated to be 32.4 kcal/mol and estimated to be 34 kcal/mol), (b) the lack of directionality in the Co−C bond (as discussed previously), and (c) the increased $d^8$ character of the metal.. The fact that there is no barrier for the initial C−H insertion is another encouraging sign that such processes are facile.

### 8.6.2 1,2-Dehydrogenation of Alkanes by $Rh^+$

The problem of $Rh^+$ dehydrogenation is perhaps a bit more puzzling. This reaction has been observed to occur at thermal energies[3,4] yet we find that the initial C−H insertion step is unfavorable. Due to the stability of the $Rh(H)_2(C_2H_4)^+$ complex, however, we inferred that this was a probable intermediate on the reaction profile. It was then a question of how it was arrived at.

In early calculations, we attempted optimization of the $Rh(H)_2(C_2H_4)^+$ stucture at the MCPF level, with four variable degrees of freedom. These were the Co−H bond length, the Co−$C_2H_4$ distance, the H−Co−H angle and the dihedral angle between the H−Co−H and C−Co−C planes. We were struck by how floppy the latter coordinate was and decided to investigate further. As this dihedral angle decreases to 0°, the $^1A_1$ $C_{2v}$ $Rh(C_2H_6)^+$ molecular complex results. This is outlined in Scheme I. Surprisingly, we find the energetics of such a direct conversion between the molecular complex and the dihydride is favorable and we propose that 1,2-dehydrogenation of alkanes by $Rh^+$ occurs by such a concerted mechanism.

A true evaluation of the energetics associated with this mechanism is difficult. The mechanism involves insertion of the $^1D$ $d^8$ state of $Rh^+$ into the two C−H bonds and this state is not well described by a single configuration. Thus, the MCPF level overestimates the promotion energy for this state by 17.7 kcal/mol ($^3F$-$^1D$ = 36.3 kcal/mol, calculated and 18.6 kcal/mol experiment). The ACPF method does a bit better, overestimating the splittings by only 8.5 kcal/mol (27.1 kcal/mol calculated splitting). The remaining error is mostly due to the limitations in the basis set rather than the method.

**Scheme I**

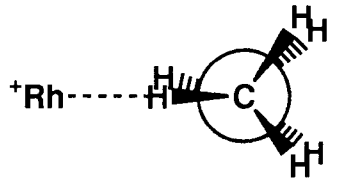


**0°**

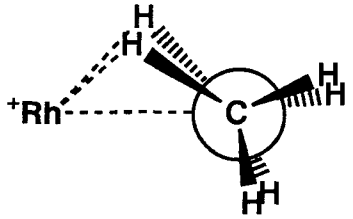


**30°**

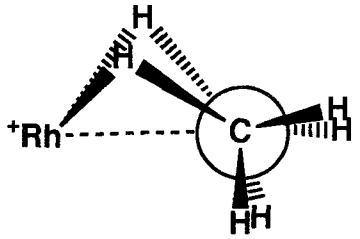


**50°**

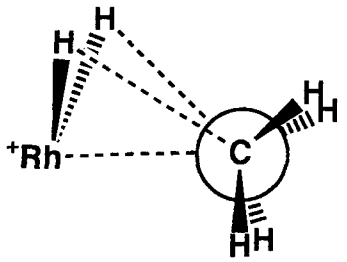


**70°**

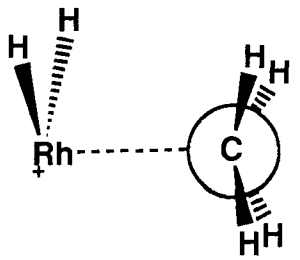


**90°**

Optimizing a geometry for the molecular complex at the HF level (with $C_{2v}$ symmetry and two C−H bonds coordinated to the $Rh^+$ and the $d_{yz}$ orbital of the metal empty), we obtained energetics at both the MCPF (based on HF orbitals) and ACPF (based on CASSCF orbitals) levels. At the MCPF level, the complex is bound by $D_e$=25.9 kcal/mol with respect to the $^1$D state of $Rh^+$. At the more reliable ACPF level, the complex is bound by $D_e$=20.2 kcal/mol. The larger bond energy at the MCPF level results from the fact that complexation to the metal reduces the multi-configurational nature of the wavefunction. (It is most favorable for the $d_{yz}$ orbital to be empty and this configuration then dominates.) As a result, the single reference MCPF method does a better job with the complex than with the atom, and this is reflected in the bond energy. The ACPF method is consistent, however. To obtain the best bond energy, we optimized the $Rh^+-C_2H_4$ coordinate at the ACPF level. This led to a bond energy of $D_e$=22.5 kcal/mol, with respect to $^1$D, which is $D_e$=3.9 kcal/mol, with respect to $^3$F (using an empirical correction). We estimate the complex is bound by $D_0$=4.5 kcal/mol.

To investigate a barrier for concerted insertion, the molecular complex (with an energy corrected to $D_0$=4.5 kcal/mol) should be used as the reference energy. This removes the error in the state splittings as much as possible from the energetics. Due to the reduction in symmetry from $C_{2v}$ to $C_s$ and the concomitant increase in computational cost, we considered only the MCPF potential energy surface. While there is a danger that the MCPF calculations could lead to too low a barrier because of the problem with the method being single reference, other factors such as the use of HF geometries should lead to too high a barrier. All things considered, the resulting calculated barrier should represent a conservative upper limit to the true barrier for this concerted mechanism.

We calculate that the barrier for insertion on the singlet surface occurs at a dihedral angle of 32°. This barrier is only 2.3 kcal/mol above the energy of the singlet molecular complex. We estimate that this is 3 kcal/mol below the energy of the reactants ($^3$F $Rh^+ + C_2H_6$) and thus insertion is viable with this concerted mechanism. Our best estimate to the potential energy surface is given in Figure 13. It is necessary for the spin to change from triplet to singlet, and the crossing of these curves should occur at an angle of 30°−40°, *below* the threshold energy.

This mechanism is entirely plausible when one considers the nature of the orbitals active in the chemistry (Figure 14). To a first approximation, in the molecular complex, the $a''$ $d_{yz}$ orbital (in the Rh−C−C plane) is empty and the other $d$ orbitals are doubly occupied. The C−H $a'$ and $a''$ orbitals and the $d_{z^2}$ orbital should be considered active. In the dihydride complex, the $a'$ $d_{z^2}$ orbital is empty and the Rh−H $a'$ and $a''$ orbitals and the C−C $a'$ $\pi$ bond should be considered active. In both complexes, there are six active electrons in orbitals of $a'$, $a'$, and $a''$ symmetries. These orbitals easily convert from those of the molecular complex to those of the dihydride complex, thus facilitating the concerted insertion.

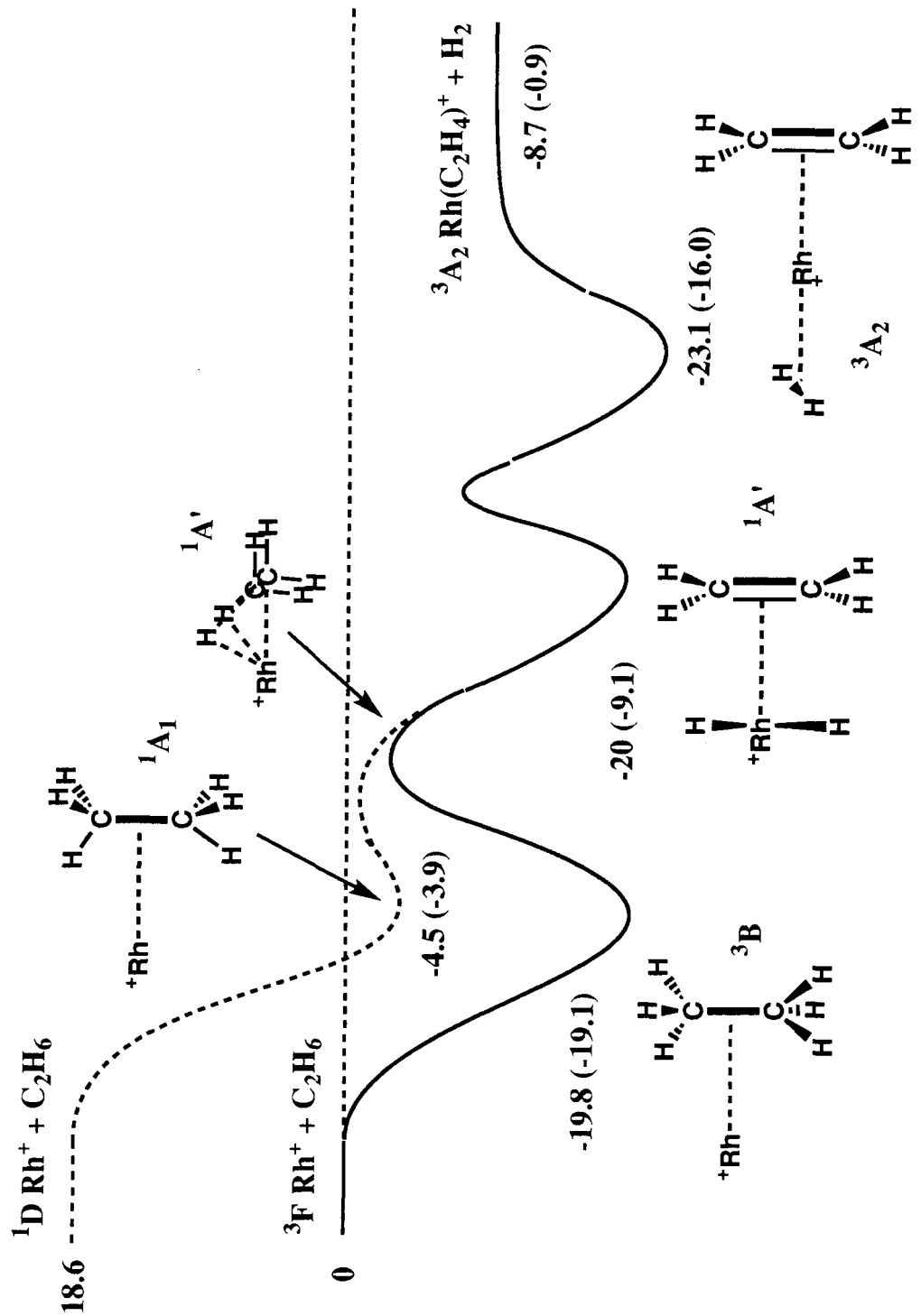


**Figure 13.** Best estimate for the potential energy surface for dehydrogenation of ethane by $Rh^+$. A concerted insertion into two C-H bonds on the singlet surface is the initial step. Energies represent our best estimate. Energies in parenthesis are our calculated well depths. In kcal/mol

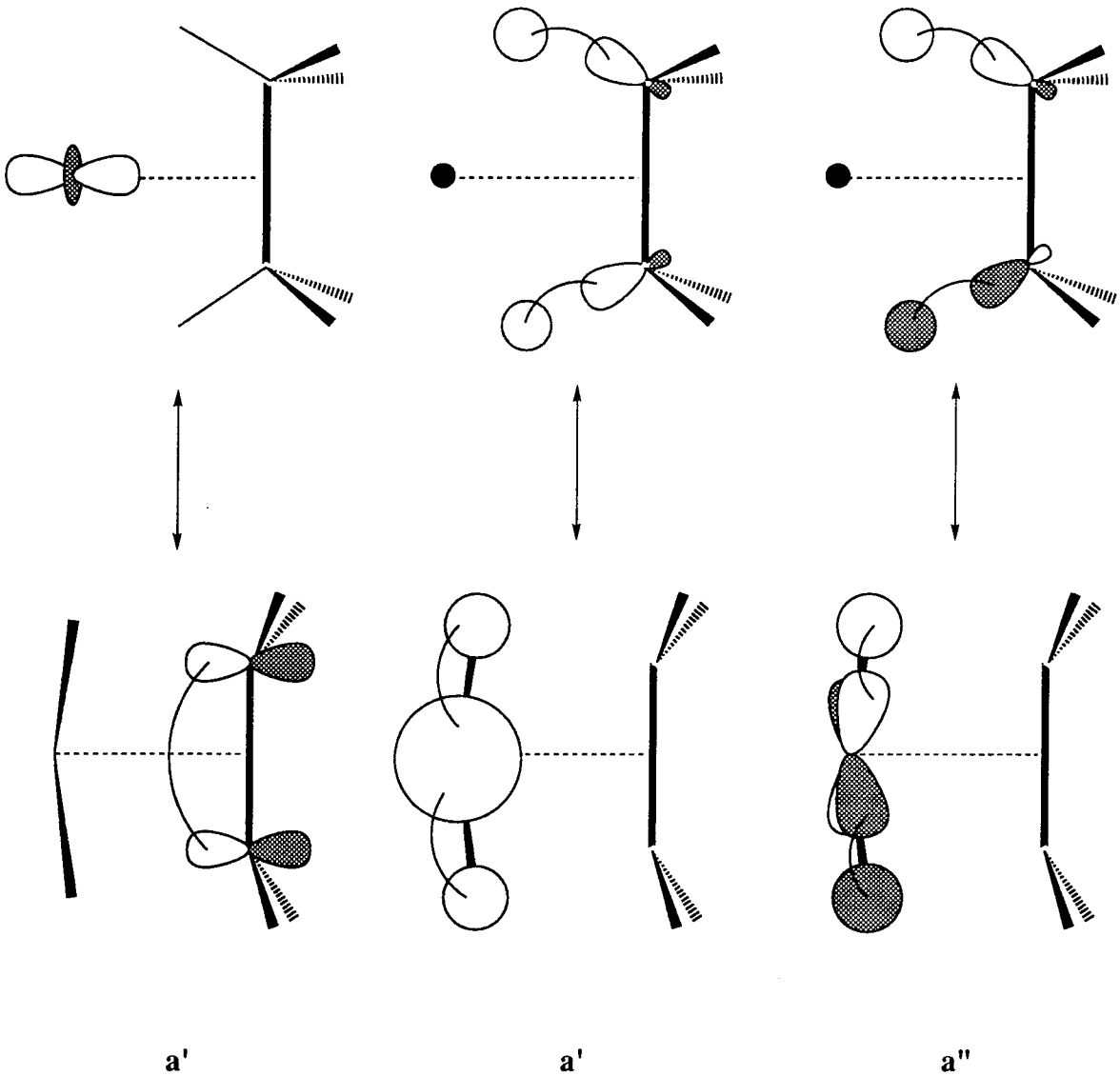


**Figure 14.** Evolution of active orbitals from $Rh(C_2H_6)^+$ to $Rh(H)_2(C_2H_4)^+$.

## 8.7 Conclusions

We have found 1,2-dehydrogenation of ethane to be an exothermic process for $Co^+$, $Rh^+$, and $Ir^+$. Based on a combination of theory and experiment, we have proposed three unique mechanisms for this reaction.

For $Co^+$, we find that the intermediate complex, $Co(H)_2(C_2H_4)^+$, is not stable to reductive elimination of $H_2$. Since experiment has determined that the initial C−H oxidative addition is rate determining for propane dehydrogenation, we conclude that this step is followed by a multi-center transition state corresponding to a concerted $\beta$-H shift and $H_2$ elimination. We estimate the barrier for the initial C−H insertion is 1 to 5 kcal/mol above the threshold energy. The nature of this barrier is such that the initial insertion into the C−H bond must be extensive enough that the Co−H bond can freely rotate about the Co−C bond.

For $Rh^+$, we find that the initial C−H insertion is unfavorable and crosses the threshold energy at an H−Rh−C angle of only 50°-60°. This angle is not large enough to proceed via the mechanism outlined for $Co^+$. However, unlike $Co^+$, the pyramidal $^1A'$ $Rh(H)_2(C_2H_4)^+$ intermediate complex is stable (by an estimated 20 kcal/mol). In addition, the $^1A_1$ $Rh(C_2H_6)^+$ complex is below the threshold energy by 4.5 kcal/mol. We find that there is only a minimal barrier on this singlet surface for a concerted insertion into two C−H bonds to go directly from the molecular complex to the dihydride. Via this mechanism, ethane dehydrogenation should occur at thermal energies, as observed.

For $Ir^+$, we expect that a number of reaction channels are available but dehydrogenation occurs via the standard oxidative addition/$\beta$-H shift/reductive elimination mechanism. This reaction is exothermic by 43 kcal/mol with a global

minimum for the $Ir(H)_2(C_2H_4)^+$ complex, bound by 82 kcal/mol with respect to the reactants.

Much of the difference in the chemistry stems from the two most important factors detailed in this work. The first is the effectiveness of *sd* hybridization and the second is the state splittings between the $d^8$ and $s^1d^7$ configurations. Poor *sd* hybridization destabilizes the $Co(H)_2(C_2H_4)^+$ intermediate while an unfavorable $s^1d^7$ configuration destabilizes the $Rh(H)(C_2H_5)^+$ intermediate. As a result, the above reaction mechanisms were proposed which did not invoke these structures. In contrast, efficient *sd* hybridization and favorable state splittings lead to a facile and strongly exothermic reaction profile for $Ir^+$.

## Appendix

Geometry optimizations at the MCPF level on the $Co(H)_2(C_2H_4)^+$ structure used a TZ basis on Co and a TZP basis set on C and H. The single d polarization function on the C had an exponent of 0.55 and the single p polarization function on the H had an exponent of 0.727.

## References


(1) (a) Eller, K.; Schwartz, H. *Chem. Rev.* **1991**, *91*, 1121. (b) Armentrout, P.B.; Beauchamp, J.L. *Acc. Chem. Res.* **1989**, *22*, 319.

(2) Tolbert, M.A.; Beauchamp, J.L. *J. Am. Chem. Soc.* **1984**, *106*, 8117.

(3) Byrd, G.D.; Freiser, B.S. *J. Am. Chem. Soc.* **1982**, *104*, 5944.

(4) Tolbert, M.A.; Mandich, M.L.; Halle, L.F.; Beauchamp, J.L. *J. Am. Chem. Soc.* **1986**, *108*, 5675.

(5) Tonkyn, R.; Ronan, M.; Weisshaar, J.C. *J. Phys. Chem.* **1988**, *92*, 92.

(6) Ranasinghe, Y.A.; MacMahon, T.J.; Freiser, B.S. *J. Phys. Chem.* **1991**, *95*, 7721.

(7) Huang, Y.; Wise, M.B.; Jacobson, D.B.; Freiser, B.S. *J. Am. Chem. Soc.* **1985**, *107*, 6744.

(8) Irikura, K.; Beauchamp, J.L. *J. Am. Chem. Soc.* **1989**, *111*, 75.

(9) Armentrout, P.B.; Beauchamp, J.L. *J. Chem. Phys.* **1981**, *74*, 2819.

(10) (a) Hanratty, M.A.; Beauchamp, J.L.; Illies, A.J.; van Koppen, P.; Bowers, M.T. *J. Am. Chem. Soc.* **1988**, *110*, 1. (b) Georgiadis, R.; Fisher, E.R.; Armentrout, P.B. *J. Am. Chem. Soc.* **1989**, *111*, 4251.

(11) van Koppen, P.A.M.; Brodbelt-Lustig, J.; Bowers, M.T.; Dearden, D.V.; Beauchamp, J.L.; Fisher, E.R.; Armentrout, P.B. *J. Am. Chem. Soc.* **1991**, *113*, 2359.

(12) Perry, J.K.; Goddard, W.A., III *J. Am. Chem. Soc.*, in press.

(13) Crabtree, R.H. *The Organometallic Chemistry of the Transition Metals*; Wiley: New York, 1988, Chap. 5.

(14) Sodupe, M.; Bauschlicher, C.W., Jr.; Langhoff, S.R.; Partridge, H. *J. Phys. Chem.* **1992**, *96*, 2118.

(15) Bauschlicher, C.W. Personal communication.

(16) (a) Low, J.J.; Goddard, W.A., III *J. Am. Chem. Soc.* **1984**, *106*, 6928. (b) Low, J.J.; Goddard, W.A., III *J. Am. Chem. Soc.*, **1984**, *106*, 8321.

(c) Low, J.J.; Goddard, W.A., III *J. Am. Chem. Soc.* **1986**, *108*, 6115.
(d) Low, J.J.; Goddard, W.A., III *Organometallics*, **1986**, *5*, 609.

(17) Schultz, R.H.; Armentrout, P.B. *J. Am. Chem. Soc.* **1991**, *113*, 729.

(18) Blomberg, M.R.A.; Siegbahn, P.E.M., Svensson, M. *New J. Chem.* **1991**, *15*, 727.

(19) van Koppen, P.A.M.; Bowers, M.T.; Fisher, E.R.; Armentrout, P.B. *J. Am. Chem. Soc.*, submitted.